UNIVERSITÀ DEGLI STUDI FIRENZE

DOTTORATO DI RICERCA IN SCIENZE BIOMEDICHE

CICLO XXXVI

COORDINATORE Prof. Chiti Fabrizio

STUDY OF THE EFFECTS OF AMINOSTEROLS AND BERBERINE ON THE STRUCTURAL AND DYNAMICAL PROPERTIES OF BIOLOGICAL MEMBRANES AND QUANTIFICATION OF THEIR PROTECTIVE ROLE AGAINST MISFOLDED PROTEIN OLIGOMERS

Settore Scientifico Disciplinare BIO/10

Dottorando

Dott.ssa Errico Silvia

Supervisore

Prof. Chiti Fabrizio

Coordinatore

Prof. Chiti Fabrizio

Anni 2020 – 2023

Table of content

Abstract

Many neurodegenerative diseases, such as Alzheimer's and Parkinson's diseases, are associated with the self-assembly of peptides and proteins into fibrillar aggregates. Soluble misfolded oligomers formed during the aggregation process, or released by mature fibrils, play a relevant role in neurodegenerative processes through their interactions with neuronal membranes. Natural aminosterols are considered promising drug candidates against neurodegeneration, and one relevant protective mechanism occurs via their binding to biological membranes and inhibiting the binding of amyloidogenic proteins and their cytotoxic oligomers. Another natural compound with a potential therapeutic effect is the plant alkaloid berberine, which has been reported to possess antioxidant and anti-inflammatory activities and to protect neuronal cells from death induced by oxidative stress, but its mechanism of action is not yet clear, and there is no evidence whether it exerts its protective effects through the interaction with biological membranes.

In the first part of this thesis, we obtained a quantitative measurement of the affinity of a pair of toxic/nontoxic oligomers of the model protein HypF-N for the lipid membranes of liposomes in the form of large unilamellar vesicles (LUVs) by using fluorescence quenching experiments with probes embedded in the polar and apolar regions of the LUV bilayer and toxic/nontoxic oligomers, and another oligomer-membrane binding assay using fluorescently labelled oligomers and unlabeled LUVs. With both approaches, we found that toxic oligomers have a membrane affinity 20-25 times higher than nontoxic oligomers. Circular dichroism spectroscopy, intrinsic fluorescence measurements and fluorescence resonance energy transfer (FRET) indicated that neither oligomer type changes its structure upon membrane interaction. LUVs enriched with trodusquemine had a significantly decreased affinity for these toxic species. The affinity of the oligomers for the lipid membranes increased and slightly decreased with GM1 ganglioside and cholesterol content, respectively, indicating that physico-chemical properties of lipid membranes modulate their affinity for misfolded oligomers.

In the second part of this thesis, we compared three natural chemically different aminosterols, namely squalamine, trodusquemine and the newly discovered

aminosterol ENT-03. Using unlabelled LUVs and fluorescently labelled aminosterols and an aminosterol-membrane binding assay we quantified the different binding affinities of the three aminosterols for the membrane. Moreover, the three aminosterols caused different (i) LUV charge neutralization, as observed with ζ potential measurements; (ii) LUV bilayer mechanical reinforcement, as observed with breakthrough force measurements on supported lipid bilayers (SLBs) with atomic force microscopy (AFM); and (iii) redistributions of key lipids within membranes of LUVs, as inspected with lipid-lipid FRET. Following a dose-dependent quantification of their different abilities in protecting cultured cells against Ca^{2+} influx induced by amyloid-β oligomers, a global fitting analysis led to an analytical equation describing quantitatively the protective effects of aminosterols as a function of their concentration and relevant membrane perturbations, and furthermore correlated aminosterol-mediated protection with well-defined chemical moieties, linking quantitatively their chemistry to their protective effects on biological membranes.

In the third part of this thesis, we focused on the plant alkaloid berberine, and we demonstrated its ability to interact with the membrane of LUVs, with a slightly higher affinity for the hydrophobic core of the lipid bilayer, as investigated using berberine-induced fluorescence quenching of LUVs containing fluorescent probes, light scattering and equilibrium dialysis experiments with unlabeleld LUVs and berberine. Concentration- and temperature-dependent fluorescence anisotropy measurements indicated that the interaction between berberine and LUVs induced an overall stiffening of the membrane. Moreover, berberine decreased the affinity of toxic oligomers for the membrane, as observed with fluorescence quenching experiments with fluorescent probes embedded in LUVs bilayer and toxic oligomers. An ANS binding assay and circular dichroism spectroscopy in the absence of LUVs highlighted the ability of this alkaloid to shield the exposure of hydrophobic clusters to the solvent of toxic oligomers, without significantly altering their secondary structure, suggesting an additional therapeutic potential of this molecule against misfolded oligomers based on its direct effect on oligomers, in addition to its protective binding to the membranes.

Abbreviations

AD, Alzheimer's disease; Aβ, amyloid-β; ADDLs, $A\beta_{42}$-derived diffusible ligands; AFM, atomic force microscopy; APoE, apolipoprotein E; APP, amyloid precursor protein; A594, Alexa Fluor® 594 NHS Ester; AM-A594, Alexa Fluor® 594-labelled aminosterol; AM-BODIPY, BODIPY™ TMR-X-labelled aminosterol; BACE, β-APP cleaving enzyme; Brb, berberine; BODIPY, BODIPY™ TMR-X NHS Ester; BTF, breakthrough force; CD, circular dichroism; COC, cyclic olefin copolymer; CSF, cerebrospinal fluid; CHOL, cholesterol; DMEM, Dulbecco's Modified Eagle's Medium; DMF, dimethylformamide; DMPS , 1,2-dimyristoyl-sn-glycero-3-phospho-L-serine; DMSO, dimethyl sulfoxide; DOPC, 1,2-dioleoyl-sn-glycero-3-phosphocoline; DPH, 1,6-Diphenyl-1,3,5-hexatriene; DTT, dithiothreitol; EMA , European Medicines Agency; ENS, enteric nervous system; FBS, fetal bovine serum; FDA, Food and Drug Administration; FDG, [^{18}F] fluorodeoxyglucose; FRET, fluorescence resonance energy transfer; FWHM, full width at half maximum; GBA , glucocerebrosidase 1; GdnHCl, guanidine hydrochloride; GSH, reduced glutathione; GUVs , giant unilamellar vesicles; GWASs, genome-wide association studies; HEPES, 4-(2-Hydroxyethyl) piperazine-1-ethanesulfonic acid; HO-1, heme oxygenase-1; IPTG, isopropyl β-D-thiogalactopyranoside; kcps, kilocounts per second; LUVs, large unilamellar vesicles; MD, molecular dynamics; MLVs, multilamellar vesicles; MVVs , multivesicular vesicles; MWCO, molecular weight cut-off; NAC, non-amyloid component; NIA-AA, National Institute on Aging and Alzheimer's Association; NMDA , N-methyl-D-aspartate; OAs, type A HypF-N oligomers; OBs, type B HypF-N oligomers; PBS, phosphate-buffered saline; PD, Parkinson's disease; PTP1B, protein tyrosine phosphatase 1B; PSEN1, presenilin 1; PSEN2, presenilin 2; QCM, quartz crystal microbalance; ROS, reactive oxygen species; SLBs, supported lipid bilayers; SM, sphingomyelin; SNARE, soluble N-ethylmaleimide-sensitive factor activating protein receptor; SQ, squalamine; SUVs, small unilamellar vesicles; TCEP, tris(2-carboxyethyl)phosphine hydrochloride; TFE, trifluoroethanol; TFA, trifluoroacetic acid; T_m, transition temperature; TMA-DPH, 1-(4-trimethylammoniumphenyl)-6-phenyl-1,3,5-hexatriene p-toluenesulfonate; TRO, trodusquemine; ULVs , unilamellar vesicles; αS, α-synuclein; ^{123}ImIBG, iodine-123-meta-iodobenzylguanidine; 1,5-IAEDANS, 5-((((2-iodoacetyl)amino)ethyl)amino)naphthalene-1-sulfonic acid; 6-IAF, 6-iodoacetamidofluorescein; 6-OHDA, 6-hydroxydopamine.

1. Introduction

1.1 Alzheimer's disease (AD)

1.1.1 Pathophysiological basis of AD

In 1906, Alois Alzheimer, a clinical psychiatrist and neuroanatomist, first described "a peculiar severe disease process of the cerebral cortex" affecting a patient who suffered from memory loss, disorientation, hallucinations, aggression and confusion (Hippius 2003; Cipriani et al 2011). In 1910, Emil Kraepelin, a German psychiatrist, named the condition with the eponym of ''Alzheimer's disease'' (AD) (Cipriani et al 2011) that is, now, the world's main cause of dementia, accounting for 60-80% of dementia cases and an estimated 55 million patients worldwide (statistical data from: www.alz.org).

Initially, the diagnosis of AD was restricted to the stage of dementia, a clinical syndrome characterised by substantial progressive cognitive impairment affecting several domains, or neurobehavioral symptoms of enough severity to cause evident functional impact on daily life (Dubois et al. 2007; Scheltens et al. 2021). In 2011, some important biomarkers were integrated into the diagnostic formulations for probable and possible AD-associated dementia for use in research settings, in order to enhance the pathophysiological specificity of the diagnosis of AD dementia (McKhann et al., 2011; Albert et al., 2011). Based on these important integrations, it was possible to define different clinical phases or stages of AD: (i) pre-symptomatic AD, which can last for years, characterized by mild or even undetectable memory loss, but significant pathological changes in cortex and hippocampus, until the overproduction and accumulation of Aβ in the brain reaches a critical level that triggers the amyloid cascade; (ii) mild or early stage

of AD, in which cognitive impairment becomes apparent, although mild, and early-stage pathology is present, ranging from mild neuronal dystrophy to early-stage Braak pathology; (iii) moderate AD stage, in which the disease spreads to cerebral cortex areas that results in an increased memory loss; (iv) clinically defined AD dementia, in which there is severe accumulation of neuritic plaques and neurofibrillary tangles in the entire cortex area (De-Paula et al. 2012; Dubois et al., 2016; Breijyeh & Karaman 2020).

Since biomarkers have become increasingly important to understanding the biology of AD and provide measures of relevant pathophysiology in living persons, the National Institute on Aging and Alzheimer's Association (NIA-AA) recently proposed a research framework based on the definition of AD that can be documented by postmortem examination or in living patients by biomarkers, following the "AT(N)" system (Jack et al. 2016; Jack et al. 2018). In particular, the major biomarkers of AD can be divided into 3 binary categories based on the nature of the underlying pathophysiology that each of them measures (Jack et al. 2016; Jack et al. 2018): (i) β amyloid deposition (A): high amyloid-specific ligand retention on PET in specific areas of the brain or low $A\beta_{42}$ in cerebrospinal fluid (CSF) (Klunk et al. 2004; Fagan et al. 2007; Mattsson et al. 2009; Visser et al. 2009); (ii) tau pathology (neurofibrillary tangles) (T): elevated CSF phosphorylated tau (p-tau) and tangle-specific ligand retention on PET (Buerger et al. 2006; Mattson et al. 2009); (iii) AD-like neurodegeneration or neuronal injury (N): CSF total tau (t-tau), [^{18}F] fluorodeoxyglucose (FDG) hypometabolism on PET, and atrophy on structural MRI in regions characteristic of AD (Besson et al. 2015).

From a pathological point of view, AD is characterized by the presence of neuritic plaques and neurofibrillary tangles, typically accumulating in the entorhinal cortex in the hippocampus and then spreading to cortical regions of the brain, that are related to the

deposition and accumulation of the amyloid-β peptide (Aβ) in the extracellular space and to cytoskeletal changes that arise from the hyperphosphorylation of microtubule-associated tau protein in neurons, causing its deposition in neuronal cells, respectively (**Fig. 1.1**) (Serpell 2000; Selkoe 1991; De-Paula et al 2012; Loof & Schoofs, 2019).

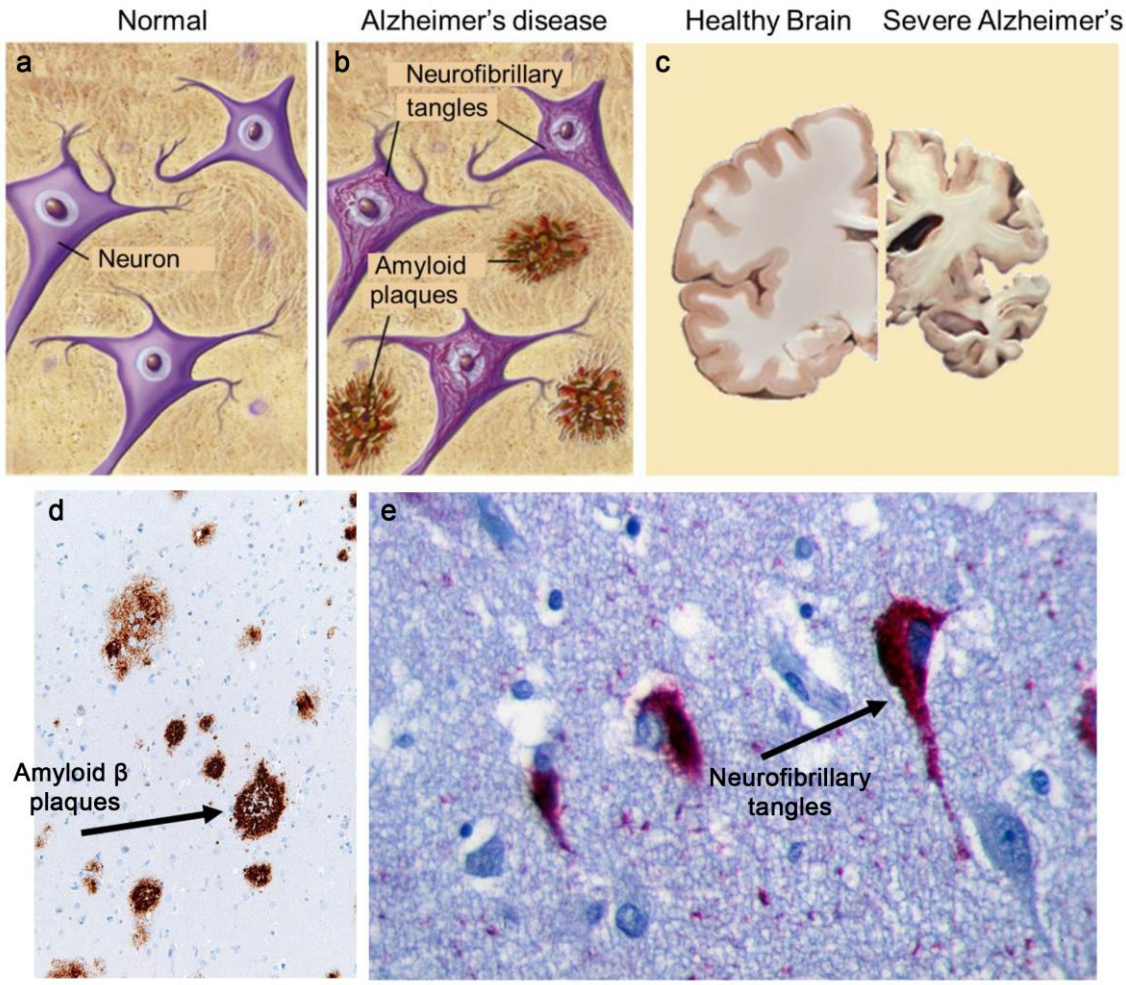

Figure 1.1. Hallmarks of AD. (A,B) Representation of healthy brain tissue **(A)** compared to pathological AD **(B)** with the presence of characteristic neuritic plaques and neurofibrillary tangles. **(C)** Brain slices showing the massive apoptosis occurring in later stages of the development of AD in the human brain. **(D)** Aβ plaque within the cortex visualised via anti-amyloid antibodies and immunohistochemistry. **(E)** Antibodies against tau showing paired helical filaments-containing neurites. Figure adapted from Loof & Schoofs, 2019; Wikimedia Commons.

According to the amyloid hypothesis, these alterations lead to the onset of the typical symptoms of AD, represented by the progressive impairment of cognitive

function and often behavioural disorders such as aggression, depression, and wandering (Francis et al., 1999; Atri, 2019; Jack et al., 2019). The underlying cause of pathological changes in AD is not clear and there is still debate on a unique theory for explaining its pathogenesis, with one dominant hypothesis of AD pathogenesis emerging, that is the amyloid hypothesis, which suggests that alterations in Aβ protein production and processing are the main initiating factors of AD (Hardy & Selkoe, 2002; Anand & Singh, 2013; Armstrong, 2019; Breijyeh & Karaman, 2020; Karran & De Strooper, 2022).

The first evidence that led to the articulation of the amyloid hypothesis of AD was the discovery of an autosomal dominant form of AD, caused by a missense mutation in the gene coding for amyloid precursor protein (APP) (Goate et al., 1991), the holoprotein from which the Aβ-peptide is excised via sequential scission by the β-APP cleaving enzyme (BACE) (Hussain et al., 1999; Sinha et al., 1999) and γ-secretase (De Strooper et al., 1998; Karran et al., 2011). After a few years, this hypothesis was further supported after the identification of other mutations causing autosomal dominant forms of AD in the gene coding for APP (Goate et al., 1991), but also in genes coding for presenilin 1 (PSEN1) (Sherrington et al., 1995) and presenilin 2 (PSEN2) (Rogaev et al., 1995), which are both homologous proteins that can form the catalytic active site of γ-secretase (Karran et al., 2011; Karran & De Strooper, 2022). Moreover, it was observed that trisomy of chromosome 21 (Downs syndrome) leads inevitably to the histopathological changes typical of AD (Olson & Shaw, 1969), and the gene encoding APP is located in this chromosome (Kang et al., 1987; Tanzi et al., 1987; Robakis et al., 1987), reinforcing this proposal of AD pathogenesis. A further strengthening element of the amyloid hypothesis is the observation that anti-Aβ antibodies, which will be widely discussed in section 1.1.5, represent the only disease-modifying drugs capable to mediate the removal of

amyloid plaques from brains of patients with AD and consequent amelioration of cognitive decline (Karran & De Strooper, 2022; Budd Haeberlein et al., 2022; Sims et al., 2023; van Dyck et al., 2023).

On the other hand, considering neurofibrillary tangles formed by the protein tau, which represent the second hallmark of AD, an alternative hypothesis was proposed, specifically the tau hypothesis, that postulates that tau phosphorylation and aggregation represent the main cause of neurodegeneration in AD (Brier et al., 2016; Kametani & Hasegawa, 2018; Agarwal et al., 2020). This hypothesis was named the tau hypothesis (Frost et al., 2009). The role of the protein tau in AD will be widely discussed in section 1.1.3.

Another hypothesis for the pathogenesis of AD is the cholinergic hypothesis, which is the oldest known hypothesis of AD and proposes that degeneration of cholinergic neurons in the basal forebrain and the associated loss of cholinergic neurotransmission represent a critical pathological change that contributes significantly to the deterioration in cognitive function observed in AD patients (Bartus et al., 1982; Francis et al., 1999; Terry & Buccafusco, 2003). A loss of cholinergic innervation in the cerebral cortex of patients with AD is an early pathogenic event that correlated with cognitive impairment and led to the development of cholinesterase inhibitor therapies, which are one of the few drugs actually used in the treatment of AD, even if they only provide a symptomatic relief (Hampel et al., 2018; Cummings et al., 2019; Passeri et al., 2022).

The oxidative stress hypothesis for the pathogenesis of AD is based on the particular vulnerability of the brain to oxidative stress, since the brain utilizes more oxygen than other tissues and undergoes mitochondrial respiration, which increases the potential for reactive oxygen species (ROS) formation and reduces levels of antioxidants

(Evans, 1993; Markesbery, 1997; Padurariu et al., 2013). Moreover, it is known that Aβ can induce oxidative stress, and AD is typically highly associated with cellular oxidative stress, including augmentation of protein oxidation, protein nitration, glycoloxidation and lipid peroxidation (Butterfield et al., 2002; Cheignon et al., 2018; Du et al., 2018). This evidence led to the postulation of the oxidative stress hypothesis for the pathogenesis of AD (Padararíu et al., 2013; Du et al., 2018).

Inflammation, and particularly neuroinflammation, is another typical hallmark of AD and other neurodegenerative diseases, including PD, and it is attributed to activated microglia cells and release of numerous cytokines surrounding amyloid plaques (Kinney et al., 2018; Du et al., 2018). Neuroinflammation is therefore considered an early, fundamental player in the progression of AD and led to the inflammation hypothesis (Kinney et al., 2018). However, non-steroid anti-inflammatory drugs did not show convincing evidence of benefits, suggesting that the relationship between inflammatory and AD pathogenesis is very complex, probably involving many players (Miguel-Álvarez et al., 2015; Kinney et al., 2018; Du et al., 2018).

1.1.2 Amyloid-β (Aβ) peptide and AD pathogenesis

Aβ-peptide originates from the single transmembrane receptor-like protein APP, that is enriched in neuronal synapses and that seems to be involved in synaptogenesis and synaptic plasticity (Gralle et al., 2007; Haas & Selkoe, 2007; Knopman et al., 2021). The partially intramembrane Aβ region can be liberated as a free peptide from its precursor following the sequential cleavage of APP by β-secretases and γ-secretases, and the precise site of the γ-cleavage produces several Aβ species, including the most abundant 40 amino-acid species ($Aβ_{40}$) and a number of minor species, including $Aβ_{42}$, which are

more hydrophobic and prone to aggregate in a concentration dependent manner, and are the principal species deposited in the brain (**Fig. 1.2**) (Steiner & Haass, 2000; Holtzman et al., 2011; Thinakaran & Koo, 2008; Murphy & Levine, 2010; Knopman et al., 2021).

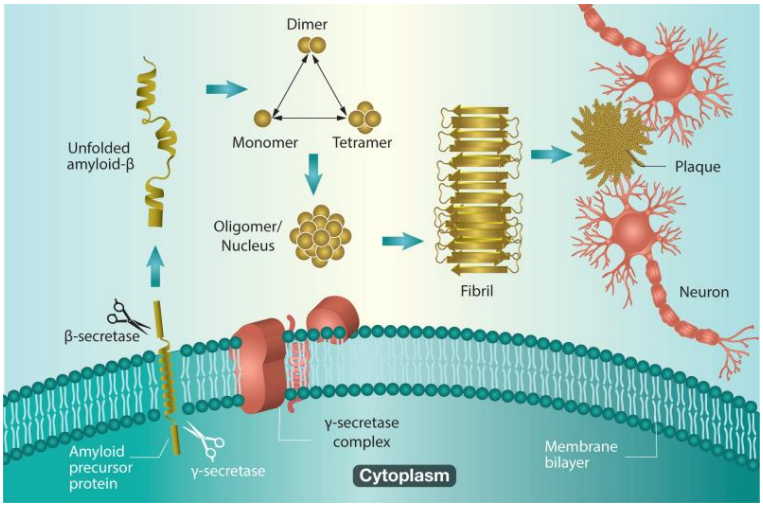

Figure 1.2. Scheme of Aβ formation from APP, aggregation and deposition in amyloid plaques. Figure adapted from Jokar et al., 2020.

In fact, Aβ is produced and secreted physiologically in all cells but is present at the highest concentrations in the central nervous system, and its levels seem to be directly influenced by synaptic activity (Seubert et al., 1992; Shoji et al., 1992; Cirrito et al., 2005; Knopman et al., 2021). The increase in $A\beta_{42}$ peptide concentration, either due to an increased production or decreased clearance, or an increase in the ratio of $A\beta_{42}$ to $A\beta_{40}$, induces Aβ assembly into insoluble β-sheet fibrillar aggregates that deposit extracellularly in the brain parenchyma and cerebral vasculature, causing the damage of synaptic structure and function, and neuronal atrophy in the hippocampus area and then spreading to cortical regions, resulting in the cognitive impairment and dementia typical of AD (**Fig. 1.2**) (Selkoe, 1991; Hardy & Higgins, 1992; Hardy & Selkoe, 2002; Lu et al.,

2013; Ricciarelli & Fedele, 2017; Paroni et al., 2019; Breijyeh & Karaman, 2020; Shi et al., 2022; Jokar et al., 2020).

There are two forms of AD: the genetic form of AD, which can be caused by mutations in APP, PSEN1 or PSEN2 genes, occurs before the age of 65 and represents less than 1% of cases; and the sporadic form, that accounts for most of the patients affected by this disease (Passeri et al., 2022). In the context of late-onset sporadic AD, many putative susceptibility genes have been reported, but the ε4 isoform of the lipid-carrier protein apolipoprotein E (APoE) remains the strongest confirmed genetic risk factor (Corder et al., 1993; Strittmatter et al., 1993; Kim et al., 2009; Serrano-Pozo et al., 2021). The APOE gene encodes the ApoE protein, which is produced in the brain predominantly by astrocytes and activated microglia, and in humans exist in three common isoforms, ApoE ε2, ApoE ε3 and ApoE ε4 (Kim et al., 2009; Knopman et al., 2021). The three different ApoE isoforms are known to modulate Aβ metabolism to varying extents, with ApoE ε4 having the strongest effect on the slowing of clearance, therefore individuals carrying ApoE ε4 isoform show an early Aβ accumulation in a dose-dependent manner before the onset of clinical symptoms (Kim et al., 2009; Reiman et al., 2009; Knopman et al., 2021). However, the details of this process as well as the role ApoE plays in non-Aβ mediated mechanisms in AD pathogenesis remain to be fully clarified (Small & Duff, 2008; van der Kant et al., 2020). At present, *ca*. 75 risk loci were identified as genetic risk factors thanks to genome-wide association studies (GWASs), involving mainly amyloid/tau pathways and highlighting microglia implication in the pathophysiological process (Bellenguez et al., 2022).

Regardless of the cause of Aβ accumulation, it was interestingly found that protein deposition could precede cognitive decline, leading to a pre-symptomatic stage with

neuropathologic changes and positive biomarkers of AD pathology that could last many years before the appearance of any symptoms (Sengupta et al., 2016; Buccellato et al., 2023). Moreover, a lack of correlation was observed between the severity of the disease and the plaque burden, with neuronal death occurring in brain regions devoid of plaques and Aβ plaques found in cognitively normal individuals (Sloane et al., 1997; Erten-Lyons et al., 2009). This suggests that large insoluble Aβ aggregates are not the main responsible factor of AD neurodegeneration (Erten-Lyons et al., 2009; Sengupta et al., 2016). On the other hand, small soluble Aβ oligomers have been shown to produce cognitive deficits in the absence of plaques and more effectively than Aβ fibrils, and individuals with clinical AD symptoms could show no pathological changes in their brains (Gandy et al., 2010; Petersen et al., 2013). Moreover, a correlation was found between disease severity and total Aβ (McLean et al., 1999; Shankar et al., 2008). These findings therefore suggest that larger aggregates are not directly responsible for neurodegeneration but rather small soluble Aβ oligomers represent the highest toxic and disease-relevant species of Aβ and appear before the first neuropathological signs of AD (De Felice et al., 2007; Chiti & Dobson, 2017; Wang et al., 2016; Fani & Chiti, 2022).

1.1.3 Tau and AD pathogenesis

Neurofibrillary tangles in cell bodies and dendrites composed of hyperphosphorylated tau protein are the second neuropathological hallmark of AD in addition to extracellular Aβ plaques (Eftekharzadeh et al., 2018; Tiwari et al., 2019; Knopman et al., 2021). Neurofibrillary tangles of hyperphosphorylated tau are associated not only with AD but with a group of neurodegenerative disorders called tauopathies (Sarkar, 2018). The tau protein is a microtubule-associated protein that co-assembles with tubulin to form

mature and stable microtubules (Claeysen et al., 2012; Tiwari et al., 2019). It is normally present in the cytoplasm of axons, in both presynaptic and postsynaptic compartments and associated with the nuclear membrane (Pooler et al., 2014; Gallardo et al., 2019).

Tau is regulated during both normal homeostasis and in stress-induced responses by several post-translational modifications, including phosphorylation (Medeiros et al., 2011), but in AD and other tauopathies, the phosphorylation level of tau is significantly higher. The consequence of this increased phosphorylation is not completely comprehended but it results in lowering tau's affinity for the microtubules as well as increasing its resistance to degradation by the ubiquitin-proteosome pathway (Mandelkow et al., 1995; Iqbal et al., 2009), and eventually leads to fibrillization and aggregation into pairs of helical filaments to form the neurofibrillary tangles typical of AD and other tauopathies (Grundke-Iqbal et al., 1986; Sengupta et al., 1998; Wells et al., 2021).

It is becoming increasingly clear how soluble forms of Aβ and tau cooperate leading healthy neurons to death, independently of their accumulation into plaques and tangles (Ittner et al., 2010; Shipton et al., 2011; Jackson et al., 2016). This could explain why the pharmacological removal of Aβ or tau alone have not shown a complete resetting of the rate of AD progression once symptoms of AD are present (Picket et al., 2019; Busche & Hyman, 2020; Budd Haeberlein et al., 2022; Sims et al., 2023; van Dyck et al., 2023). Soluble Aβ species seem to act upstream of tau in AD pathogenesis, as suggested by studies that blocked Aβ production in cultures and resulted in prevented formation of tau pathology (Israel et al., 2012; Lee et al., 2016). Moreover, synaptic disfunction and neurotoxicity induced by Aβ has been shown to essentially require the presence of soluble cytoplasmic tau (Takashima et al., 1993) and Aβ fibrils can

significantly accelerate the formation of neurofibrillary tangles in mouse models (Götz et al., 2001). These pieces of evidence, taken together, suggest that Aβ could initiate a pathological feedback loop with tau and that these two proteins then work with a synergistical relation (Picket et al., 2019; Busche & Hyman, 2020).

1.1.4 Pharmacological approaches for AD

Up to the present, only four drugs have been approved by both the Food and Drugs Agency (FDA) and the European Medicines Agency (EMA) for treatment in AD and only provide modest improvement in cognitive impairment, without significantly altering the outcome of the disease, therefore representing symptomatic drugs (Tayeb et al., 2012; Shi et al., 2022). Three of these are acetylcholinesterase inhibitors, named donepezil, galantamine, and rivastigmine, and one is a N-methyl-D-aspartate (NMDA) receptor antagonist, named memantine (Cummings et al., 2019; Yiannopoulou & Papageorgiou, 2020; Vaz & Silvestre 2020; Shi et al., 2022; Buccellato et al., 2023).

It is known that in AD patients cholinergic pathways in the cerebral cortex and basal forebrain are compromised, and this cholinergic deficit contributes significantly to the cognitive impairment and related symptoms (Katzman & Saitoh, 1991; McGleenon et al, 1999; Shi et al., 2022). The use of acetylcholinesterase inhibitors aims to block the enzymes that break down acetylcholine, in order to compensate the breakdown of synaptic acetylcholine due to the death of cholinergic neurons and to offer symptomatic relief by inhibiting acetylcholine turnover (Davies & Maloney, 1976; Rees & Brimijoin, 2003; Hampel et al., 2018; Moss, 2020). Donepezil, rivastigmine, and galantamine have been shown to significantly improve cognition, daily and global function, and some

behavioural manifestations of AD (Massoud & Gauthier, 2010; Hampel et al., 2018; Buccellato et al., 2023).

NMDA receptors are ionotropic glutamate receptors that exert a crucial role in excitatory synaptic neurotransmission in the mammalian central nervous system, mediating the vast majority of excitatory transmission in neuronal networks (Scheefhals & MacGillavry, 2018; Fani & Chiti, 2022). These receptors are known to be involved in the neurotoxicity mediated by the Aβ oligomers (Snyder et al., 2005; De Felice et al., 2007; Acosta et al., 2017; Fani & Chiti, 2022). Indeed, it has been observed that toxic Aβ oligomers activate aberrantly extrasynaptic NMDA receptors leading to an extracellular Ca^{2+} ions influx into the cytoplasm and consequently to the cascade of biochemical changes that lead to the neuronal dysfunction and death observed in AD (Li et al., 2011; Acosta et al., 2017; Fani & Chiti, 2022). The NMDA receptor antagonist memantine exerts its therapeutic effect by acting as a low-to-moderate affinity, non-competitive antagonist that binds preferentially to open NMDA receptor-operated Ca^{2+} channels and therefore blocks NMDA-mediated Ca^{2+} ion influx induced by Aβ oligomers (Danysz & Parsons, 2003; Matsunaga et al., 2015; Vaz & Silvestre, 2020; Buccellato et al., 2023).

1.1.5 Anti-Aβ monoclonal antibodies

Since current treatment for AD is only symptomatic, has modest benefits and does not restrain the progressive deterioration of cognition, the development of drugs aimed at changing the progression of the disease has been a priority for decades (Vaz & Silvestre, 2020). The abnormal accumulation of Aβ peptides in the brain in AD patients, and the high toxicity exerted by these small soluble species, led to the focus on Aβ as a potential target of disease-modifying therapies (Lord et al., 2009; Selkoe & Hardy, 2016; Vaz &

Silvestre, 2020). In particular, the focus on soluble Aβ oligomers has also increased the interest in antibodies that are selective for different Aβ conformations (Grover et al., 2023). Seven antibodies have reached phase III clinical trials: bapineuzumab, solanezumab, crenezumab, gantenerumab, aducanumab, lecanemab and donanemab, and the last three appeared to be the most promising ones (Shi et al., 2022; Budd Haeberlein et al., 2022; Sims et al., 2023; van Dyck et al., 2023).

Aducanumab is a human immunoglobulin G1 monoclonal antibody, that is able to selectively target aggregated Aβ, but excludes Aβ monomers (Sevigny et al., 2016; Linse et al., 2020; Shi et al., 2022). Aducanumab showed a significant decrease of Aβ and potential slowing of cognitive decline in 3285 patients in two randomized, multicenter, double-blind, placebo-controlled phase III clinical trials (Budd Haeberlein et al., 2022). In June 2021, aducanumab was approved by the FDA to treat mild AD, but has caused considerable medical and scientific controversy (Howard & Liu, 2020; Schneider, 2020; Tampi et al., 2021; Orini et al., 2022; Huang et al., 2023), that eventually led the EMA to conclude that the risk-benefit balance was unfavourable and decided against approval and the withdrawal of marketing application for aducanumab for the treatment of AD in Europe by Biogen on April 2022 (Whitehouse & Saini, 2022; Ashique et al., 2023).

Lecanemab is a humanized G1 monoclonal antibody that preferentially targets soluble aggregated Aβ, with activity across oligomers, protofibrils, and insoluble fibrils (Logovinsky et al., 2016; Swanson et al., 2021). The administration of this monoclonal antibody in a 18-months, randomized multicenter, double-blind, placebo-controlled phase III clinical trial on about 1800 participants was found to reduce markers of amyloid in early AD and resulted in a 27% slower decline on measures of cognition and function in early AD patients (van Dyck et al., 2022). Based on this clinical trial, on July 6, 2023,

the FDA granted traditional approval for lecanemab for the treatment of AD and this antibody represents the second disease-modifying AD treatment to be approved by the FDA and at present the only approved treatment for AD (https://www.fda.gov/news-events/press-announcements/fda-converts-novel-alzheimers-disease-treatment-traditional-approval).

Donanemab is a humanized G1 monoclonal antibody directed against insoluble, modified, N-terminal truncated form of Aβ present only in brain amyloid plaques (Sims et al., 2023). The administration of this monoclonal antibody in a 18-month multicenter, randomized, double-blind, placebo-controlled, phase III clinical trial that enrolled 1736 participants with early symptomatic AD resulted in a reduced a 35% less decline in ability to perform activities of daily living and reduced amyloid plaque on average by 84% compared to placebo (Sims et al., 2023). The Lilly company submitted donanembad to the FDA for traditional approval and regulatory action are expected by the end of this year (https://investor.lilly.com/news-releases/news-release-details/results-lillys-landmark-phase-3-trial-donanemab-presented).

1.2 Parkinson's disease (PD)

1.2.1 Pathophysiological basis of PD

Parkinson's disease (PD) is a neurodegenerative disorder affecting both the central and peripheral nervous systems, which affects more than 10 million people worldwide (https://www.apdaparkinson.org). The first detailed description of PD was made more than two centuries ago, in 1817, by the British medical doctor James Parkinson (Parkinson, 1817; Kalia & Lang, 2015). Most cases of PD are considered sporadic or

idiopathic, and they probably result from a complex interaction of environmental and genetic factors (Kouli et al., 2018). Moreover, there is a minority of cases (10–15%) that record family history, and approximately 5% exhibit Mendelian inheritance, and are considered familial cases of PD (Deng et al., 2018; Kouli et al., 2018).

PD is characterized by early prominent death of dopaminergic neurons in the *substantia nigra pars compacta* and the presence of α-synuclein (αS) positive cytoplasmic inclusions, called Lewy bodies, in surviving neurons (**Fig. 1.3**) (Stefanis, 2012; Kalia & Lang, 2015; Cerri et al., 2019; Karaman et al., 2021; Menšíková et al., 2022).

The resulting dopamine deficiency within the basal ganglia leads to a movement disorder characterised by classical parkinsonian motor symptoms, which include bradykinesia, rigidity, resting tremor and gait disturbances (Kalia & Lang, 2015; Moustafa et al., 2016; Cerri et al., 2019). However, the symptomatology of PD is now recognised as heterogeneous, with clinically significant non-motor features, such as autonomic dysfunctions, cognitive abnormalities, psychiatric symptoms such as anxiety, depression and apathy, and sleep disorders (Kalia & Lang, 2015; Cerri et al., 2019). Due to the heterogeneity of PD symptoms and the implication of multiple neuroanatomical areas, with gradual development of nonmotor symptoms for years before movement symptoms begin, diagnostic tests which allow for definitive diagnosis at early stages of the disease are challenging (Kalia & Lang, 2015; Armstrong & Okun, 2020). The Movement Disorder Society has set up a series of clinical diagnostic criteria for PD, to be used in clinical research but also to guide clinical diagnosis (Postuma et al., 2015).

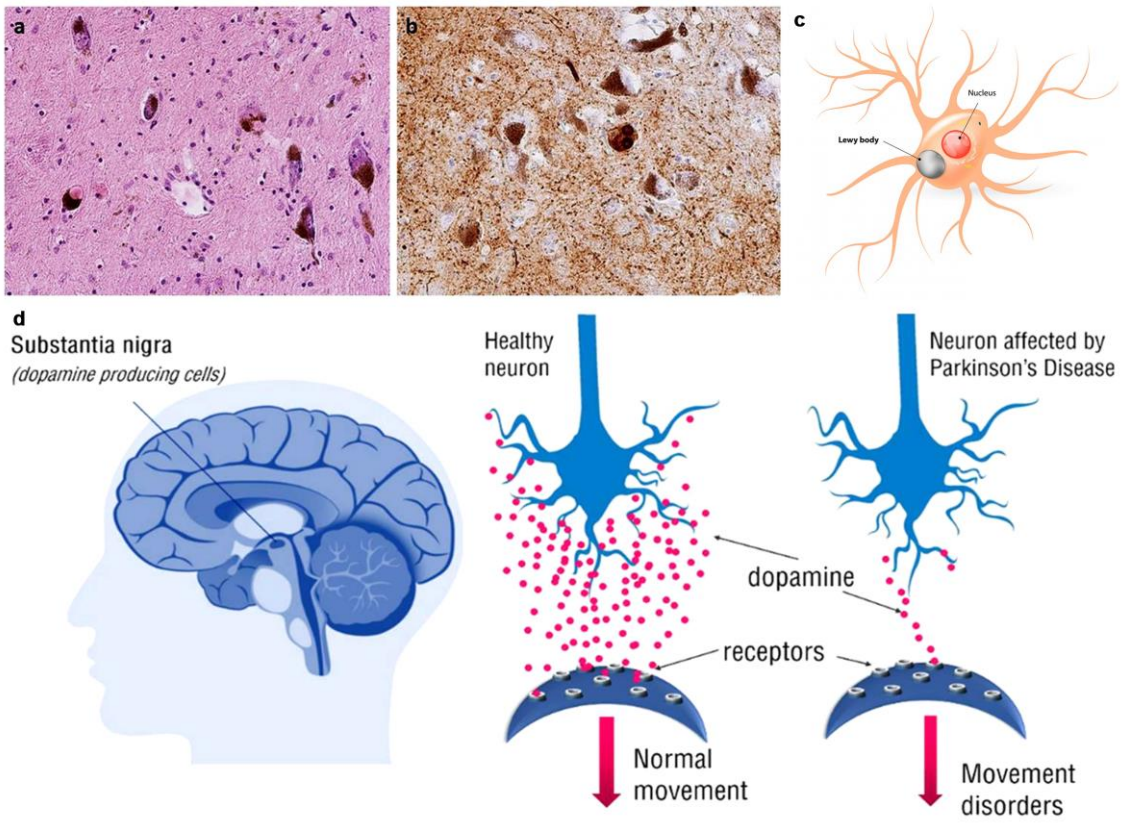

Figure 1.3. Hallmarks of PD. (A) Classical Lewy bodies in the pigmented neurons of *substantia nigra*, haematoxylin and eosin staining, original magnification ×200. **(B)** Pathological deposits of αS in *substantia nigra*, granular cytoplasmic positivity, and dystrophic neurites, stained with a monoclonal antibody against αS, original magnification ×200. **(C)** Illustrative diagram of a neuron containing deposits of αS in the form of Lewy bodies. **(D)** Illustrative diagram showing a region of the brain responsible for dopamine production and the difference in dopamine levels at a synapse between neurons in a healthy person (left) and a patient with PD (right). Figure adapted from Karaman et al., 2021; Menšíková et al., 2022; https://alzheimersnewstoday.com/.

The first essential criterion is parkinsonism, motor-symptom defined as bradykinesia, in combination with at least one other symptom between rest tremor or rigidity (Postuma et al., 2015; Armstrong & Okun, 2020). Once parkinsonism has been diagnosed, the diagnosis of clinically established PD requires at least two of four supportive criteria: (i) rest tremor, (ii) a dramatic improvement with dopaminergic therapy, (iii) the presence of levodopa-induced dyskinesias, or (iv) the presence of either olfactory loss or cardiac sympathetic denervation on iodine-123-meta-iodobenzylguanidine (^{123}ImIBG) myocardial scintigraphy, which is an imaging test that

assesses decreased cardiac norepinephrine uptake (Postuma et al., 2015; Armstrong & Okun, 2020). The gold standard for pathologic confirmation of PD has been the presence of *substantia nigra pars compacta* degeneration and abnormal aggregates of αS protein, called Lewy bodies and Lewy neurites at post-mortem pathological examination (Kalia & Lang, 2015).

1.2.2 α-synuclein (αS) and PD pathogenesis

The first correlation between αS and PD dates back to the early-1990s and followed the observation that genetic markers on human chromosome 4q21–q23, where αS gene was mapped, segregated with the PD phenotype in a large family of Italian descent (Golbe et al., 1990; Polymeropoulos et al., 1997). The members of this family affected by autosomal-dominant PD manifested typical clinical PD traits, including Lewy bodies, except for early onset at a mean age of 46.5 years (Golbe et al., 1990). Some years later, a mutation in the αS gene was discovered in the Italian kindred and in three unrelated families of Greek origin with the same autosomal dominant inheritance for the PD phenotype (Polymeropoulos et al., 1997; Krüger et al., 1998; Zarranz et al., 2004; Miller et al., 2004). These findings led to the development of specific antibodies against αS to localize this protein on histopathological sections of PD patients, and it was observed that αS is robustly expressed within Lewy bodies of both sporadic and familial PD (Spillantini et al., 1997; Spillantini et al., 1998; Baba et al. 1998).

αS is a small intrinsically disordered protein composed of 140 amino acid residues, which is expressed in neurons of the central and peripheral nervous system as well as in blood cells and other tissues (Burré et al., 2018). αS is a member of the synuclein family, which also include β- and γ-synuclein, and is abundantly expressed in the nervous

system, comprising 1% of total cytosolic protein and under physiological conditions it localizes preferentially to presynaptic terminals (George, 2002; Kahle, 2008; Stefanis, 2012). αS is composed of three different regions: the basic N-terminal region (residues 1–60), in turn divided in H1 (1–30) and H2 (31–62) regions, that shows helical propensity in solution and assumes a helical structure when the protein is bound to lipid vesicles (Ulmer et al., 2005; Menon & Mondal, 2023); the central hydrophobic region (residues 61–95), called non-amyloid component (NAC), which constitutes the minimal segment needed for toxic aggregation; and the C-terminal region (residues 96–140) which is highly acidic (Gallardo J. et al., 2020).

Even if the precise physiological role of αS is not completely understood, it is proposed to interact with biological membranes and membrane proteins, acting as a modulator of synaptic transmission by controlling the neurotransmitter release (Murphy et al., 2000; Stefanis, 2012; Bendor et al., 2013; Galvagnion, 2017). One mechanism by which αS modulates synaptic transmission is the promotion of the assembly of the soluble N-ethylmaleimide-sensitive factor activating protein receptor (SNARE) complex through the formation of a multimer at the surface of synaptic vesicles (Burré et al., 2010; Galvagnion, 2017). The neuronal SNARE complex includes three proteins, characterized by sequences of about 65 residues called SNARE motifs that have propensity to form coiled cols, and allow them to anchor to the plasma and synaptic vesicle membranes forming a bridge between these two membranes (Ramakrishnan et al., 2012). Therefore, this protein complex brings the plasma membrane of neuronal cell and the membrane of synaptic vesicles into close proximity, which is critical for membrane fusion and the consequent neurotransmitter release (Söllner et al., 1993; Poirier et al., 1998; Rizo, 2018). In physiological conditions, αS was observed to stabilize

and chaperone the SNARE complex to regulate neurotransmission enhances SNARE-dependent vesicle docking (Burré et al., 2014; Sun et al., 2019).

αS is mainly localized in presynaptic terminals and therefore, synaptic vesicle trafficking in neurons is particularly susceptible to the accumulation of pathological αS species, as observed in PD (Yoo et al., 2023). Monomeric αS appears to be intrinsically disordered in aqueous solution, but under certain conditions, the NAC region can form a cross-β structure, leading to αS amyloid fibrillation, similarly to what is observed with Aβ peptide, and amyloid-like fibrils on prolonged incubation in solution forming the basis of the mature Lewy bodies and neurites present in PD (Kingwell, 2017; Conway et al. 2000; Xu et al., 2018) (**Fig. 1.4**). αS aggregation generates a variety of intermediate species prior to the formation of insoluble fibrils and Lewy bodies, starting from initially soluble oligomeric forms of αS that assume spherical, ring-, and stringlike characteristics when seen under the electron microscope, that gradually become insoluble and coalesce into fibrils (Stefanis, 2012) (**Fig. 1.4**). Synaptic disfunction observed from the initial stages of PD is thus induced by the reduction of functionally αS combined with the accumulation of various toxic intermediates of αS in the presynaptic region (Kramer & Schulz-Schaeffer, 2007; Roberts et al., 2015; Calo et al., 2017). These observations provided important parallels to the pathogenetic basis for the two most common neurodegenerative diseases, *i.e.* AD and PD (Xie et al., 2014; Stefanis, 2012; Chiti & Dobson, 2017).

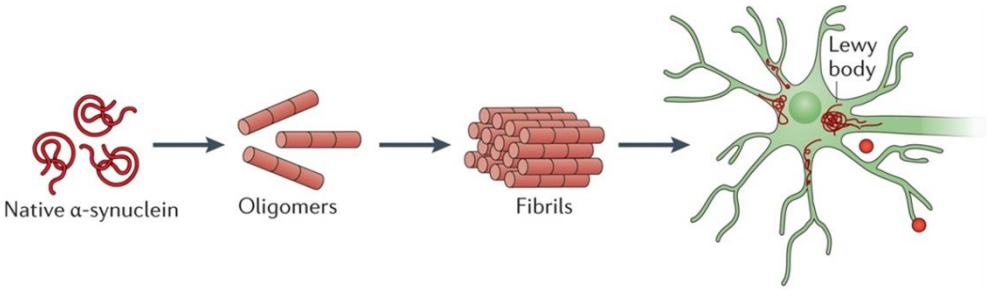

Figure 1.4. αS aggregation. From left to right: monomeric αS in normal conditions in a soluble random coil state; misfolded oligomeric intermediates that form during αS aggregation under pathological conditions that further aggregate into higher order structures which ultimately are converted into Lewy bodies. Figure adapted from Kingwell, 2017.

1.2.3 Pharmacological approaches for PD

In the absence of a disease-modifying therapy, PD treatment is currently mainly based on the control of motor symptoms of the disease and improve patient quality of life, by the administration of dopamine-based drugs that enhance intracerebral dopamine concentrations or stimulate dopamine receptors (Connolly & Lang, 2014; Kalia & Lang, 2015; Armstrong & Okun, 2020). Levodopa preparations, dopamine agonists, and monoamine oxidase-B inhibitors are useful initial therapies (Connolly & Lang, 2014; Armstrong & Okun, 2020).

Levodopa is the immediate precursor to dopamine, which can cross the blood–brain barrier and enable the reduced number of dopaminergic neurons to replace the depleted endogenous neurotransmitter and alleviate motor-symptoms (Hayes, 2019; Deuschl et al., 2022). Levodopa is usually administrated to patients in combination with carbidopa, which reduces metabolism of levodopa in the periphery, increasing central nervous system, and helps to reduce peripheral side effects, such as nausea, vomiting, low blood pressure, and restlessness (Hayes, 2019). However, it was observed that long-term therapy with levodopa leads to the development of motor complications, such as levodopa-induced-dyskinesia, mainly associated with sustained levodopa plasma levels

(Connolly & Lang, 2014; Deuschl et al., 2022). Another option for the treatment of PD are dopamine agonists, that exert their antiparkinsonian effects by acting directly on dopamine receptors and mimicking the endogenous neurotransmitter (Quinn, 1995). Dopamine agonists are less efficient than levodopa, but are frequently used because they are less likely to cause dyskinesias than levodopa and tend to have a longer half-life, so they are usually introduced as initial treatment for patients younger than 60 years (Brooks, 2000; Hayes, 2019).

As an alternative to pharmacological therapy, deep brain stimulation is a surgical treatment for patients with PD who do not respond well to medications or have medication-responsive motor symptoms but with complications such as off periods or dyskinesias, typical of long-term use of dopamine-based drugs (Hayes, 2019). Deep brain stimulation involves surgical placement of unilateral or bilateral leads in the subthalamic nucleus (Pilitsis et al., 2008; Groiss et al., 2009; Armstrong & Okun, 2020). This surgical treatment frequently allows a significant reduction of dyskinesias and improvement of motor symptoms with sustained long-term benefits and allows the reduction of dopaminergic medication (Pilitsis et a., 2008; Groiss et al., 2009; Fox et al., 2018; Armstrong & Okun, 2020).

1.3 Role of misfolded protein oligomers in neurodegenerative diseases

1.3.1 Molecular basis of amyloid aggregation

AD, PD and many other neurodegenerative and non-neuropathic protein misfolding diseases are rooted in the aberrant misfolding and aggregation of peptides and proteins into highly ordered aggregates, called amyloid fibrils that histopathologists observe as

dense clusters such as neuritic plaques, neurofibrillary tangles and Lewy bodies (Haass & Selkoe, 2007; Chiti & Dobson, 2017; Wells et al., 2021). Interestingly, amyloid fibrils formed by different peptides and proteins, such as Aβ and αS, but also other proteins not related to protein deposition diseases, share highly conserved morphological, structural, and tinctorial properties (Chiti & Dobson, 2017; Limbocker et al., 2023). Amyloid fibrils are filamentous structures with a typical diameter of 7–13 nm, as observed by electron microscopy or atomic force microscopy (AFM) techniques, and often microns in length (Sunde & Blake, 1997; Gras et al., 2011; Cava & Vélez, 2022). They generally comprise 2–8 protofilaments, each approximately 2–7 nm in diameter, that often twist around each other or associate laterally as flat ribbons 2–7 nm high and up to 30 nm wide (Wasmer et al., 2008; Paravastu et a., 2008; Chiti & Dobson, 2017; Gallardo R. et al., 2020). Moreover, amyloid fibrils share a common cross-β architecture, consisting of laminated β-sheets whose strands run perpendicular to the long-axis of the fibril when observed in X-ray diffraction (Nelson & Eisenberg, 2006; Morris & Serpell, 2012). Amyloid fibrils also share typical tinctorial properties since they can bind specific dyes such as thioflavin T, Congo red or their derivatives, mainly because of their β-structured core (Elghetany & Saleem, 1988; Glenner et al., 1972; Nilsson, 2004; Biancalana & Koide, 2010; Yakupova et al., 2019).

The molecular mechanisms by which initially native peptides and proteins can rearrange into an amyloid core structure and then form amyloid fibrils, is not completely understood. However, it appears increasingly clear that amyloidogenesis passes through the formation of transient non-native prefibrillar intermediates known as misfolded protein oligomers (Karamanos et al., 2015; Chiti & Dobson, 2017; Birol et al., 2018; Gallardo R. et al., 2020). These prefibrillar species appear in the beginning from primary

nucleation processes and later from secondary nucleation processes once a critical concentration of fibrils have formed (Buell et al., 2014; Habchi et al., 2017; Limbocker et al. 2023); moreover oligomers can also accumulate as off-pathway species (Dear et al., 2020), or be generated after their detachment from fibril ends (Martins et al., 2008; Cohen et al., 2013; Cascella et al., 2021; Limbocker et al., 2023).

These small soluble metastable aggregates are important in protein misfolding diseases, and in particular in neurodegenerative diseases such as AD and PD, not only because of their role in the process of amyloid formation, but also because they are thought to represent the most pathogenic species in the diseases (Haass & Selkoe, 2007; Chiti & Dobson, 2017; Wells et al., 2021; Cline et al., 2018; Limbocker et al., 2023). In fact, misfolded protein oligomers have been detected both in AD and PD brains (Gong et al., 2003; Kayed et al., 2003; Kayed et al., 2007; Paleologou et a., 2009; Esparza et al., 2013; Kayed & Lasagna-Reeves, 2013; Cline et al., 2018; Limbocker et al., 2023) and have been hypothesized to correlate more directly with neuronal toxicity than amyloid fibrils (Shankar et al., 2008; Esparza et al., 2013). Interestingly, even if the accumulation of Aβ plaques is one of the pathological hallmarks of AD, these fibrillar aggregates have been observed also in cognitively normal subjects (Katzman et al., 1988; Hulette et al., 1998; Price et al., 1999; Aizenstein et al., 2008), whereas the presence or the administration of soluble oligomeric species of Aβ have reported to induce direct adverse effects (Kayed et al., 2003; Selkoe, 2008; Esparza et al., 2013; Cline et al., 2018).

1.3.2 Structural determinants of oligomer toxicity

A variety of different types of oligomers have been isolated and characterized for both Aβ and αS (Lambert et al., 1998; Barghorn et al., 2005; Kayed et al., 2009; Lorenzen et

al., 2014; Chen et al., 2015; Fusco et al., 2017) and, even though they display a high structural heterogeneity, most of them affect cellular viability, suggesting that toxicity induced by oligomers is correlated with their misfolded nature rather than with particular characteristics of their amino acid sequences or specific patterns of their three-dimensional structure (Campioni et al., 2010; Bucciantini et al., 2002; Chiti & Dobson, 2017). These observations led to extensive work over the past two decades focused on the elucidation of their conformational and structural properties in order to understand the structural determinants of oligomer toxicity (Chiti & Dobson, 2017; Limbocker et al., 2023).

So far, the most important determinant of oligomer toxicity is the exposure of hydrophobic residues on the oligomer surface (Mannini et al., 2014; Chiti & Dobson, 2017). A crucial point in the understanding the structural determinants of oligomer toxicity was the development of pairs of toxic and nontoxic oligomers formed by several protein, directly linked with known neurodegenerative diseases, such as Aβ (Ladiwala et al., 2012) and αS (Fusco et al., 2017; Cascella et al., 2021) or not correlated with any disease but able to form *in vitro*, under specific conditions, toxic and nontoxic species (Campioni et al., 2010; Krishnan et al., 2012).

Another important determinant has been shown to be the small size of the oligomers (Mannini et al., 2012; Chiti & Dobson, 2017). In the context of AD, an inverse correlation between the size of Aβ assemblies and the potency of their exerted toxicity was observed, with the maximum toxicity exhibited by small oligomers (Lambert et al., 2001; Gong et al., 2003; Kayed et al., 2007; Kayed et al., 2009), and as the size of the oligomers increases, their deleterious effects decrease (Sengupta et al., 2016; Chiti & Dobson, 2017). A similar observation was also reported in the context of PD, where small

soluble non-fibrillar αS aggregates smaller than 200 nm in length were found to exert the highest toxicity, causing lipid membrane permeabilization and inflammation (Emin et al., 2022). A possible explanation of why small oligomeric species are more toxic than larger species is that small aggregates have a larger surface:volume ratio, which increases the extent of active surface per protein molecule; moreover, their small size allows them to diffuse more rapidly and hence form aberrant interactions more readily (Mannini et al., 2012; Chiti & Dobson, 2017).

1.3.3 The model protein HypF-N

The first observation on the possibility to obtain a pair of toxic and nontoxic oligomers from the same protein under different conditions dates back in 2010 from HypF-N (Campioni et al., 2010), the acylphosphatase-like domain of the bacterial protein HypF, which plays an essential role in [NiFe]-hydrogenases maturation, enzymes involved in the prokaryotic hydrogen metabolism (Rosano et al., 2002). Under physiological conditions, HypF-N displays a highly compact globular shape, stabilized in order to disfavour intermolecular interactions and aggregation processes (Rosano et al., 2002). However, in particular conditions, it can be induced to form amyloid fibrils *in vitro*, incubating it in conditions that destabilize its native globular fold (Campioni et al., 2010). In particular, under different solution conditions, HypF-N can form two distinct types of highly stable oligomers, named type A (OAs) and type B (OBs), that share similar sizes with a diameter of 2–6 nm, appear roughly spherical under atomic force microscopy, and have a similar β-sheet core structure, but different molecular structure and ability to cause cell dysfunction (**Fig. 1.5**) (Campioni et al., 2010; Capitini et al., 2018).

OAs displayed a strong ability to penetrate cell membranes and initiate a series of downstream events associated with cytotoxicity, when added to cultured cells (Campioni et al., 2010; Zampagni et al., 2011), and induced loss of cholinergic neurons and cognitive impairment when microinjected into rat brains, similarly to what has been observed with misfolded oligomers directly related to neurodegenerative diseases (Zampagni et al., 2011; Tatini et al., 2013).

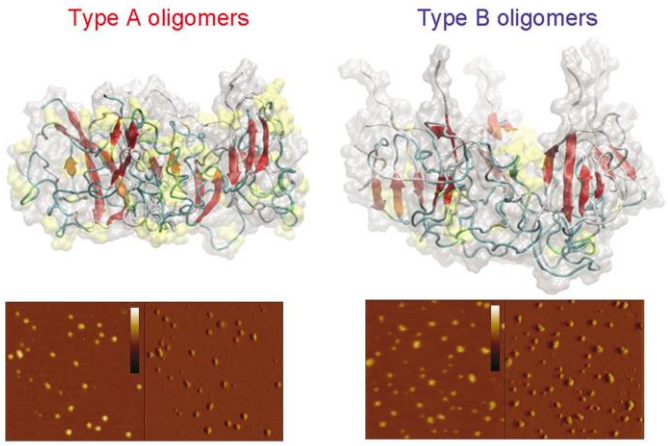

Figure 1.5. Toxic and nontoxic oligomers of HypF-N. Schematic representation of toxic OAs and nontoxic OBs of HypF-N indicating disordered regions (grey/green), b-strands (red) and hydrophobic side chains (yellow). TM-AFM images of HypF-N samples pre-incubated under conditions A (left) and B (right) and then resuspended at pH 7.0. Scan size, 500 nm. The colour bar corresponds to a Z range of 7 nm. Figure adapted from Capitini et al., 2018; Campioni et al., 2010.

From a structural point of view, OAs and OBs display important differences that explain their different toxicities. In particular, nontoxic oligomers have a higher overall flexibility that allows to bury the hydrophobic residues in a compact hydrophobic core (Campioni et al., 2010; Capitini et al., 2018). By contrast, toxic oligomers showed a more rigid and compact structure leading to structural constraints that cause several of the hydrophobic residues to remain exposed and establish aberrant intermolecular interactions with cell membranes (Campioni et al., 2010; Capitini et al., 2018).

1.4 Importance of membrane-oligomer interactions in oligomer toxicity

1.4.1 The plasma membrane

The cell membrane consists of a lipid bilayer composed of amphipathic lipids and proteins, such as receptors, transporters, enzymes, and cytoskeletal proteins, that interacts with lipids by hydrophobic and electrostatic interaction, with a thickness of 5-10 nm (Casares et al., 2019). Cell membranes are highly dynamic structures yet are simultaneously required to maintain cell and compartment identity and integrity and in fact a damage to the membrane, if not promptly repaired, results in cell death (Gould, 2018).

A typical plasma membrane contains hundreds of different lipid species that are actively regulated by the cell and that in turn are able to modulate membrane proteins and their functions through specific chemical interactions between individual lipid molecules and proteins, but also through non-specific interactions due to the comprehensive macrostructure of the bilayer such as its thickness, intrinsic monolayer curvature or elastic moduli (van Meer et al., 2008; Lundbaek et al., 2010; Ingólfsson et al., 2017) (**Fig. 1.6**). Plasma membranes are usually enriched in sphingolipids and sterols (**Fig. 1.6**), packed at high density in order to resist to the mechanical stress to which they are subjected (van Meer et al., 2008). Moreover, lipids are non-uniformly distributed within the membrane plane, in fact the preferential associations between cholesterol (CHOL) and saturated lipids drive the formation of relatively packed membrane domains, called lipid rafts, that selectively recruit certain lipids and proteins, further modulating their local concentration, aggregation and trafficking (**Fig. 1.6**) (Sezgin et al., 2017; Ingólfsson et al., 2017).

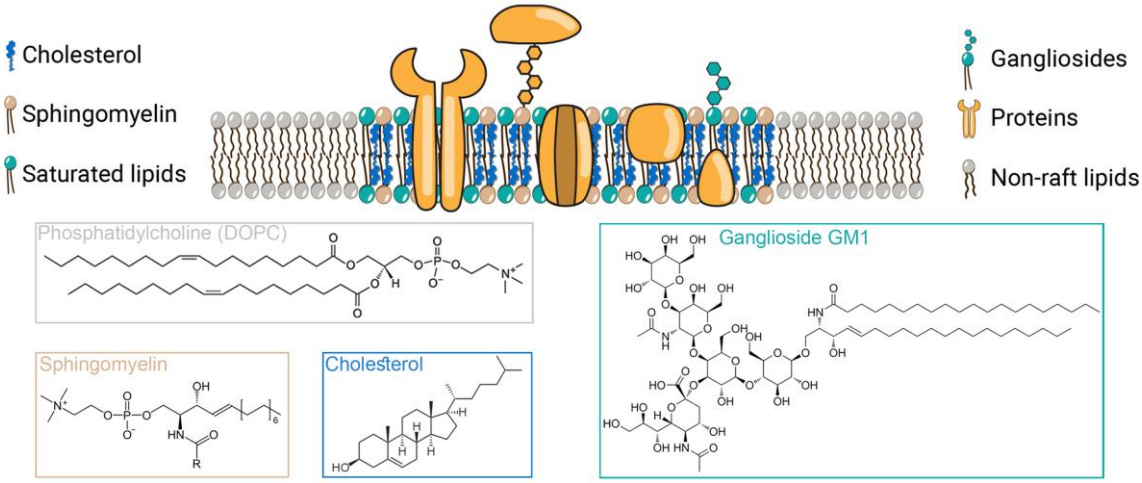

Figure 1.6. The plasma membrane and its lipids. Schematic representation of the plasma membrane, containing membrane proteins, and an example of a lipid rafts domain, enriched in CHOL, gangliosides, sphingomyelin (SM) and saturated lipids. Chemical structure of some representative lipids usually contained in plasma membranes, including CHOL, SM, phosphatidylcholine and gangliosides. Figure adapted from Nieto-Garai et al., 2022.

1.4.2 Oligomer-membrane interactions and resulting toxicity in neurodegeneration

In neurodegenerative diseases, including AD and PD, a fundamental interaction by misfolded protein oligomers involves biological membranes, such as plasma and mitochondrial membranes, and is one of the primary events causing cytotoxicity (Chiti & Dobson, 2017; Gonzalez-Garcia et al., 2021). These aberrant interactions result in calcium imbalance, mitochondrial dysfunction, and intracellular reactive oxygen species, eventually leading to cell death (Chiti & Dobson, 2017; Gonzalez-Garcia et al., 2021). In fact, oligomers expose on their surface flexible hydrophobic regions that mediate aberrant interactions with plasma membranes and membrane proteins, resulting in their functional impairment and sequestration (Campioni et al., 2010; Bolognesi et al., 2010; Evangelisti et al., 2016; Andreasen et al., 2015). In addition, their small size allows them to diffuse more rapidly and hence form aberrant interactions more readily, and they have a larger surface:volume ratio than larger species, which increases the extent of active surface per protein molecule (Chiti & Dobson, 2017).

Oligomer-mediated cytotoxicity seems to be influenced not only by the type, size, structure and physicochemical properties of the protein aggregates themselves, but also by the lipid composition and physicochemical features of the membranes with which the oligomers interact (Evangelisti et al., 2012; Evangelisti et al., 2016; Oropesa-Nuñez et al., 2016; Galvagnion et al., 2022). The ganglioside GM1, particularly enriched in neuronal membranes (Ingòlfsson et al., 2017), seems to play a critical role in Aβ neurotoxicity both by contributing to Aβ oligomer nucleation and growth into toxic fibrils (Matsubara et al., 2013; Matsubara et al., 2018) and by sequestering Aβ oligomers from brain interstitial fluid onto neuronal membranes (Hong et al., 2014; Evangelisti et al., 2016). Moreover, GM1 appeared to be able to recruit toxic protein aggregates to lipid raft domains of the cell membrane, and this ability seems to be primarily linked its negative charge (Oropesa-Nuñez et al., 2016).

CHOL seems to play an important role in AD as well as GM1, even though its precise role is still controversial, since it has displayed both neuroprotective and aggravating effects in relation to the development of AD (Rudajev & Novotny, 2022). In fact, it has been observed that this lipid could exert a protective role by influencing Aβ-membrane interaction and Aβ-induced bilayer disruption, and that enrichment of cultured cells with CHOL made the cells resistant to the calcium-mediated cytotoxic effect of Aβ (Arispe et al., 2002; Evangelisti et al., 2012; Evangelisti et al., 2014). On the other hand, the binding of Aβ to CHOL has been observed in senile plaques in the brain, where CHOL accumulates along with ApoE (Panchal et al., 2010), it was found to bind to membranes and facilitate seeding and aggregation (Mizuno et al., 1999; Yanagisawa et al., 2005).

1.4.3 Lipid homeostasis and its association with neurodegenerative diseases

Altered membrane lipid composition and homeostasis are known to be linked to many diseases, including neurodegenerative diseases such as AD and PD (Alecu et al., 2019; Liu et al., 2021). In fact, the brain appears to be particularly vulnerable to disease states that are characterised by an altered lipid composition (Mattson et al., 2006; Müller et al., 2015). In the context of neurodegenerative diseases, particularly AD, the ganglioside GM1, that plays a crucial role in oligomer-toxicity, has been found increased in concentration in cell membranes purified from AD patients compared to healthy controls (Fujita et al., 2007; Molander-Melin et al., 2005), and altered ganglioside metabolism resulting in an increase in GM1 levels has also been reported in AD brains (Yamamoto et al., 2008).

In PD, mutations of the glucocerebrosidase 1 (GBA) gene, known to represent a prevalent risk factor, affect the sphingolipid content and metabolism, resulting in higher levels of total sphingolipids, enhanced amounts of short-chain sphingolipid molecules and decreased content of long-chain sphingolipid that correlates with the promotion of αS aggregation and progression of the disease (Galvagnion et al., 2022). Moreover, accumulation of short-chain sphingolipid could alter the structural order of membrane lipid bilayers, modify membrane curvature, and disrupt membrane fluidity (Niemelä et al., 2006; Ben-David & Futerman, 2010). Taken together, all these findings confirm how homeostasis of membrane lipids is a critical point for normal brain function (Litvinov et al., 2018; Kao et al., 2020; McFarlane & Kedziora-Kornatowska, 2020) and there is a strong correlation between age-related alterations of the lipid homeostasis and neurodegenerative diseases (Molander-Melin et al., 2005; Yamamoto et al., 2008; Liu et al., 2015; Gonzalez-Garcia et al., 2021; Galvagnion et al., 2022).

1.4.4 Liposomes as a model system for biological membranes

Studying the role of lipids and biological membranes in the pathogenesis of neurodegenerative diseases and the eventual protective role of putative drugs on natural cell membranes is challenging as they have a highly complex architecture, with factors that cannot be controlled or fully known, such as their exact composition and interferences by their protein components (Andersson & Köper, 2018). To address this, several membrane models have been developed to mimic the physicochemical characteristics of lipid bilayers, without the high complexity typical of natural membranes (Andersson & Köper, 2018). Lipid vesicles or liposomes are membrane model that mimic many properties of biological membranes, since they are lipid bilayers with a spherical shape that can be composed of one or more types of lipids, such as phospholipids, CHOL, and others (Shaheen et al., 2006; Akbarzadeh et al., 2013). They consist of one or more lipid bilayers surrounding an aqueous core, where the polar head groups are oriented towards the interior and exterior aqueous phases. Depending on the method of preparation and their lipid composition, liposomes can be obtained by modulating their dimensions, structure and charge (Akbarzadeh et al., 2013). On the basis of their number of bilayers, liposomes can be classified into unilamellar vesicles (ULVs), multilamellar vesicles (MLVs), and multivesicular vesicles (MVVs) (Jash et al., 2021) (**Fig. 1.7**). Moreover, based on their size ULVs can be classified into small unilamellar vesicles (SUVs), large unilamellar vesicles (LUVs), and giant unilamellar vesicles (GUVs) (Jash et al., 2021) (**Fig. 1.7**).

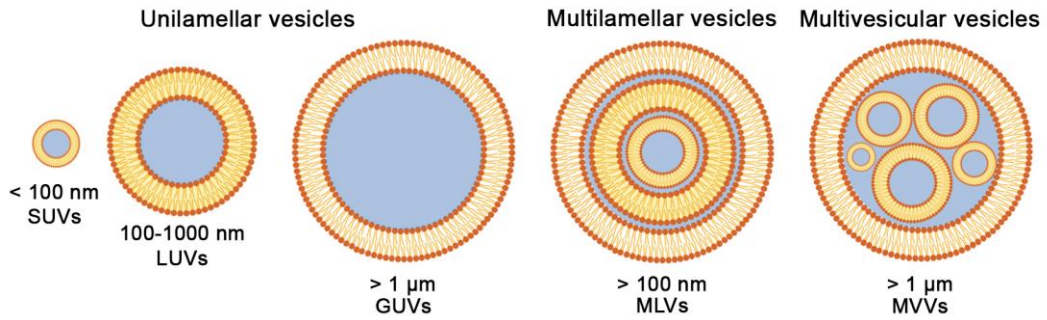

Figure 1.7. Classification of liposomes based on their lamellarity and size. Figure adapted from Jash et al., 2021.

Liposomes are therefore extremely versatile structures, which can be formed with various combinations of different lipids, in order to simulate the physiological composition of the cellular membrane (Bendas et al., 1997; Oropesa-Nuñez et al., 2016) and with a wide range of sizes, up to those of cells, making them great models for biological membranes and for the study of the interaction of various molecules with membrane lipids in the absence of proteins (Evans & Kwok, 1982; Angelova & Dimitrov, 1986; Relini et al., 2004; Galvagnion et al., 2015; Oropesa-Nuñez et al., 2016).

In the context of neurodegenerative diseases, for example, SUVs composed of 1,2-dimyristoyl-sn-glycero-3-phospho-L-serine (DMPS), a negatively charged phospholipid enriched in the membrane of synaptic vesicles (Takamori et al., 2006; Galvagnion et al., 2015), were used to investigate perturbations of the kinetics of αS amyloid formation in the presence of lipid surfaces (Galvagnion et al., 2015). Furthermore, SUVs with a lipid composition mimicking the most abundant lipids in membranes of synaptic vesicles, were used to investigate the capability of natural compounds to alter the binding of αS to lipid membranes (Perni et al., 2017; Perni et al., 2018).

It is known that CHOL can promote phase separation between lipids with a low transition temperature (T_m), such as 1,2-dioleoyl-sn-glycero-3-phosphocoline (DOPC)

and lipids with higher T_m, such as sphingomyelin (SM) at an intermediate temperature when the fraction of one lipid is too low to phase separate in the absence of CHOL (de Almeida et al., 2003), so a ternary system of lipids SM/DOPC/CHOL can be used to model lipid rafts in synthetic vesicles or synthetic supported lipid bilayers (SLBs) (de Almeida et al., 2003). On the basis of these observations, SLBs with a ternary SM/DOPC/CHOL and quaternary SM/DOPC/CHOL/GM1 systems of lipids were used to investigate the role of the content of the ganglioside GM1 in the toxicity of toxic oligomers formed by the model protein HypF-N separating it from that of the protein component in the evaluation of the oligomer-membrane interaction (Oropesa-Nuñez et al., 2016). With these lipid compositions, SLBs displayed segregation of lipid species in well distinct, differently ordered, domains: domains with low level of order, considered as fluid domains (L_α phase domains), enriched in DOPC, and domains with a higher level of order, considered as gel phase domains (L_β phase domains), enriched in SM, CHOL and GM1 (when present) (**Fig. 1.8**) (de Almeida et al., 2003; Oropesa-Nuñez et al., 2016). The use of membrane models with lipid phase segregations allows to mimic the important distinction between lipid rafts and the surrounding disordered plasma membrane domains in natural cells, and to study the interaction of misfolded oligomers with at the sub-microscopic level with high and unprecedented resolution (Oropesa-Nuñez et al., 2016).

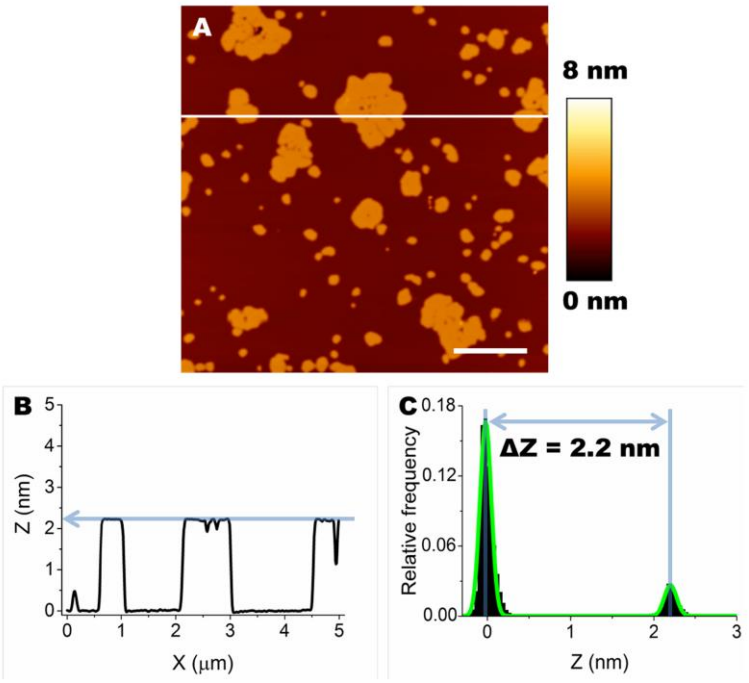

Figure 1.8. Formation of Lα and Lβ domains by segregation of lipid species in SLBs. (A) Typical morphology of SLBs containing DOPC, SM, CHOL and GM1. Scale bar: 1.0 µm. **(B)** A cross section was taken along the white line in A (X axis). The difference in height between L_β and L_α is ≈ 2.2 nm. **(C)** The height distribution of Z values shows the difference in thickness (ΔZ) between L_β and L_α domains. Figure taken from Oropesa-Nuñez et al., 2016.

1.5 Natural compounds against neurodegenerative disease

1.5.1 Natural compounds in drug discovery

Natural compounds and their structural analogues have historically played a major role in pharmacotherapy and drug discovery, for several therapeutics areas, such as cancer and infectious diseases (Atanasov et al., 2015; Harvey et al., 2015), cardiovascular diseases (Waltenberger et al., 2016; Koushki et al., 2021), metabolic diseases (Waltenberger et al., 2016), multiple sclerosis (Tintore et al., 2019), and other neurodegenerative diseases (Castelli et al., 2018; Cicero et al., 2019). Natural products possess special features compared to conventional synthetic molecules, which can confer advantages for pharmacotherapy and drug discovery: they are characterized by enormous scaffold diversity and structural complexity, typically have a higher molecular

mass, higher numbers of H-bond acceptors and donors, and greater molecular rigidity compared with synthetic compound libraries (Feher et al., 2003; Clardy & Walsh, 2004; Atanasov et al., 2015). Moreover, natural compounds are structurally optimized by evolution to serve specific biological functions, and the fact that they have been used for millennials in traditional medicine may provide insights regarding efficacy and safety (Atanasov et al., 2015; Atanasov et al., 2021).

Several natural compounds have been studied and proposed as potential therapeutic candidates or useful dietary supplements to complete and/or support the traditional therapies of neurodegenerative disorders (Lökk & Nilsson, 2010; Bagli et al., 2016; Deshpande et al., 2019). A new prospect is now represented by aminosterols, a category of natural compounds initially discovered in the gastrointestinal tract of dogfish sharks *Squalus acanthias*, that have demonstrated promising therapeutic properties for the treatment of PD and AD (Limbocker et al., 2022).

1.5.2 Squalamine (SQ) and trodusquemine (TRO): aminosterols from the shark *S. acanthias*

In 1993, a search for antimicrobial compounds aimed to study the evolution of antibiotics across vertebrates, led to the discovery in stomach extracts of the dogfish sharks *Squalus acanthias* of a novel molecule with antimicrobial activity, represented by a bile salt with a cholestane steroid ring, with hydroxyl and sulphate groups at C-7 and C-24, respectively, coupled to a spermidine moiety at C-3 (**Fig. 1.9**) (Moore et al., 1993; Wehrli et al., 1993). This natural product was named squalamine (SQ), after the *Squalus* genus from which it was extracted and its characteristic polyamine group (Moore et al., 1993). At physiological pH, SQ exists as a positively charged zwitterionic molecule,

soluble in both water and organic solvents, and was shown to strongly bind to membranes containing phospholipids with negatively charged headgroups, (Selinsky et al., 1998; Selinsky et al., 2000), and to be able to displace membrane-bound cationic proteins (Zasloff et al., 2011). These biophysical properties are thought to be the explanation of some of the pharmaceutical properties of this aminosterol; in fact SQ exhibited a broad spectrum of anti-infective activity against Gram-positive and Gram-negative bacteria, fungi, certain protists, and viruses against both RNA- and DNA-envelopes (Moore et al., 1993; Zasloff et al., 2011).

A few years later, in 2000, following a tentative procedure of extraction of SQ from larger amounts of dogfish liver, which is the richest source of SQ in this animal, at least seven other aminosterols were discovered in *Squalus acanthias*, structurally very similar to the first discovered aminosterol, with slight variations involving mainly the cholestane-like side chain, from position 20 to position 27 (Rao et al., 2000). One of these compounds, initially referred to as MSI-1436 (Rao et al., 2000) and later named trodusquemine (TRO) by a biopharmaceutical company (Salmi et al., 2008), shares the same steroid cholestane scaffold as SQ, but carries at position C-3 a longer polyamine chain, which is a spermine rather than a spermidine (**Fig. 1.9**) (Rao et al., 2000).

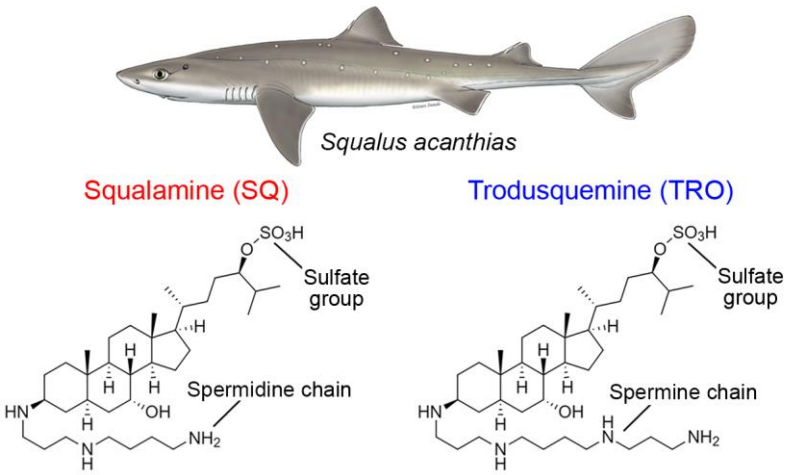

Figure 1.9. Structural formulas of SQ and TRO. Figure adapted from Limbocker et al., 2022; Errico et al., 2023.

Similarly to SQ, TRO was found to exhibit a broad spectrum activity against Gram-negative and Gram-positive bacteria and fungi (Brunel et al., 2005). Interestingly, TRO was shown to cross the blood brain barrier, after peripheral injection, and suppress appetite and increase insulin sensitivity in rodents, monkeys and dogs (Zasloff et al., 2001; Ahima et al., 2002). These potent appetite suppressant and antidiabetic properties exhibited by TRO are most likely resulting from the inhibition of the protein tyrosine phosphatase 1B (PTP1B), an endosomal phosphatase that downregulates many physiologically important signalling pathways, including that of insulin, leptin, as well as many growth factors and cytokines (Lantz et al., 2010). These findings led to numerous other studies aimed to better understand the potential curative role of this aminosterol in metabolic disorder and other therapeutics areas (Pandey et al., 2013; Krishnan et al., 2014; Pandey et al., 2014; Thompson et al., 2017; Smith et al., 2017; Qin et al., 2020).

1.5.3 Pharmacological role of SQ and TRO in neurodegenerative diseases

The first evidence of a possible therapeutic potential of aminosterols in the context of neurodegenerative diseases dates to 2017, when SQ was shown to inhibit lipid-induced αS aggregation, protect cultured human neuroblastoma cells (SH-SY5Y cells) from the action of toxic oligomers formed by this protein by reducing their interactions with lipid membranes, and ameliorate deficits of motility and paralysis in a *C. elegans* model of PD over-expressing human αS (Perni et al., 2017). One year later, TRO displayed similar effects on the inhibition of αS lipid-induced aggregation and on the protection of cultured cells against αS oligomers, as well as on the protection of *C. elegans* PD models against over-expressed human αS (**Fig. 1.10 and 1.11**) (Perni et al., 2018).

The study of the potential therapeutic effects of TRO in the context of neurodegenerative diseases was the extended to AD and the related $A\beta_{42}$ aggregation. TRO was found to significantly influence $A\beta_{42}$ aggregation but accelerating, rather than inhibiting, the rate of aggregation, predominantly by stimulating the secondary nucleation (**Fig. 1.10**) (Limbocker et al., 2019). The overall resulting effect of TRO was the reduction of $A\beta_{42}$ oligomer-toxicity, albeit with this paradoxical effect on aggregation, because it appeared to shift the $A\beta_{42}$ oligomer population towards the fibrillar form, therefore reducing the population of $A\beta_{42}$ oligomers, known to represent the main responsible of cytotoxicity (**Fig. 1.10**) (Limbocker et al., 2019).

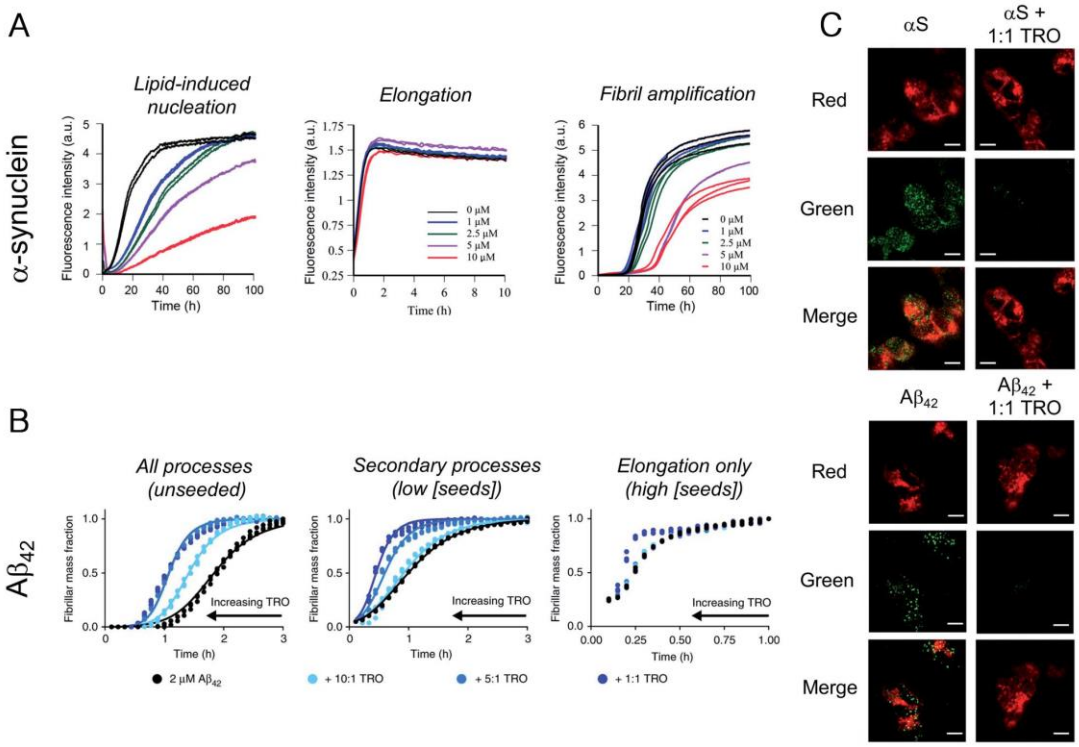

Figure 1.10. Impact of TRO on αS and Aβ$_{42}$ aggregation. (A) TRO inhibits the lipid-induced nucleation and fibril amplification reactions in αS aggregation, corresponding to primary and secondary nucleation events, respectively, without impacting fibril elongation. **(B)** TRO accelerates the unseeded and seeded aggregation reactions of Aβ$_{42}$ to varying degrees, reducing the steady-state population of oligomers. **(C)** Confocal microscopy analysis of the extent of αS or Aβ$_{42}$ oligomer binding to the membranes of human neuroblastoma cells in the absence (left panels) or presence (right panel) of TRO. Red and green channels indicate cell membranes and oligomers, respectively. Scale bars, 10 μm. Figure adapted from Limbocker et al., 2022.

On cultured neuroblastoma cells, TRO was reported to displace or inhibit the binding of Aβ$_{42}$ oligomers, similarly to what observed with αS oligomers (Perni et al., 2018; Limbocker et al., 2019). Similarly to observations on *C. elegans* models of PD over-expressing human αS, both SQ and TRO exhibited important protective effects in *C. elegans* models of AD over-expressing human Aβ$_{42}$ (**Fig. 1.11**) (Perni et al., 2017; Perni et al., 2018; Limbocker et al., 2019).

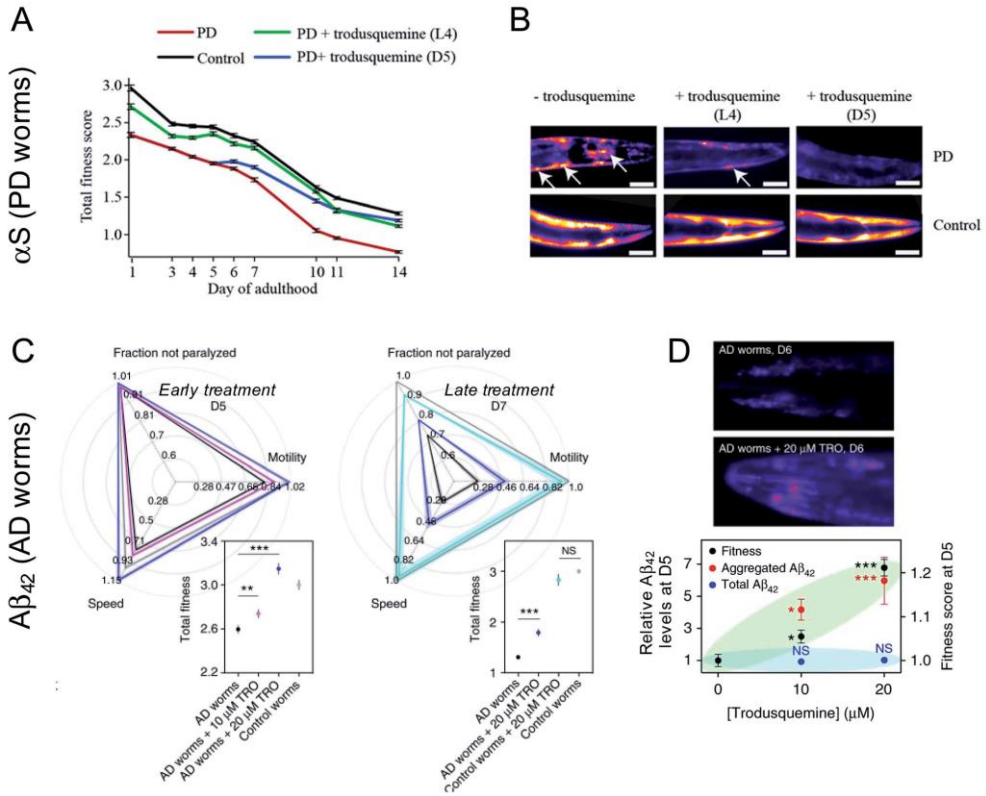

Figure 1.11. Impact of TRO on AD and PD model worms. (A) TRO significantly improves the health of *C. elegans* model of PD over-expressing αS-YFP in their muscle cells, when administered before (L4) or after (D5) the onset of toxicity in these animals. **(B)** TRO decreases the number of αS-YFP inclusions in PD worms, when administered before (L4) or after (D5) the onset of toxicity in these animals, a finding that is consistent with its *in vitro* mechanism of action. Scale bars, 80 µm. **(C)** TRO also improves the health of *C. elegans* model of AD over-expressing $A\beta_{42}$ in their muscle cells, when administered before (L4) or after (D5) the onset of toxicity in the animals. **(D)** TRO stimulates the aggregation of $A\beta_{42}$ in AD worms, which may shift the reactive flux away from the oligomeric state towards the less toxic fibrillar form. Figure taken from Limbocker et al., 2022.

Following all these findings, SQ has entered human clinical trials for the treatment of PD in 2018, as an orally administered phosphate salt named ENT-01. In this clinical trial, ENT-01 was developed to target αS aggregates within the enteric nervous system (ENS), since PD patients often manifest constipation due to diminished peristalsis caused by the reduced excitability of the neurons of the myenteric plexus as a result of accumulation of a-synuclein aggregates (Lin et al., 2014; Fornai et al., 2016). The results of this 1/2a clinical trial showed that ENT-01 was able to restore bowel motility in over 80% of PD patients with severe constipation (Hauser et al., 2019). Moreover, ENT-01 has

just completed a multicenter, randomized, double-blind, placebo-controlled phase-2b clinical trial in patients with PD-related constipation (KARMET, identifier NCT03781791), with improvement in constipation and benefits in other neurological symptoms, such as memory, hallucinations, motor functioning and circadian rhythm (Camilleri et al., 2022).

1.5.4 Membrane physicochemical perturbation induced by TRO

In principle, the ability of aminosterols to prevent the binding of misfolded protein oligomers formed by different proteins, including αS, $A\beta_{42}$ and HypF-N, to cell membranes and to suppress their toxicity could be due to at least two non-mutually exclusive mechanisms: (i) the aminosterols bind to the oligomers preventing them from binding to cell membranes, or (ii) the aminosterols bind to cell membranes preventing them from binding the oligomers (Errico et al., 2020). It was recently observed that neither SQ nor TRO significantly alter either the size or the hydrophobicity of cytotoxic aggregates at therapeutically meaningful concentrations of aminosterol, ruling out that aminosterol-oligomer binding is responsible for the aminosterol-mediated inhibition of oligomer-membrane binding (Limbocker et al., 2020). These results rather suggest that the aminosterol-mediated protective effects can be exerted through their binding to membrane bilayers.

A recent work investigated, at a molecular level, the mechanism by which TRO binds to biological membranes and reinforces them against the toxicity of misfolded protein oligomers (Errico et al., 2020). In this study, LUVs and SLBs composed of DOPC, SM, CHOL and GM1 were used to mimic biological membranes and reproduce the lipid segregation in different ordered domains (de Almeida et al., 2003; Oropesa-Nuñez et al., 2016). TRO was found to bind to these membrane models strongly and stably, as well as

to the membrane of cultured human neuroblastoma cells (Errico et al., 2020). By applying fluorescence quenching and anisotropy experiments with probes that localized in different portions of the membrane, quartz crystal microbalance (QCM) analysis and molecular dynamics (MD) simulations, it was also possible to determine the location and orientation of TRO within the bilayer: it appeared positioned within the external hydrophilic face, with its steroidal portion extending downward and penetrating the external hydrophilic layer down to the interface between the hydrophilic and hydrophobic layers, and the polyamine moiety sticking out of the membrane into the bulk medium (**Fig. 1.12**) (Errico et al., 2020). Moreover, the embedding of TRO in the lipid bilayer occurred with a well-defined oblique angle (about 55°) for the major axis of the molecule with respect to the normal to the bilayer plane (**Fig. 1.12**) (Errico et al., 2020).

Importantly, the incorporation of TRO into the lipid bilayer was shown to induce significant effects on the physicochemical properties of the membrane (**Fig. 1.12**): (i) it decreased the total negative charge of the lipid bilayer, contributed by the anionic headgroup of GM1, as determined with zeta potential (ζ) measurements; (ii) it caused an increment of the breakthrough force (BTF) applied perpendicularly to its surface, corresponding to a higher mechanical resistance of the bilayer to indentation, and an increase of the membrane phase transition temperature, reflecting a more stable packing of the lipids; (iii) it changed the spatial distances between lipids, proportionally to its concentration, as observed with lipid–lipid fluorescence resonance energy transfer (FRET) experiments, inducing a separation of GM1 from CHOL molecules, and the formation of clusters of CHOL molecules and of clusters of GM1 molecules, probably caused by a preferential binding of this aminosterol nearby these two lipids.

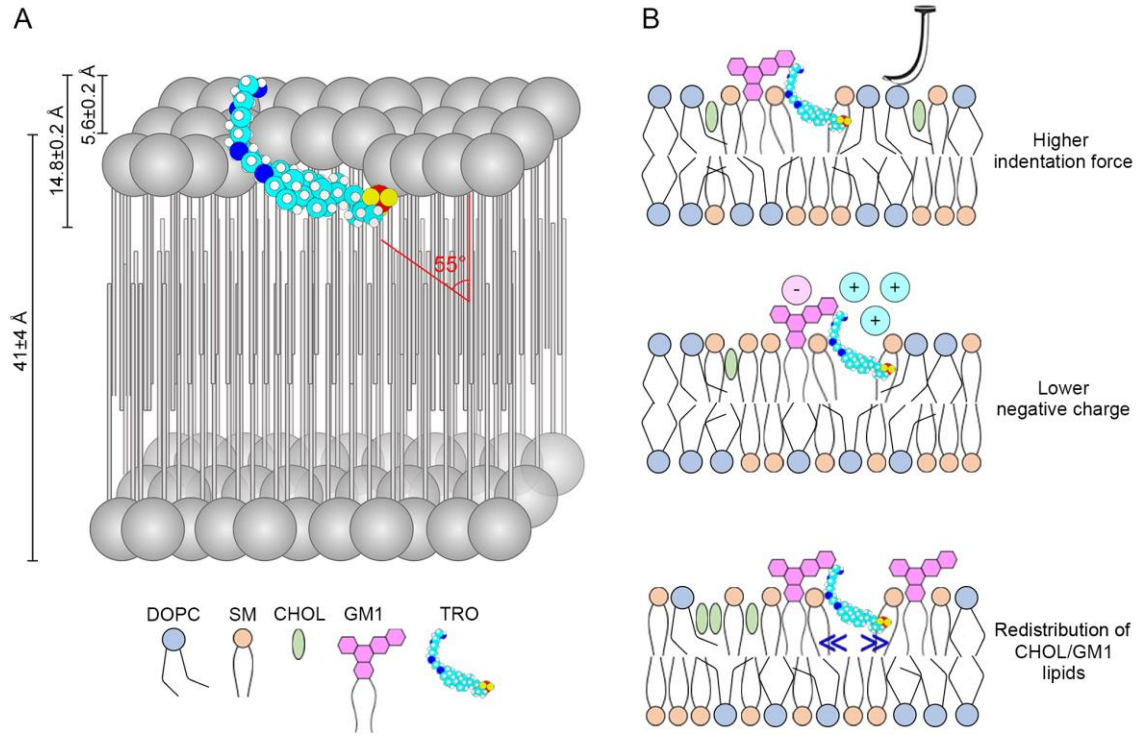

Figure 1.12. Membrane insertion and perturbation induced by TRO. (A) Schematic representation of the insertion and localization of TRO within biological membranes. The 55° angle refers to the whole molecule, rather than the steroid group or polyamine group only. The 14.8±0.2 and 5.6±0.2 Å distances refer to the space occupied by the molecule and portion sticking out of the membrane along the normal to the bilayer plane, respectively. **(B)** Schematic representation of the three major physico-chemical effects on cell membranes induced by the insertion of TRO, all possibly mediating the TRO-induced protection against the toxicity of misfolded protein oligomers. Figure adapted from Errico et al., 2023.

All these perturbations contribute significantly to improve the resistance of biological membranes to the toxic action of misfolded protein oligomers, explaining from a physicochemical perspective how aminosterols can reinforce the membranes making them resistant to the deleterious action of these aberrant species, and also suggest the intriguing possibility that these natural compounds may exert regulatory functions within the lipid homeostasis system, known to be altered in neurodegenerative diseases (Errico et al., 2020; Limbocker et al., 2022).

1.5.5 Discovery of a new aminosterol in mammals: ENT-03

Very recently, it was reported the discovery of ENT-03, a spermine-bile acid, in the neonatal mouse brain (Barbut et al., 2023, under revision). ENT-03 shares a high structural similarity with sharks aminosterols, with a sterol group, an alkyl moiety of the cholestane-type fused to the sterol at C-17, and an alkyl polyamine tail fused to the sterol at C-3 and replacing the hydroxyl group (**Fig. 1.13**). However, ENT-03 does not have the sulphate moiety linked at C-24 like sharks aminosterols, it has rather a carboxylate group at position C-25, replacing the methyl group, and it carries a spermine group as alkyl polyamine like TRO (**Fig. 1.13**).

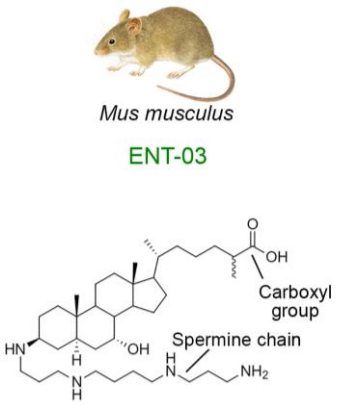

Figure 1.13. Structural formula of ENT-03. Figure adapted from Errico et al., 2023.

ENT-03 was detected in brain, liver, kidney, and gastrointestinal tract of neonatal mice, with highest concentrations detected in brain (Barbut et al., 2023, under revision). The concentration in brain was low at birth, reached peak concentrations over the first postnatal week, and declined rapidly as the animals aged. The low concentrations of ENT-03 in the gastrointestinal tract suggested that milk was not the source of the compound, and weaning occurred between 18-22 days, followed by a rapid increase in body weight (Barbut et al., 2023, under revision). ENT-03 was shown to increase insulin

sensitivity in both lean and insulin resistant, obese diabetic rodents within 24 hours of administration, by enhancing the peripheral uptake of glucose (Barbut et al., 2023, under revision). Moreover, following repeated administration of ENT-03 for several days, reduction in food intake and sustained weight loss occurs, which persists for several weeks after dosing has stopped (Barbut et al., 2023, under revision). Following the similar chemical structure of TRO and SQ and the similar pharmacological properties in metabolic disorders, ENT-03 could also exert similar effects in the context of neurodegenerative diseases.

1.5.6 The plant alkaloid berberine (Brb) and its putative therapeutic role in neurodegeneration

Berberine (Brb) is a cationic alkaloid present in many commonly used medicinal plants, such as *Coptis chinensis, Hydrastis canadensis, Berberis vulgaris* and *Berberis aristate*, that has been used in traditional medical systems in China and India for more than 3000 years (**Fig. 1.14**) (Dev, 1999; Chen et al., 2014; Song et al., 2020; Xu et al., 2021). Recently, it was observed that Brb can exert therapeutic effects in the context of metabolic disorders; in particular it was shown to reduce hyperlipidaemia in animal models and patients with high cholesterolemia, to lower blood glucose levels and improve insulin resistance by promoting glucose uptake and glycolysis, and glucose-stimulated insulin secretion (Xu et al., 2021). Moreover, similarly to aminosterols, Brb was found to inhibit the phosphatase activity of PTP1B (Chen et al., 2010). Brb has also important antioxidant and anti-inflammatory activities in the context of metabolic disorders, as observed in cells cultured with high glucose-containing media (Liu et al., 2008) and in a series of diabetic animal models (Bhutada et al., 2011; Moghaddam et al., 2014; Xie et al., 2013).

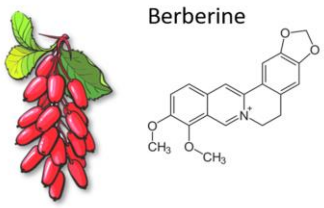

Figure 1.14. Structural formula of Brb. Figure adapted from Bellavite et al., 2023.

Oxidative stress and inflammation play a crucial role also in neurodegenerative diseases, since the aberrant aggregation of misfolded proteins can trigger ROS production as inflammatory response in the brain, and it is known that neuronal cells are particularly vulnerable to oxidative damage because of their high polyunsaturated fatty acid content in membranes, high oxygen consumption, and weak antioxidant defences (Rego et al., 2003; Liu et al., 2017). Brb was reported to protect neuronal cells from cell death induced by the PD neurotoxin 6-hydroxydopamine (6-OHDA), which is a hydroxylated analog of dopamine able to induce massive oxidative stress leading to the damage of dopaminergic neurons (Bae et al., 2013). This protective effect exerted by Brb occurs by reducing ROS generation and upregulating heme oxygenase-1 (HO-1) expression, a cytoprotective enzyme with neuroprotector functions (Bae et al., 2013). Furthermore, Brb was found to inhibit human acetylcholinesterase according to computational screening of synthetic molecules and dietary phytochemicals, and dysfunction and death of forebrain cholinergic is typically observed in AD patients (Amat-Ur-Rasool et al., 2015). Taken together, all these pharmacological properties of Brb suggest a therapeutic potential of Brb against neurodegenerative diseases (Ahmed et al., 2015; Jiang et al., 2015; Shou & Shaw, 2022).

1.6 Aim of the thesis

In the first part of this thesis (Section 3.1), we aimed at obtaining a quantitative measurement of the affinity of toxic and nontoxic misfolded protein oligomers for lipid bilayers of liposomes (LUVs), and we then investigated the change of this affinity by changing lipid composition and by adding the aminosterol TRO. To this aim, we used LUVs with a variable and biologically compatible lipid composition and OAs/OBs formed by the model protein HypF-N to measure the affinity of these different oligomeric species to lipid membranes. We also investigated whether oligomers change their structure upon interaction with the LUVs and if they preferentially bind to specific lipids of LUVs. Then, we added TRO to our LUV system, to quantify the influence exerted by this aminosterol on the affinity of the membrane for OAs and, again in a quantitative manner, how the lipid composition of LUVs can influence the affinity of the membrane for these toxic species. The results of this part of the thesis have been published in Errico et al., 2021.

In the second part of this thesis (Section 3.2), we performed a comparative study at the chemical and physical levels on SQ, TRO and ENT-03, to quantitively measure their affinities for lipid membranes of LUVs, to investigate whether these aminosterols can affect the physicochemical and molecular properties of the lipid bilayer to different extents, and whether they result in different protective effects. We then related all these chemical, physical, molecular, and biological measurables using an approach of quantitative chemical biology to obtain the identification and quantification of: (i) the chemical groups within aminosterols mainly responsible for their protective effect against oligomers of Aβ, and (ii) the specific physicochemical changes of the membrane

that most mediate this protective effect. The results of this part of the thesis have been published in Errico et al., 2023.

In the third part of this thesis (Section 3.3), we focused on the plant alkaloid Brb, investigating its possible interaction with LUVs and its potential role against misfolded protein oligomers. To this aim, we first studied whether Brb interacts with the membrane of LUVs with different lipid compositions, whether the interaction involves the polar or nonpolar portion of the membrane, and if this interaction could affect the packing of lipids contained in them. Then, we investigated whether the interaction of Brb with LUVs could induce a variation of the affinity of OAs for the membrane, similarly to what is observed with TRO. Eventually, we examined whether this alkaloid was also able to directly interact with misfolded protein oligomers and affect their morphology and structure. The results of this part have not yet been published and are collected in a manuscript that will soon be submitted for publication.

2. Experimental section

2.1 Expression and purification of wild-type and mutant forms of HypF-N

Cultures of *E. coli* XL10 Gold harbouring the pQE30-Th plasmids for the expression of wild-type HypF-N and its mutational variants (Campioni et al., 2010) were grown overnight at 37 °C under shaking in 200 ml of 20 g/L LB medium (Merck) containing 100 µg/ml of ampicillin (Merck). The cells were then diluted 1:20 in 4 l of fresh medium and grown at 25 °C under shaking until ~ 0.6 optical density at 600 nm (OD_{600}), monitored with a Jasco V-630 UV-VIS spectrophotometer. Protein expression was induced overnight at 25 °C under shaking by the addition of 1 mM isopropyl β-D-thiogalactopyranoside (IPTG, Thermo Scientific). The bacterial cells were then harvested by centrifugation for 15 min at 7000 g at 4 °C; the pellet was resuspended in ~ 30 ml of lysis buffer (50 mM phosphate buffer, 300 mM NaCl, 10 mM imidazole, pH 8.0) and stored at -20 °C overnight. The cell suspension was defrosted at 37 °C in a Thermo Haake C25P water bath and then incubated for 1 h with 1 mg/ml lysozyme (Merck) in ice under shaking followed by 5 cycles of sonication at 50 kHz for 30 s alternated to 30 s in ice. The cell lysate was then centrifuged for 45 min at 38,700 g at 4 °C and the supernatant containing the protein was filtered using filters with a cut-off of 0.45 µm. The filtered supernatant was applied to an affinity chromatography column packed with HIS-Select® Nickel Affinity Gel (Merck), previously equilibrated with the lysis buffer at 4 °C. The column was then washed with the washing buffer (50 mM phosphate buffer, 300 mM NaCl, 20 mM imidazole, pH 8.0), equilibrated with the cutting buffer (50 mM phosphate buffer, 50 mM NaCl, pH 8.0) and incubated with 50 units of human thrombin (Merck) dissolved in 5 ml of cutting buffer for 1 h at 37 °C, and then overnight at 4 °C under slight shaking. The

pure wild-type and mutated HypF-N were then eluted using 50 mM phosphate buffer, 50 mM NaCl, 10 mM imidazole, pH 8.0. Wild-type and mutant HypF-N were then buffer-exchanged and concentrated in 5 mM acetate buffer, 2 mM dithiothreitol (DTT), pH 5.5, and in 20 mM phosphate buffer, 2 mM tris(2-carboxyethyl)phosphine hydrochloride (TCEP), pH 7.0, respectively, using an ultrafiltration cell with a 3000 Da molecular weight cut-off (MWCO) cellulose membrane (Biorad) at 4 °C. The final solution containing the pure protein was centrifuged for 10 min at 16,100 g to eliminate any aggregates and/or impurities, and its concentration was measured with a Jasco V-630 UV-VIS spectrophotometer using ε_{280} = 12490 $M^{-1}cm^{-1}$. Samples were checked for their purity with SDS-PAGE and DLS, as described below, and then stored at -80 °C until use.

2.2 SDS-PAGE analysis of HypF-N

Samples of the various HypF-N purification steps were denatured with a 4X sample buffer (0.25 M Tris, 5.4 M glycerol, 0.3 M β-mercaptoethanol, 277 mM SDS, 6 mM bromophenol blue), and then incubated at 98 °C for 2 min. The resulting samples and a molecular weight marker (Precision Plus Protein™ Standard, Bio-Rad) were loaded in a precast gel with a gradient of 4-20% of acrylamide (Mini-PROTEAN TGX Precast Gels, Bio-Rad) and then run for about 90 min at 20 mA, using the Bio-Rad Laboratories electrophoresis kit. The running chambers were filled with a running buffer (25 mM Tris, 19.2 mM glycine, 0.1% SDS). The gel was then stained with Coomassie Blue dye (40% methanol, 10% acetic acid, 0.1% Coomassie Blue) for 30 min at 37 °C with slow agitation and then washed in a destaining solution (40% methanol, 10% acetic acid) for at least 1 h at room temperature to remove the excess of dye. The purified protein featured a single band at 10 kDa, in agreement with its expected molecular weight of 10,464 Da.

2.3 Dynamic light scattering (DLS) analysis of HypF-N

The monomeric state of purified HypF-N was assessed acquiring its size distribution on a Zetasizer Nano S DLS device from Malvern Panalytical (Malvern), thermostated at 25 °C with a Peltier temperature controller and using a 10 mm reduced-volume plastic cell. The refractive index and viscosity were 1.33 and 0.89 cP, respectively. The measurement was acquired with the cell position 4.65, attenuator index 8, at 25 °C. The DLS distribution in volume mode featured a single population with a hydrodynamic diameter of 5.4±1.0 nm, which is compatible with a monomeric folded HypF-N, as previously determined with X-ray crystallography (Rosano et al., 2002).

2.4 Labelling of HypF-N mutant with BODIPY FL

The C7S/C65A mutant of HypF-N (containing only Cys40) was diluted to a final concentration of 150 µM in 20 mM phosphate buffer, pH 7.0, and incubated with 2.25 mM BODIPY™ FL N-(2-aminoethyl)maleimide, previously dissolved at high concentration in dimethyl sulfoxide (DMSO) for 2 h at 25 °C in the dark on a mechanical shaker. The labelled sample was dialysed (membrane MWCO of 3500 Da) in the dark against 1.5 l of 20 mM phosphate buffer, pH 7.0, overnight and then centrifuged to remove any precipitate. The concentration of the dye in the BODIPY FL-labelled HypF-N mutant was determined spectrophotometrically, using ε_{505}=76000 $M^{-1}cm^{-1}$, whereas the concentration of the protein was determined using ε_{280}=12490 $M^{-1}cm^{-1}$. The labelling degree of the sample was then estimated by determining the ratio between the measured dye and protein molar concentrations.

2.5 Labelling of HypF-N mutants with 1,5-IAEDANS and 6-IAF

The C7S/C40S/C65A/Q18C (named C18) and C7S/C40S/C65A/N34C (named C34) mutants of HypF-N (containing one cysteine residue at position 18 and 34, respectively) were labelled with 5-((((2-iodoacetyl)amino)ethyl)amino)naphthalene-1-sulfonic acid (1,5-IAEDANS) and 6-iodoacetamidofluorescein (6-IAF) dyes (Thermo Fisher Scientific), respectively, as previously reported (Capitini et al., 2018). The C18 variant was diluted to a final concentration of 180 µM in 100 mM potassium phosphate buffer, pH 7.0, with 2.7 mM 1,5-IAEDANS (15-fold molar excess of dye) and 3 M guanidine hydrochloride (GdnHCl), whereas the C34 variant was diluted to the same final concentration of 180 µM in 100 mM potassium phosphate buffer, pH 7.0, with 1.8 mM 6-IAF (10-fold molar excess of dye) and 3 M GdnHCl. Both dyes were previously dissolved in dimethylformamide (DMF) at high concentration. The two labelling mixtures were left in the dark under shaking for 2 h at 30 °C and then overnight at 4 °C. They were then dialysed in the dark (membrane MWCO of 3000 Da) against: (i) 0.25 l of 100 mM potassium phosphate buffer, pH 7.0, with 1.5 M GdnHCl for 4 h, (ii) 0.25 l of 100 mM potassium phosphate buffer, pH 7.0 for 4 h, (iii) 0.5 l of 50 mM potassium phosphate buffer, pH 7.0, overnight, (iv) 1.0 l of 20 mM or 5 mM potassium phosphate buffer (depending on whether the labelled mutants were used to produce type A or type B oligomers, respectively), at pH 7.0, for 6 h. The samples were then centrifuged to remove any precipitate. The concentrations of the dye in the 1,5-IAEDANS-C18 variant and in the 6-IAF-C34 variant were determined spectrophotometrically, using ε_{336}= 5700 $M^{-1}cm^{-1}$ and ε_{491}=8200 $M^{-1}cm^{-1}$, respectively. The protein concentration was determined spectrophotometrically using ε_{280}=12490 $M^{-1}cm^{-1}$ after subtraction of the absorbance contribution of the 1,5-IAEDANS/6-IAF probe at the same wavelength of 280 nm. The

labelling degree was estimated as the ratio between the two measured dye and protein molar concentrations.

2.6 Preparation of HypF-N type A (OAs) and type B (OBs) oligomers

OAs and OBs of wild-type HypF-N were obtained at a protein concentration of 0.5 mg/ml, corresponding to 48 µM (monomer equivalents), by incubating the protein for 4 h at 25 °C in: (i) 50 mM acetate buffer, 12% (v/v) trifluoroethanol (TFE), 2 mM DTT, pH 5.5 and (ii) 20 mM trifluoroacetic acid (TFA), 330 mM NaCl, pH 1.7, respectively, as previously described (Campioni et al., 2010).

BODIPY FL-labelled OAs and OBs used for the binding experiments were obtained under the same conditions, but using 4.4 µM of BODIPY FL-labelled C7S/C65A HypF-N and 43.6 µM of unlabelled C7S/C65A HypF-N, in order to obtain a 1:10 molar ratio for labelled:unlabelled protein.

OAs and OBs for intra-oligomer FRET were formed under the same conditions by 24 µM C18 variant labelled with the donor dye 1,5-IAEDANS (18D) and 24 µM C34 variant labelled with the acceptor dye 6-IAF (34A), at a molar ratio 18D:34A of 1:1. These oligomers were named 18D_34A. Oligomers 18D_10 and 10_34A (with 34A and 18D replaced by the unlabelled HypF-N mutant with only one cysteine residue at position 10, respectively) were also produced in a 1:1 molar ratio between labelled and unlabeled variant.

OAs and OBs for LUV-oligomer FRET were initially formed under the same conditions using C7S/C65A HypF-N. They were then centrifuged at 16,100 g for 15 min at 20 °C. The supernatants were removed, the pellets were gently dried with nitrogen flow and then resuspended in 20 mM phosphate buffer, 2 mM TCEP, pH 7.0, to a final

HypF-N concentration (monomer equivalents) of 160 µM. They were then incubated with a 12.5-fold molar excess of 1,5-IAEDANS, previously dissolved at high concentration in DMF for 2 h at 25 °C in the dark on a mechanical shaker. The labelled samples were dialysed (membrane MWCO of 3500 Da) in the dark against 1.5 l of 20 mM phosphate buffer, pH 7.0, overnight and then centrifuged to remove any precipitate. The concentration of the dye in the samples was determined spectrophotometrically, using and ε_{336} = 5700 $M^{-1}cm^{-1}$, whereas the concentration of the protein was determined using ε_{280} = 12490 $M^{-1}cm^{-1}$ after subtraction of the absorbance contribution of 1,5-IAEDANS at 280 nm. The labelling degree was estimated as the ratio between the measured dye and protein molar concentrations.

2.7 Labelling of aminosterols with BODIPY TMR and Alexa Fluor 594

SQ and TRO were synthetized by coupling spermidine and spermine, respectively, to the (5α, 7α, 24R)-3-keto-7-hydroxycholestan-24-ol sulphate steroid intermediate as previously described (Zhang et al., 1998; Jones et al., 1998; Zasloff et al., 2001). The synthesis of ENT-03 was carried out similarly to the other aminosterols, by coupling a polyamine tail to a steroidal skeleton (Barbut et al., 2023, under revision); the step-by-step procedure is reported in a deposited patent and will be published in a separate paper (Patent CN114929724; 2022). The >95% chemical purities of all aminosterols were assessed by HPLC-ELSD and ^{1}H-NMR. All aminosterols were stored as powders until use. For the labelling procedure, aminosterols were dissolved in distilled water to obtain a 100 mM stock solution and stored at 4 °C. BODIPY™ TMR-X NHS Ester and Alexa Fluor® 594 NHS Ester (BODIPY and A594, respectively, ThermoFisher Scientific) were both dissolved in anhydrous DMSO to obtain 15 mM and 10 mM stock solutions, respectively,

and stored at -20 °C. For labelling, 5 mM aminosterol, 0.5 mM dye, 0.1 M sodium bicarbonate buffer, pH 8.3 for BODIPY and pH 7.0 for A594, were incubated in a final volume of 20 µl at 25 °C for 2 h under mild orbital shaking. During labelling with BODIPY the aminosterol precipitates; therefore, after the incubation, the solution was centrifuged at 18,000 g for 15 min, the pellet was dried with a nitrogen flow and resuspended in 20 µl DMSO to maintain the initial concentrations. During labelling with A594, TRO remains in solution, whereas SQ and ENT-03 precipitate. Hence, the solution with TRO labelled with A594 was directly used after incubation, while those with SQ and ENT-03 were centrifuged and resuspended in DMSO as described for the BODIPY labelling. With these procedures the labelled:total aminosterol was 1:10 in all cases. No unreacted dye was detected using mass spectrometry, following a previously described procedure (Errico et al., 2020). As a negative control, L-Arg was labelled with both BODIPY and A594 under the same conditions used for aminosterol labelling and no precipitate was observed.

2.8 Preparation of large unilamellar vesicles (LUVs)

LUVs were produced with a lipid mixture composed of DOPC (Avanti Polar Lipids), SM (Sigma-Aldrich), CHOL (Sigma-Aldrich) and GM1 (Avanti Polar Lipids), as previously reported (Errico et al., 2020). In particular, the lipid composition of “model-LUVs” was 65% DOPC (mol), 33% SM (mol), 1% CHOL (mol) and 1% GM1 (mol), as used in previous work (Errico et al., 2020). These lipid species are known to be present in the neuronal membranes (Calderon et al., 1995; Pike, 2004; Ingólfsson et al., 2014; Ingólfsson et al., 2017). The non-natural percentages of the various lipids were chosen to favour well-separated L_β domains and L_α regions (Seghezza et al., 2014). In particular, the CHOL

percentage of 1% was already adopted in other works (Seghezza et al., 2014; Leri et al., 2016; Oropesa-Nuñez et al., 2016; Leri et al., 2018; Canepa et al., 2020; Errico et al., 2020) and it is necessary to obtain model membranes with well distinct L_α and L_β phases and relatively extended L_β domains. It was demonstrated that the L_β domains significantly decreased their size by increasing the CHOL concentration, becoming indistinguishable for microscopic analyses (Seghezza et al., 2014). The ordered domains of LUVs, enriched in GM1 and CHOL, partially mimic the complex features of lipid rafts in neurons (Ingólfsson et al., 2017; Staneva et al., 2021). Moreover, the progressive increase of CHOL and GM1 content in our experiments, aim at better mimicking the real composition of neuronal membranes.

LUVs were obtained by dissolving the desired lipid mixture in chloroform/methanol (2:1) and by removing the organic solvent by evaporation in vacuo (Univapo 150H, UniEquip) for at least 3 h. The mixtures were hydrated with distilled water to form MLVs to a total lipid concentration of 2 mg/ml for quenching experiments, 3.5 mg/ml for binding experiments, 1 mg/ml for LUV-oligomer FRET experiments, and 3 mg/ml for circular dichroism (CD), tryptophan fluorescence and intra-oligomer FRET experiments (mother solutions). MLVs were left to swell for 1 h at 60 °C and then extruded 17 times through a polycarbonate membrane with 100 nm pores using a mini-extruder (Avanti Polar Lipids) at the same temperature, to form LUVs. After cooling to room temperature, LUVs were stored at 4 °C for a maximum of 1 week.

For the measurement of the ζ potential and BTF, and for the lipid-lipid FRET experiments, 5 µM of each aminosterol was added during the hydration phase of LUVs preparation.

2.9 Atomic force microscopy (AFM)

2.9.1 Interaction between OAs/OBs and supported lipid bilayers (SLBs) using AFM

The interaction was tested on SLBs with three different lipid mixtures: (i) 66% DOPC (mol), 33% SM (mol), 1 % CHOL (mol); (ii) DOPC/SM 2:1 (mol/mol), 1 % (mol) CHOL, 1 % (mol) GM1; (iii) 63% DOPC (mol), 31% SM (mol), 1 % (mol) CHOL, 5 % GM1 (mol). 40 µl aliquots of LUVs suspension (0.1 mg/ml), were deposited onto a 1.0×1.0 cm^2 freshly cleaved mica substrate with 10 µl of a 10 mM $CaCl_2$ solution. The samples were kept 15 min at room temperature and then incubated for 15 min at 60 °C in a close chamber with 100% relative humidity to form a uniform SLB. Subsequently, the samples were cooled at room temperature and gently rinsed three times with Milli-Q water. A Nanowizard III (JPK Instruments) mounted on an Axio Observer D1 (Carl Zeiss) inverted optical microscope was used to acquire the AFM images. V-shaped DNP silicon nitride cantilevers (Bruker), with a typical tip curvature radius of 20-60 nm, nominal spring constant 0.24 N/m, and a resonance frequency in air ranging from 40 kHz to 75 kHz were used. The measurements were carried out in water using the intermittent contact mode in the constant-amplitude mode, working with an oscillating frequency of 10-20 kHz. The amplitude setpoint was kept above 70% of free oscillation amplitude in all cases. OAs and OBs were administered under the AFM head at a final concentration of 12 µM and left standing to interact with the SLBs for 30 min. AFM images (512×512 image data points) were processed using the JPK Data Processing software (JPK Instruments). The difference in thickness (ΔZ) between gel (L_β) and fluid (L_α) lipid domains was determined by considering image height distributions. The distributions were fitted to the sum of two Gaussian functions, and the ΔZ value was determined as the difference between the

peaks of the two Gaussian functions. This procedure was repeated for at least 10 different images for each experiment.

2.9.2 Breakthrough force (BTF) measurement in the absence and presence of aminosterols

SLBs were obtained as described above. Prior to AFM imaging, samples were kept again at room temperature in a closed chamber at 100% relative humidity. AFM imaging usually started 1.5 h after rinsing.

Force spectroscopy measurements were performed under liquid environment with a Multimode SPM (Bruker) equipped with "E" scanning head (maximum scan size 15 µm) and driven by a Nanoscope V controller (Bruker). Triangular silicon nitride cantilevers (DNP-10, Bruker, nominal spring constant 0.24 N/m) were used. The actual spring constant of each cantilever was determined in-situ using the thermal noise method (Hutter & Bechhoefer, 1993). Force maps consisting of 128x128 force distance curves were acquired point-by-point on scan areas of 5×5 μm^2 or 2.5×2.5 μm^2. The maximum force load was 15-18 nN. Breakthrough forces were evaluated from the force-distance curves data sets using a home-built software.

2.10 Intrinsic tryptophan fluorescence assay

OAs, OBs and native HypF-N were diluted in 20 mM phosphate buffer, pH 7.0, in the presence of different concentrations of unlabelled model-LUVs (0, 0.04, 0.08, 0.12, 0.24, 0.30, 0.50, 1.00, 1.50 mg/ml) to a final HypF-N concentration (monomer equivalents) of 1.9 µM (OAs and OBs) and 20 µM (native HypF-N) for 15 min at 25 °C. DLS was used to

assess the integrity of LUVs upon change of solution conditions from distilled water (in which they were prepared) to 20 mM phosphate buffer, pH 7.0. The structural integrity of OAs and OBs upon change of solution conditions was assessed previously (Campioni et al., 2010). Intrinsic tryptophan fluorescence spectra were then acquired at 25 °C from 300 to 450 nm (excitation at 280 nm) using a 3×3 mm black wall quartz cell on a Perkin-Elmer LS 55 spectrofluorimeter equipped with a thermostated cell-holder attached to a Haake F8 water-bath, or on an Agilent Cary Eclipse spectrofluorimeter (Agilent Technologies) equipped with a thermostated cell holder attached to a Agilent PCB 1500 water Peltier system.

2.11 Far ultraviolet circular dichroism (Far-UV CD) spectroscopy

2.11.1 Far-UV CD spectroscopy of HypF-N oligomers incubated with LUVs

OAs, OBs and native HypF-N were diluted in 20 mM phosphate buffer, pH 7.0, in the presence of different concentrations of model-LUVs (0, 0.04, 0.08, 0.12, 0.24, 0.30, 0.50, 1.00, 1.50 mg/ml), to a final HypF-N concentration (monomer equivalents) of 20 µM for 10 min at 25 °C. The far-UV CD spectra were collected over the 190–260 nm wavelength range at 25 °C using a 1 mm path-length cell on a Jasco J-810 spectropolarimeter equipped with a thermostated cell holder attached to a Thermo Haake C25P water bath. All spectra were truncated at HT > 700 V, blank-subtracted and normalized to mean residue ellipticity using:

$$[\theta] = \frac{\theta}{\left(\frac{10 \cdot N.\ residues \cdot optical\ path \cdot concentration}{molecular\ weight}\right)} \quad (1)$$

where [θ] is the mean residue ellipticity in deg cm^2 $dmol^{-1}$, θ is the ellipticity in mdeg, optical path is in cm, concentration is in g/l and molecular weight is in g/mol.

2.11.2 Far-UV CD spectroscopy of HypF-N OAs incubated with Brb

HypF-N OAs were diluted to 10 μM (monomer equivalents) in 20 mM phosphate buffer, pH 7.0 and incubated with 0, 5, 10, 30, 40, 50, 100 μM Brb for 15 min at 25 °C in the dark. Similar solutions containing Brb in the absence of OAs were also prepared. The far-UV CD spectra were collected over the 190–260 nm wavelength range by averaging 7 spectra with a data pitch of 0.1 nm, a scanning speed of 50 nm/min and a response time of 1 s at 25 °C using a 1 mm path-length cell on the Jasco spectropolarimeter described above. All spectra were truncated at HT > 700 V, blank-subtracted and normalized to mean residue ellipticity using Eq. 1. Then, [θ] at 222 nm and 208 nm was plotted as a function of Brb concentration.

2.11.3 FAR-UV CD spectroscopy of αS incubated with LUVs

5 μM αS was incubated with DMPS LUVs (250 μM total lipids, corresponding to 0.2 mg/ml total lipids) for 30 min and then with increasing concentrations of TRO, SQ or ENT-03 (0, 10, 20, 30, 40, 50, 60 and 70 μM) for 15 additional min, in 20 mM sodium phosphate buffer, pH 6.5, at 30 °C. LUVs were prepared with the same procedure reported above, but using 100% DMPS. Far-UV CD spectra were recorded on the Jasco spectropolarimeter described above CD spectra were recorded from 180 to 260 nm by averaging 5 spectra with a data pitch of 0.2 nm, a scanning speed of 50 nm/min and a response time of 1 s. All spectra were blank subtracted and truncated at HT>700 V, then

normalized to mean molar residue ellipticity using Eq. 1. For all analyses, [θ] at 222 nm and 192 nm was plotted as a function of aminosterol concentration.

2.12 Fluorescence resonance energy transfer (FRET)

2.12.1 HypF-N intra-oligomer FRET

OAs and OBs (18D_34A, 18D_10 and 10_34A) formed at a total monomer concentration of 48 µM were diluted in 20 mM and 5 mM potassium phosphate buffer (for OAs and OBs, respectively), pH 7.0, to obtain a final HypF-N concentration (monomer equivalents) of 20 µM, and in the presence of different concentrations of model-LUVs (0.12, 0.30, 0.50, and 0.70 mg/ml), prepared as described above. Oligomers and LUVs were incubated for 10 min at 25 °C. The samples were diluted to a final HypF-N concentration of 2 µM immediately before fluorescence acquisition. Fluorescence emission spectra were recorded on a Perkin-Elmer LS55 spectrofluorimeter equipped with a thermostated cell-holder attached to a Haake F8 water-bath. The measurements were performed using a 2×10 mm quartz cell at 25 °C with excitation at 336 nm. The FRET efficiency (*E*) values between 18D and 34A in OAs and OBs were calculated as:

$$E = \frac{(F_{DA}A_A - F_A A_A)}{F_A A_D} \quad (2)$$

where A_A and A_D represent the absorbance values at 336 nm of acceptor (A_A = 0.05) and donor (A_D = 0.07), respectively, obtained in the presence of a concentration of dye of 120 µM; F_{DA} and F_A represent the acceptor fluorescence emission at 1 mM (excitation 336 nm) obtained in the presence and in the absence of donor, respectively, determined from the area between 490 nm and 600 nm below the corresponding curves (Capitini et al., 2018).

2.12.2 LUVs-HypF-N-oligomers FRET

Model-LUVs were prepared at a total lipid concentration of 1 mg/ml, as described above, in the presence of either BODIPY-FL C5-ganglioside GM1 (GM1-A, commercial name BODIPY-FL C5-Ganglioside GM1, ThermoFisher Scientific), BODIPY-FL-CHOL (CHOL-A, commercial name TopFluor® cholesterol, Avanti Polar Lipids), BODIPY-FL-SM (SM-A, commercial name TopFluor® Sphingomyelin, Avanti Polar Lipids) or BODIPY-FL-DOPC (DOPC-A, commercial name TopFluor® PC, Avanti Polar Lipids) used as acceptors, with a molar fraction of each labelled lipid of 1% relative to total lipids in all cases. OAs from the C7S/C65A mutant labelled on their surface with 1,5-IAEDANS were prepared at a total protein concentration of 160 µM, as described above, and used as donor (OA-D). Fluorescence spectra of 0.3 mg/ml nonlabelled LUVs incubated with 20 µM OA-D (OA-D spectra), 0.3 mg/ml LUVs containing lipid-A incubated with 20 µM nonlabelled OAs (Lipid-A spectra), and 0.3 mg/ml LUVs containing lipid-A incubated with 20 µM OA-D (OA-D+Lipid-A spectra) were acquired after 15 min of incubation on a Perkin-Elmer LS 55 spectrofluorimeter equipped with a thermostated cell-holder attached to a Haake F8 water bath. The spectra were acquired from 350 to 600 nm using a 3×3 mm black wall quartz cell at 25 °C, with excitation at 336 nm. The FRET *E* was calculated as:

$$E = 1 - \left(\frac{F_{DA}}{F_D}\right) \quad (3)$$

where F_{DA} is the fluorescence intensity of D in the presence of A, and F_D is the fluorescence intensity of D in the absence of A.

2.12.3 Lipid-lipid FRET in the absence and presence of aminosterols

Model-LUVs were prepared at a total lipid concentration of 1.0 mg/ml, as described above. TRO, SQ and ENT-03, when present, were added during the hydration phase to a final concentration of 5 μM. BODIPY-FL C5-ganglioside GM1 (GM1-D), BODIPY-FL-CHOL (CHOL-D), BODIPY-FL-SM (SM-D) and BODIPY-FL-DOPC (DOPC-D) were used as donor lipids. Cholesteryl 4,4-difluoro-5-(4-methoxyphenyl)-4-bora-3a,4a-diaza-s-indacene-3-undecanoate (CHOL-A, commercial name CholEsteryl BODIPY™ 542/563 C11, ThermoFisher Scientific) was used as acceptor lipid. The molar fraction of each lipid labelled with D or with A was 0.0625% of total lipids in all cases.

Fluorescence spectra of LUVs containing only lipid-D, only CHOL-A, and both lipid-D and CHOL-A were acquired using the cell and spectrofluorometer described above, at 25 °C, with excitation at 450 nm and emission from 480 to 640 nm. FRET efficiencies (*E*) were calculated using Eq. 3 and then converted into distance between D and A (*r*) using (Lakowicz, 2006):

$$r = \sqrt[6]{\frac{R_0^6 - E \cdot R_0^6}{E}} \tag{4}$$

where R_0 is the Forster distance and was previously calculated for this D/A probe pair (Errico et al., 2020).

2.13 Fluorescence quenching of TMA-DPH and DPH in LUVs

2.13.1 Fluorescence quenching with HypF-N OAs, OBs and native protein

1,6-Diphenyl-1,3,5-hexatriene (DPH, Merck) and 1-(4-trimethylammoniumphenyl)-6-phenyl-1,3,5-hexatriene p-toluenesulfonate (TMA-DPH, ThermoFisher scientific) were

dissolved in chloroform/methanol (2:1) and added to the lipid mixture to obtain a probe:lipid molar ratio of 1:300. LUVs were then prepared at 2 mg/ml as described above, diluted with distilled water to 0.3 mg/ml and incubated with increasing concentrations of OAs, OBs and native protein (0 to 32.5 µM) at 25 °C for 15 min in the dark. The lipid mixtures: i) 65% DOPC (mol), 33% SM (mol), 1% CHOL (mol), 1% GM1 (mol); ii) 66% DOPC (mol), 33% SM (mol), 1% CHOL (mol); iii) 63% DOPC (mol), 31% SM (mol), 1% CHOL (mol) and 5% GM1 (mol); iv) 66% DOPC (mol), 33% SM (mol), 1% (mol) GM1; v) 63% DOPC (mol), 31% SM (mol), 5% CHOL (mol) and 1% GM1 (mol); vi) 59% DOPC (mol), 30% SM (mol), 10% CHOL (mol) and 1% GM1 (mol). LUVs containing TRO were obtained by adding the aminosterol during the hydration phase to obtain final TRO and total lipid concentrations of 5 µM and 0.3 mg/ml, respectively. The fluorescence spectra of the resulting samples were acquired at 25 °C from 380 to 550 nm (excitation 355 nm) using a 3×3 mm black walls quartz cell on an Agilent Cary Eclipse spectrofluorimeter (Agilent Technologies) equipped with a thermostated cell holder attached to an Agilent PCB 1500 water Peltier system. The quenching of TMA-DPH and DPH was then analysed with the Stern-Volmer equation:

$$\frac{F_0}{F} = 1 + K_{SV} \cdot [Q] \quad (5)$$

where F_0 and F are the integrated fluorescence intensity areas at 400-500 nm in the absence and presence of the quencher (OAs, OBs, or native proteins), respectively; [Q] is the concentration of the quencher and K_{SV} is the Stern-Volmer constant. The plot of quenching of TMA-DPH and DPH in 0.3 mg/ml LUVs containing 5 µM TRO was analysed from 12.5 µM OAs with an equation derived from the Stern-Volmer equation:

$$\frac{F_0}{F} = q + K_{SV} \cdot [Q] \quad (6)$$

where q is the intercept and all the other parameters have the same meaning as in Eq. 5.

2.13.2 Fluorescence quenching with Brb and HypF-N OAs

Brb was dissolved in 100 mM potassium phosphate buffer, pH 7.0 at a concentration of 3 mM and stored at 4 °C until use. TMA-DPH and DPH were added to the lipid mixture to obtain a probe:lipid molar ratio of 1:300 as described above. LUVs were then prepared at 2 mg/ml as described above, diluted with distilled water to 0.5 mg/ml and incubated with increasing concentrations of Brb (0 to 1 mM) at 25 °C for 15 min in the dark. The lipid mixtures were: i) Model-LUVs, composed of 65% DOPC (mol), 33% SM (mol), 1% CHOL (mol), 1% GM1 (mol); ii) Neuronal-LUVs, composed of 44% DOPC (mol), 16% SM (mol), 35% CHOL (mol), 5% GM1 (mol). The fluorescence spectra of the resulting samples were acquired at 25 °C from 380 to 550 nm (excitation 355 nm) using a 3×3 mm black walls quartz cell on the Agilent Cary Eclipse spectrofluorimeter described above. The quenching of TMA-DPH and DPH fluorescence induced by Brb were then analysed considering fluorescence emission at 427 nm and 429 nm, respectively, previously normalised in order to obtain F_0 = 1000 a.u. and fluorescence emission values (F_0/F) were plotted *versus* [Brb]. The upward curvature of the F_0/F *versus* Brb concentration plot suggested the coexistence of dynamic or collisional quenching, and static quenching, with the latter determined by the formation of a nonfluorescent ground-state complex between the fluorophore (TMA-DPH or DPH) and the quencher (Brb) (Lakowicz, 2006). We therefore isolated collisional quenching considering F_0/F values until 30 µM Brb for

DPH and 50 µM Brb for TMA-DPH and fitting these data with Eq. 5 to obtain K_{SV} values, and then we obtained K_{ST} values by applying:

$$\frac{F_0}{F} = (1 + [Brb] \cdot K_{SV}) exp([Brb] \cdot K_{ST}) \quad (7)$$

where K_{SV} was the value previously obtained with Eq. 5.

The quenching of TMA-DPH induced by 0-32 µM HypF-N OAs in 0.3 mg/ml model- and neuronal- LUVs, preincubated for 15 min with and without 30 µM Brb, was analysed from 7.5 µM OAs for model-LUVs and from 12.5 µM OAs for neuronal-LUVs with Eq. 6. The quenching of TMA-DPH induced by by 0-32 µM HypF-N OAs in 0.3 mg/ml LUVs+CHOL composed of 43% DOPC, 21% SM, 35% CHOL, 1% GM1 in the absence and presence of 30 µM Brb (15 min incubation) was analysed from 10 µM OAs with Eq. 6. The quenching of TMA-DPH induced by by 0-32 µM HypF-N OAs in 0.3 mg/ml LUVs+GM1, composed of 63% DOPC, 31% SM, 1% CHOL, 5% GM1 in the absence and presence of 30 µM Brb (15 min incubation) was analysed with Eq. 5 and from 12.5 µM OAs with Eq. 6, respectively.

2.14 Binding assays

2.14.1 Binding assay of fluorescently labelled OAs, OBs and native HypF-N to LUVs

OAs, OBs and native HypF-N formed by BODIPY FL-labelled and unlabelled HypF-N C7S/C65A mutant (molar ratio 1:10) were diluted in 20 mM phosphate buffer, pH 7.0, to obtain a final HypF-N mutant concentration of 20 µM (monomer equivalents), and were incubated for 15 min at 25 °C, with increasing concentrations (from 0 to 2.0 mg/ml) of model-LUVs, prepared as described above. In experiments involving TRO-containing LUVs, the concentration of the small molecule was variable but the TRO:lipid molar ratio

was maintained and corresponded to 5 µM in 0.3 mg/ml LUVs. The fluorescence spectra were acquired at 25 °C from 490 to 560 nm (excitation 480 nm) using a 3×3 mm black walls quartz cell on the Agilent Cary Eclipse spectrofluorimeter described above. The fluorescence emission at 512 nm was then plotted *versus* LUV concentration and analysed with:

$$F = [\mathrm{OA}] \cdot f_U + m[Lipid] - (f_U - f_B) \cdot \frac{[\mathrm{OA}] \cdot [\mathrm{Lipid}]}{K_D + [\mathrm{Lipid}]} \quad (8)$$

where *F* is the observed fluorescence at 512 nm, [OA] is the molar concentration of OAs (monomer equivalents), f_U and f_B are the fluorescence emission of the unbound and bound OAs at unitary concentration of OAs, respectively, *m* is the dependence of *F* on [Lipid] after binding (drift), [Lipid] is the molar concentration of total lipids in LUVs and K_D is the dissociation constant.

2.14.2 Binding assay of fluorescently-labelled aminosterols to LUVs

BODIPY or A594-labelled aminosterols and L-Arg (negative control) were diluted with distilled water to 10 µM and incubated with increasing concentrations of unlabelled model-LUVs, (from 0.0 to 1.0 mg/ml) for 15 min at 25 °C in the dark. Fluorescence emission of BODIPY and A594-labelled aminosterols and L-Arg were then acquired at 572 nm (excitation at 535 nm), and at 612 nm (excitation at 590 nm), respectively, using the cell and spectrofluorometer described above. The weak fluorescence contribution of unlabelled LUVs was subtracted from fluorescence emission spectra and resulting values were then normalized to the value obtained in the absence of LUVs (taken as 100%). The fluorescence emission intensity was then plotted *versus* LUV concentration and data points were then fitted with:

$$F = F_0 - A \cdot \frac{[LUVs]}{K_D + [LUVs]} \quad (9)$$

where *F* is the fluorescence intensity at a given LUV concentration, F_0 is fluorescence intensity at 0.0 mg/ml LUVs, *A* is the difference between the fluorescence emission of unbound and bound aminosterols and K_D is the dissociation constant of the LUV-aminosterol complex.

2.15 Fluorescence anisotropy

2.15.1 Fluorescence anisotropy of fluorescently-labelled aminosterols

BODIPY or A594-labelled aminosterols and L-Arg (negative control) were diluted with distilled water to 10 µM. The fluorescence anisotropy (*r*) values were then acquired at 570 nm after excitation at 544 nm and at 617 nm after excitation at 590 nm, respectively, in the absence and presence of 0.5 mg/ml unlabelled model-LUVs, incubated for 15 min in the dark, using a 3x3 mm black walls quartz cell at 25 °C on the Agilent Cary Eclipse spectrofluorometer described above.

2.15.2 Fluorescence anisotropy of TMA-DPH and DPH in LUVs in the presence of Brb

Model- and neuronal-LUVs labelled with TMA-DPH and DPH were prepared as described above. LUVs were diluted with distilled water to 0.5 mg/ml and incubated with increasing concentrations of Brb (0 to 100 µM) at 25 °C for 15 min in the dark and fluorescence anisotropy (*r*) values were acquired at 25 °C from 429 nm for DPH-LUVs and 429 nm for TMA-DPH LUVs, (excitation 350 nm) using a 3×3 mm black walls quartz cell on the Agilent

Cary Eclipse spectrofluorimeter described above. The obtained *r* values were then plotted *versus* [Brb].

The fluorescence anisotropy values (*r*) of model- and neuronal-LUVs labelled with TMA-DPH and DPH preincubated without and with 10, 30, 50 and 100 µM Brb for 15 min at 25 °C were acquired in a temperature range between 20 and 50 °C with intervals of 2 °C, after excitation at 355 and 350 nm for TMA-DPH and DPH-labelled LUVs respectively, using the Agilent Cary Eclipse spectrofluorimeter described above. *r* values were acquired at 427 and 429 nm for TMA-DPH and DPH-labelled LUVs respectively.

2.16 Fluorescence emission of fluorescently-labelled aminosterols

BODIPY or A594-labelled aminosterols and L-Arg (negative control) were diluted with distilled water to 10 µM. Fluorescence emission spectra of aminosterols and L-Arg labelled with BODIPY and A594 were acquired from 550 to 650 nm (excitation at 544 nm) and from 600 to 700 nm (excitation at 590 nm), respectively, in the absence and presence of 0.5 mg/ml unlabelled model-LUVs, incubated for 15 min in the dark, using the cell and spectrofluorometer described above.

2.17 Stopped-flow kinetic analysis of TRO-LUV binding

TRO-A594 (50 µM) was diluted 5-fold into solutions containing different concentrations of model-LUVs dissolved in H_2O. We used a Bio-logic SFM-3 stopped-flow device attached to a fluorescence detection system, an FC-08 cuvette (path length 0.08 cm), an excitation at 380 nm and a band pass filter to collect emission above 475 nm. The flow rate was 2.19 ml/s. The injection time, total volume and dead-time were 160 ms, 350 µl

and 14 ms, respectively. The final conditions after dilution were 10 µM TRO-A594, with LUV concentrations ranging from 0.12 mg/ml to 1.00 mg/ml, 25 °C. Each trace was averaged over 2 – 7 experiments, normalized to the maximum fluorescence and then analysed with a double exponential equation:

$$f(t) = m \cdot t + q + A_1 \cdot e^{-k_1 \cdot t} + A_2 \cdot e^{-k_2 \cdot t} \quad (10)$$

where $f(t)$ is the fluorescence recorded at time t, m and q are the slope and intercept of the plateau signal, A_1 and A_2 the amplitudes of the exponential phases and k_1 and k_2 are their apparent rate constants. Plots of k_1 and k_2 *versus* LUV concentration were fitted to straight lines (Copeland, 2000):

$$k_1 = k_{on(1)} \cdot [LUVs] + k_{off(1)} \quad (11)$$

$$k_2 = k_{on(2)} \cdot [LUVs] + k_{off(2)} \quad (12)$$

2.18 Light scattering analysis

2.18.1 Light scattering analysis of LUVs in in the presence of saturating concentrations of aminosterols

Model-LUVs were diluted with distilled water to 0.5 mg/ml and incubated for 15 min at 25 °C with increasing concentrations of aminosterols (from 0 to 100 µM). The size distributions (light scattering *versus* apparent hydrodynamic diameter) and count rate (kilocounts per second, kcps) were then recorded at 25 °C, using a Zetasizer Nano S (Malvern), thermostatted with a Peltier temperature controller, measurement position 4.20 mm, attenuator 6, and using disposable low volume (45 µl) plastic cuvettes.

According to the laws of light scattering, the following equation holds:

$$I = n \cdot m^2 \cdot I_0 \quad (13)$$

where *I* is the total intensity of light scattered by LUVs in kcps, *n* is the number of LUVs, *m* is the mass of a single LUV and I_0 is the intensity of light scattered by a single unitary mass of LUV in kcps. LUV hydrodynamic diameter did not change with addition of any of the aminosterols, indicating that *n* and I_0 remain constant. By contrast, when the aminosterol is incorporated into the LUVs, *m* increases. The relative increase of LUV mass determined by the addition of aminosterols was then calculated with:

$$\frac{m_{AM}}{m_{NO}} = \sqrt{\frac{I_{AM}}{I_{NO}}} \quad (14)$$

where I_{AM} and I_{NO} are the intensities of light scattered by LUVs in the presence and absence of a given concentration of aminosterol, m_{AM} and m_{NO} are the LUV mass concentrations in the presence and absence of a given concentration of aminosterol. The obtained data were then plotted *versus* aminosterol concentration.

2.18.2 Light scattering analysis of LUVs in in the presence of saturating concentrations of Brb

Model- and neuronal-LUVs were diluted with distilled water to 0.5 mg/ml and incubated for 15 min at 25 °C with increasing concentrations of Brb (from 0 to 100 µM). The count rate (kcps) were then recorded at 25 °C, using a Zetasizer Nano S (Malvern), thermostatted with a Peltier temperature controller, measurement position 4.20 mm, attenuator 9, and using disposable low volume (45 µl) plastic cuvettes. The count rate was recorded for the same concentrations of Brb in the

absence of LUVs and the light scattering intensity of the small molecule was subtracted from the count rate resulting from the incubation of LUVs and Brb to remove Brb scattering contribution. The mass of Brb inserted in the LUVs at saturation was obtained with:

$$m_{Brb} = m_{NO} \cdot \sqrt{\frac{I_{Brb}}{I_{NO}}} \quad (15)$$

where m_{NO} is the mass of LUVs in our conditions (0.2 mg/ml) and I_{Brb}/I_{NO} is the ratio of the mean of count rates at saturating concentration of Brb (>30 µM) and the count rate in the absence of Brb.

2.19 Microfluidics of TRO in presence of LUVs

Model-LUVs were diluted with distilled water to 0.5 mg/ml and incubated for 15 min at 25 °C with 10-100 µM TRO-A594 or 20 µM TRO-BODIPY (1:10 dye:TRO) or 2 µM CHOL-BODIPY (1:1 dye:CHOL); samples with 10 or 50 µM TRO-A594 without LUVs were also prepared. The diffusion of the fluorescently labelled molecule in the various samples was evaluated with the microfluidic technique using a Fluidity One-W instrument (Fluidic Analytics) and placing a 5 µl drop of the sample on a disposable microfluidic chip made of cyclic olefin copolymer (COC) manufactured using injection moulding (Fluidic Analytics). The diffusion was evaluated as the ratio of fluorescence values in the diffused *versus* that in the undiffused channels (F_d/F_{und}) or as the ratio of fluorescence values in the diffused channel *versus* total fluorescence [$F_d/(F_d+F_{und})$]. This ratio parameter correlated directly with diffusion rapidity and inversely with size of the fluorescent

molecule or its complex with LUVs. When this value was in the appropriate range, it was converted automatically by the instrument into a hydrodynamic radius (R_h).

2.20 Zeta potential (ζ) measurements

ζ potential measurements were performed with a Zetasizer Pro Red Label (Malvern). Model-LUVs were co-vesiculated with 5 µM of each aminosterol at a total lipid concentration of 1 mg/ml. About 600 µl of each LUV sample was diluted to obtain a total lipid concentration of 0.25 mg/ml, with phosphate buffer, 5.57 mM ionic strength, pH 7, 20 °C, and put in a disposable folded capillary cell (polycarbonate, Malvern). Each ζ potential value is the average of three independent runs; for each temperature the ζ potential was determined as the mean of 5-8 measurements; The reported error is the standard deviation of the measurements. The measurements were performed in the range 10-60 °C, every 2 °C (except every 1 °C in the range 38-50 °C for ENT-03 containing LUVs, to better appreciate the transition). The electrophoretic mobility measurements were converted into ζ values according to the Smoluchowsky model (Hunter, 1981). The temperature was internally controlled (accurancy ±0.1 °C). The ζ potential measurements were also used to determine the T_m in LUVs systems (Sierra et al., 2016). The T_m values were determined by analysing the first order derivative of ζ with respect to temperature (dζ/dT) as a function of temperature: the T_m correspond to the minimum of the curve, while the amplitude of the transition was assumed to correspond to the full width at half maximum (FWHM) of the derivative curves.

2.21 Preparation of $A\beta_{42}$-derived diffusible ligands (ADDLs)

Lyophilised $A\beta_{42}$ (Bachem) was dissolved in HFIP to 1.0 mM and incubated for 1 h at room temperature to allow complete peptide monomerization. $A\beta_{42}$-derived diffusible ligands (ADDLs) were prepared as described previously (Lambert et al., 2001). In particular, the HFIP was evaporated with a gentle flow of N_2 and the dried protein was resuspended to 5 mM with DMSO and then diluted with phenol red free F-12 HAM to 100 µM. The sample was then incubated at 4 °C for 24 h and centrifuged at 12000 g for 10 min, 4 °C, to collect the supernatant containing the oligomers.

2.22 Cell culture

Authenticated human SH-SY5Y neuroblastoma cells were purchased from A.T.C.C. and cultured in Dulbecco's Modified Eagle's Medium (DMEM), F-12 Ham with 25 mM 4-(2-Hydroxyethyl) piperazine-1-ethanesulfonic acid (HEPES) and $NaHCO_3$ (1:1) supplemented with 10% fetal bovine serum (FBS), 1 mM glutamine and 1% penicillin and streptomycin solution (Sigma-Aldrich). Cells were maintained in a 5% CO_2 humidified atmosphere at 37° C and grown until 80% confluence for a maximum of 20 passages, and routinely tested to ensure that they were free form mycoplasma contamination (Cascella et al., 2017). The cell line was authenticated by the European Collection of Authenticated Cell Cultures using short tandem repeat loci analyses.

2.23 Interaction of fluorescently labelled aminosterols with cells

SH-SY5Y cells were plated in 12-well plates containing coverslips at a density of 50,000 cells per well. 24 h after plating, the cells were washed with phosphate-buffered saline

(PBS) and incubated at room temperature for 30 min with 5 µM TRO-BODIPY, SQ-BODIPY, ENT-03-BODIPY or L-Arg-BODIPY (1:10 dye:molecule) diluted in the Leibovitz's L-15 (ThermoFisher Scientific), a medium designed for supporting cell growth in the absence of CO_2 equilibration. Ten min before the incubation ending, the Hoechst 33342 dye was added to the culture medium (10 µg/ml). The analysis of aminosterol-derived fluorescence and nuclei-derived fluorescence were performed on a Nikon Eclipse TE300 C2 confocal laser scanning microscope (Nikon) equipped with a Nikon 60x immersion oil objective (Apo Plan, NA 1.4) and with Coherent CUBE (diode 405 nm) and Coherent Sapphire (Sapphire 561 nm) lasers. The emission filters for imaging were 452/45 nm and 595/60 nm. All settings, including pinhole diameter, detector gain and laser power, were optimized for each analysis.

2.24 Measurement of cytosolic Ca^{2+} levels

SH-SY5Y cells were plated in 12-well plates containing coverslips at a density of 40,000 cells per well. 24 h after plating, the cells were washed with PBS and incubated at 37 °C for 15 min with ADDLs (1 µM, monomer equivalents) in the absence or presence of increasing concentrations (0.05, 0.1, 0.5, 1, 2.5 and 5 µM) of TRO, SQ or ENT-03. Cytosolic Ca^{2+} levels were measured in living SH-SY5Y cells after the different treatments, by loading the cells with 4 µM Fluo-4 AM (Thermo Fisher Scientific) for 10 min, as previously reported (Cascella et al., 2017). Ca^{2+} levels were detected after excitation at 488 nm and emission at 520-580 nm, by a TCS SP8 scanning confocal microscopy system (Leica Microsystems), equipped with an argon laser source. A series of 1 µm thick optical sections (1024 × 1024 pixels) was taken through the cell depth for each sample using a Leica Plan Apo 63× oil immersion objective, and all sections were projected as a single

composite image by superimposition. The confocal microscope was set at optimal acquisition conditions, e.g., pinhole diameters, detector gain and laser powers. Settings were maintained constant for each analysis. Images were then analysed using the ImageJ (NIH) software (Rasband 1997–2018). Fluorescence intensities were typically expressed as a percentage of that measured in untreated cells.

2.25 Equilibrium dialysis

Model- and neuronal-LUVs were prepared at a total lipid concentration of 2 mg/ml and diluted with 100 mM sodium phosphate buffer, pH 7.0. Brb was diluted to 1 mM in 100 mM sodium phosphate buffer, pH 7.0. 0.2 mg/ml LUVs were incubated with 30 µM Brb in a final volume of 2 ml and then dialysed using a Float-A-Lyzer® (Sigma-Aldrich) device with a 100 kDa MWCO, against 3 ml of 100 mM sodium phosphate buffer, pH 7.0 for 24 h at 4 °C, to let the two solutions reach the equilibrium. 30 µM Brb in the absence of LUVs was also dialysed with the same experimental settings to obtain a negative control. The fluorescence spectra from 450 to 650 nm of the permeates derived from model-LUVs with Brb, neuronal-LUVs with Brb and Brb alone were recorded using the 3×3 mm black walls quartz cell and the Agilent Cary Eclipse spectrofluorimeter described above after excitation at 345 nm. A calibration curve was obtained from the fluorescence emission at 550 nm of increasing concentrations of Brb (from 1 to 20 µM) using the same experimental settings but in the absence of dialysis. The latter data were fitted using:

$$F_{Brb} = 15.179 + 23.539 \cdot [Brb] \quad (16)$$

where F_{Brb} is the observed fluorescence emission at 550 nm and *[Brb]* is the concentration of Brb. Values of fluorescence emission at 550 nm determined from the three permeates were interpolated into the calibration curve to determine the corresponding Brb concentrations.

2.26 8-anilinonaphtalene-1-solfonate (ANS) fluorescence assay

ANS was added at a concentration of 50 or 100 µM to 10 µM HypF-N OAs preincubated with 0, 5, 10, 20, 30, 50, 100 µM Brb for 15 min at 25 °C. Fluorescence emission spectra were acquired at 25 °C between 435 and 650 nm (excitation at 380 nm), immediately after addition of the dye, using a 10x2 mm quartz cell and the Agilent Cary Eclipse spectrofluorimeter described above. ANS spectra were also acquired in the absence of protein. A spectrum recorded with 10 µM OAs in the absence of ANS was subtracted from each spectrum obtained with ANS and OAs, to subtract the scattering contribution of these oligomeric species.

3. Results

3.1 Quantitative measurement of the affinity of toxic and nontoxic misfolded protein oligomers for lipid bilayers, and of its modulation by lipid composition and TRO

3.1.1 The binding affinity of OAs to LUVs is 20-25 times higher than that of OBs

Toxic OAs and nontoxic OBs were pre-formed from purified HypF-N at a total concentration of 0.5 mg/ml, corresponding to 48 μM (monomer equivalents), as previously reported (Campioni et al., 2010; Capitini et al., 2018). LUVs were prepared with a lipid mixture composed of 65% (mol) DOPC, 33% (mol) SM, 1% (mol) CHOL and 1% (mol) GM1, as used in previous work (Errico et al., 2020) and at various mass concentrations (mg/ml); at a total lipid concentration of 1 mg/ml, for example, molar concentrations were 836 μM DOPC, 418 μM SM, 13 μM CHOL and 13 μM GM1.

First, the group of Annalisa Relini at the Department of Physics of the University of Genoa, checked whether OAs and OBs bound to LUVs using AFM. To this purpose, SLBs with the same lipid composition as LUVs were formed separately, treated with 12 μM OAs or 12 μM OBs (monomer equivalents) and then imaged with AFM. The images showed that OAs bind to the gel-phase domains (L_β or S_o) and to the liquid-disordered phase (L_α or L_d) of the SLBs with 1% GM1, whereas only few OBs were found to be bound to them (**Fig. 3.1**), in agreement with previous results obtained with 5% GM1 as the only difference in LUV composition relative to our LUV preparations (Oropesa-Nuñez et al., 2016). Furthermore, the difference in the thickness between the L_β and L_α domains (ΔZ) appeared altered by the presence of OAs, but not OBs, clearly indicating the presence of

structural changes of the overall bilayer (**Fig. 3.1M**), again in agreement with the result obtained with 5% GM1 (Oropesa-Nuñez et al., 2016).

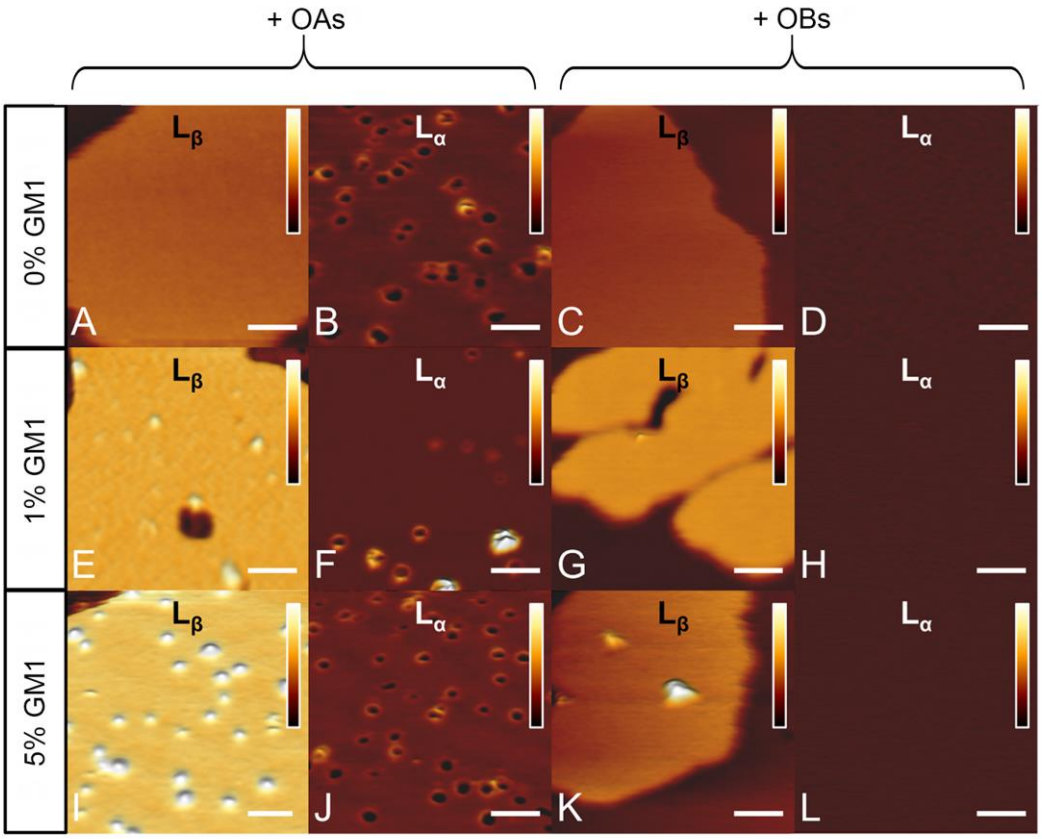

M

Lipid composition (molar fraction)	ΔZ (nm)		
	Untreated	Treated with OAs	Treated with OBs
0% GM1	1.1 ± 0.3	2.2 ± 0.1	1.0 ± 0.1
1% GM1	2.0 ± 0.3	2.8 ± 0.1	2.1 ± 0.1
5% GM1	2.1 ± 0.1	3.7 ± 0.1	2.2 ± 0.1

Figure 3.1. Tapping mode AFM images of SLBs treated with OAs (A,B,E,F,I,J) and with OBs (C,D,G,H,K,L). The concentration of GM1 varied from 0% **(A-D)**, to 1% **(E-H)** and 5% **(I-L)** molar fraction. OAs bind the L_β ordered phase domains in the presence of GM1 (**E,I**), whereas the binding for OBs involves a lower number of oligomers (**G,K**). Neither OAs nor OBs are binding the L_β ordered phase domains in the absence of GM1 (**A,C**) and the number of oligomers on SLBs depends on the GM1 concentration. Toxic OAs also form annular structures on the disorder L_α phase domains **(B,F,J),** but these were not found to correlate with oligomer toxicity (Oropesa-Nuñez et al. 2016). The interaction between OBs and SLBs is weak in all cases **(C,D,G,H,K,L)**. Scale bars: 100 nm. Vertical color scale: 5 nm. **(M)** ΔZ measured on SLBs with different GM1 contents, the values obtained for untreated samples are compared with those after treatment with OAs or OBs. The modification of the bilayer structure induced by OAs is reflected in the variation of ΔZ.

In order to obtain a more quantitative measure of the binding affinity of the OAs and OBs for lipid membranes, we evaluated the ability of these oligomers to quench DPH and its derivative TMA-DPH, two fluorescent probes that incorporate within the hydrophobic region (Kaiser & London, 1998) and polar head region (Illinger et al., 1995) of the lipid bilayer, respectively. The 15-min incubation of increasing concentrations of OAs (from 0 to 32.5 μM monomer equivalents) with TMA-DPH- and DPH-labelled LUVs (0.3 mg/ml, 384 μM total lipids) caused a marked and concentration-dependent reduction of the fluorescence emission of both fluorescent probes, with a more consistent quenching of TMA-DPH (**Fig. 3.2A,B**). The K_{SV} constant is a measure of the quenching of the dye fluorescence operated by the oligomers and obtained by fitting the data to Eq. 5 (see Section 2.13) and is also a measure of the affinity of the oligomers for the membrane-embedded probe, as it reports on the collisions between OAs and the probe (Lakowicz, 2006). The K_{SV} value was found to be 48.2±2.0 mM^{-1} for TMA-DPH and 14.5±1.7 mM^{-1} for DPH (**Fig. 3.2**). The incubation of OBs with TMA-DPH- and DPH-labelled LUVs under identical conditions caused a significantly weaker fluorescence quenching (**Fig. 3.2A,B**), with K_{SV} values of 3.7±0.7 mM^{-1} and 2.2±0.4 mM^{-1}, respectively, which reflected a lower binding to the membrane and the absence of lipid membrane alteration (**Fig. 3.2**). Native HypF-N showed a substantially absent ability to quench both TMA-DPH and DPH (**Fig. 3.2A,B**), with K_{SV} values of 1.2±1.1 mM^{-1} and 1.6±0.4 mM^{-1}, respectively, reflecting the absence of binding to the membrane (**Fig. 3.2**). By subtracting these two background values from the corresponding ones obtained for OAs and OBs, one can determine that OAs have K_{SV} values *ca.* 20-fold higher than OBs with both probes.

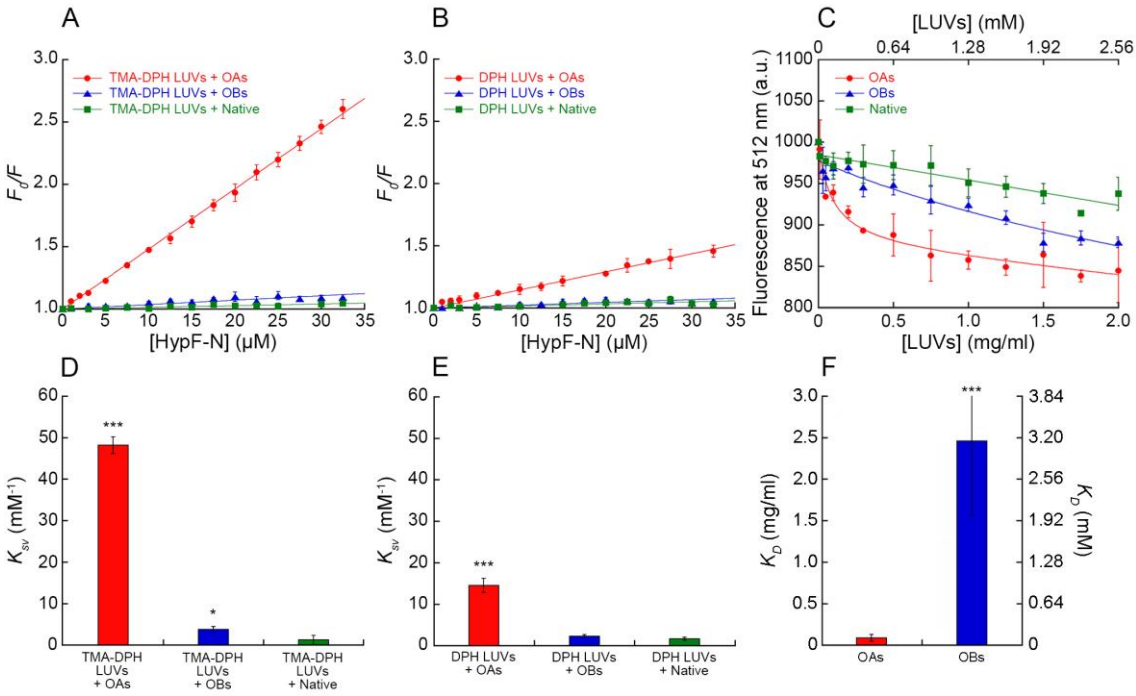

Figure 3.2. Binding of OAs/OBs/native HypF-N to LUVs. (A,B) Stern-Volmer plots reporting the ratio of fluorescence of TMA-DPH **(A)** and DPH **(B)** in 0.3 mg/ml LUVs in the absence (F_0) or presence (F) of various concentrations (monomer equivalents) of OAs (red circles), OBs (blue triangles) and native HypF-N (green squares). The straight lines through the data points represent the best fits to Eq. 5. **(C)** Binding plots reporting the fluorescence at 512 nm of 20 μM BODIPY-FL-labelled OAs (red circles), OBs (blue triangles) and native HypF-N (green squares) *versus* LUV concentration reported in mg/ml units (bottom *x* axis) or mM units (top *x* axis). The lines through the data points represent the best fits to Eq. 8. **(D,E)** Bar plots reporting the K_{SV} values obtained from TMA-DPH **(D)** and DPH **(E)** fluorescence quenching using Eq. 5. **(F)** Bar plots reporting the K_D values from binding using Eq. 8. Experimental errors represent SEM of 2-5 experiments. The symbols * and *** refer to p values <0.1 and <0.001, respectively, relative to K_{SV} values of the native protein **(D,E)** and relative to the K_D value of OAs **(F)**.

To obtain an independent measure of the binding affinity of the three HypF-N species for the LUV membrane, we labelled HypF-N with BODIPY FL and then prepared samples of OAs, OBs and native proteins using the labelled and unlabelled protein at a molar ratio of 1:10. The 15 min incubation of native HypF-N (20 μM) with increasing concentrations of unlabelled LUVs (0.0-2.0 mg/ml, 0.0-2.6 mM total lipids) caused a weak decrease of protein fluorescence that was found to correlate linearly with LUV concentration (**Fig. 3.2C**). A similar decrease, even with the same slope, was observed for the highly soluble reduced glutathione (GSH) labelled with BODIPY FL (**Fig. 3.3**),

indicating that it consists of a LUV-induced fluorescence drift, most probably arising from light scattering as the LUV concentration increases. The 15 min incubation of OAs (20 µM monomer equivalents) with increasing concentrations of unlabelled LUVs (0.0-2.0 mg/ml, 0.0-2.6 mM) caused a marked decrease of OA fluorescence from 0 to *ca*. 0.4 mg/ml LUVs (corresponding to 0.5 mM total lipids), followed by the same drift at higher LUV concentrations (**Fig. 3.2C**). By fitting the data points to a binding function (Eq. 8), we obtained a dissociation constant (K_D) value of 0.09±0.04 mg/ml, corresponding to 0.12±0.05 mM of total lipids, indicating binding of OAs to the LUV bilayer. The fluorescence of OBs also decreased significantly with LUV concentration, to an extent lower relative to that of OAs, but larger relative to native HypF-N or GSH (**Fig. 3.2C and 3.3**), indicating real binding. The fitting of the data points to Eq. 8 led to a K_D value of *ca*. 2.5 mg/ml, corresponding to *ca.* 3.2 mM of total lipids, indicating an affinity for LUVs lower, by *ca.* 25-fold, relative to OAs.

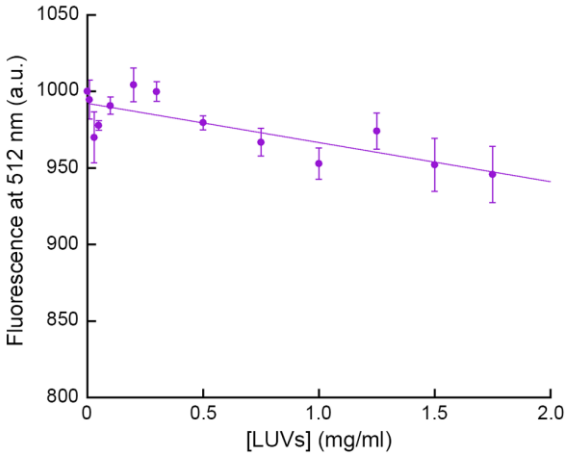

Figure 3.3. Binding plot reporting the fluorescence at 512 nm of 20 µM GSH labelled with BODIPY FL *versus* LUV concentration. The line through the data points represents the best fits to a linear function. Experimental errors represent SEM of 3 experiments.

Hence, under the conditions used here, we have quantified the binding affinity of toxic OAs and nontoxic OBs of a sample protein for the bilayer of lipid vesicles (LUVs) by measuring the K_{SV} values of fluorescence quenching of membrane-embedded TMA-DPH and DPH caused the oligomers (0.3 mg/ml LUVs or 384 µM total lipids) and the oligomer-membrane K_D values (20 µM protein in monomer equivalents). Although K_{SV}^{-1} has been shown to correspond to K_D (Lakowicz, 2006) these values are not immediately comparable in our system because they were measured in different conditions, that is at constant LUV concentration (0.3 mg/ml) upon varying OAs concentration and at constant OAs concentration (20 µM), upon varying that of LUVs, respectively. The molarities of K_{SV}^{-1} and K_D also refer to protein and total lipids, respectively, and are not, therefore, comparable. In both cases, however, the binding affinity of the toxic OAs for the membrane appears to be ca. 20-25 times higher than nontoxic OBs. Albeit with much lower affinity, nontoxic OBs also bind to the LUV membrane, unlike the native protein.

Can we relate the data obtained here with LUVs to cell cultures and brain tissues? By using a mean diameter of 7.5±0.5 µM known for human neuroblastoma SH-SY5Y cells (Maqoud et al., 2018), a lipid density of a membrane bilayer estimated from LUVs of 425±3 ng/cm^2 (Errico et al., 2020), and a cell density value of neuroblastoma SH-SY5Y cells commonly used to test the toxicity of OA/OB species of *ca*. 7.5±0.7 10^4 cells/cm^2 (Fani et al., 2021), and then extrapolating this value to the three-dimensional space, one can determine a lipid concentration of 0.06±0.01 mg/ml in SH-SY5Y cell cultures where OA/OB species are tested. The K_D value of 0.09±0.04 mg/ml lipids measured here for OAs, and referred to total lipid concentration, implies that a significant fraction of OAs (40±15%) is bound to the lipid membranes of cells, as soon as the equilibrium between membrane-bound and membrane-unbound OAs is established and before they enter

into the cells. By contrast, the K_D value of ~2.5 mg/ml lipids measured for OBs, implies that a very minor fraction of OB species interacts with the cell membrane (~2%).

3.1.2 The binding to LUVs does not detectably affect the structures of OAs and OBs

One of the questions that is often raised when studying the structure-toxicity relationship of misfolded protein oligomers is whether the structural characteristics determined for the oligomers in aqueous suspension are maintained or changed upon the interaction with biological membranes. Difficulties to address this issue arise from interferences by cellular or membrane proteins that make it very difficult to monitor the structural characteristics of the oligomers with conventional spectroscopic probes. Here we circumvented this problem using protein-free LUVs and three optical probes to which LUVs are spectroscopically silent, making it possible to monitor the secondary and tertiary structure of the oligomers before and after their binding to the membrane.

First, Hassan Ramshini, who was a Professor on sabbatical leave working in our laboratory at the University of Florence, acquired far-UV CD and intrinsic fluorescence spectra of OAs, OBs and native HypF-N incubated with increasing concentrations of LUVs. The far-UV CD spectra of OAs, OBs and native HypF-N (20 μM monomer equivalents) were not found to be significantly different in the absence or presence of the various LUV concentrations (0-1.5 mg/ml), indicating that their secondary structure was maintained upon interaction with LUVs (**Fig. 3.4A-C**). The intrinsic tryptophan fluorescence spectra of the three species (1.9 μM monomer equivalents) were also similar in the absence or presence of the various LUV concentrations (0-1.5 mg/ml) in terms of wavelength of maximum fluorescence and overall shape, featuring only a linear intensity decrease as the LUV concentration increases, again attributable to light

scattering caused by LUVs, as explained above. This indicates that the presence of LUVs did not influence the chemical environment around the tryptophan residues of the protein (**Fig. 3.4D-F**).

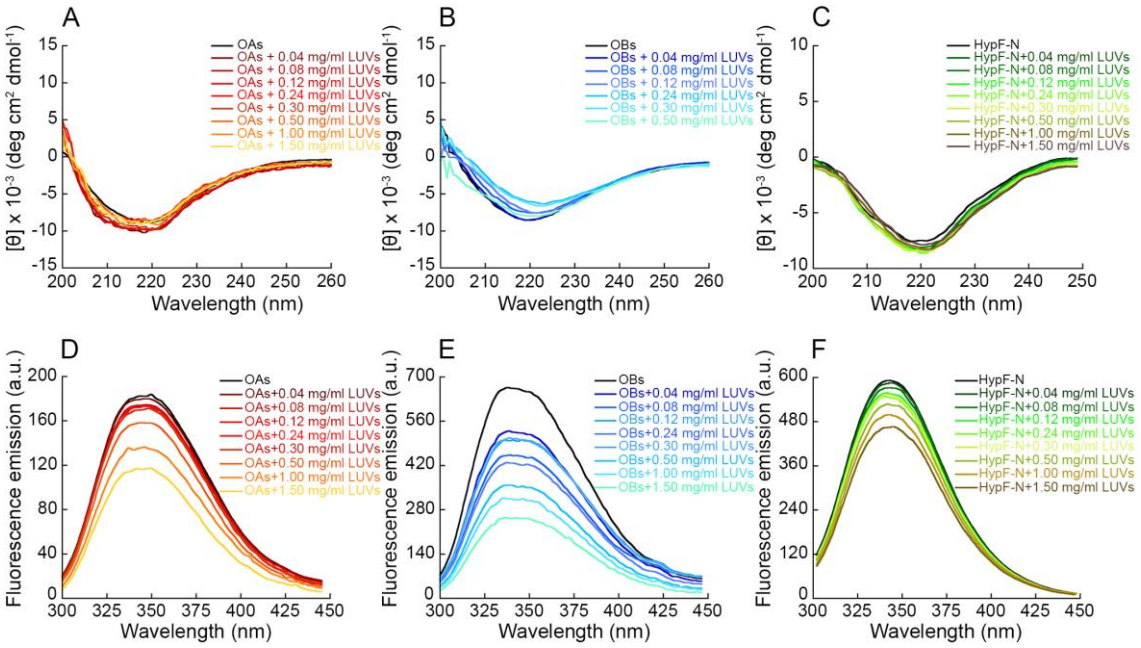

Figure 3.4. Far-UV CD and intrinsic fluorescence spectra of OAs, OBs and native HypF-N. (A-C) Far-UV CD spectra of OAs **(A)**, OBs **(B)** and native HypF-N **(C)** in the presence of increasing concentrations of LUVs. Spectra were blank-subtracted and normalised using Eq. 1. **(D-F)** Intrinsic tryptophan fluorescence emission spectra of OAs **(D)**, OBs **(E)** and native HypF-N **(F)** in the presence of increasing concentrations of LUVs.

In addition, Hassan Ramshini also performed experiments of intra-oligomer FRET in the presence of increasing concentrations of LUVs. Two HypF-N mutants having only one cysteine residue at positions 18 and 34 were labelled with the donor dye 1,5-IAEDANS and the acceptor dye 6-IAF, respectively, and then mixed in a 1:1 molar ratio to form OAs and OBs to a final protein concentration of 20 µM monomer equivalents. The FRET *E* values determined by analysing the resulting fluorescence spectra acquired following 10 min-incubation with unlabelled LUVs (0.0-0.7 mg/ml) were not found to significantly change when varying LUV concentration, either for OAs or for OBs (**Fig. 3.5**).

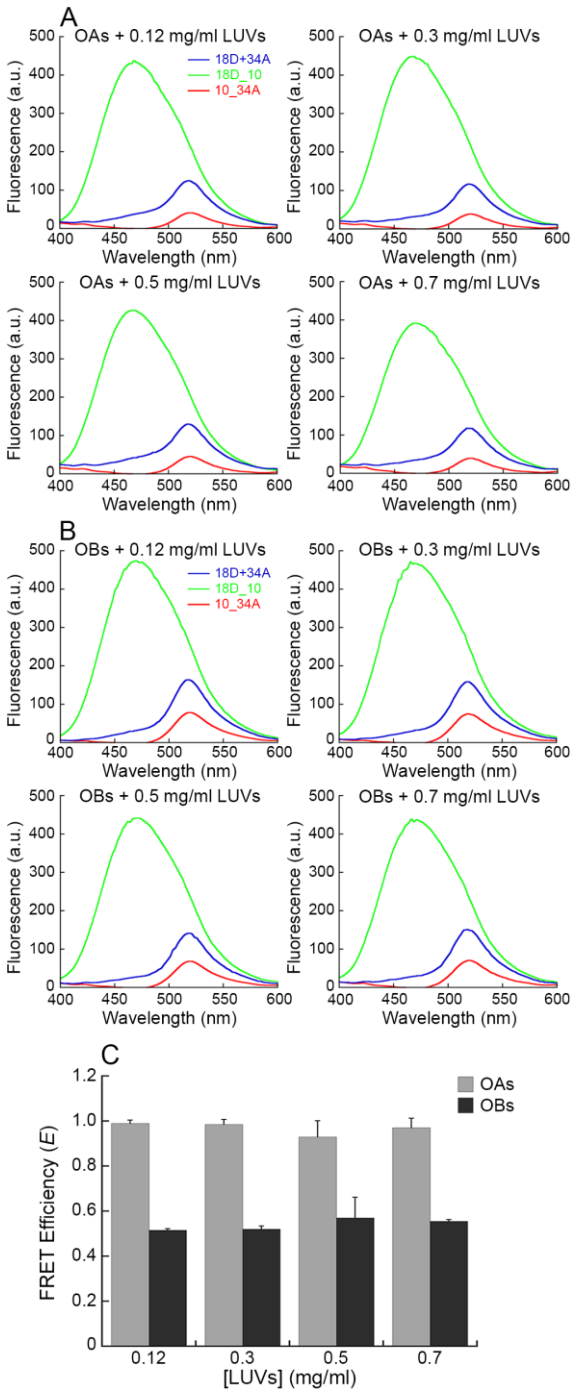

Figure 3.5. Intra-oligomer FRET between OAs and OBs LUVs. (A,B) Fluorescence emission spectra of OAs **(A)** and OBs **(B)** formed by 18D_10 (green), 10_34A (red), and 18D+34A (blue), obtained in the presence of increasing concentrations of LUVs (0.12, 0.3, 0.5, and 0.7 mg/ml). **(C)** FRET *E* values of OAs (grey) and OBs (black) in the presence of increasing concentrations of LUVs, determined using Eq. 2. Experimental errors are S.D.

This result indicates that the mean shortest donor-acceptor distance in the oligomers does not change upon LUV addition and suggests that the intermolecular structure of the oligomers was not significantly altered by the presence of LUVs.

3.1.3 The OA-LUV binding does not involve specific lipid species

Since only OAs were found to have a high affinity for LUVs, we continued our study with this species. In order to investigate whether the binding between LUVs and OAs could depend on a specific interaction with one of the lipids contained in LUVs, we performed FRET experiments using 20 µM (monomer equivalents) OAs labelled with 1,5-IAEDANS as a donor probe (OA-D) and 0.3 mg/ml LUVs containing one of the four lipids labelled with BODIPY-FL as an acceptor probe (Lipid-A).

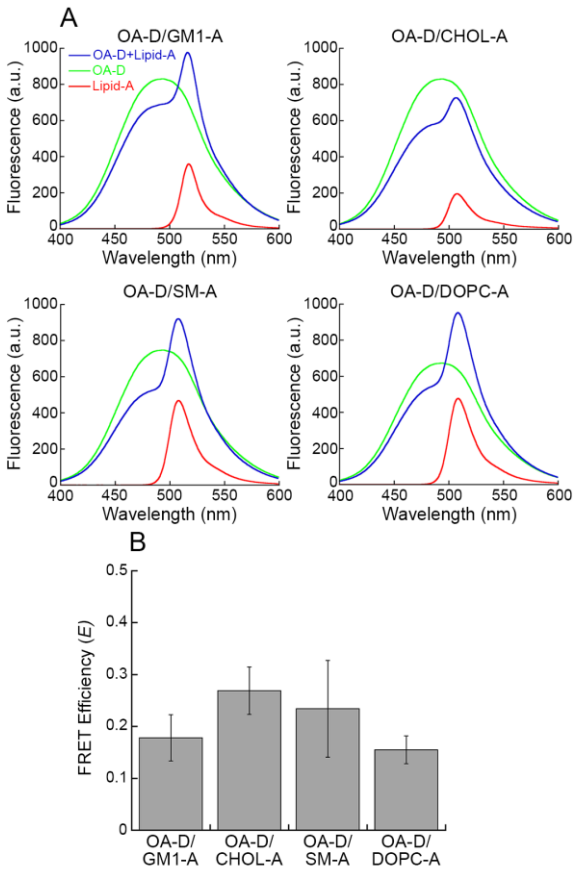

Figure 3.6. FRET between OAs labeleld with donor **(D)** and the various lipids labelled with acceptor **(A)** contained in LUVs. **(A)** Fluorescence emission spectra of OA-D+Lipid-A (blue), OA-D (green) and Lipid-A (red). **(B)** FRET *E* values of the indicated FRET pairs examined, obtained using Eq. 3. Experimental errors represent SEM of 5 experiments.

These experiments were carried out separately by using each of four lipids contained in the LUVs labelled with A. The FRET *E* values were obtained by the analysis of the fluorescence spectra acquired after 15 min (**Fig. 3.6A**) and were found to be 0.18±0.04 for OA-D/GM1-A, 0.27±0.05 for OA-D/CHOL-A, 0.23±0.09 for OA-D/SM-A and 0.15±0.03 for OA-D/DOPC-A, without significant differences between the various FRET pairs examined (**Fig. 3.6B**).

This analysis indicates that OAs bind to LUVs, but do not have a preferential interaction with any of the four lipids. Therefore, the role played by GM1 in the oligomer-membrane interaction, observed here and previously (Evangelisti et al., 2012; Evangelisti et al., 2016; Oropesa-Nuñez et al., 2016), involves a change of the bilayer physical properties, without a direct preferential interaction of the lipid with the oligomers. Indeed, it is clear that GM1 changes the overall negative net charge of the membrane (Errico et al., 2020), increases the thickness of the membrane, particularly of the L_β phase (Reich et al., 2008; Oropesa-Nuñez et al., 2016) and increases its rigidity to lateral diffusion (Calamai et al., 2016), all known to contribute to a higher resistance to oligomer insertion.

3.1.4 TRO reduces the binding affinity of OAs for LUVs

We then investigated whether TRO (**Fig. 1.7**), which has been reported to displace toxic oligomers from lipid membranes (Perni et al., 2018; Limbocker et al., 2019; Limbocker et al., 2020), could induce a variation of the affinity of OAs for the membrane, as measured with TMA-DPH and DPH fluorescence quenching and OAs fluorescence change upon LUV binding. To this aim we prepared TMA-DPH and DPH-labelled LUVs (0.3 mg/ml, 384 μM total lipids) containing 5 μM TRO, and we incubated them with increasing concentrations

of unlabelled OAs (0-32.5 μM monomer equivalents). Previous experiments have shown that TRO has a high affinity for LUVs of this type and partitions completely in the bilayer at this concentration (Errico et al., 2020). The presence of TRO in the bilayer caused a significant reduction of the TMA-DPH fluorescence quenching, with an almost complete absence of quenching at low concentrations of OAs up to *ca*. 10 μM (**Fig. 3.7A**). At higher concentrations of OAs, the TMA-DPH quenching was evident, but remained lower than that observed in the absence of TRO at corresponding OAs concentrations, showing a reduction of the affinity of OAs for LUVs (**Fig. 3.7A**). A similar profile was observed by repeating the experiment with DPH-labelled LUVs (**Fig. 3.7B**).

Interestingly, the absence of TMA-DPH and DPH fluorescence quenching at the concentrations of OAs that normally cause dysfunction and toxicity to cell cultures (<10 μM monomer equivalents), and at the 5 μM concentration of TRO that causes protection, indicates that this small molecule provides protection by preventing OA-LUV binding. By contrast, at higher OAs concentrations the oligomer-displacing effect of the molecule is overcome, most probably because in the excess of OAs TRO partitions to OAs more markedly (Limbocker et al., 2020) and populates the membrane to a lower extent. However, under these excess OAs concentrations and in the presence of 5 μM TRO, the K_{SV} constant remains lower than that observed in the absence of the small molecule. This phenomenon indicates that at the toxic OAs concentrations and protective TRO concentrations the molecule is largely effective as a protective factor, but partly loses its protective action in the presence of excess oligomers.

We then incubated BODIPY FL-OAs (20 μM) with increasing concentrations of unlabelled LUVs (0-2.0 mg/ml, 0-2.6 mM total lipids) containing the same molar fraction

of TRO, and we repeated the analysis described above in the absence of the small molecule, but this time with the molecule (**Fig. 3.7C**).

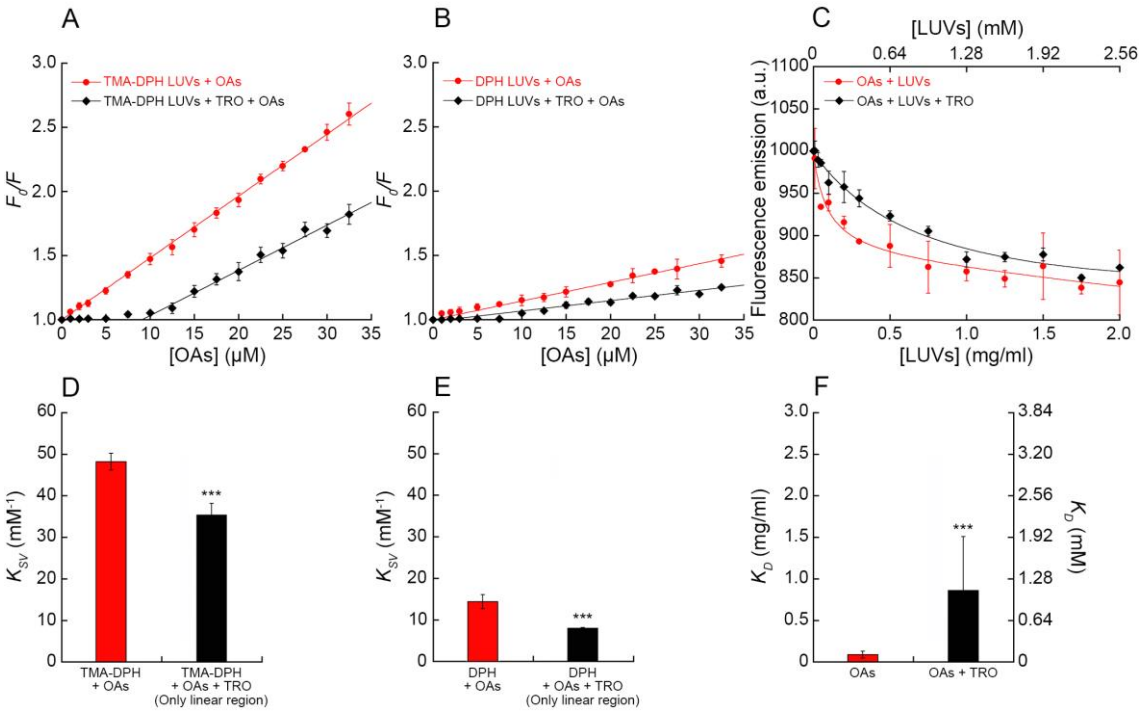

Figure 3.7. Interaction of OAs with LUVs with and without TRO. (A,B) Stern-Volmer plots reporting the ratio of fluorescence of TMA-DPH **(A)** and DPH **(B)** in the absence (F_0) or presence (F) of various concentrations (monomer equivalents) of OAs, in the absence (red circles) and presence (black diamonds) of 5 μM TRO in 0.3 mg/ml LUVs. The straight lines through the data points represent the best fits to Eq. 5 (red line) and Eq. 6 (black line). Experimental errors represent SEM of 2-5 experiments. **(C)** Binding plots reporting the fluorescence at 512 nm of OAs in the absence (red circles) and presence (black diamonds) of TRO in LUVs, *versus* LUV concentration. The lines through the data points represent the best fits to Eq. 8. **(D,E)** Bar plots reporting the K_{SV} values obtained from TMA-DPH (**D**) and DPH (**E**) fluorescence quenching in the absence (red) and presence (black) of 5 μM TRO. **(F)** Bar plots reporting the K_D values obtained from the binding experiments of OAs in the absence (red) and presence (black) of 5 μM TRO. Experimental errors represent SEM of 2-5 experiments. The symbols *** refer to p values <0.001 relative to K_{SV} **(D,E)** and K_D **(F)** values of OAs in the absence of TRO.

TRO was found to significantly increase the K_D, from a value of 0.09±0.04 mg/ml in its absence (corresponding to 0.12±0.05 mM lipids) to a value of 0.86±0.65 mg/ml in its presence (corresponding to 1.10±0.83 mM lipids), therefore reducing the binding affinity of OAs to LUVs by one order of magnitude (**Fig. 3.7C**). Using the same arguments

described above to translate these data into a cell culture context, under these conditions of analysis TRO induces a decrease of membrane-bound OAs from ~40% in the absence of the molecule to ~6% in its presence. Numerical values of K_{SV} and K_D with and without TRO are reported in **Fig. 3.7D-F**.

3.1.5 Change of OA-LUV binding affinity with LUV composition

As widely discussed in section 1.4, it is increasingly clear that membrane lipids have a crucial role in the binding of misfolded protein oligomers to the bilayer (Williams & Serpell, 2011; Andreasen et al., 2015; Oropesa-Nuñez et al., 2016; Galvagnion et al., 2022), particularly GM1 and CHOL (Evangelisti et al., 2012; Evangelisti et al., 2016; Matsubara et al., 2013; Matsubara et al., 2018). In order to better mimic the physiological content of GM1 and CHOL in neuronal plasma membranes, and in light of the fact that the content of these two lipids plays a crucial role in the interaction with LUVs and toxicity of misfolded protein oligomers (Evangelisti et al., 2012; Evangelisti et al., 2016; Oropesa-Nuñez et al., 2016), we decided to explore whether the variation of these two lipids in LUVs could affect the affinity of OAs for LUVs (**Fig. 3.8**). To this aim, we performed the TMA-DPH quenching experiment with OAs and LUVs with 0%, 0.5%, 1% and 5% (molar fractions) GM1 (**Fig. 3.8A**). In the absence of GM1, OAs showed a significantly reduced affinity for the membrane of LUVs (K_{SV} value of 34.7±2.0 mM^{-1}), which was then found to increase with GM1 content (K_{SV} value up to 49.2±0.4 mM^{-1} with 5% GM1), confirming the crucial role of this lipid in the membrane-oligomer interaction (**Fig. 3.8A,C**). We then changed the CHOL content and performed the TMA-DPH quenching experiment with OAs and LUVs with 0%, 1%, 5% and 10% (molar fractions)

CHOL (**Fig. 3.8B**). In this case we observed a small but non-significant decrease in the K_{SV} parameter (**Fig. 3.8B,D**).

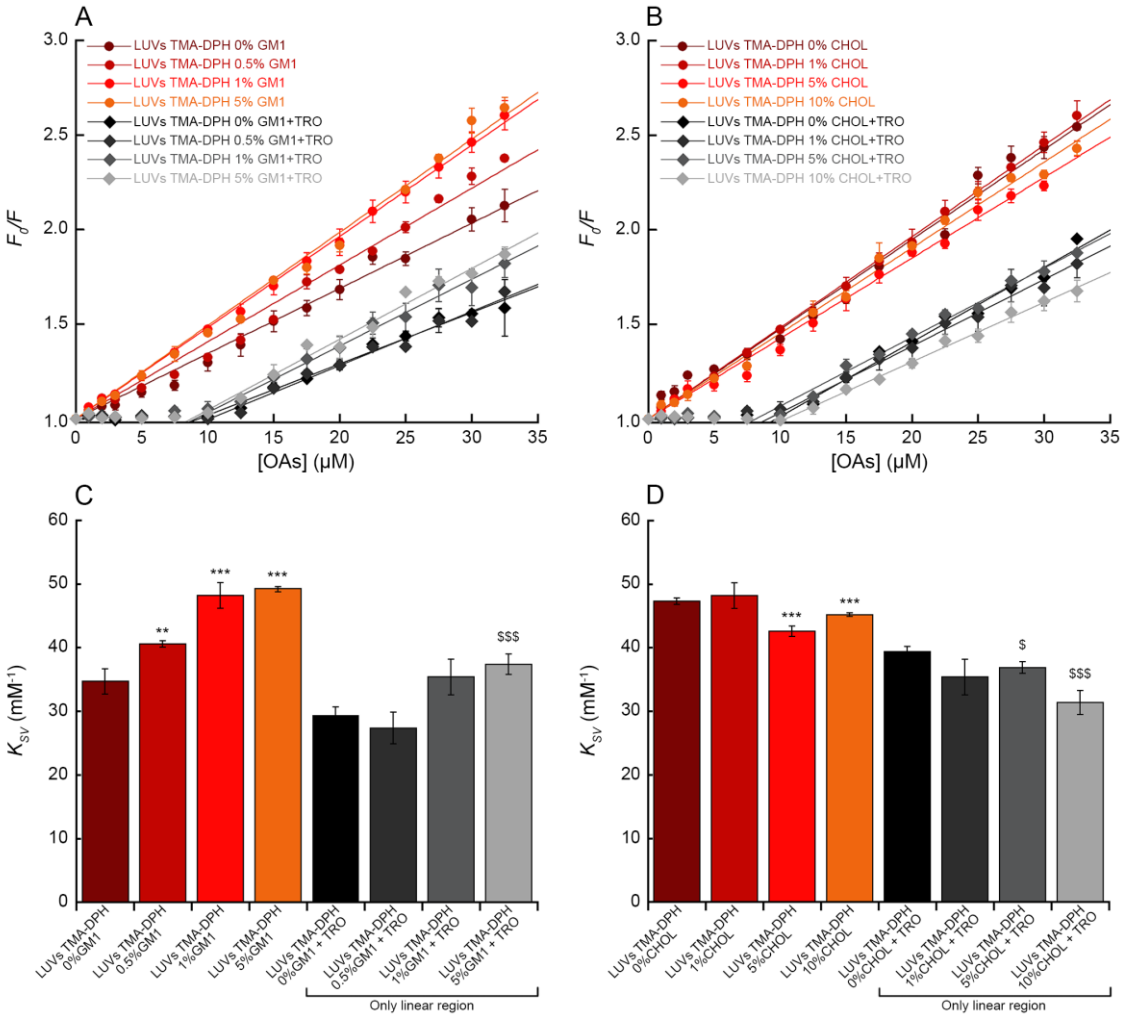

Figure 3.8. Binding of OAs to LUVs with various lipid compositions. (**A,B**) Stern-Volmer plots reporting the ratio of fluorescence of TMA-DPH in the absence (F_0) or presence (F) of various concentrations (monomer equivalents) of OAs, in the absence (various shades of red circles) and in the presence (various shades of grey diamonds) of 5 μM TRO in 0.3 mg/ml LUVs containing different percentage of GM1 **(A)** and CHOL **(B)**. The straight lines through the data points represent the best fits to Eq. 5 (various shades of red lines) and Eq. 6 (various shades of grey lines). **(C,D)** Bar plots reporting the K_{SV} values obtained from TMA-DPH fluorescence quenching in LUVs containing different percentages of GM1 **(C)** and CHOL **(D)** in the absence (various shades of red) and in the presence (various shades of grey) of 5 μM TRO. Experimental errors represent SEM of 2-5 experiments. The symbols ** and *** refer to p values <0.01 and <0.001, respectively, relative to K_{SV} values of OAs without GM1 **(C)** and without CHOL **(D)** in the absence of TRO; $ and $$$ refer to p values <0.05 and <0.001, respectively, relative to K_{SV} values of OAs without GM1 **(C)** and CHOL **(D)** in the presence of TRO.

Since TRO was found to preferentially bind to GM1 and CHOL in LUVs (Errico et al., 2020) we repeated the TMA-DPH quenching experiment using LUVs containing TRO and various contents of GM1 and CHOL, in order to investigate whether the reduction of the K_{SV} induced by this aminosterol could be affected by the lipid composition of LUVs. TRO induced a significant reduction of the TMA-DPH fluorescence quenching at all GM1 and CHOL concentrations, with an almost complete protection from quenching at low OAs concentration, and an evident quenching at higher concentration of OAs, but still lower than the corresponding values in the absence of the aminosterol (**Fig. 3.8**). In the presence of TRO, the K_{SV} value in the linear portion of the plot was found to increase with GM1 content and to slightly decrease with CHOL content, confirming the relationships observed in the absence of the small molecule (**Fig. 3.8C,D**).

3.2 Quantitative attribution of the protective effects of aminosterols against protein aggregates to their chemical structures and ability to modulate biological membranes

3.2.1 All three aminosterols bind to LUVs

Following the observation that TRO appeared able to strongly interact with lipid membranes and partially penetrate them (Errico et al., 2020), we first investigated whether the other aminosterols SQ and ENT-03 (**Fig. 1.9 and 1.13**) were able to bind to our LUV system. To this aim, the fluorescence anisotropy (*r*) values of 10 µM BODIPY™ TMR-X-labelled aminosterol (AM-BODIPY) and Alexa Fluor® 594-labelled aminosterol (AM-A594) were measured in the absence and presence of 0.5 mg/ml LUVs incubated with the three aminosterols for 15 min. BODIPY and A594 labelled the distal primary amino group of the polyamine chain, which is known to stick out of the membrane from previous studies on TRO (Errico et al., 2020) and is not expected, therefore, to affect the aminosterol-membrane binding affinity significantly. In addition, the two probes have different chemical properties. BODIPY has a lower molecular weight, is hydrophobic and has a neutral net charge, whereas A594 has a higher molecular weight, is hydrophilic and has a negative net charge. These differences enable the assessment of whether the probe chemistry affects dramatically the LUV-aminosterol binding affinity.

The incubation of all BODIPY-labelled aminosterols with LUVs showed a highly significant increment of *r* ($p<0.001$, unpaired, two-tailed Student's *t*-test, **Fig. 3.9A, Table 3.1**), suggesting a lower rotational freedom of the probe in presence of LUVs. A similar result was obtained with A594-labelled aminosterols ($p<0.001$, **Fig. 3.9B, Table 3.1**). *r* values of 10 µM L-Arg-BODIPY and L-Arg-A594, used here as negative controls of similarly

labelled small molecules that have no predicted ability to bind to LUV bilayers, increased only marginally or did not increase significantly in the presence of LUVs (**Fig. 3.9A,B**).

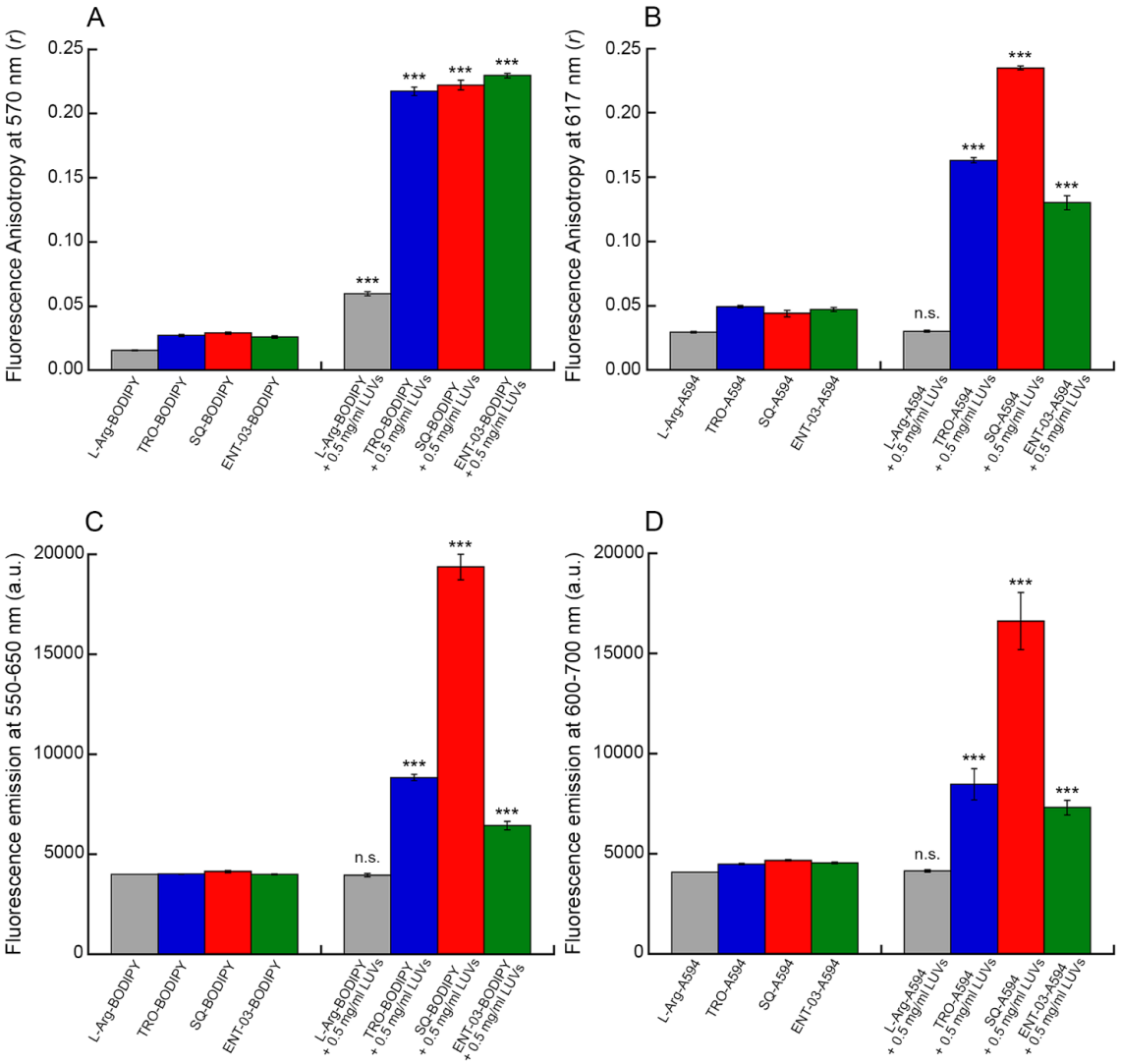

Figure 3.9. Changes in fluorescence anisotropy and emission of the three fluorescently labelled aminosterols in the presence of LUVs. (A,B) Fluorescence anisotropy (*r*) values at 570 nm for BODIPY **(A)** and at 617 nm for A594 **(B)**, of 10 µM L-Arg (grey), TRO (blue), SQ (red) and ENT-03 (green) labelled with BODIPY **(A)** and A594 **(B)**, obtained in the absence and presence of 0.5 mg/ml LUVs. **(C,D)** Fluorescence emission corresponding to the integrated area between 550-650 nm for BODIPY **(C)** and 600-700 nm for A594 **(D)**, of 10 µM L-Arg (grey), TRO (blue), SQ (red) and ENT-03 (green) labelled with BODIPY **(C)** and A594 **(D)**, obtained in the absence and presence of 0.5 mg/ml LUVs. Bars indicate mean ± SEM (n=5. n.s., non-significant; ***, p<0.001 relative to corresponding values in the absence of LUVs (Student's t-test).

L-Arg-BODIPY displayed a slight, but significant, increase of *r* when incubated with LUVs, that was not reproduced with L-Arg-A594, possibly due to the hydrophobic nature of the BODIPY dye that caused clustering of L-Arg-BODIPY molecules or transient interactions with the membrane. We also investigated possible fluorescence emission changes of fluorescently labelled aminosterols (10 μM) when incubated with LUVs (0.5 mg/ml) for 15 min (**Fig. 3.9C,D, Table 3.1**).

Table 1. Fluorescence anisotropy and intensity of aminosterols incubated with LUVs

AM	*r* (- LUVs)	*r* (+ LUVs)	Fluorescence (- LUVs) (a.u.)	Fluorescence (+ LUVs) (a.u.)	K_D (mg/ml)	K_D (μM)
L-Arg-BODIPY	0.0155±0.0004	0.0595±0.0016	3994±8	3964±87	-	-
TRO-BODIPY	0.0271±0.0008	0.2173±0.0033	4010±8	8828±154	0.0302±0.0032	38.7±4.1
SQ-BODIPY	0.0289±0.0009	0.2221±0.0038	4136±51	19358±635	0.0169±0.0023	21.6±2.9
ENT-03-BODIPY	0.0258±0.0010	0.2296±0.0017	3994±15	6435±201	0.0321±0.0064	41.1±8.2
L-Arg-A594	0.0294±0.0007	0.0302 ± 0.0007	4085±7	4141±63	-	-
TRO-A594	0.0493±0.0009	0.1630±0.0020	4483±29	8471±779	0.1516±0.0545	195±70
SQ-A594	0.0440±0.0025	0.2349±0.0014	4678±23	16612±1431	0.0620±0.0093	79±12
ENT-03-A594	0.0471±0.0014	0.1301±0.0057	4541±38	7304±362	0.1164±0.0603	148±81

Table 3.1. Anisotropy (*r*) at 570 and 617 nm and intensity area between 550-650 and 600-700 nm for BODIPY and A594-labelled L-Arg and aminosterols, respectively, in the absence and in the presence of 0.5 mg/ml LUVs. K_D values obtained from the binding experiments expressed in mg/ml and μM of total lipids. Experimental errors are standard error of the mean (SEM) of n=5 technical replicates.

All aminosterols displayed a highly significant increase in fluorescence emission when incubated with LUVs, confirming their ability to bind to LUVs ($p<0.001$). Notably,

SQ labelled with both dyes showed a greater increase compared to the other two aminosterols, as noticed also for the *r* value of SQ-A594 ($p<0.001$). This can be attributed to the shorter polyamine group of SQ relative to TRO and ENT-03, which reduces the distance of the dye probe from the membrane. Fluorescence of 10 µM L-Arg-BODIPY and L-Arg-A594 did not change significantly upon LUV addition (**Fig. 3.9B,C, Table 1**).

3.2.2 SQ exhibits the highest affinity among the three aminosterols for LUVs

Since all three labelled aminosterols increase their fluorescence upon LUV binding, we exploited this spectroscopic property to obtain quantitative measurements of the affinity of the three labelled aminosterols for LUVs. They were therefore incubated for 15 min (10 µM) with increasing concentrations of unlabelled LUVs and observed in all cases a significant increase in fluorescence emission (**Fig. 3.10**). By fitting the data points to a standard binding curve (Eq. 9, see Section 2.14), it was possible to obtain K_D values of all labelled aminosterols (**Fig. 3.10, Table 3.1**). With both fluorescent dyes, SQ confirmed the highest increase of fluorescence upon LUV binding and also showed a K_D value approximately 2-fold lower relative to the other two aminosterols, ($p<0.05$), indicating a higher affinity for LUVs compared to the other two aminosterols. This observation can be attributed to the shorter hydrophilic spermidine moiety of SQ, as opposed to the longer hydrophilic spermine moiety of TRO and ENT-03, which increases the overall hydrophobicity of SQ and explains its higher affinity for LUVs. By contrast, TRO and ENT-03 displayed similar K_D values in both analyses with BODIPY and A594 ($p=0.8198$ and $p=0.7380$, respectively, non significant).

The K_D value determined with BODIPY for a given aminosterol was about 4-fold lower than that determined for the same aminosterol with A594, indicating that the

chemistry of the probe affects the aminosterol-LUV affinity to some extent. However, the rankings and relative differences of the K_D values determined for the three aminosterols are similar when determined with either probe, indicating in both cases that TRO and ENT-03 have similar affinities for the LUV membrane, within experimental error, and that SQ has a *ca*. 2-fold higher affinity.

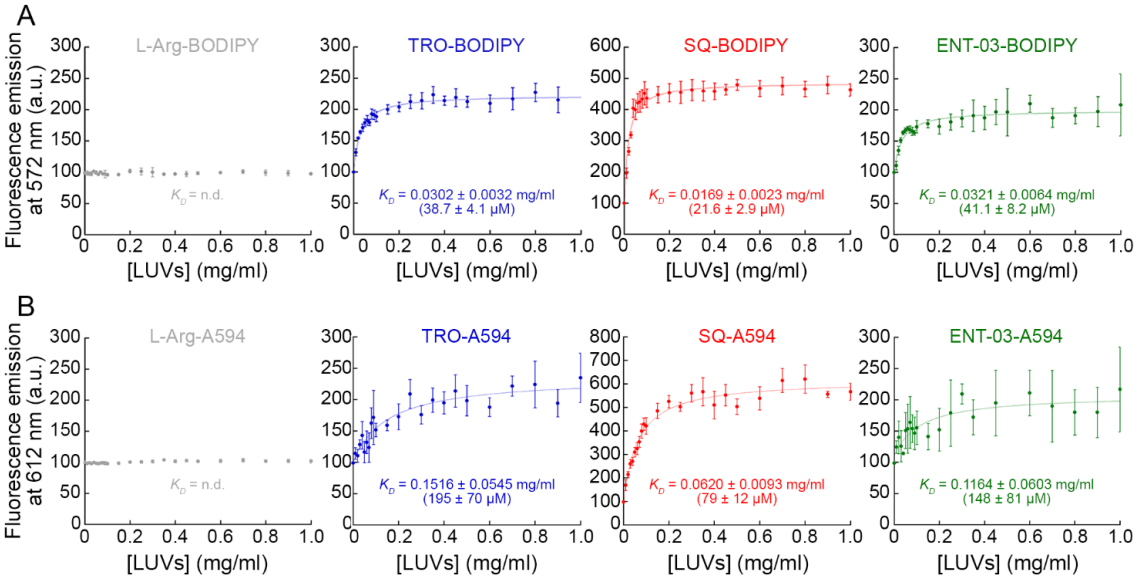

Figure 3.10. Binding of the three aminosterols to LUVs. Binding plots reporting the fluorescence emission at 572 nm **(A)** and 612 nm **(B)**, of 10 μM BODIPY **(A)** and A594 **(B)** labelled TRO (blue), SQ (red), ENT-03 (green) and L-Arg (grey) *versus* LUV concentration. The lines through the data points represent the best fits to Eq. 9. Each graph reports the obtained K_D value in units of mg/ml and μM of total lipids. Experimental errors are SEM (n=5).

Since the two probes add a hydrophilic and hydrophobic component to the aminosterols, it is likely that the binding constant of a given unlabelled aminosterol is intermediate between these two values. Negative controls with labelled L-Arg and increasing concentrations of LUVs showed the lack of variation in fluorescence, confirming that the binding abilities of labelled aminosterols to LUVs were mediated by the aminosterol rather than the fluorescent probe bound to them (**Fig. 3.10**).

To explore the kinetics of the aminosterol-LUV binding, TRO-A594 as a representative aminosterol and LUVs were rapidly mixed using a stopped-flow apparatus to final concentrations of 10 µM and 0.5 mg/ml, respectively, and the TRO-A594 fluorescence change during the binding process was monitored in real time (**Fig. 3.11A**). Two kinetic phases were observed, occurring on the time scales of *ca*. 500 ms and 10 s, respectively, therefore indicating that the binding was very rapid and that after a time of 15 min explored here binding has attained equilibrium. This holds true even at the lowest LUV concentration (0.12 mg/ml) tested (**Fig. 3.11B,C**). These two phases may either represent the signature of a two-step binding mechanism, or reflect two ligand subpopulations that bind LUVs with different kinetics. Assignment of the two phases to well defined molecular events is beyond the scope of the present analysis.

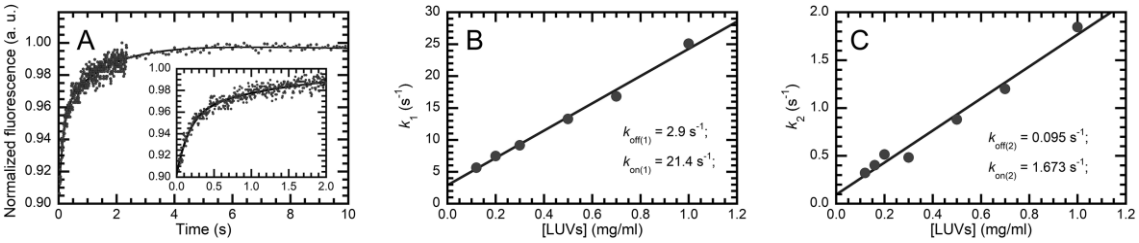

Figure 3.11. Investigation of the binding between TRO-A594 and LUVs in real-time. (A) Representative trace, showing the fluorescence emitted during the binding of 10 µM TRO-A594 with 0.20 mg/ml LUVs. The inset shows the first two seconds of recording, to highlight the first fast phase. The continuous line represents the best fit of experimental data to Eq. 10. **(B,C)** Plots of the apparent rate constants k_1 **(B)** and k_2 **(C)** obtained from best fits of the experimental traces to Eq. 10 *versus* [LUVs]. The continuous lines represent linear fits of the experimental values to Eq. 11 **(B)** and 12 **(C)**.

3.2.3 SQ exhibits the lowest occupancy within LUVs among the three aminosterols

The steric hindrance and chemical properties of the dyes bound to aminosterols could in principle have an impact on the interaction of aminosterols with LUVs. Therefore, we sought an additional experimental approach to probe the incorporation of TRO, SQ and

ENT-03 in their free unlabelled form with LUVs. To this aim, a light scattering analysis using only unlabelled species was carried out (0-100 µM aminosterols, 0.5 mg/ml LUVs, 15 min). Since light scattering intensity is proportional to the second power of the mass of the light scattering particles, by incubating LUVs with increasing concentrations of the three aminosterols, it was possible to obtain a measure of the increase of LUV mass due to aminosterol incorporation in these three cases (**Fig. 3.12**).

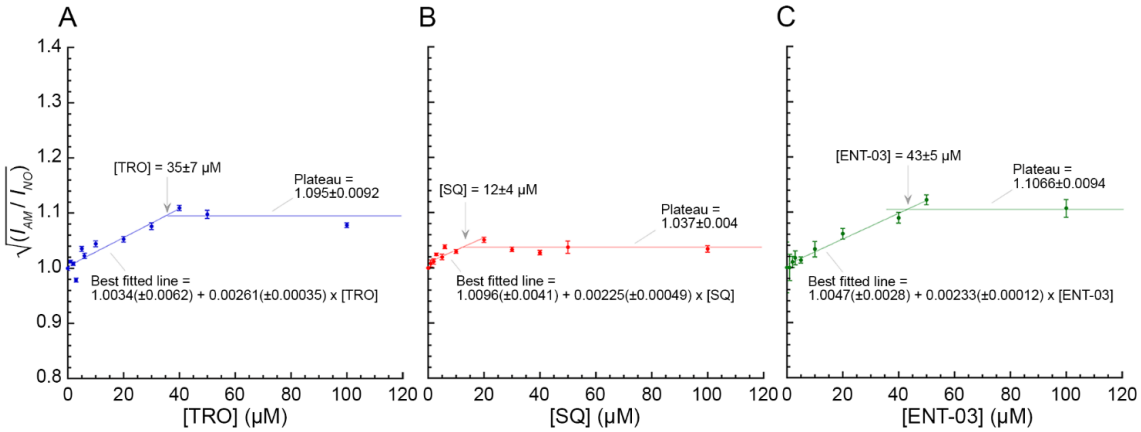

Figure 3.12. Light scattering intensity of LUVs in the presence of increasing concentrations of the three aminosterols. Plots reporting the square root of the light scattering intensity of LUVs with (I_{AM}) and without (I_{NO}) aminosterol, respectively, *versus* aminosterol concentration, representing the increase in LUV mass due to TRO **(A)**, SQ **(B)** and ENT-03 **(C)** incorporation. The indicated aminosterol concentrations correspond to the values reported on the *x* axis at saturation points. Experimental errors are SEM (n=3).

All aminosterols induced an increase in light scattering intensity, and thus LUV mass, until a saturating concentration, after which they exhibited a plateau phase, where no more aminosterols were incorporated. SQ reached the plateau at a significantly lower concentration compared to the other aminosterols (**Fig. 3.12B**, $p<0.05$), whereas TRO and ENT-03 displayed similar saturating concentrations (**Fig. 3.12A,C**, $p>0.05$). The saturating concentrations were found to be 35±7 µM, 12±4 µM and 43±5 µM for TRO, SQ and ENT-03, respectively. These values can also be obtained from the LUV mass

increase at saturation, which yields the mass of incorporated aminosterols, which were found to be 35±4 µM, 15±2, 43±4 µM for TRO, SQ and ENT-03, respectively, in very good agreement with those estimated above. All aminosterols did not show a significant increment of LUV diameter (**Fig. 3.13**), ruling out that the observed increase of light scattering intensity upon aminosterol addition was due to an increase in LUV size. This analysis indicates that aminosterols bind to LUVs even without fluorescent labelling and allows the maximum aminosterol occupancy to be estimated for all three aminosterols.

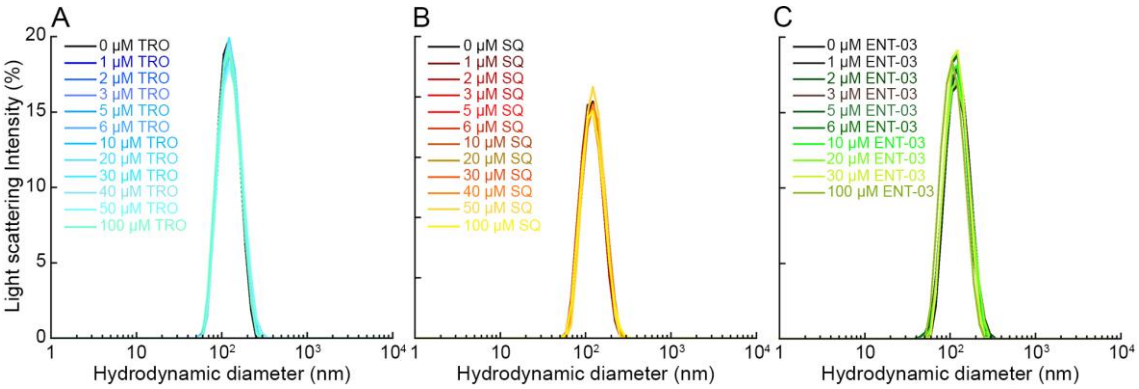

Figure 3.13. Size distributions of LUVs incubated with the three aminosterols. Plots reporting the size distributions of LUVs incubated with the indicated increasing concentrations of **(A)** TRO, **(B)** SQ and **(C)** ENT-03.

To obtain an independent estimate of the aminosterol occupancy at LUVs at saturation, we employed a microfluidic technique using LUVs and TRO as a representative aminosterol, obtaining a value of ca. 28−35 µM TRO at saturation, in agreement with the value of 35±4 µM TRO estimated with light scattering (**Fig. 3.14**). In details, TRO-A594 displayed a high ratio of fluorescence values in the diffused channel *versus* total fluorescence ($F_d/(F_d+F_{und})$), which is typical of a small highly diffusible molecule and led to a value of apparent hydrodynamic radius of 725±35 pm, consistent with that of a molecule of the size of TRO-A594 in a monomeric form (expected value of

700-800 pm). Moreover, the small value of $F_d/(F_d+F_{und})$ measured for TRO-BODIPY in the presence of LUVs ruled out that the molecule was even in part monomeric or assembled into low-molecular weight micelles and rather indicates that the molecule was entirely bound to LUVs, in agreement with the binding plot showing that binding saturation was achieved at these concentrations of TRO-BODIPY and LUVs (**Fig. 3.10A**).

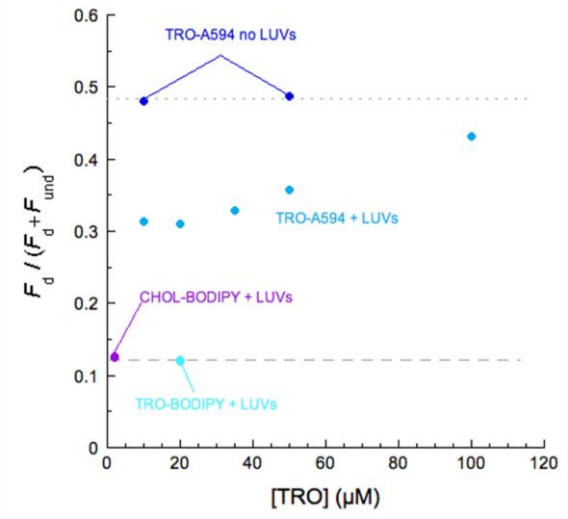

Figure 3.14. Microfluidics of different concentrations of TRO-A594 in the absence or presence of LUVs. Ratio of fluorescence values in the diffused channel *versus* total fluorescence [$F_d/(F_d+F_{und})$], determined with the microfluidic technique, for 10 µM and 50 µM TRO-A594 (1:10 of dye:TRO) in the absence of LUVs (dark blue), for 10-100 µM TRO-A594 (1:10 of dye:TRO) in the presence of 0.5 mg/ml LUVs (n=1, medium blue), for 20 µM TRO-BODIPY (1:10 of dye:TRO) in the presence of 0.5 mg/ml LUVs (pale blue) and for 2 µM CHOL-BODIPY (1:10 of dye:TRO) in the presence of 0.5 mg/ml LUVs used as a positive control of a molecule bound to LUVs (purple).

The similar value of $F_d/(F_d+F_{und})$ measured for CHOL-BODIPY in the presence of LUVs, used here as a positive control of a molecule bound to LUVs, confirmed full binding of TRO-BODIPY to LUVs. Values of $F_d/(F_d+F_{und})$ measured at low concentrations of TRO-A594, in the presence of LUVs, were intermediate, indicating partial binding of the labelled molecule to LUVs, in agreement with the binding plots showing pre-saturation conditions at these concentrations of TRO-A594 and LUVs (**Fig. 3.10B**). As the concentration of TRO-A594 increases, the value of $F_d/(F_d+F_{und})$ also increases, with a

value at 100 μM TRO-A594 close to that of TRO-A594 in the absence of LUVs. This indicates that LUVs are saturated with TRO-A594 under these conditions and the excessive TRO-A594 pool remains unbound. The TRO-A594 concentration at which $F_d/(F_d+F_{und})$ starts to increase is roughly 28-35 μM, in agreement with that determined with the light scattering analysis (**Fig. 3.12A**). Moreover, the $F_d/(F_d+F_{und})$ value measured at 100 μM TRO-A594 is consistent with concentrations of *ca.* 65 μM and *ca.* 35 μM unbound and bound in pre-saturating conditions, respectively, lending further support to a saturating value of *ca*. 35 μM determined with the light scattering analysis.

3.2.4 All three aminosterols partially neutralise the negative charge of LUVs, with an efficacy TRO ≅ ENT-03 > SQ

Since 5 μM aminosterol and 1.0 mg/ml LUVs are concentrations at which binding is complete (all aminosterol is bound to LUVs and LUVs are not yet saturated), we carried out the following analyses at these concentrations, in all cases after co-vesiculating aminosterols with the lipids of LUVs to rule out incomplete binding. In particular, we evaluated the effect of the three aminosterols on three physicochemical properties of the LUV lipid bilayer previously found to be altered by TRO and thought to represent important factors for the vulnerability of the lipid plasma membrane to misfolded protein oligomers (Errico et al., 2020): the membrane negative charge, monitored with ζ potential measurements, the resistance of the bilayer to a BTF perpendicular to the bilayer plane, monitored with AFM on SLBs, and the distribution of lipids in the membrane, monitored with lipid-lipid FRET.

The ζ potential was measured by Gabriella Caminati's group at the Department of Chemistry of the University of Florence, using naked LUVs and LUVs co-vesiculated

with TRO, SQ or ENT-03 (**Fig. 3.15A, Table 3.2**). For naked LUVs, a negative value of ζ of −23.6±0.7 mV was found at 20 °C (Errico et al., 2020), whereas values of -18.7±0.3, -21.0±0.5 and -18.7±0.3 mV (mean±SEM) were obtained for LUVs co-vesiculated with TRO, SQ and ENT-03, respectively, at the same temperature (**Fig. 3.15A, Table 3.2**). These variations indicate, in all cases, a partial neutralization of the total negative surface charge of LUVs, or molecular packing of the charged lipid heads, upon aminosterol addition ($p<0.001$, $p<0.05$, $p<0.001$, respectively). SQ induced a smaller decrease compared to TRO and ENT-03 ($p<0.01$), which showed by contrast comparable decreases ($p>0.05$). This is in agreement with the chemical properties of the three aminosterols, with SQ carrying a spermidine group, which is shorter and less positively charged than the spermine group of TRO and ENT-03.

ζ measurements *versus* temperature were then used to determine the phospholipid gel to liquid-crystalline phase T_m of LUVs in the absence and presence of each aminosterol (**Fig. 3.15A,B**). The transition is described by a sharp change in the ζ potential (**Fig. 3.15A**), that is more evident in corresponding first derivative plots (**Fig. 3.15B**). The T_m of this LUV system is dominated by SM (T_m of 35-40 °C), since DOPC (T_m of -17 °C), which is the most abundant lipid, is already in a fluid-like phase in the examined temperature range (Attwood et al., 2013; Shaw et al., 2012).

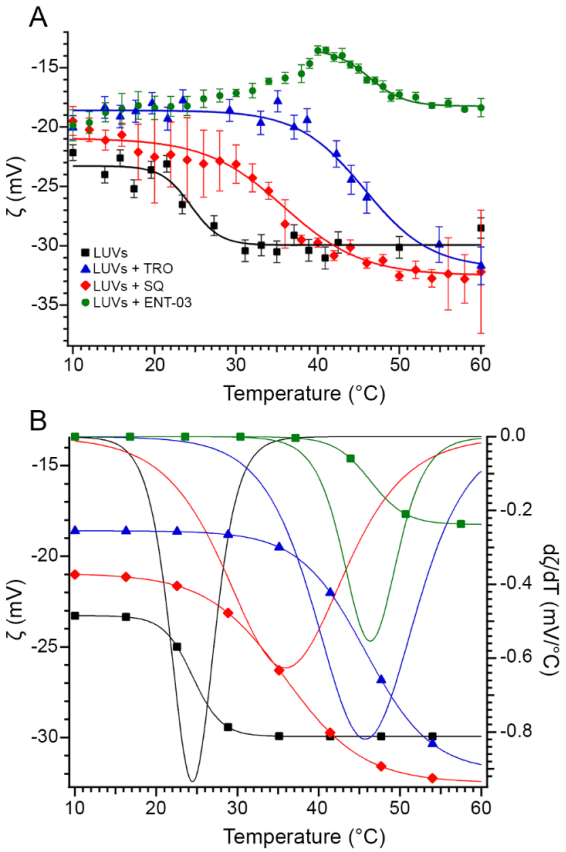

Figure 3.15. The three aminosterols increase the transition temperatures of LUVs. (A) ζ potential and **(B)** fitted curves (left axis) and first derivative curves (right axis) of ζ values as a function of temperature for naked LUVs (black square), and aminosterol-containing LUVs: TRO (blue), SQ (red), and ENT-03 (green). Experimental errors are standard deviations (n=5). In each case, the T_m corresponds to the minimum of the first derivative curve.

Table 3.2. Experimental values of the physicochemical perturbations of the membrane induced by aminosterols (AMs)

	ζ (mV)	**Δζ (%)**	***BTF* (nN)**	***ΔBTF* (%)**	**$r_{GM1\text{-}CHOL}$ (Å)**	**$\Delta r_{GM1\text{-}CHOL}$ (%)**	**$r_{CHOL\text{-}CHOL}$ (Å)**	**$\Delta r_{CHOL\text{-}CHOL}$ (%)**
- AMs	-23.6±0.7	0%	2.73±0.09	0%	65±1	0%	72±1	0%
+ TRO	-18.7±0.3	100%	4.2±0.2	100%	79±1	100%	58±1	100%
+ SQ	-21.0±0.5	53%	3.5±0.2	52%	72±1	50%	64±1	57%
+ ENT-03	-18.7±0.3	100%	3.0±0.1	18%	73±1	57%	63±2	64%

Table 3.2. ζ potential, BTF, GM1/CHOL and CHOL/CHOL mean shortest distance (*r*) experimental values and their corresponding normalized percent values obtained in the absence and presence of TRO, SQ and ENT-03. BTF errors were evaluated as half of the range of variability of mean values from different series of measurements for each condition. Experimental r errors are SEM (n=3 technical replicates). ζ potential errors are standard deviations (n=5).

For naked LUVs, the T_m was observed at 24.5±2 °C. All aminosterols induced an increase of the transition temperature of LUVs, up to values of 46±2 °C ($p<0.01$), 35±2 °C ($p<0.05$) and 46±2 °C ($p<0.01$) with LUVs co-vesiculated with TRO, SQ and ENT-03, respectively, indicating trend variations similarly to those measured with ζ at 20 °C. The transition width is about 6 °C for the naked LUVs, but becomes larger with aminosterol, up to 16 °C in the case of TRO-containing LUVs, confirming that aminosterols modify the packing of the bilayer and the system disorder (Biruss et al., 2007).

3.2.5 All three aminosterols increase the BTF of SLBs, with an efficacy of TRO > SQ > ENT-03

The resistance of the bilayer to a force applied perpendicular to its plane was analysed by AFM by the Annalisa Relini's group at the University of Genoa, which allowed us to determine the BTF required to penetrate the bilayer with the AFM tip. Measurements were performed on SLBs in the absence and presence of each aminosterol (**Fig. 3.16**). As previously described, SLBs with this lipid composition display the coexistence of two different phases: gel-phase domains, called L_β or S_o, enriched with SM, CHOL and GM1, that float in a liquid-disordered phase, called L_α or L_d, enriched with DOPC (Errico et al., 2020; Oropesa-Nuñez et al., 2016). The largest fraction of breakthroughs was observed on L_α regions, while most of the L_β regions displayed the absence of breakthrough events (Errico et al., 2020). The presence of aminosterols determined an increase in BTF values relative to aminosterol-devoid SLBs (BTF of 2.73±0.09 nN; **Table 3.2**). TRO caused the largest increase, followed by SQ and then ENT-03, with BTF values of 4.2±0.2 nN, 3.5±0.2 nN and 3.0±0.1 nN, respectively (**Fig. 3.16; Table 3.2**).

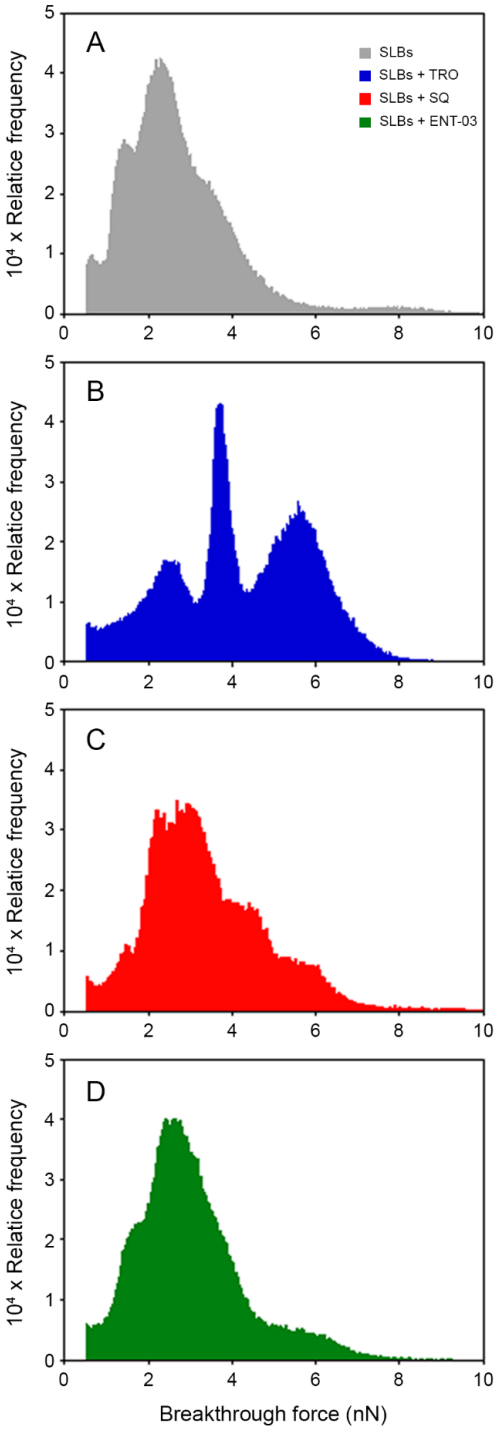

Figure 3.16. The three aminosterols increase the mechanical resistance of lipid bilayers to indentation or BTF. BTF distributions measured on SLBs formed from LUVs prepared in the absence (**A**, grey) and in the presence of 5 µM TRO (**B**, blue), SQ (**C**, red) and ENT-03 (**D**, green). Distributions were obtained from at least six independent force maps. The statistically significant difference between aminosterols was calculated using a Kruskal-Wallis test, which resulted in $p<0.001$, and a Dunn test, which highlighted a difference between each group with $p<0.05$.

3.2.6 All three aminosterols redistribute cholesterol (CHOL) and GM1 lipids in LUVs, with efficacy TRO > SQ ≅ ENT-03

Using lipid-lipid FRET, TRO was previously found to reorganize the spatial distribution of CHOL and GM1 molecules in LUVs, therein clustering CHOL molecules, separating CHOL from GM1 molecules, clustering GM1 molecules and maintaining mutual distances of SM and DOPC from CHOL (Errico et al., 2020). To investigate whether SQ and ENT-03 could have a similar impact, we carried out a series of lipid–lipid FRET experiments in the absence and presence of each aminosterol. In these experiments, 0.0625% of a given lipid (relative to the total lipid content in LUVs) was labelled with a donor (D) fluorescent probe and the same fraction of CHOL was labelled with an acceptor (A) fluorescent probe, namely BODIPY FL and BODIPY 542/563, respectively. Four different combinations of FRET pairs (GM1-D/CHOL-A, CHOL-D/CHOL-A, SM-D/CHOL-A and DOPC-D/CHOL-A) were then analysed in the presence of SQ and ENT-03 and then compared to data obtained with LUVs without aminosterols and with LUVs with TRO (**Fig. 3.17A-D**). Both SQ and ENT-03 induced a similar and significant increment of FRET efficiency (*E)* in the CHOL-D/CHOL-A pair ($p<0.001$) and a reduction in the GM1-D/CHOL-A pair ($p<0.01$), indicating a reduction of the mean shortest distance between CHOL molecules or GM1 molecules and an increase of the distance between CHOL and GM1 molecules (**Fig. 3.17E,F; Table 3.2)**. This behaviour was similar to that induced by TRO ($p<0.001$ relative to absence of aminosterol), but was found to occur to a significantly lesser extent (**Fig. 3.17E,F; Table 3.2**). Neither SQ nor ENT-03 showed variations in the FRET *E* for the SM-D/CHOL-A and DOPC-D/CHOL-A pairs ($p>0.05$), in agreement with the effect of TRO (**Fig. 3.17E,F; Table 3.2**).

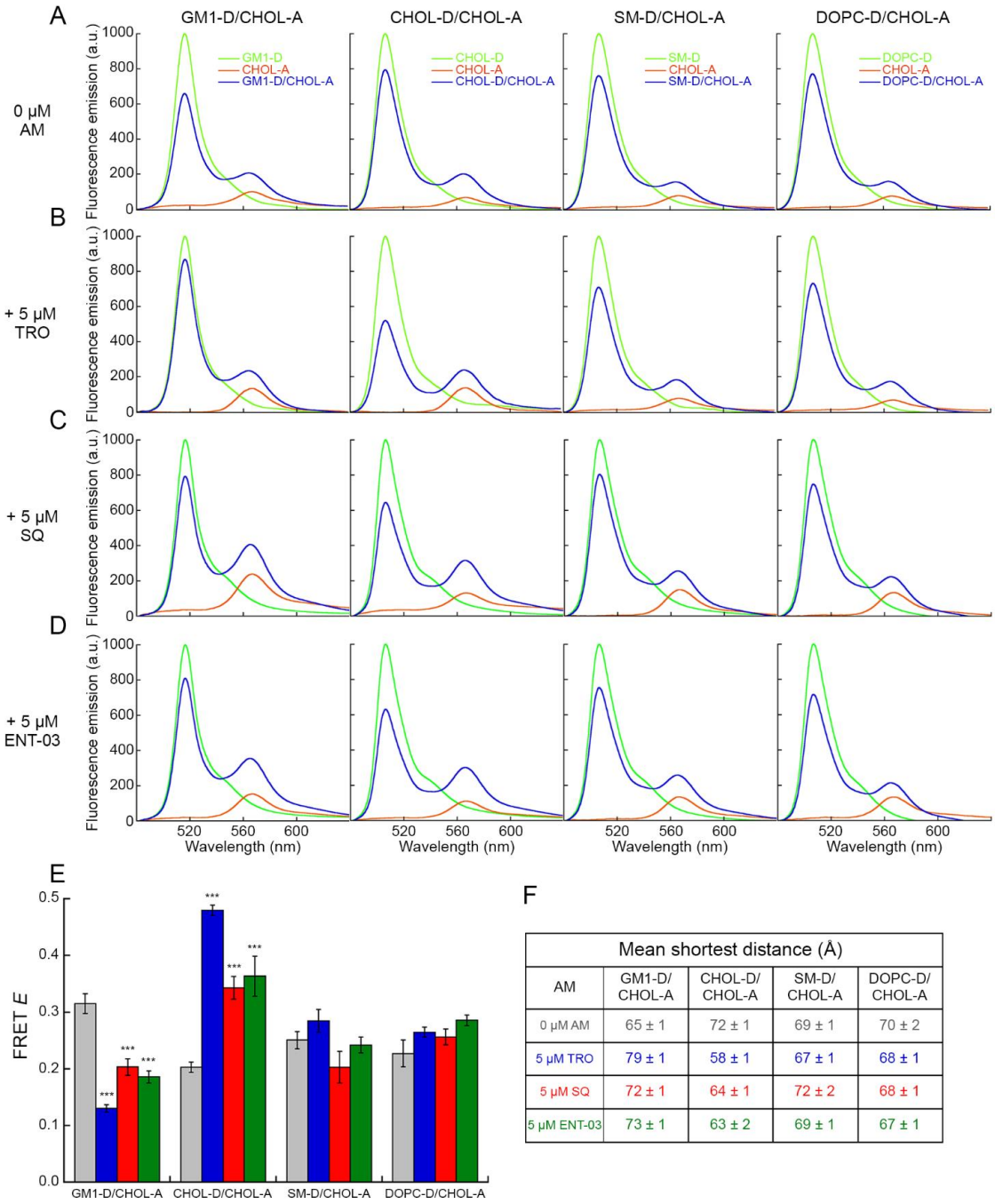

Mean shortest distance (Å)				
AM	GM1-D/ CHOL-A	CHOL-D/ CHOL-A	SM-D/ CHOL-A	DOPC-D/ CHOL-A
0 μM AM	65 ± 1	72 ± 1	69 ± 1	70 ± 2
5 μM TRO	79 ± 1	58 ± 1	67 ± 1	68 ± 1
5 μM SQ	72 ± 1	64 ± 1	72 ± 2	68 ± 1
5 μM ENT-03	73 ± 1	63 ± 2	69 ± 1	67 ± 1

Figure 3.17. The three aminosterols redistribute CHOL and GM1 molecules in LUVs. (A-D) Fluorescence spectra of LUVs containing the indicated D-labelled lipid (green), A-labelled CHOL (orange), and both (blue) in the absence **(A)** and in the presence of TRO **(B)**, SQ **(C)** and ENT-03 **(D)**. **(E)** FRET efficiency (*E*) values obtained for the various pairs using Eq. 3 in the absence (grey) and presence of TRO (blue), SQ (red), ENT-03 (green). Experimental errors are SEM (n=5). The symbols *** refer to p values of <0.001 relative to *r* values obtained in the absence of aminosterols. **(F)** Mean shortest distances (*r*) between the indicated lipid-D and CHOL-A in absence and presence of aminosterols obtained from FRET *E* values reported in panel E using Eq. 4.

3.2.7 All three aminosterols displace αS from DMPS LUVs, with efficacy TRO ≅ ENT-03 > SQ

Previous works showed that TRO and SQ were able to displace αS from SUVs composed of DMPS (Perni et al., 2017; Perni et al., 2018), and that this displacement could be monitored as a change from a LUV-bound αS conformation enriched with α-helical structure and a free, unbound, substantially disordered αS conformational state (Perni et al., 2017; Perni et al., 2018). We repeated the experiments with TRO and SQ, and also extended the analysis to ENT-03, using DMPS LUVs rather than our ordinary LUVs to replicate the previously established protocol (Perni et al., 2017; Perni et al., 2018) and because the strength of the binding of αS to lipids is strongly influenced by the chemical properties of the lipids (Zhu et al., 2003; Galvagnion et al., 2015; Galvagnion et al., 2016). To this aim, 5 μM αS was incubated with 0.2 mg/ml DMPS LUVs for 30 min and then with increasing aminosterol concentrations for 15 additional min. All aminosterols were found to displace αS from LUVs in a dose-dependent manner, as shown by the progressive apparent two-state change from a typical α-helical CD spectrum, with negative peaks at 222 and 208 nm and a positive peak at 192 nm, to a typical random-coil spectrum, with a single negative peak at 198 nm (**Fig. 3.18A-C**). This conformational change was compared for the three aminosterols as a progressive increase of mean residue ellipticity at 222 nm, showing that SQ is slightly less effective, as it requires higher concentrations to displace the protein from the membrane relative to TRO and ENT-03, which had similar displacement activities (**Fig. 3.18D**). This ranking suggests that the aminosterol-induced displacement of αS from DMPS LUVs is mainly driven by electrostatic effects, given that TRO and ENT-03 are more positively charged than SQ at physiological pH.

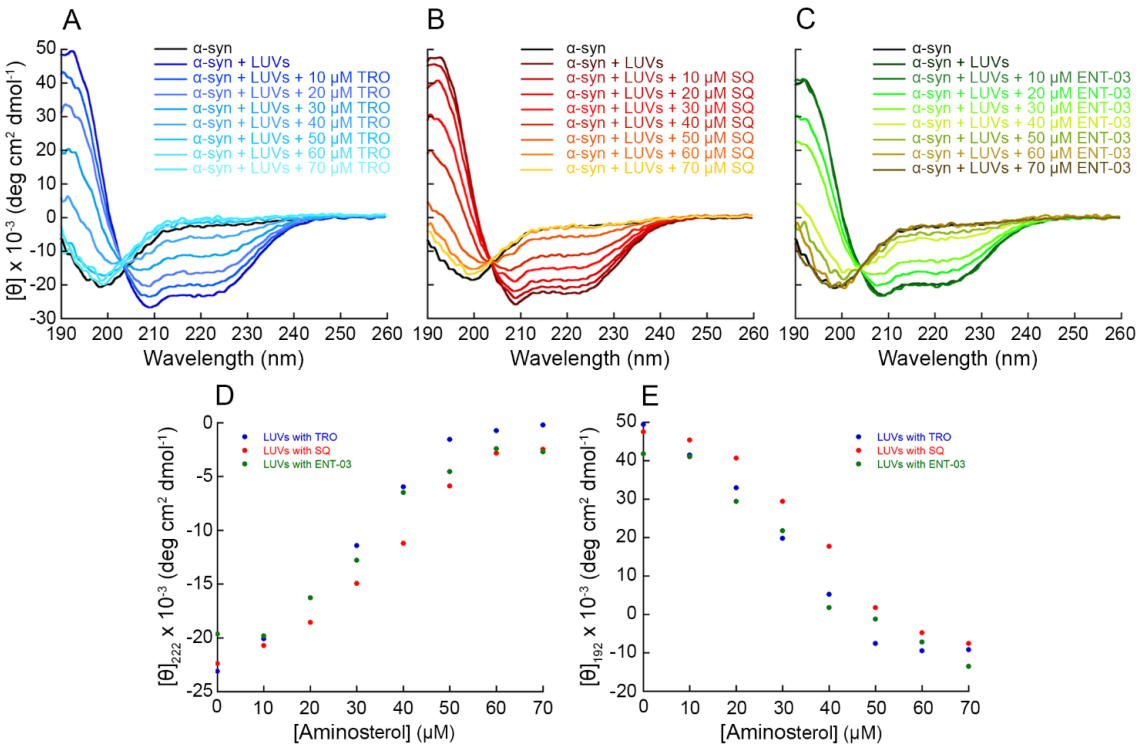

Figure 3.18. Far-UV CD analysis of αS displacement exerted by the 3 aminosterols. (A-C) Far-UV CD spectra of αS in the absence and presence of DMPS LUVs incubated with increasing concentrations of TRO **(A),** SQ **(B)** and ENT-03 **(C)**. Spectra were blank subtracted and normalized using Eq. 1. **(D,E)** Mean residue ellipticity at 222 nm **(D)** and 192 nm **(E)** of αS incubated with DMPS LUVs and increasing concentrations of TRO (blue), SQ (red) and ENT-03 (green).

3.2.8 All three aminosterols protect the plasma membrane of cultured cells from Aβ oligomers, with efficacy TRO > ENT-03 > SQ

Thanks to a collaboration with Claudia Capitini from the European Laboratory for Non-Linear Spectroscopy (LENS) at the University of Florence, we then pursued our comparative analysis from LUVs to cultured cells (human neuroblastoma SH-SH5Y cells) to investigate whether all three aminosterols would bind to the plasma membrane of cells and protect them from misfolded protein oligomers. All three aminosterols were labelled with BODIPY™ TMR, which is a neutral and hydrophobic probe that does not alter the positive net charge of the aminosterol. SH-SY5Y cells were treated with 5 μM TRO-BODIPY, SQ-BODIPY, or ENT-03-BODIPY for 30 min at room temperature and analysed with confocal scanning microscopy (**Fig. 3.19A**). All three aminosterols

prominently bind to the plasma membrane, in accordance with the results obtained with LUVs. Moreover, cells treated with L-Arg-BODIPY, used here as a negative control, show the total absence of BODIPY-derived fluorescence (**Fig. 3.19A**), confirming that the binding observed using AM-BODIPY is fully attributable to the aminosterol, rather than the hydrophobic probe.

The protective effect of the three aminosterols against the ability of misfolded protein oligomers to cause cell dysfunction was evaluated by Roberta Cascella from our lab in Florence using ADDLs comprised of $A\beta_{42}$ as sample oligomers and evaluating the influx of calcium ions (Ca^{2+}) from the extracellular space to the cytosol of cultured SH-SY5Y cells, which is thought to be the earliest insult following the oligomer-membrane interaction (Demuro et al., 2005; Diaz et al., 2009; Decker et al., 2010; Alberdi et al., 2010; Fani et al., 2022). SH-SY5Y cells were treated for 15 min with ADDLs (1 μM, monomer equivalents) in the absence or presence of different concentrations of aminosterols and then their Ca^{2+} levels were evaluated with a specific fluorescent probe that enters inside the cells and produces green fluorescence (*F*) only when bound to Ca^{2+} (**Fig. 3.19B,C**). ADDLs caused a 660±30% increase of Ca^{2+} relative to untreated cells, indicating a markedly heightened state of toxicity. Co-incubation of the ADDLs with aminosterols caused a decrease of Ca^{2+} levels with a clear dose-dependence and aminosterol type dependence. In particular, TRO was found to be more effective than ENT-03 at corresponding concentrations, and the difference was statistically significant when all doses were analysed together ($p<0.01$). TRO and ENT-03 were both more effective than SQ ($p<0.001$ in both cases). At the highest aminosterol concentration tested (5 μM), all three aminosterols were able to completely suppress the ADDL-induced Ca^{2+} influx down to the levels of untreated cells (**Fig. 3.19C**).

3.2.9 A global fitting analysis determines quantitatively the chemical factors of aminosterols and the physico-chemical determinants of membrane involved in aminosterol-induced membrane protection

All data of Ca^{2+}-derived fluorescence (*F*) shown in **Fig. 3.19C** were converted into normalized response (*R*) values ranging from 0% (no effect) to 100% (full effect) using:

$$R = 100 \cdot \frac{(F_0 - F)}{(F_0 - F_{untreated})} \quad (17)$$

where F_0 and $F_{untreated}$ are the *F* values with and without ADDLs, respectively, both without aminosterols (corresponding to 659±30% and 100±15%, respectively). The obtained *R* values were plotted *versus* aminosterol concentration in one single semi-log plot to obtain the typical dose-response curve used in pharmacology (**Fig. 3.19D**). The resulting plot was then fitted to the Hill equation, typically used to analyse dose-response curves and found to satisfactorily fit most dose-response curves (Di Veroli et al., 2015):

$$R = \frac{100}{1 + \left(\frac{EC_{50}}{[AM]}\right)^n} \quad (18)$$

where [*AM*] is the aminosterol molar concentration, EC_{50} is the molar aminosterol concentration at which *R* was 50% and *n* is the Hill coefficient. EC_{50} and *n* were parameters free to float in the fitting procedure and values of $1.62\pm0.25\cdot10^{-7}$ M and 0.78±0.09 were obtained, respectively (**Fig. 3.19D**, r=0.9291, RMSD=8.17%). A fairly good agreement was found between theoretical *R* values re-determined with Eq. 18 for all three aminosterols and corresponding experimental *R* values (**Fig. 3.19E**, r=0.9291, RMSD=8.17%). Nevertheless, the agreement was not entirely satisfactory due to differences among the three aminosterols.

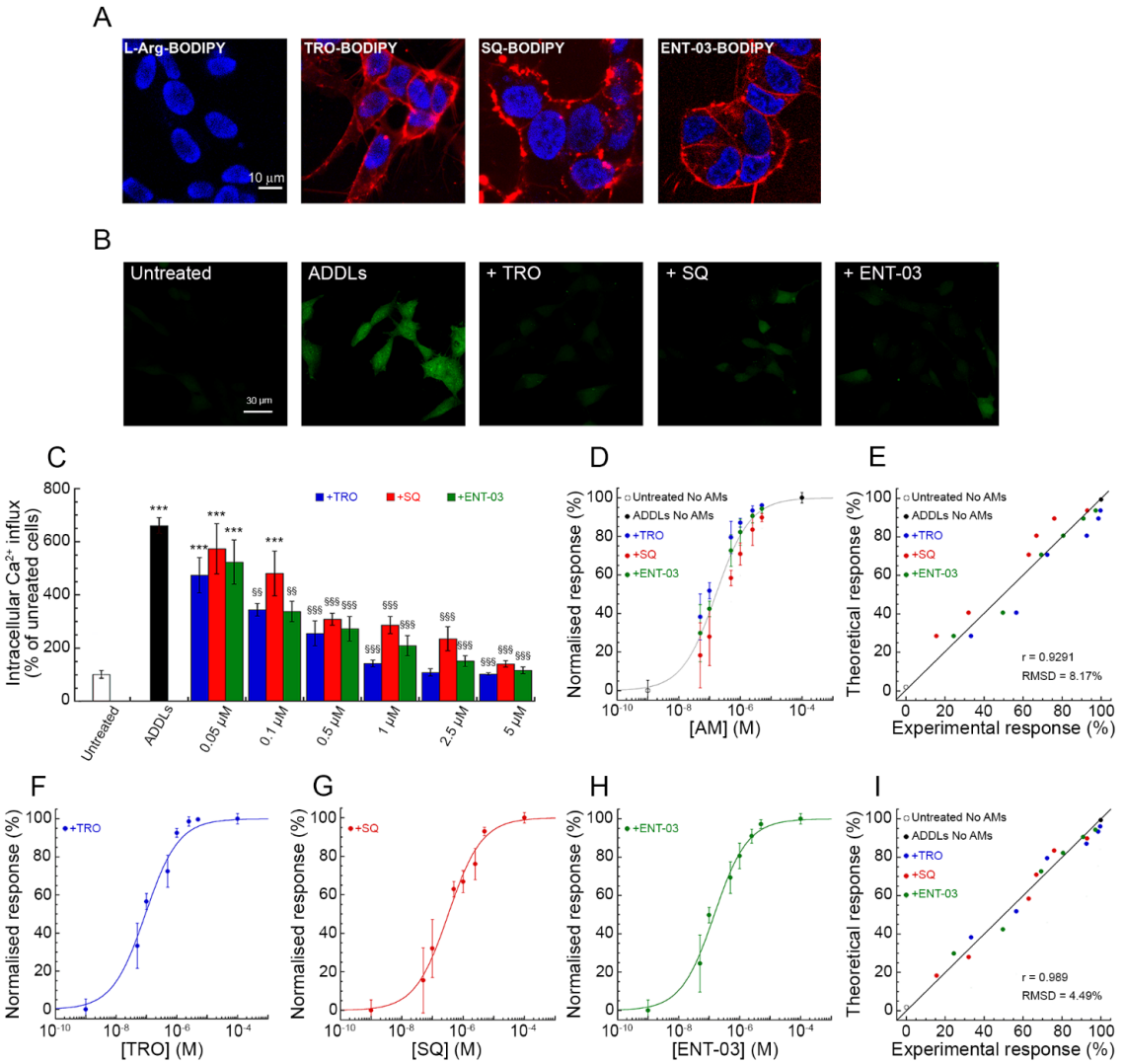

Figure 3.19. The three aminosterols bind to the plasma membrane of SH-SY5Y cells and prevent the increase of intracellular Ca^{2+} levels induced by ADDLs (global fitting analysis). (A) Representative confocal microscopy images of SH-SY5Y cells incubated for 30 min at RT with 5 µM of L-Arg-BODIPY, TRO-BODIPY, SQ-BODIPY, or ENT-03-BODIPY (probe:molecule of 1:10). Blue and red fluorescence indicate Hoechst-labelled nuclei and AM-BODIPY, respectively. **(B)** Representative confocal scanning microscopy images of free Ca^{2+} levels in untreated SH-SY5Y cells or in cells treated for 15 min with 1 µM ADDLs in the absence or presence of 1 µM aminosterols. **(C)** Intracellular free Ca^{2+}-derived fluorescence in untreated SH-SY5Y cells or in cells treated for 15 min with ADDLs in the absence or presence of the indicated concentrations of aminosterols. Experimental errors are SEM (n=4). *** symbols refer to p values <0.001 relative to untreated cells. §§ and §§§ symbols refer to p values <0.01 and <0.001, respectively, relative to ADDLs without aminosterols. **(D)** Normalised dose-response curve obtained from Ca^{2+}-derived fluorescence data of all aminosterols in **(C)** and fitted to Eq. 18. **(E)** Plot reporting theoretical *versus* experimental response values obtained from Eq. 18. **(F,G,H)** Normalised dose-response curves for TRO (blue), SQ (red) and ENT-03 (green) obtained from Ca^{2+}-derived fluorescence data in **(C)**. In each plot, the lines through the data do not represent independent fitting procedures using Eq. 18, but result from global fitting using only Eq. 20, in all cases with corresponding values of ζ potential, *BTF* and FRET data. Experimental errors are SEM (n=4). **(I)** Plot reporting theoretical *versus* experimental response values obtained from Eq. 20.

To improve the agreement and identify the aminosterol-induced membrane alterations responsible for the observed changes of *R* values at corresponding aminosterol concentrations, we recognise two different contributions to the EC_{50} of the aminosterols: the change in charge and the change in packing, which add to an offset EC_{50} value in the absence of these two changes (EC'_{50}):

$$EC_{50} = EC'_{50} + k_{charge} \cdot \Delta\zeta + k_{packing} \cdot \Delta p \tag{19}$$

The two contributions were considered additive, in the absence of knowledge of a well-defined relationship, as generally done in empirical equations (Hastie & Tibshirani, 1990). This leads to a phenomenological Hill equation, where all *R* values were analysed in a multi-variable and multi-parameter global fitting procedure:

$$R = \frac{100}{1 + \left\{\frac{\left(EC'_{50} + k_{charge} \cdot \Delta\zeta + k_{packing} \cdot \Delta p\right)}{[AM]}\right\}^{n}} \tag{20}$$

where $\Delta\zeta$ is the experimentally determined and normalized change of ζ observed upon aminosterol addition (corresponding to the percent values reported in **Table 3.2**); Δp is the experimentally determined and normalized change of lipid distribution and packing observed upon aminosterol addition (corresponding to the averaged three remaining percent values reported in **Table 3.2**); k_{charge} and $k_{packing}$ are the proportionality constants for $\Delta\zeta$ and Δp, respectively; EC'_{50} is a parameter corresponding to EC_{50} when $\Delta\zeta$ and Δp are both equal to 0 and corresponds to the EC_{50} for a hypothetical non-natural aminosterol that does not affect ζ and *p; n* has the same meaning described for Eq. 18.

This equation represents a Hill equation integrated with the $k_{charge} \cdot \Delta\zeta$ and $k_{packing} \cdot \Delta p$ factors. Its three independent variables *(*[*AM*], $\Delta\zeta$ and Δp) are used to express one dependent variable (*R*), upon the global fitting of the four constants (EC'_{50}, k_{charge},

$k_{packing}$ and n) using all the available data. Fitting all R values to Eq. 20 yielded values of $5.94\pm0.59\cdot10^{-7}$ M, $-3.99\pm0.82\cdot10^{-7}$ M, $-1.03\pm0.22\cdot10^{-7}$ M and 0.795 ± 0.015 for EC'_{50}, k_{charge}, $k_{packing}$ and n, respectively. The equation can describe well the behaviour of the three aminosterols plotted separately in three independent graphs (**Fig. 3.19F-H**), where the three solid lines through the data do not represent the results of three independent fitting procedures, but are rather the result of one equation determined from the global fitting. A very good and improved agreement was found between theoretical R values re-determined with Eq. 21 for all three aminosterols and the corresponding experimental R values (**Fig. 3.19I**, r=0.9890, RMSD=4.49%).

The model and resulting Eq. 20 were validated using the leave-one-out cross-validation (LOOCV) method, in which each experimental R value was left out from the analysis, one by one, to re-determine, through the global fitting, the four constants of Eq. 20 and the resulting theoretical R value corresponding to the left-out experimental R value. A good agreement was found between re-determined theoretical *versus* experimental R values (**Fig. 3.20**, r=0.982, RMSD=5.70%), indicating the ability of Eq. 20 to predict new R values that are not present in the analysis.

What can we learn from this analysis? The k_{charge} and $k_{packing}$ values are both negative, indicating that both the partial charge neutralization and compaction of the membrane contribute to the increase of aminosterol potency (corresponding to a decreased EC_{50} value). Their relative contributions amount to 79±7% and 21±7%, respectively, indicating that the charge effect is predominant. A hypothetical non-natural aminosterol that does not affect ζ and p (for example having a monoamine group and a shorter tail on the other side) would have a potency 6-7-fold lower than that of TRO. TRO appears the most effective aminosterol because it produces the highest effects in terms

of both membrane neutralization and compaction. ENT-03 is marginally, albeit significantly, less effective because it has a much lower effect on membrane compaction. This feature accounts for only 21±7% of the effect, therein explaining why its potency is only slightly lower. By contrast, SQ appears markedly less effective because it leads to a much lower change in charge than TRO and ENT-03, despite a packing effect similar to that of ENT-03.

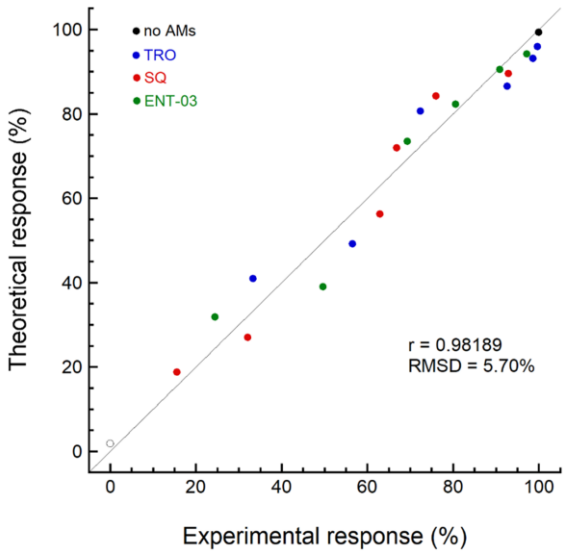

Figure 3.20. Plot reporting theoretical *versus* experimental *R* values obtained using the leave-one-out cross-validation (LOOCV) method. To obtain this plot, each experimental *R* value was left out from the analysis and Eq. 20 was re-determined using the remaining experimental *R* values (four constants and theoretical *R* value corresponding to the one left out).

We also included the different binding affinities (K_D) of the aminosterols for LUVs as a parameter in the global fitting, but this has not resulted in any improvement, particularly because the least protective SQ has also the highest binding affinity for the lipid bilayer, suggesting that binding affinity is a less relevant factor. This can be rationalized by the fact that the lipid concentration is very high in the two-dimensional carpets of cells, making the aminosterols work in a saturation regime similar to that of

high LUV concentration in the conditions explored in **Fig. 3.10**. On different grounds, aminosterol occupancy on the membrane is also not a factor because all aminosterol concentrations tested here on cells (0-5 µM) are well below the aminosterol concentrations determined experimentally at saturation on LUVs (12-50 µM), and the latter are certainly even higher in cell cultures.

3.2.10 Potency and membrane perturbations can be attributed to specific aminosterol chemical groups

To attribute the potency as well as the k_{charge} and $k_{packing}$ parameters and their numerical values to discrete chemical groups within the aminosterols, we repeated the analysis using modifiers of the Hill equation that account for chemical differences between the three aminosterols ($a_{polyamine}$ and $a_{SO3/COO}$) rather than experimental observables ($\Delta\zeta$ and Δp):

$$R = \frac{100}{1 + \left\{\frac{(EC'_{50} + a_{polyamine} + a_{SO3/COO})}{[AM]}\right\}^{n}} \quad (21)$$

where *[AM]* and *R* are the independent and dependent variables, respectively; EC'_{50}, $a_{polyamine}$ and $a_{SO3/COO}$ are constants free to float in the global fitting analysis using all the available data. $a_{polyamine}$ and $a_{SO3/COO}$ are parameters accounting for the change of the EC'_{50} parameter when a spermine, rather than a spermidine, and a $-SO_3^-$, rather than a $-COO^-$ group, are present in the aminosterol, respectively. The two parameters were constrained to 0 when the spermine and $-SO_3^-$ groups were absent and replaced by spermidine and carboxylate, respectively. Fitting all *R* values to Eq. 21 yielded values of

$3.83\pm0.39\cdot10^{-7}$ M, $-2.36\pm0.47\cdot10^{-7}$ M and $-0.55\pm0.12\cdot10^{-7}$ M for EC'_{50}, $\alpha_{polyamine}$ and $\alpha_{SO3/COO}$, respectively (r=0.9820, RMSD=4.50%).

The $\alpha_{polyamine}$ and $\alpha_{SO3/COO}$ values were again found to be negative, indicating that the longer spermine and SO_3^--containing tail cause a potency increase (or EC_{50} decrease) relative to a hypothetical non-natural aminosterol having a spermidine and carboxylate group. They account for 81±7% and 19±7% of the effect, respectively, in good agreement with the values obtained with the experimental analysis and confirming that the charge effect of the polyamine is predominant over the chemistry of the tail on the other side of the molecule that causes a redistribution of lipids and increased packing. The net positive charge of aminosterols allows a larger decrease of the negative charge of the cell membrane provided by GM1, which is a physicochemical change reported to be crucial in protecting biological membranes from Aβ oligomer binding and resulting cell toxicity also using other compounds, such as europium positive ions (Williams et al., 2015). The EC'_{50} value obtained for the hypothetical non-natural aminosterol with spermidine and carboxylate ($3.83\pm0.39\cdot10^{-7}$ M), which is higher than that of any aminosterol analysed here having at least the spermine (triamine) or SO_3^- group, is lower than the hypothetical non-natural aminosterol of the previous analysis having a monoamine group and a shorter tail on the other side ($5.94\pm0.59\cdot10^{-7}$ M). Since all natural and non-natural aminosterols studied here have a steroid scaffold their EC_{50} values remain in the 10^{-8}-10^{-7} M range.

3.3 Study of the interaction of Brb with lipid membranes and its potential role against misfolded protein oligomers

3.3.1 Brb interacts with the membrane of LUVs

The natural compound Brb possesses a predominantly hydrophobic structure and has been reported to be able to cross the blood–brain barrier (Wang et al., 2005; Tan et al., 2013; Shou & Shaw, 2022), so we first assessed whether this alkaloid could be able to interact with the membrane of LUVs with different lipid compositions. Therefore, we used LUVs with two different lipid compositions: model-LUVs composed of 65% (mol) DOPC, 33% (mol) SM, 1% (mol) CHOL and 1% (mol) GM1, known to exhibit an optimal segregation of lipids into distinct domains and widely used in the previous sections and works (Oropesa-Nuñez et al., 2016; Errico et al., 2020; Barletti et al., 2023); and neuronal LUVs composed of 44% (mol) DOPC, 16% (mol) SM, 35% (mol) CHOL and 5% (mol) GM1, enriched in CHOL and GM1 content to better mimic the lipid composition of neuronal membranes (Ingólfsson et al., 2017).

In a first experiment, we labelled LUVs with TMA-DPH and DPH, incubated them with increasing concentrations of Brb, and we observed a reduction in the fluorescent emission of these two lipophilic probes with the increase of Brb concentration using both LUV compositions (**Fig. 3.21**). In particular, in all conditions we observed a linear quenching at low concentrations of Brb, and an exponential trend at higher concentrations, suggesting the coexistence of both dynamic and static quenching (Lakowicz, 2006) (**Fig. 3.21**). We then first fitted the obtained data with a linear Stern-Volmer equation (Eq. 5) up to 30 and 50 µM for LUVs labelled with DPH and TMA-DPH, respectively, in order to obtain K_{SV} values, and then we obtained K_{ST} values with Eq. 7, as

described in section 2.13 (**Fig. 3.21**). Brb induced a higher quenching on DPH-labelled LUVs (**Fig. 3.21C,D**) than TMA-DPH-labelled (**Fig. 3.21A,B**), suggesting that, unlike aminosterols, this alkaloid interacts more deeply within the hydrophobic core of the bilayer. Moreover, the quenching was higher in neuronal-LUVs (**Fig. 3.21B,D**) than model-LUVs (**Fig. 3.21A,C**) with both the probes used, suggesting a higher affinity of Brb for neuronal LUVs. More generally, these results indicate that Brb is able to interact with both model- and neuronal-LUVs.

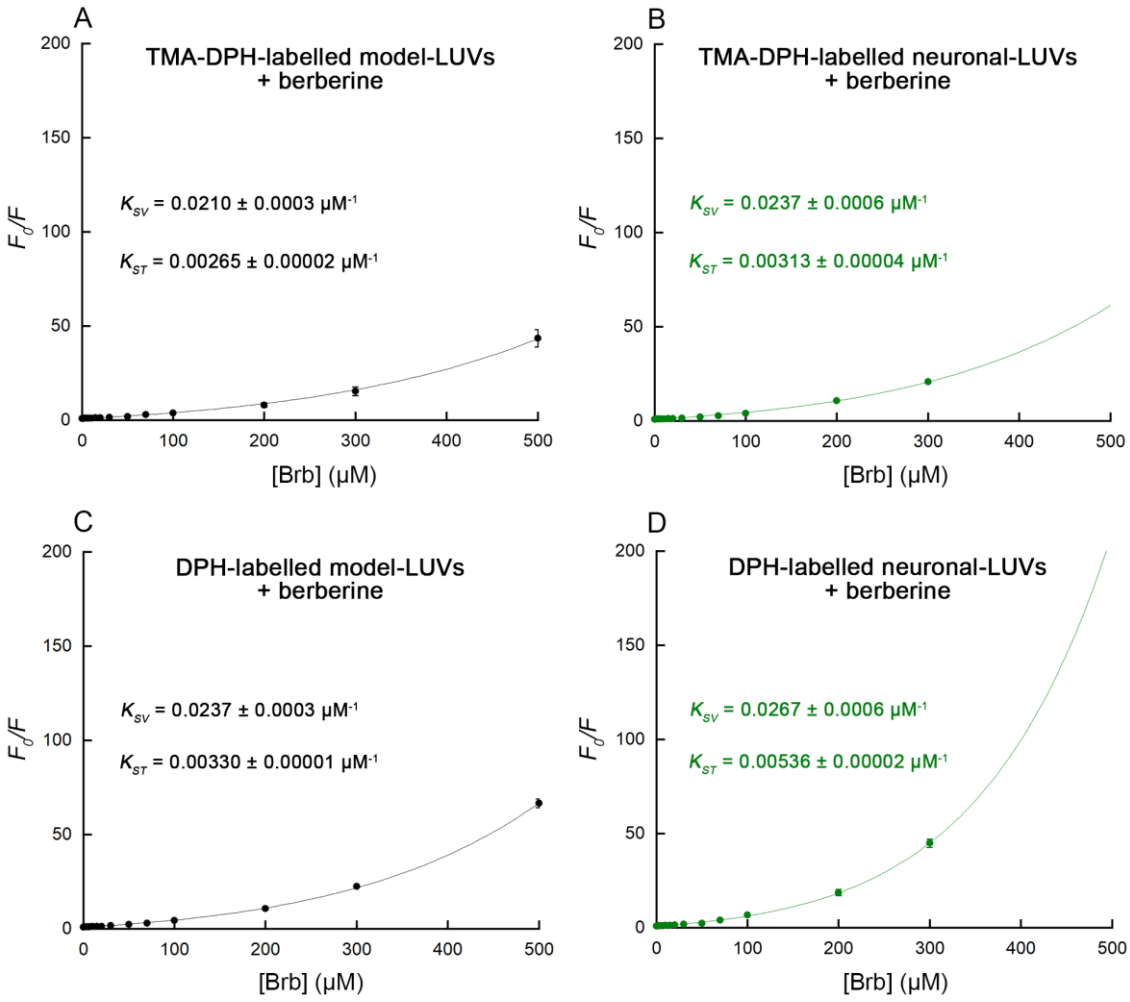

Figure 3.21. Interaction of Brb with LUVs. Stern-Volmer plot of (**A,C**) model-LUVs and (**B,D**) neuronal-LUVs labelled with TMA-DPH (**A,B**) and DPH (**C,D**) and incubated with increasing concentrations of Brb. K_{SV} and K_{ST} values were obtained by fitting the plots with Eq. 5 and Eq. 7, as described in section 2.13. Experimental errors are SEM of 3-7 experiments.

To obtain an independent measure of the interaction between Brb and LUVs, and to rule out that the interaction observed with fluorescence quenching experiments could depend on the lipophilic probe's properties, we then probed the incorporation of Brb within unlabelled LUVs. To this aim, a light scattering analysis was carried out using model-LUVs and neuronal-LUVs incubated with increasing concentrations of Brb, on the theoretical grounds that incorporation of Brb within LUVs membranes causes an increase of LUV mass and, consequently, light scattering intensity (**Fig. 3.22**). As reported in section 3.2.3, light scattering intensity is proportional to the second power of the mass of the light scattering particles, so by plotting the square root of the ratio of light scattering intensity with Brb and light scattering intensity without Brb ($sqrt(I_{Brb}/I_{NO})$) *versus* Brb concentration, it was possible to measure the increase of mass upon Brb addition (**Fig. 3.22**).

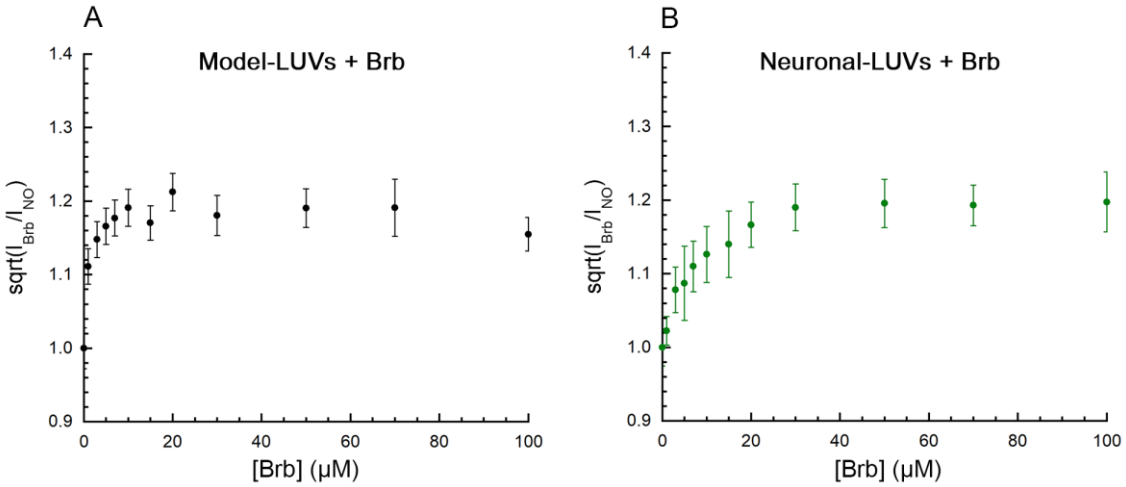

Figure 3.22. Light scattering intensity of LUVs in the presence of increasing concentrations of Brb. Plot reporting the square root of the light scattering intensity of (**A**) model-LUVs and (**B**) neuronal-LUVs with (I_{Brb}) and without (I_{NO}) Brb, respectively, *versus* Brb concentration, representing the increase in LUV mass due to Brb incorporation. The count rate values measured with corresponding Brb concentrations in the absence of LUVs were subtracted from those measured with both Brb and LUVs to remove Brb light scattering contribution. Experimental errors are SEM of at least 3 experiments.

In particular, at saturating concentration of Brb, mass increases of 1.17 ±0.008 and 1.194±0.002 were obtained for model- and neuronal-LUVs, respectively. Brb was therefore able to bind to both types of LUVs, confirming fluorescence quenching results. Moreover neuronal-LUVs displayed a higher mass increase upon Brb addition compared to model-LUVs, indicating a higher incorporation of Brb in this type of LUVs, in agreement again with fluorescence quenching results where higher K_{SV} values were obtained for neuronal-LUVs. DLS experiments ruled out an increase of LUV diameter upon Brb addition (data not shown). Therefore, the remarkable mass increase by about 15-20% suggests that Brb micelles also incorporate on LUV surfaces, causing an increase of mass and light scattering intensity.

In a third experiment, we performed an equilibrium dialysis experiment incubating Brb without and with model- and neuronal-LUVs and then dialysing these samples against phosphate buffer, to investigate the binding of Brb to LUVs, and a possible incorporation of this alkaloid within LUV membranes. In particular, 2 ml of a solution containing 30 µM Brb with 0.2 mg/ml model-LUVs, 30 µM Brb with 0.2 mg/ml neuronal-LUVs and 30 µM Brb without LUVs were dialysed against 3 ml of 100 mM sodium phosphate buffer, pH 7.0 for 24 h. Then, the fluorescence spectra of the permeates resulting from these three different samples were acquired by exploiting the intrinsic fluorescence of Brb (**Fig. 3.23A**). By interpolating the measured fluorescence emission value of the permeate with a calibration curve obtained from different known concentrations of Brb (Eq. 16), it was possible to measure the fraction of Brb that was free to cross the dialysis membrane and, by difference, the fraction that was retained in the inner chamber (retentate), which interacted stably with LUVs or that was incorporated within them (**Fig. 3.23B**).

The permeate derived from 30 µM Brb in the absence of LUVs contained a concentration of 9.8±0.2 µM Brb (**Fig. 3.23B**) rather than an expected concentration of 12 µM, indicating that a small fraction of this alkaloid (2.2±0.2 µM) interacted with the dialysis membrane and could not cross it. The permeates derived from 30 µM Brb incubated with 0.2 mg/ml of model- and neuronal-LUVs contained 7.7±0.8 µM and 5.3±0.9 µM, respectively (**Fig. 3.23B**). By subtracting the permeate Brb concentration in the presence of LUVs from that measured in the absence of LUVs, in was possible to obtain the actual Brb concentration incorporated in LUVs, which appeared to be 2.1±0.8 µM and 4.5±0.9 µM for model- and neuronal-LUVs, respectively. These results confirmed the interaction of Brb with both types of LUVs and indicated that neuronal-LUVs incorporated a slightly higher fraction of Brb than model-LUVs, in agreement with the fluorescence quenching and light scattering results.

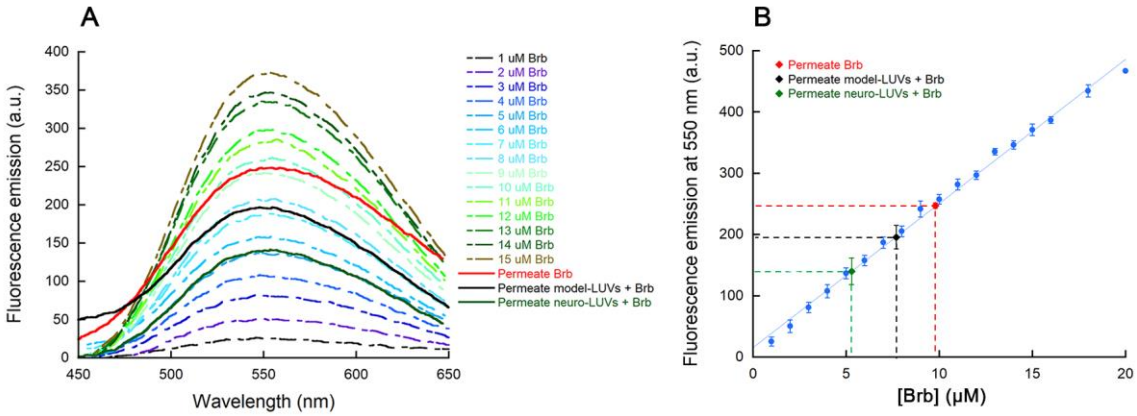

Figure 3.23. Equilibrium dialysis of Brb incubated with LUVs. (A) Fluorescence spectra of the permeates derived from 24 h dialysis of 30 µM Brb (red); 30 µM Brb incubated with 0.2 mg/ml model-LUVs (black) and 30 µM Brb incubated with 0.2 mg/ml neuronal-LUVs (green). The plot also reports the fluorescence spectra of different known Brb concentrations (dashed lines). **(B)** Calibration curve reporting the fluorescence emission values at 550 nm of known concentrations of Brb. Data were fitted with Eq. 16. Fluorescence emission values at 550 nm of the three permeates described in (**A**) are also indicated, using the same colour code. Experimental errors are SEM of 3 experiments.

3.3.2 Brb stiffens the membrane of LUVs

Since Brb exhibited the ability to interact with the lipid bilayer of labelled and unlabelled LUVs, we then investigated the effect of this alkaloid on the rotational diffusion of TMA-DPH and DPH embedded in LUVs, and then on the packing of lipids in LUVs. To this aim, we performed fluorescence anisotropy experiments as a function of Brb concentration, using model- and neuronal-LUVs labelled with TMA-DPH and DPH, and incubating them with increasing concentrations of Brb. In the absence of Brb, the anisotropy (*r*) of DPH was lower than that of TMA-DPH in both model- and neuronal-LUVs, reflecting the lower degree of molecular packing of the lipids in the hydrophobic portion of the bilayer relative to the polar region, with consequent higher rotational freedom of DPH than TMA-DPH (Collins et al., 1990). Moreover, with both probes, neuronal-LUVs exhibited higher *r* values than model-LUVs in the absence of Brb, reflecting the greater packing of lipids induced by the higher CHOL content in the former type of LUVs (Chakraborty et al., 2020).

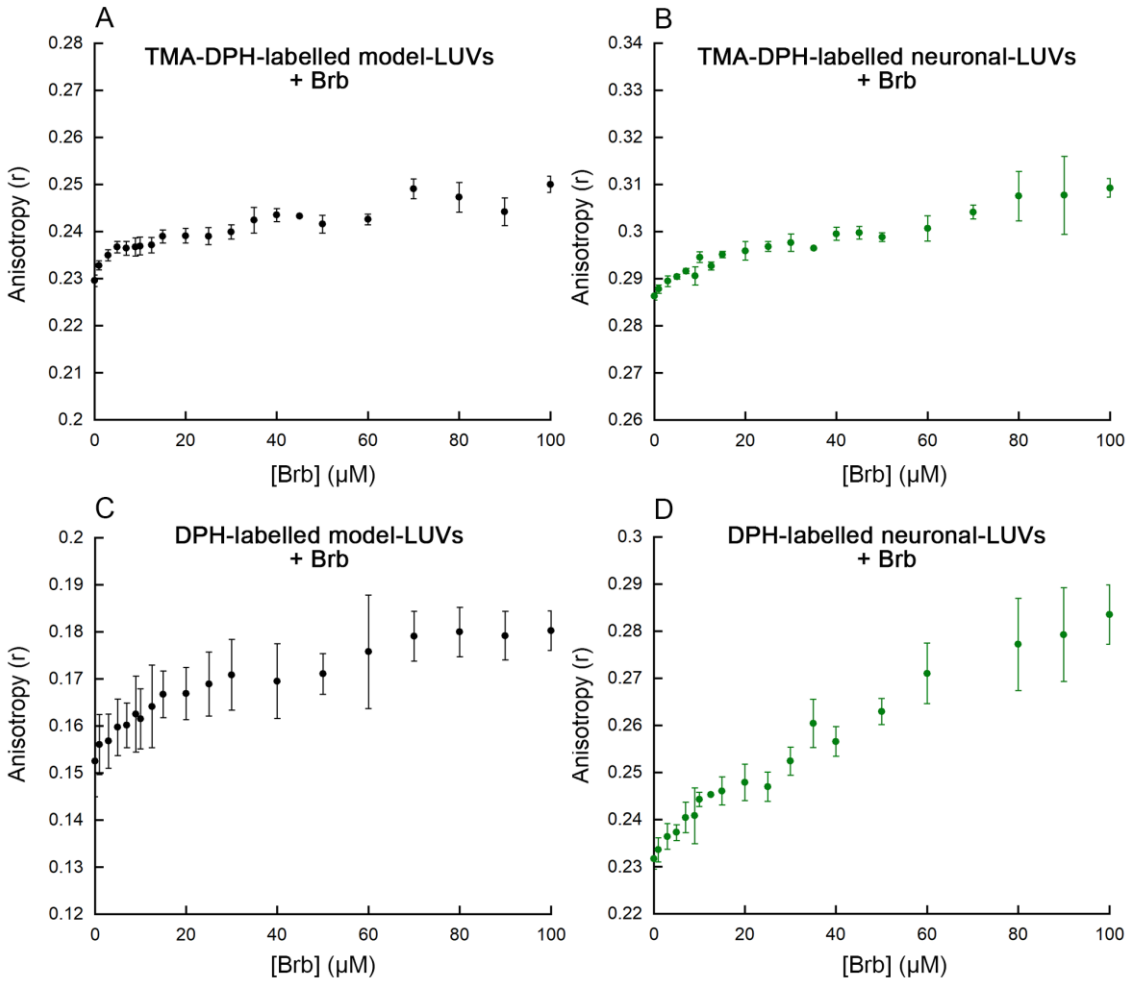

Figure 3.24. Fluorescence anisotropy of probes embedded in LUVs as a function of Brb concentration. Anisotropy (*r*) values of model-LUVs (**A,C**) and neuronal-LUVs (**B,D**) labelled with TMA-DPH (**A,B**) and DPH (**C,D**) in the presence of increasing concentrations of Brb. Experimental errors are SEM of at least 5 experiments.

The addition of Brb appeared to further stiffen their membranes, as indicated by an increase of probe fluorescence anisotropy in the presence of increasing concentration of Brb. The higher packing of lipids induced by Brb involved both the superficial polar heads region of the bilayer, as observed with TMA-DPH-labelled LUVs (**Fig. 3.24A,B**), and its hydrophobic core, as observed with DPH-labelled LUVs (**Fig. 3.24C,D**). Nevertheless, the increase of fluorescence anisotropy was higher for DPH than TMA-DPH in both LUV types, suggesting a larger stiffening of the membrane in the hydrophobic core of the lipid bilayer (**Fig.3.24**), probably as a result of the higher affinity of Brb for this portion of the

membrane, as indicated by fluorescence quenching experiments. From these data it emerges that the interaction of Brb with LUVs influences the degree of rotational diffusion of both TMA-DPH and DPH embedded in LUVs, particularly the latter, in both model- and neuronal-LUVs, stiffening the bilayer in a concentration-dependent manner.

The impact of Brb on the rotational diffusion of TMA-DPH and DPH in LUVs, and therefore, on the packing of lipids, was also investigated by temperature-dependent probe fluorescence anisotropy. In fact, changes in the temperature-dependent fluorescence anisotropy upon Brb addition reflect perturbations in the probe rotational correlation time (Lúcio et al., 2006; Alves et al., 2017). As the temperature increased, the fluorescence anisotropy decreased for both probes and in both types of LUVs (**Fig. 3.25**), as expected following the temperature-dependent increase of fluidity of the membrane with temperature with resulting increase of the rotational freedom of the two fluorophores (Collins et al., 1990; Alves et al., 2017; Errico et al., 2020). The presence of Brb induced a significant increase of the fluorescence anisotropy of both TMA-DPH and DPH, particularly the latter, at all temperatures and with both model- and neuronal-LUVs (**Fig. 3.25**), confirming that Brb interacts with both the polar heads and the hydrophobic regions of the bilayer, and that this effect exerts an overall stiffing of the lipid bilayer.

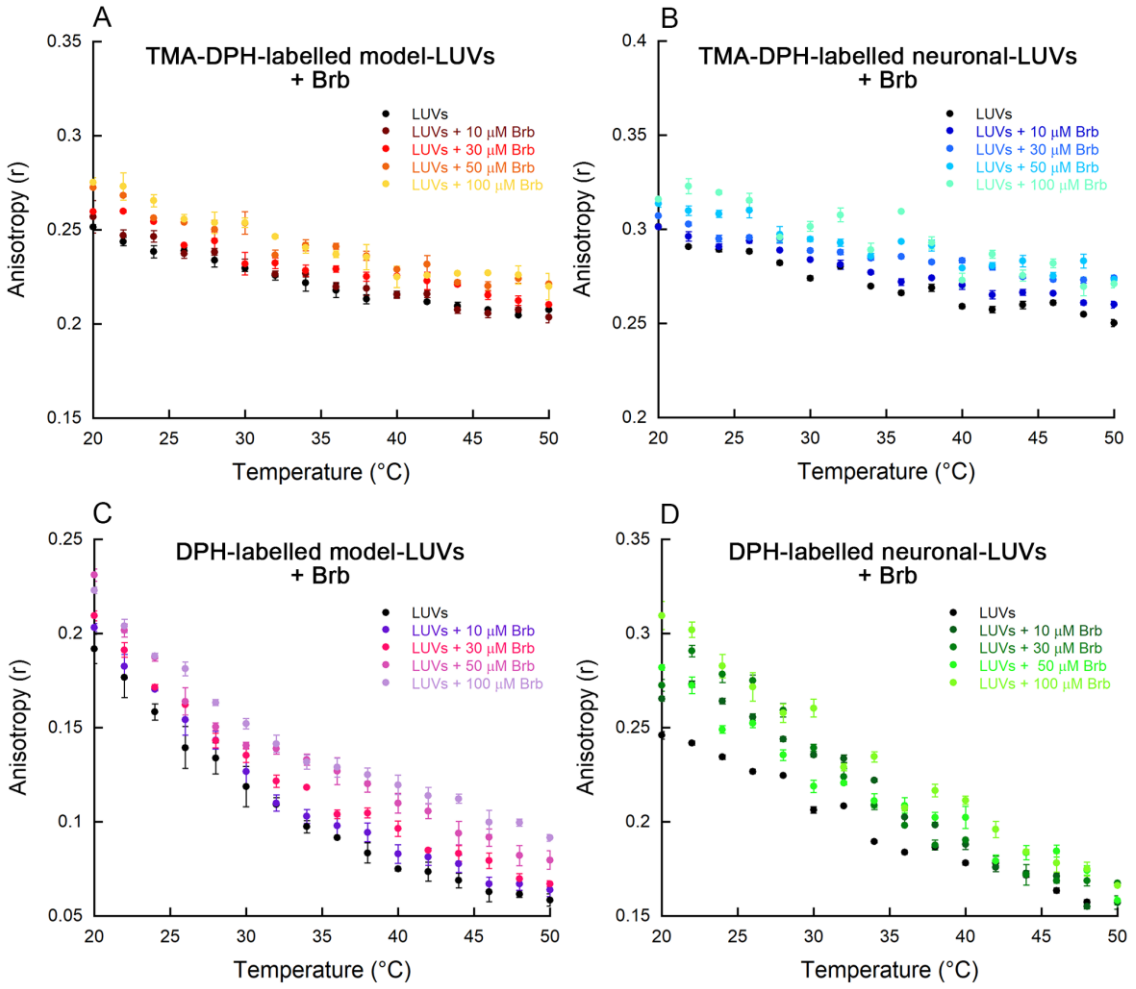

Figure 3.25. Temperature-dependent fluorescence anisotropy of probes embedded in LUVs in the presence of Brb. model-LUVs (**A,C**) and neuronal-LUVs (**B,D**) labelled with TMA-DPH (**A,B**) and DPH (**C,D**) in the absence and presence of the indicated concentrations of Brb. Experimental errors are SEM of at least 3 experiments.

3.3.3 Brb reduces the binding affinity of OAs for LUVs

Since Brb displayed the ability to bind to the membrane of LUVs, and to induce an overall stiffening of the lipid bilayer, we then investigated whether Brb could induce a variation of the affinity of OAs for the membrane, similarly to what was observed with TRO in Section 3.1.4. To this aim, we prepared TMA-DPH-labelled model- and neuronal-LUVs incubated with 30 µM Brb, and then we incubated them with increasing concentrations of unlabelled OAs (**Fig. 3.26**). The presence of Brb in model-LUVs induced a significant reduction of TMA-DPH fluorescence quenching relative to the same LUVs without Brb,

with an almost complete absence of quenching at low concentrations of OAs up to *ca*. 6 µM (**Fig. 3.26A**). At higher concentrations of OAs, the TMA-DPH quenching was evident, but remained lower than that observed in the absence of Brb at corresponding OAs concentrations, showing a reduction of the affinity of OAs for LUVs (**Fig. 3.26A**). With neuronal-LUVs, data were more challenging to decipher, since at low concentrations of Brb we observed an increased quenching, that then decreased until *ca.* 10 µM OAs, and then again proportionally increased as observed with OAs in the absence of Brb (**Fig. 3.26B**).

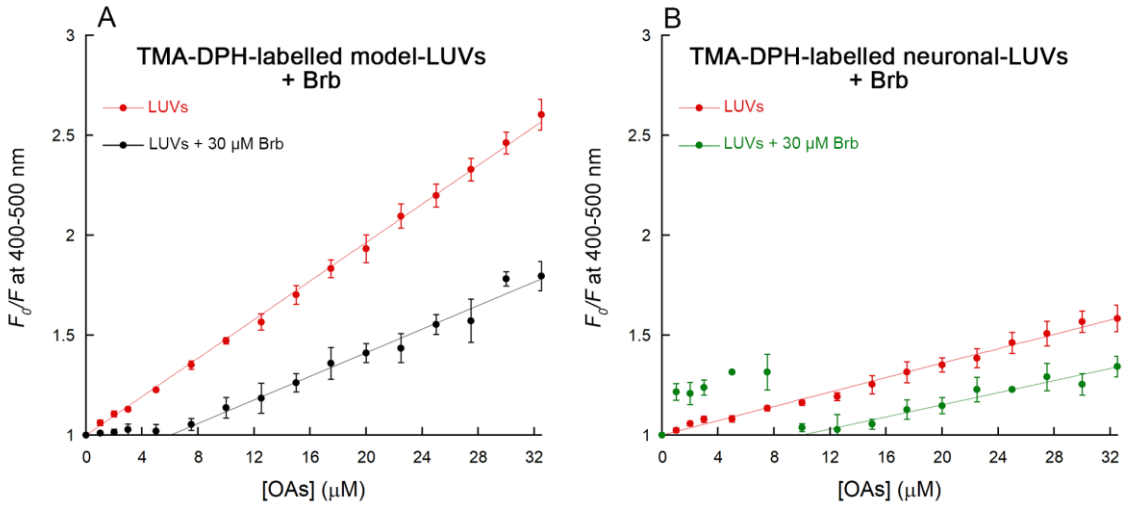

Figure 3.26. Interaction of OAs with LUVs with and without Brb. Stern−Volmer plots reporting the ratio of fluorescence of TMA-DPH in the absence (F_0) or presence (F) of various concentrations (monomer equivalents) of OAs, in the absence (red) and presence of 30 µM Brb in (**A**) model-LUVs and (**B**) neuronal-LUVs. The straight lines through the data points represent the best fits to Eq.6 and 5, in the presence and absence of Brb, respectively. Experimental errors SEM of 5 experiments.

This atypical trend could reflect the differences in lipid proportions used in neuronal-LUVs compared to model-LUVs. In neuronal-LUVs the proportion between DOPC and SM were maintained in a molar ratio of ca. 2:1 (mol/mol), but CHOL and GM1 contents were significantly increased from 1% (mol) to 35% (mol) and from 1% (mol) to

5% (mol), respectively. To investigate whether the increased content of one of these two lipids could affect the quenching trend, we repeated the experiment increasing one lipid species at a time in modified LUVs: LUVs+CHOL, composed of 43% DOPC, 21% SM, 35% CHOL, 1% GM1; and LUVs+GM1, composed of 63% DOPC, 31% SM, 1% CHOL, 5% GM1. First, we incubated LUVs for 15 min with increasing concentrations of OAs, and then we repeated the experiment pre-incubating LUVs for 15 min with 30 µM Brb (**Fig. 3.27**).

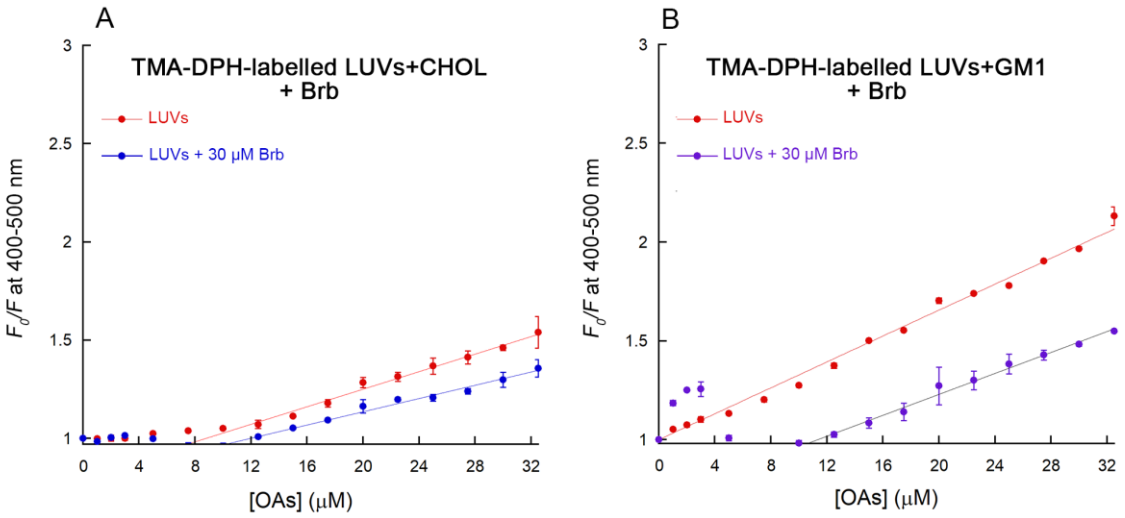

Figure 3.27. Interaction of OAs with LUVs enriched with CHOL or GM1 with and without Brb. Stern–Volmer plots reporting the ratio of fluorescence of TMA-DPH in the absence (F_0) or presence (F) of various concentrations (monomer equivalents) of OAs, in the absence (red) and presence of 30 µM Brb in (**A**) LUVs enriched in CHOL content (43% DOPC, 21% SM, 35% CHOL, 1% GM1) and (**B**) LUVs enriched in GM1 content (63% DOPC, 31% SM, 1% CHOL, 5% GM1). The straight lines through the data points represent the best fits to Eq. 6 (**A**) and to Eq. 6 and 5 (**B**), in the presence and absence of Brb, respectively. Experimental errors SEM of 3 experiments.

The fluorescence quenching of TMA-DPH in LUVs+CHOL in the absence of Brb was significantly lower than that observed with model-LUVs, and similar to that observed with neuronal-LUVs (**Fig. 3.27A**). This interesting behaviour was observed in previous studies, where membrane CHOL modulation, and in particular CHOL enrichment, affected oligomer-induced cell disfunction, resulting in a significant decrease of interaction of toxic oligomer with the cell membrane and internalisation (Evangelisti et

al., 2012; Evangelisti et al., 2016). The incubation of LUVs+CHOL with Brb displayed a further decrease of OAs quenching ability and therefore a further lower affinity of these toxic species for LUVs (**Fig. 3.27A**), similarly to observations with neuronal-LUVs. On the other hand, the quenching of TMA-DPH in LUVs+GM1 in the absence of Brb was linearly dependent on OAs concentration and fitted well with Eq. 5, as observed in model- and neuronal-LUVs. The addition of Brb determined the same atypical trend observed in neuronal-LUVs in the presence of Brb, but the overall OA-induced fluorescence quenching was lower than in neuronal-LUVs (**Fig. 3.27B**).

These results suggest that the content of GM1 somehow alters the quenching trend of low concentrations of OAs in the presence of Brb, and in the future we will need to better understand this effect, since it could indicate a direct binding of Brb to this key lipid.

3.3.4 Brb reduces OAs ANS binding

Since Brb appeared to interact with the membrane of our LUVs and inhibit the binding of OAs to them, we then decided to investigate whether this alkaloid was also able to directly interact with misfolded protein oligomers in the absence of LUVs and possibly affect their morphology and structure. To this aim, we used the fluorescent probe 8-anilinonaphthalene-1-sulfonate (ANS) to see whether the incubation of OAs with Brb could affect the hydrophobic exposure of this misfolded species. ANS is a fluorescent probe able to bind to solvent-exposed hydrophobic clusters and generates a marked increase in its fluorescence emission intensity and a blue shift of its maximum emission wavelength (Cardamone et al., 1992; Thirunavukkuarasu et al., 2008); ANS is widely used

to study hydrophobic exposure of misfolded protein oligomers (Campioni et al., 2010; Chiti & Dobson, 2017).

Since Brb is a predominantly hydrophobic molecule, we first performed a control experiment with ANS and Brb alone in the absence of OAs, to rule out a possible direct binding of Brb to ANS. We incubated 50 and 100 µM ANS with increasing concentrations of Brb (**3.28A,B**). The absence of changes in the fluorescence spectra of ANS at all Brb concentrations confirmed the absence of a binding between this alkaloid and the fluorescent probe.

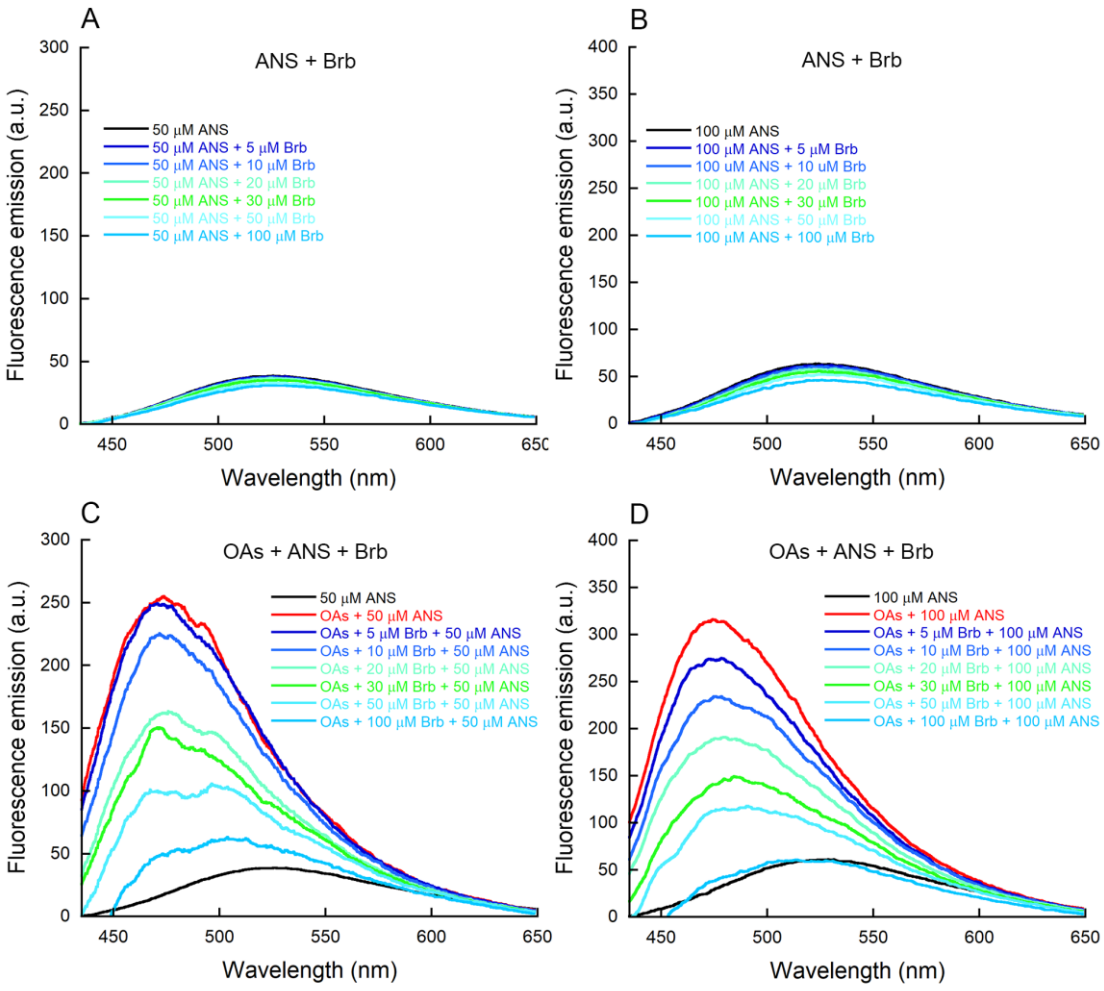

Figure 3.28. OAs binding to ANS in the absence and presence of Brb. Fluorescence spectra of 50 µM (**A**) and 100 µM (**B**) ANS incubated with increasing concentrations of Brb alone without OAs. Fluorescence spectra of 50 µM (**C**) and 100 µM (**D**) ANS incubated with OAs in the absence and presence of increasing concentration of Brb (5-100 µM).

The fluorescence spectra of ANS alone displayed a low fluorescence emission and a peak at *ca.* 510-530 nm, whereas we observed a significant increase in fluorescence emission and a blue shift of the peak wavelength to 470-490 nm when ANS was incubated with OAs, revealing the exposure of hydrophobic groups on the surface of the OAs (**Fig. 3.28C,D**). After the pre-incubation of OAs with increasing concentrations of Brb, we observed a progressive decrease in ANS fluorescence emission and a red shift of the peak wavelength to values similar to unbound ANS (**Fig. 3.28C,D**). These results suggest that the pre-incubation between Brb and OAs induced a reduction of the exposure to the solvent of hydrophobic clusters of these oligomeric species.

3.3.5 Brb does not affect the secondary structure of OAs

To further study the interaction between Brb and OAs, we used far-UV CD spectroscopy to investigate whether Brb could change the secondary structure of OAs. We incubated OAs with increasing concentrations of Brb for 15 min and then we acquired far-UV CD spectra (**Fig. 3.29A**). In the presence of Brb, we observed a modest flattening of the far-UV CD spectrum of OAs, without significant changes in the spectrum shape (**Fig. 3.29A**). To evaluate whether this flattening of the spectra could be related to a real change in secondary structure or rather to the impact of Brb on the overall absorbance of the sample, we measured the HT signal at 208 nm (**Fig. 3.29B**) and 222 nm (**Fig. 3.29C**) of Brb alone and we compared these data with those of OAs incubated with the corresponding concentrations of Brb. The HT signals at the two wavelengths increased linearly and proportionally with Brb concentration alone, and the same trends and slopes were observed for Brb in the presence of OAs (**Fig. 3.29B,C**). This suggests that the flattening of the far-UV CD spectra of OAs in the presence of Brb is not determined

by changes in secondary structure induced by Brb, but rather by the progressive increase in the HT signal.

Overall, Brb appears to bind to OAs in the absence of LUVs and decrease their solvent exposure of hydrophobic clusters while maintaining their intact secondary structure.

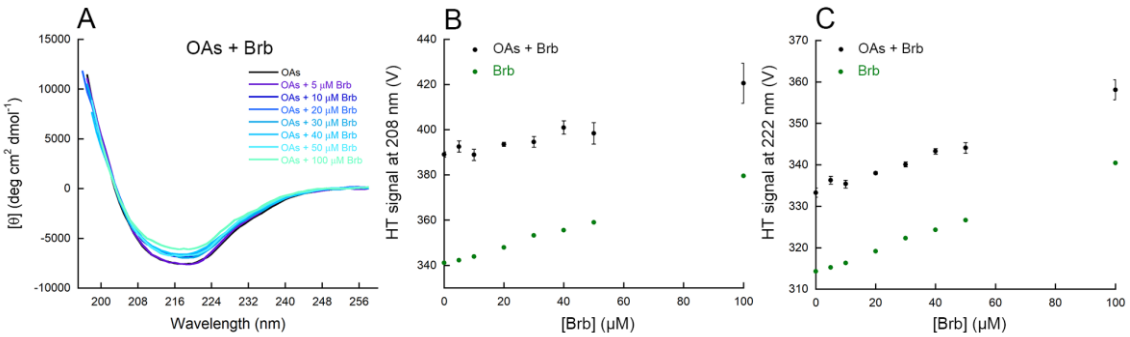

Figure 3.29. Far-UV CD spectra of OAs incubated with Brb. (**A**) Far-UV CD spectra of 10 µM OAs (monomer equivalents) in the absence and presence of increasing concentrations of Brb. (**B,C**) HT values at 208 and 222 nm as a function of Brb concentration.

4. Discussion and conclusion

Many neurodegenerative diseases are associated with the self-assembly of peptides and proteins into fibrillar aggregates. Soluble misfolded oligomers formed during the aggregation process, or released by mature fibrils, play a relevant role in neurodegenerative processes, and their aberrant interactions with neuronal membranes represent an important event in the mechanism through which these oligomeric species manifest their toxicity.

The two natural aminosterols TRO and SQ, firstly isolated from the shark *Squalus acanthias*, are considered promising drug candidates in the context of neurodegenerative diseases, like AD and PD, since they have shown the ability to inhibit the interaction of misfolded protein oligomers with biological membranes, *in vitro* (cultured cells) and *in vivo* (*C. elegans*), as well as to dramatically change amyloid fibril formation by Aβ and αS *in vitro* using isolated proteins (Perni et al., 2017; Perni et al., 2018; Limbocker et al., 2019; Limbocker et al., 2022). One relevant protective mechanism exerted by aminosterols occurs via their binding to biological membranes, and a previous study conducted on TRO revealed that this small molecule is incorporated into lipid membranes, particularly within their superficial hydrophilic portion and the interface with the hydrophobic portion (Errico et al., 2020). Through this binding, TRO appeared able to modulate the physicochemical properties of lipid membranes, by reducing their net charge, increasing the mechanical resistance to indentation and remodelling the spatial distribution of CHOL/GM1 lipids (Errico et al., 2020). All these alterations are known to contribute significantly to an increased resistance of the cell

membranes to the toxic action of misfolded protein oligomers (Errico et al., 2020; Limbocker et al., 2022).

Another natural compound with peculiar therapeutic properties that suggest a potential protective effect in the context of neurodegenerative diseases is represented by the plant alkaloid Brb, which have been reported to possess antioxidant and anti-inflammatory activities and to protect neuronal cells from death induced by oxidative stress, by reducing ROS generation and upregulating a cytoprotective enzyme with neuroprotector functions (Bae et al., 2013). Unlike aminosterols, there is no evidence that Brb interacts with the lipid bilayer of biological membranes.

In the first part of the thesis (Section 3.1), we used liposomes in the form of LUVs composed of a variable and biologically compatible lipid composition and a pair of toxic/nontoxic oligomers formed by the same model protein HypF-N to measure quantitatively the affinity of the two oligomeric species for lipid membranes and possible changes induced by variations of lipid composition or addition of TRO. First, we measured the interaction of toxic/nontoxic oligomers and native HypF-N with the membrane through the fluorescence quenching of two lipophilic probes embedded in the polar and apolar regions of the lipid membranes, and a well-defined membrane-oligomer binding assay using fluorescently labelled oligomers and unlabelled LUVs, to determine the Stern-Vomer (K_{SV}) and dissociation constants (K_D), respectively. With both approaches, we found that toxic oligomers have a membrane affinity 20-25 times higher than that of nontoxic oligomers. Interestingly, the binding with the lipid membranes is not associated with a change in structure in none of the HypF-N species investigated, as observed with far-UV CD, intrinsic fluorescence and FRET.

Using liposomes enriched with TRO, we found that the membrane affinity of toxic oligomers was significantly lower and at protective concentrations of the small molecule (5 µM TRO and < 10 µM monomer equivalents OAs), the binding of the OAs to the lipid membranes of LUVs was fully prevented. Furthermore, the affinity of toxic oligomers for the lipid membranes of LUVs was found to increase and slightly decrease with GM1 ganglioside and CHOL content, respectively, indicating that physicochemical properties of lipid membranes of LUVs can modulate their affinity for misfolded oligomeric species (**Fig. 4.1**).

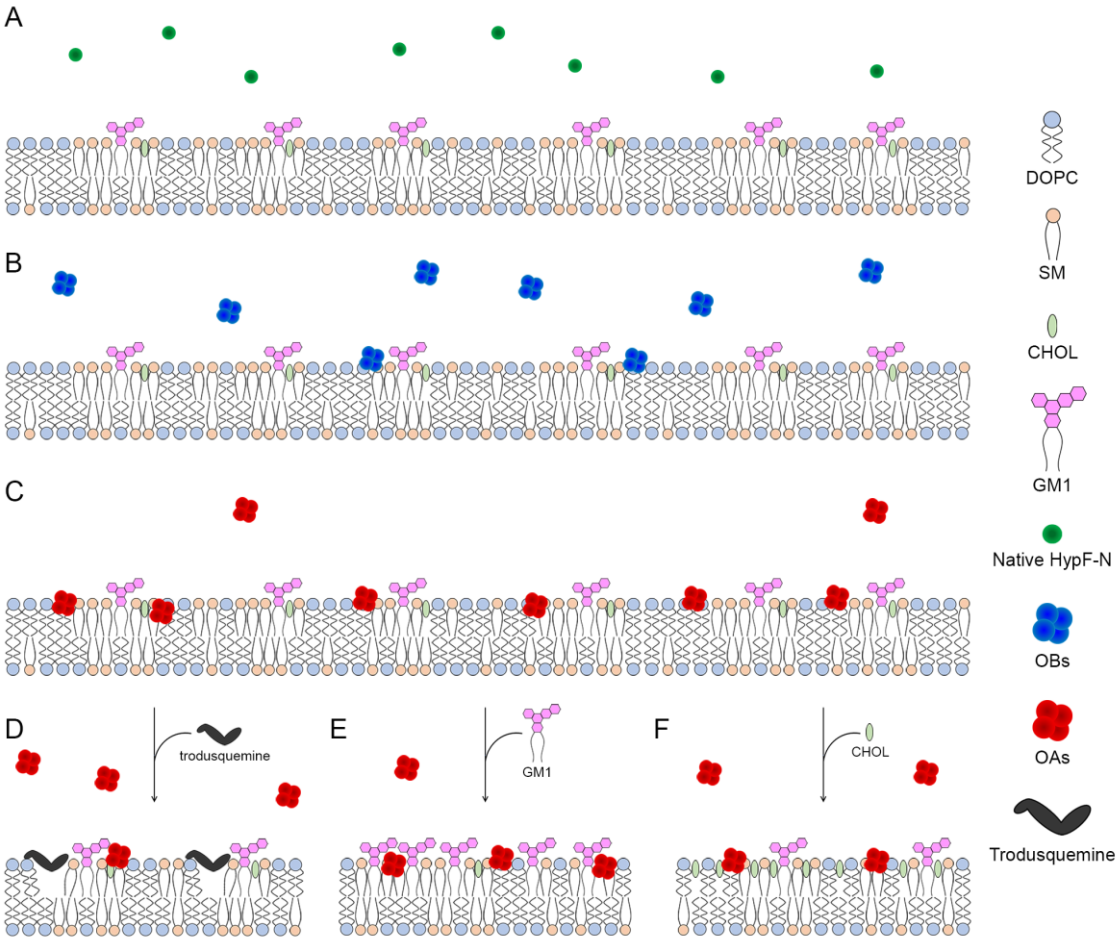

Figure 4.1. Summary of the results obtained on the affinity of OAs and OBs for LUV lipid membranes. **(A-C)** Schematic representation of the affinity of the native protein (green, no affinity) (**A**), OBs (blue, low affinity) **(B)** and OAs (red, high affinity) **(C)** for the LUV lipid membrane. **(D-F)** Change of the affinity of OAs for the membrane due to addition of TRO (decreased affinity) (**D**), increase of GM1 concentration (increased affinity) (**E**) and increase of CHOL concentration (slightly decreased affinity) (**F**) in LUVs.

Taken together, these results indicate that the toxicity of the oligomers depends on their ability to bind and penetrate the lipid membranes, whereas nontoxic oligomers and native proteins do not have this action (**Fig. 4.1A-C**). Correspondingly, we have also found that changes in the composition of the lipid membranes themselves, including those induced pharmacologically with the addition of TRO, can decrease the affinity of the toxic oligomers for the lipid membranes (**Fig. 4.1D-F**). These results therefore offer quantitative insight on one of the fundamental molecular mechanisms of cellular degeneration caused by misfolded protein oligomers and suggest pharmacological approaches to increase the resistance of the cells to this type of insult.

In the second part of the thesis (Section 3.2), we compared three chemically different aminosterols, TRO, SQ and ENT-03, characterized by different chemical and structural formulas and originally identified in different species, the latter of which was recently identified in the mouse *Mus musculus*, whereas TRO and SQ were originally isolated from the dogfish shark *Squalus acanthias*. By the application of an aminosterol-LUVs binding assay with fluorescently labelled aminosterols we found that all the three small molecules exhibited the ability to bind to the lipid membrane, albeit with different binding affinities, and SQ showed the highest affinity for our LUVs model.

The binding of the three aminosterols to the lipid bilayer of LUVs resulted in different perturbations of the physicochemical properties of the liposome bilayer, such as their surface charge, resistance to a mechanical BTF perpendicular to its plane and distribution of CHOL and GM1 lipids. Importantly, the binding of the three aminosterols to the membranes of cultured SH-SY5Y cells resulted into different degrees of protection against the action of misfolded protein oligomers of the $A\beta_{42}$ peptide to Ca^{2+} influx. The

protection depends on aminosterol concentration, level of charge neutralisation of the membrane and change of packing resulting from lipid redistribution.

Using a global fitting analysis of all the dose-response curves obtained with the three aminosterols and an equation derived from a Hill equation integrated with the contributions of the change in charge and the change in packing of the lipid bilayer induced by these molecules, we described quantitatively the level of aminosterol-mediated protection of the cell membrane as a function of all these factors, which allowed the quantification of the weights that the different types of membrane alterations have in this protection (Eq. 20) and the contributions of the various chemical groups of aminosterols in their protective mechanism against oligomers (Eq. 21). In particular, the results of this global fitting analysis allowed us to calculate the contributions of the various types of membrane alterations (**Fig. 4.2A**) and chemical groups of aminosterols (**Fig. 4.2B**) to the EC_{50} parameter in the experimental setting described here based on cultured SH-SY5Y cells and Ca^{2+} influx measurements as a readout of membrane destabilisation. This kind of approach also provides hints to anticipate the effects, on a similar experimental setting, of other aminosterols isolated from sharks (Rao et al., 2000), aminosterols present in other animals that will probably be discovered in the next few years, monoamino-steroid molecules present in plants (Janot et al., 1960; Emanoil-Ravicovitch et al., 1967; Kumar et al., 2007), as well as synthetic aminosterols (**Fig. 4.2C**). Hence, these results help establish molecular principles for the further study and rational optimization of aminosterols and, more generally, help elucidate the means by which the physicochemical properties of cell membranes can be targeted pharmacologically.

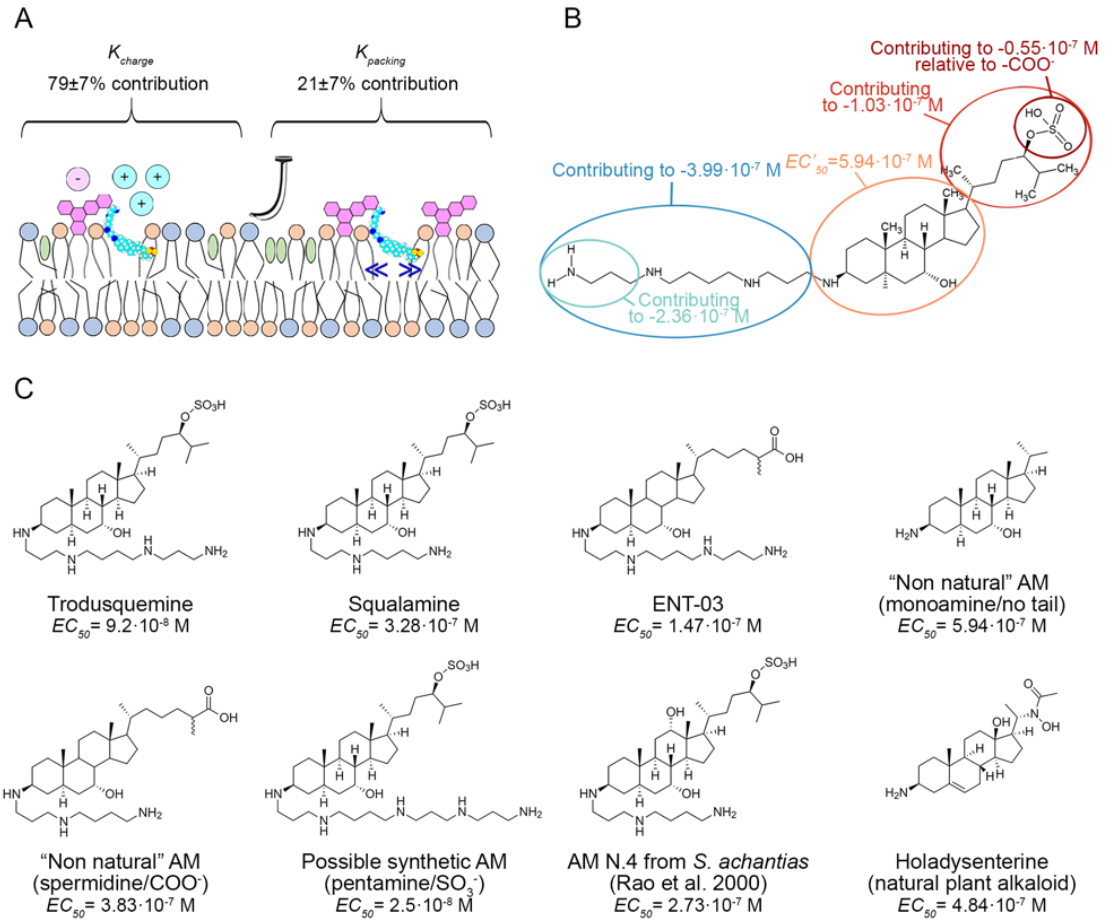

Figure 4.2. Contributions of the various membrane alterations and chemical groups of aminosterols to their potency in this experimental setting. (A) Contributions of the various types of membrane alterations and **(B)** of the chemical groups of aminosterols to the EC_{50} parameter in this experimental setting. The numbers reported in **(B)** refer to the contributions to the aminosterol potency in membrane protection of SH-SY5Y cultured cells against misfolded protein oligomers of Aβ (ADDLs, 1 µm monomer equivalents) causing Ca^{2+} influx. The chemical formula in the image refers to TRO. **(C)** Representative AMs with their potencies (EC_{50} values) predicted in our experimental setting using the values reported in **(B)**. The EC_{50} values predicted for TRO, SQ and ENT-03 are in good agreement with those observed experimentally.

In the third part of this thesis (Section 3.3), we focused on a new molecule for which the scientific literature reports a lower level of information and even the evidence for its interaction with biological membranes is missing. We therefore started our investigation on the ability of Brb to interact with LUVs and then we assessed whether Brb modulates the packing of membrane lipids and to inhibit the binding of OAs to these lipid bilayers.

The interaction of Brb with LUVs was observed with three different experiments: fluorescence quenching of lipophilic probes embedded in different regions of the bilayer of LUVs; dynamic light scattering analysis of increasing concentrations of Brb incubated with LUVs; and equilibrium dialysis of LUVs incubated with Brb against phosphate buffer. Using fluorescence quenching of two different lipophilic LUVs we found that Brb is able to interact with both the superficial polar heads region and hydrophobic core of the lipid bilayers, with a slightly higher affinity for the latter. We obtained a quantitative measure of the binding, in the form of dynamic (K_{SV}) and static (K_{ST}) quenching constants, of this alkaloid with LUVs with two different lipid composition, the first known to exhibit an optimal segregation of lipid into distinct domain and widely used in the previous (model-LUVs) (Oropesa-Nuñez et al., 2016; Errico et al., 2020; Errico et al., 2021; Barletti et al., 2023; Errico et al., 2023), and the latter enriched in CHOL and GM1 content to better mimic the lipid composition of neuronal membranes (neuronal-LUVs) (Ingólfsson et al., 2017). We measured higher K_{SV} and K_{ST} values on DPH-labelled LUVs than TMA-DPH-labelled, suggesting that, unlike aminosterols, Brb interacts more deeply within the hydrophobic core of the bilayer. Moreover, neuronal-LUVs displayed higher quenching than model-LUVs with both the probes used, suggesting a higher affinity of Brb for neuronal LUVs.

The interaction between Brb and LUVs was then confirmed using dynamic light scattering (DLS) of model- and neuronal-LUVs incubated with Brb and also allowed to measure the increase of mass consequent to Brb addition. In particular, neuronal-LUVs displayed a higher mass increase upon Brb addition than model-LUVs, indicating a higher incorporation of Brb in this type of LUVs and confirming the previous fluorescence quenching experiments. Moreover, since we did not observe an increase of LUV

diameter upon Brb addition, the remarkable mass increase by about 15-20% suggests that Brb micelles also incorporate on LUV surfaces, causing an increase of mass and light scattering intensity. An equilibrium dialysis experiment further confirmed the interaction of Brb with LUVs, allowing to measure the fraction of Brb that interacted stably with LUVs or that was incorporated within them. Moreover we observed that neuronal-LUVs incorporated a slightly higher fraction of Brb than model-LUVs, in agreement with the fluorescence quenching and light scattering result.

The interaction between Brb and LUVs determined a global stiffening of the lipid membrane, as demonstrated with Brb concentration- and temperature-dependent fluorescence anisotropy experiments. The addition of Brb to LUVs appeared to decrease the affinity of OAs for the membrane, as observed with fluorescence quenching of TMA-DPH using OAs as quenchers, with an almost complete absence of quenching at low concentrations of OAs up to *ca*. 6 µM. Eventually, using ANS binding assay and CD, we demonstrated how Brb is able to reduce the exposure to the solvent of hydrophobic clusters of OAs, without significantly altering their secondary structure.

In conclusion, in this thesis we investigated at the chemical and physical levels the therapeutic potential of different natural compounds, starting from aminosterols of the shark *Squalus acanthias*, to a new aminosterol found in mammals and eventually to a plant alkaloid that has been used in traditional medical systems in China and India. We found that all of them interact with the lipid bilayer of the membrane of LUVs and inhinit the binding of toxic oligomers for the membrane, therefore representing valuable therapeutic molecules to treat diseases associated with neurodegeneration. In the case of aminosterols, we measured the affinity of oligomers with the membrane with and without aminosterols in a quantitative manner, and we were also able, again in a

quantitative manner, to attribute the protective action of aminosterols to physicochemical perturbations of the membrane and well-defined chemical groups of these natural molecules. In the case of Brb, our study is perhaps more preliminary, but we found that this alkaloid is able to interact with LUVs with different lipid compositions and to decrease the affinity of toxic oligomers for the membrane. Moreover, we observed that Brb is able to shield the exposure to the solvent of hydrophobic clusters of toxic oligomers, without significantly altering their secondary structure. All these results suggest that Brb can also be a very promising molecule.

References

Acosta C, Anderson HD, Anderson CM (2017) “Astrocyte dysfunction in Alzheimer disease”. *J Neurosci Res*. **95**:2430-2447.

Agarwal M, Alam MR, Haider MK, Malik MZ, Kim DK (2020) “Alzheimer's Disease: An Overview of Major Hypotheses and Therapeutic Options in Nanotechnology”. *Nanomaterials (Basel).* **11**:59.

Ahima RS, Patel HR, Takahashi N, Qi Y, Hileman SM, et al. (2002) “Appetite suppression and weight reduction by a centrally active aminosterol”. *Diabetes*. **51**:2099-2104.

Ahmed T, Gilani AU, Abdollahi M, Daglia M, Nabavi SF, Nabavi SM (2015) “Berberine and neurodegeneration: A review of literature”. *Pharmacol Rep*. **67**:970-979.

Aizenstein HJ, Nebes RD, Saxton JA, Price JC, Mathis CA, Tsopelas ND, Ziolko SK, James JA, Snitz BE, Houck PR, Bi W, Cohen AD, Lopresti BJ, DeKosky ST, Halligan EM, Klunk WE (2008) “Frequent amyloid deposition without significant cognitive impairment among the elderly”. *Arch Neurol*. **65**:1509-1517.

Akbarzadeh A, Rezaei-Sadabady R, Davaran S, Joo SW, Zarghami N, Hanifehpour Y, Samiei M, Kouhi M, Nejati-Koshki K (2013) “Liposome: classification, preparation, and applications”. *Nanoscale Res Lett*. **8**:102.

Alberdi E, Sánchez-Gómez MV, Cavaliere F, Pérez-Samartín A, Zugaza JL, Trullas R, Domercq M, Matute C (2010) “Amyloid Beta Oligomers Induce Ca^{2+} Dysregulation and Neuronal Death Through Activation of Ionotropic Glutamate Receptors”. *Cell Calcium*. **47**:264-272.

Albert MS, DeKosky ST, Dickson D, Dubois B, Feldman HH, Fox NC, Gamst A, Holtzman DM, Jagust WJ, Petersen RC, Snyder PJ, Carrillo MC, Thies B, Phelps CH (2011) “The diagnosis of mild cognitive impairment due to Alzheimer's disease: recommendations from the National Institute on Aging-Alzheimer's Association workgroups on diagnostic guidelines for Alzheimer's disease”. *Alzheimers Dement*. **7**:270-279.

Alecu I, Bennett SAL. (2019) “Dysregulated Lipid Metabolism and Its Role in α-Synucleinopathy in Parkinson's Disease”. *Front Neurosci*. **13**:328.

Alves AC, Ribeiro D, Horta M, Lima JLFC, Nunes C, Reis S (2017) “A biophysical approach to daunorubicin interaction with model membranes: relevance for the drug's biological activity”. *J R Soc Interface*. **14**:20170408.

Amat-Ur-Rasool H, Ahmed M. (2015) “Designing Second Generation Anti-Alzheimer Compounds as Inhibitors of Human Acetylcholinesterase: Computational Screening of Synthetic Molecules and Dietary Phytochemicals”. *PLoS One*. **10**:e0136509.

Anand P, Singh B. (2013) “A review on cholinesterase inhibitors for Alzheimer's disease”. *Arch Pharm Res*. 2013 **36**:375-399.

Andersson J, Köper I (2018) “Reference Module in Materials Science and Materials Engineering: Biomimetic Membranes”. *Comprehensive Nanoscience and Nanotechnology, 2nd edition*, doi:10.1016/B978-0-12-803581-8.10447-3.

Andreasen M, Lorenzen N, Otzen D (2015) “Interactions between misfolded protein oligomers and membranes: A central topic in neurodegenerative diseases?” *Biochim Biophys Acta*. **1848**:1897-1907.

Angelova MI, Dimitrov DS (1986) “Liposome electroformation” *Faraday Discuss Chem Soc.* **81**:303-345.

Arispe N, Doh M (2002) “Plasma membrane cholesterol controls the cytotoxicity of Alzheimer's disease AbetaP (1-40) and (1-42) peptides”. *FASEB J*. **16**:1526-1536.

Armstrong MJ, Okun MS. (2020) “Diagnosis and Treatment of Parkinson Disease: A Review”. *JAMA*. **323**:548-560.

Armstrong R (2019) “Risk factors for Alzheimer's disease”. *Folia Neuropathol*. **57**:87-105.

Ashique S, Sirohi E, Kumar S, Rihan M, Mishra N, Bhatt S, Gautam RK, Singh SK, Gupta G, Chellappan DK, Dua K (2023) “Aducanumab in Alzheimer's disease: A critical update”. *Curr Med Chem*. Jul 27.

Atanasov AG, Waltenberger B, Pferschy-Wenzig EM, Linder T, Wawrosch C, Uhrin P, Temml V, Wang L, Schwaiger S, Heiss EH, Rollinger JM, Schuster D, Breuss JM, Bochkov V, Mihovilovic MD, Kopp B, Bauer R, Dirsch VM, Stuppner H (2015) “Discovery and resupply of pharmacologically active plant-derived natural products: A review”. *Biotechnol Adv*. **33**:1582-1614.

Atanasov AG, Zotchev SB, Dirsch VM; International Natural Product Sciences Taskforce; Supuran CT (2021) “Natural products in drug discovery: advances and opportunities”. *Nat Rev Drug Discov*. **20**:200-216.

Atri A (2019) “The Alzheimer's Disease Clinical Spectrum: Diagnosis and Management”. *Med Clin North Am*. **103**:263-293.

Attwood SJ, Choi Y, Leonenko Z (2013) “Preparation of DOPC and DPPC Supported Planar Lipid Bilayers for Atomic Force Microscopy and Atomic Force Spectroscopy”. *Int J Mol Sci*. **14**:3514-3539.

Baba M, Nakajo S, Tu PH, Tomita T, Nakaya K, Lee VM, Trojanowski JQ, Iwatsubo T (1998) “Aggregation of α-synuclein in Lewy bodies of sporadic Parkinson's disease and dementia with Lewy bodies”. *Am J Pathol* **152**:879–884.

Bae J, Lee D, Kim YK, Gil M, Lee JY, Lee KJ (2013) “Berberine protects 6-hydroxydopamine-induced human dopaminergic neuronal cell death through the induction of heme oxygenase-1”. *Mol Cells*. **35**:151-157.

Bagli E, Goussia A, Moschos MM, Agnantis N, Kitsos G (2016) “Natural Compounds and Neuroprotection: Mechanisms of Action and Novel Delivery Systems”. *In Vivo*. **30**:535-547.

Barbut D, Hecksher-Sørensen J, Zhang C, Muzzio M, Huang Z, Jones SR, Stewart AFR, Chen HH, Kinney WA, Frey WH, Fleming Z, Clendenin C, Baur JA, Zemel M, Zasloff M (submitted for publication). “Discovery of a spermine-bile acid from mouse brain that increases insulin sensitivity”. *Cell Chem Biol.*

Barletti B, Lucchesi G, Muscat S, Errico S, Barbut D, Danani A, Zasloff M, Grasso G, Chiti F, Caminati G (2023) “Reorganization of the outer layer of a model of the plasma

membrane induced by a neuroprotective aminosterol". *Colloids Surf B Biointerfaces*. **222**:113115.

Barghorn S, Nimmrich V, Striebinger A, Krantz C, Keller P, Janson B, Bahr M, Schmidt M, Bitner RS, Harlan J, Barlow E, Ebert U, Hillen H (2005) "Globular amyloid beta-peptide oligomer - a homogenous and stable neuropathological protein in Alzheimer's disease". *J Neurochem*. **95**:834-847.

Bartus RT, Dean RL 3rd, Beer B, Lippa AS (1982) "The cholinergic hypothesis of geriatric memory dysfunction". *Science*. **217**:408-414.

Bellavite P, Fazio S, Affuso F. (2023) "A Descriptive Review of the Action Mechanisms of Berberine, Quercetin and Silymarin on Insulin Resistance/Hyperinsulinemia and Cardiovascular Prevention". *Molecules*. **28**:4491.

Bellenguez C, Küçükali F, Jansen IE, Kleineidam L, Moreno-Grau S, Amin N, Naj AC, et al. (2022) "New insights into the genetic etiology of Alzheimer's disease and related dementias". *Nat Genet*. **54**:412-436.

Bendas G, Vogel J, Bakowski U, Krause A, Muller J, Rothe U (1997) "A liposome-based model system for the simulation of lectin-induced cell adhesion". *Biochim et Biophys Acta* **1325**:297–308.

Ben-David O, Futerman AH (2010) "The role of the ceramide acyl chain length in neurodegeneration: involvement of ceramide synthases". *Neuromolecular Med*. **12**:341-350.

Bendor JT, Logan TP, Edwards RH (2013) "The function of α-synuclein". *Neuron*. **79**:1044-1066.

Besson FL, La Joie R, Doeuvre L, Gaubert M, Mézenge F, Egret S, Landeau B, Barré L, Abbas A, Ibazizene M, de La Sayette V, Desgranges B, Eustache F, Chételat G (2015) "Cognitive and Brain Profiles Associated with Current Neuroimaging Biomarkers of Preclinical Alzheimer's Disease". *J Neurosci*. **35**:10402-10411.

Bhutada P, Mundhada Y, Bansod K, Tawari S, Patil S, Dixit P, Umathe S, Mundhada D (2011) "Protection of cholinergic and antioxidant system contributes to the effect of berberine ameliorating memory dysfunction in rat model of streptozotocin-induced diabetes". *Behav Brain Res*. **220**:30-41.

Biancalana M, Koide S (2010) "Molecular mechanism of Thioflavin-T binding to amyloid fibrils" *Biochim Biophys Acta*. **1804**:1405-1412.

Birol M, Kumar S, Rhoades E, Miranker AD (2018) "Conformational switching within dynamic oligomers underpins toxic gain-of-function by diabetes-associated amyloid". *Nat Commun*. **9**:1312.

Biruss B, Dietl R, Valenta C (2007) "The Influence of Selected Steroid Hormones on the Physicochemical Behaviour of DPPC Liposomes". *Chem Phys Lipids*. **148**:84-90.

Bolognesi B, Kumita JR, Barros TP, Esbjorner EK, Luheshi LM, Crowther DC, Wilson MR, Dobson CM, Favrin G, Yerbury JJ (2010) "ANS binding reveals common features of cytotoxic amyloid species". *ACS Chem Biol* **5**:735-740.

Breijyeh Z, Karaman R (2020) "Comprehensive Review on Alzheimer's Disease: Causes and Treatment". *Molecules*. **25**:5789.

Brier MR, Gordon B, Friedrichsen K, McCarthy J, Stern A, Christensen J, Owen C, Aldea P, Su Y, Hassenstab J, Cairns NJ, Holtzman DM, Fagan AM, Morris JC, Benzinger TL, Ances BM (2016) "Tau and Aβ imaging, CSF measures, and cognition in Alzheimer's disease". *Sci Transl Med*. **8**:338ra66.

Brooks DJ (2000) "Dopamine agonists: their role in the treatment of Parkinson's disease" *J Neurol Neurosurg Psychiatry*. **68**:685-689.

Brunel JM, Salmi C, Loncle C, Vidal N, Letourneux Y (2005) "Squalamine: a polyvalent drug of the future?". *Curr Cancer Drug Targets*. **5**:267-272.

Buccellato FR, D'Anca M, Tartaglia GM, Del Fabbro M, Scarpini E, Galimberti D (2023) "Treatment of Alzheimer's Disease: Beyond Symptomatic Therapies". *International Journal of Molecular Sciences*. **24**:13900.

Bucciantini M, Giannoni E, Chiti F, Baroni F, Formigli L, Zurdo J, Taddei N, Ramponi G, Dobson CM, Stefani M (2002) "Inherent toxicity of aggregates implies a common mechanism for protein misfolding diseases". *Nature*. **416**:507-511.

Budd Haeberlein S, Aisen PS, Barkhof F, Chalkias S, Chen T, Cohen S, Dent G, Hansson O, Harrison K, von Hehn C, Iwatsubo T, Mallinckrodt C, Mummery CJ, Muralidharan KK, Nestorov I, Nisenbaum L, Rajagovindan R, Skordos L, Tian Y, van Dyck CH, Vellas B, Wu S, Zhu Y, Sandrock A (2022) "Two Randomized Phase 3 Studies of Aducanumab in Early Alzheimer's Disease". *J Prev Alzheimers Dis*. **9**:197-210.

Busche MA, Hyman BT (2020) "Synergy between amyloid-β and tau in Alzheimer's disease". *Nat Neurosci*. **23**:1183-1193.

Buell AK, Galvagnion C, Gaspar R, Sparr E, Vendruscolo M, Knowles TPJ, Linse S, Dobson CM (2014) "Solution Conditions Determine the Relative Importance of Nucleation and Growth Processes in α-Synuclein Aggregation". *Proc Natl Acad Sci USA*. **111**:7671−7676.

Buerger K, Ewers M, Pirttilä T, Zinkowski R, Alafuzoff I, Teipel SJ, DeBernardis J, Kerkman D, McCulloch C, Soininen H, Hampel H (2006) "CSF phosphorylated tau protein correlates with neocortical neurofibrillary pathology in Alzheimer's disease". *Brain*. **129**:3035-3041.

Burré J, Sharma M, Tsetsenis T, Buchman V, Etherton MR, Südhof TC (2010) "Alpha-synuclein promotes SNARE-complex assembly in vivo and in vitro". *Science*. **329**:1663-1667.

Burré J, Sharma M, Südhof TC (2014) "α-Synuclein assembles into higher-order multimers upon membrane binding to promote SNARE complex formation". *Proc Natl Acad Sci U S A*. 111:E4274-4283.

Burré J, Sharma M, Südhof TC (2018) "Cell Biology and Pathophysiology of α-Synuclein". *Cold Spring Harb Perspect.* **8**:a024091.

Butterfield DA, Griffin S, Munch G, Pasinetti GM (2002) "Amyloid beta-peptide and amyloid pathology are central to the oxidative stress and inflammatory cascades under which Alzheimer's disease brain exists". *J Alzheimers Dis*. **4**:193-201.

Calamai M, Evangelisti E, Cascella R, Parenti N, Cecchi C, Stefani M, Pavone F (2016) "Single molecule experiments emphasize GM1 as a key player of the different

cytotoxicity of structurally distinct Aβ1-42 oligomers". *Biochim Biophys Acta*. **1858**:386-392.

Calderon RO, Attema B, DeVries GH (1995). "Lipid composition of neuronal cell bodies and neurites from cultured dorsal root ganglia". *J. Neurochem*. **64**:424-429.

Calo L, Wegrzynowicz M, Santivañez-Perez J, Grazia Spillantini M (2017) "Synaptic failure and α-synuclein". *Mov Disord*. 31:169-177.

Camilleri M, Subramanian T, Pagan F, Isaacson S, Gil R, Hauser RA, Feldman M, Goldstein M, Kumar R, Truong D, Chhabria N, Walter BL, Eskenazi J, Riesenberg R, Burdick D, Tse W, Molho E, Robottom B, Bhatia P, Kadimi S, Klos K, Shprecher D, Marquez-Mendoza O, Hidalgo G, Grill S, Li G, Mandell H, Hughes M, Stephenson S, Vandersluis J, Pfeffer M, Duker A, Shivkumar V, Kinney W, MacDougall J, Zasloff M, Barbut D (2022) "Oral ENT-01 Targets Enteric Neurons to Treat Constipation in Parkinson Disease : A Randomized Controlled Trial". *Ann Intern Med*. **175**:1666-1674.

Campioni S, Mannini B, Zampagni M, Pensalfini A, Parrini C, Evangelisti E, Relini A, Stefani M, Dobson CM, Cecchi C, Chiti F (2010) "A causative link between the structure of aberrant protein oligomers and their toxicity". *Nat Chem Biol*. **6**:140-147.

Canepa E, Salassi S, de Marco AL, Lambruschini C, Odino D, Bochicchio D, Canepa F, Canale C, Dante S, Brescia R, Stellacci F, Rossi G, Relini A. (2020). "Amphiphilic gold nanoparticles perturb phase separation in multidomain lipid membranes" *Nanoscale* **12**:19746-19759.

Capitini C, Patel JR, Natalello A, D'Andrea C, Relini A, Jarvis JA, Birolo L, Peduzzo A, Vendruscolo M, Matteini P, Dobson CM, De Simone A, Chiti F (2018) "Structural differences between toxic and nontoxic HypF-N oligomers". *Chem Commun (Camb).* **54**:8637-8640.

Cardamone M, Puri NK (1992) "Spectrofluorimetric assessment of the surface hydrophobicity of proteins". *Biochem J*. **282**:589-593.

Casares D, Escribá PV, Rosselló CA (2019) "Membrane Lipid Composition: Effect on Membrane and Organelle Structure, Function and Compartmentalization and Therapeutic Avenues". *Int J Mol Sci.* **20**:2167.

Cascella R, Evangelisti E, Bigi A, Becatti M, Fiorillo C, Stefani M, Chiti F, Cecchi C (2017) "Soluble Oligomers Require a Ganglioside to Trigger Neuronal Calcium Overload". *J Alzheimers Dis*. **60**:923-938.

Cascella R, Chen SW, Bigi A, Camino JD, Xu CK, Dobson CM, Chiti F, Cremades N, Cecchi C (2021) "The release of toxic oligomers from α-synuclein fibrils induces dysfunction in neuronal cells". *Nat Commun*. **12**:1814.

Castelli V, Grassi D, Bocale R, d'Angelo M, Antonosante A, Cimini A, Ferri C, Desideri G (2018) "Diet and Brain Health: Which Role for Polyphenols?" *Curr Pharm Des*. **24**:227-238.

Cava DG, Vélez M (2022) "Study of Amyloid Fibers Using Atomic Force Microscopy". *Methods Mol Biol*. **2538**:1-11.

Cerri S, Mus L, Blandini F (2019) “Parkinson's Disease in Women and Men: What's the Difference?” *J Parkinsons Dis*. **9**:501-515.

Chakraborty S, Doktorova M, Molugu TR, Heberle FA, Scott HL, Dzikovski B, Nagao M, Stingaciu LR, Standaert RF, Barrera FN, Katsaras J, Khelashvili G, Brown MF, Ashkar R (2020) “How cholesterol stiffens unsaturated lipid membranes”. *Proc Natl Acad Sci U S A*. **117**:21896-21905.

Cheignon C, Tomas M, Bonnefont-Rousselot D, Faller P, Hureau C, Collin F (2018) “Oxidative stress and the amyloid beta peptide in Alzheimer's disease”. *Redox Biol*. **14**:450-464.

Chen C, Yu Z, Li Y, Fichna J, Storr M (2014) “Effects of berberine in the gastrointestinal tract - a review of actions and therapeutic implications”. *Am J Chin Med*. **42**:1053-1070.

Chen C, Zhang Y, Huang C (2010) “Berberine inhibits PTP1B activity and mimics insulin action”. *Biochem Biophys Res Commun*. **397**:543-547.

Chen SW, Drakulic S, Deas E, Ouberai M, Aprile FA, Arranz R, Ness S, Roodveldt C, Guilliams T, De-Genst EJ, Klenerman D, Wood NW, Knowles TP, Alfonso C, Rivas G, Abramov AY, Valpuesta JM, Dobson CM, Cremades N (2015) “Structural characterization of toxic oligomers that are kinetically trapped during α-synuclein fibril formation”. *Proc Natl Acad Sci U S A*. **112**:E1994-2003.

Chiti F, Dobson CM (2017) “Protein Misfolding, Amyloid Formation, and Human Disease: A Summary of Progress Over the Last Decade”. *Annu Rev Biochem*. **86**:27-68.

Cicero AFG, Ruscica M, Banach M (2019) “Resveratrol and cognitive decline: a clinician perspective”. *Arch Med Sci*. **15**:936-943.

Cipriani G, Dolciotti C, Picchi L, Bonuccelli U (2011) “Alzheimer and his disease: a brief history”. *Neurol Sci*. **32**:275-279.

Cirrito JR, Yamada KA, Finn MB, Sloviter RS, Bales KR, May PC, Schoepp DD, Paul SM, Mennerick S, Holtzman DM (2005) “Synaptic activity regulates interstitial fluid amyloid-beta levels in vivo”. *Neuron*. **48**:913-922.

Claeysen S, Cochet M, Donneger R, Dumuis A, Bockaert J, Giannoni P (2012) “Alzheimer culprits: cellular crossroads and interplay”. *Cell Signal*. **24**:1831–1840.

Clardy J, Walsh C (2004) “Lessons from natural molecules”. *Nature*. **432**:829-837.

Cline EN, Bicca MA, Viola KL, Klein WL (2018) “The Amyloid-β Oligomer Hypothesis: Beginning of the Third Decade”. *J Alzheimers Dis*. **64**:S567-S610.

Cohen SI, Linse S, Luheshi LM, Hellstrand E, White DA, Rajah L, Otzen DE, Vendruscolo M, Dobson CM, Knowles TP (2013) “Proliferation of amyloid-β42 aggregates occurs through a secondary nucleation mechanism”. *Proc Natl Acad Sci U S A*. **110**:9758-9763.

Collins JM, Dominey RN, Grogan WM (1990) “Shape of the fluidity gradient in the plasma membrane of living HeLa cells”. *J Lipid Res*. **31**:261-270.

Connolly BS, Lang AE (2014) “Pharmacological treatment of Parkinson disease: a review”. *JAMA*. **311**:1670-1683.

Conway KA, Lee SJ, Rochet JC, Ding TT, Williamson RE, Lansbury PT Jr (2000) “Acceleration of oligomerization, not fibrillization, is a shared property of both alpha-synuclein mutations linked to early-onset Parkinson's disease: implications for pathogenesis and therapy”. *Proc Natl Acad Sci U S A*. **97**:571-576.

Copeland RA (2000) “Protein-Ligand Binding Equilibria in Enzymes: A Practical Introduction to Structure, Mechanism, and Data Analysis”. pp. 76-108, Wiley-VCH.

Corder EH, Saunders AM, Strittmatter WJ, Schmechel DE, Gaskell PC, Small GW, Roses AD, Haines JL, Pericak-Vance MA. (1993) “Gene dose of apolipoprotein E type 4 allele and the risk of Alzheimer's disease in late onset families”. *Science*. **261**:921-923.

Cummings J, Lee G, Ritter A, Sabbagh M, Zhong K (2019) “Alzheimer's disease drug development pipeline” *Alzheimers Dement (N Y).* **5**:272-293.

Danysz W, Parsons CG (2003) “The NMDA receptor antagonist memantine as a symptomatological and neuroprotective treatment for Alzheimer's disease: preclinical evidence”. *Int J Geriatr Psychiatry*. **18**:S23-32.

Davies P, Maloney AJ (1976) “Selective loss of central cholinergic neurons in Alzheimer's disease”. *Lancet*. **2**:1403.

De Almeida RF, Fedorov A, Prieto M (2003) “Sphingomyelin/phosphatidylcholine/cholesterol phase diagram: boundaries and composition of lipid rafts”. *Biophys J*. **85**:2406-2416.

Dear AJ, Meisl G, Šarić A, Michaels TCT, Kjaergaard M, Linse S, Knowles TPJ (2020) “Identification of on- and off-pathway oligomers in amyloid fibril formation”. *Chem Sci*. **11**:6236-6247.

Decker H, Jürgensen S, Adrover MF, Brito-Moreira J, Bomfim TR, Klein WL, Epstein AL, De Felice FG, Jerusalinsky D, Ferreira ST (2010) “N-methyl-D-aspartate Receptors are Required for Synaptic Targeting of Alzheimer's Toxic Amyloid-β Peptide Oligomers”. *J Neurochem*. **115**:1520-1529.

De Felice FG, Velasco PT, Lambert MP, Viola K, Fernandez SJ, Ferreira ST, Klein WL (2007) “Abeta oligomers induce neuronal oxidative stress through an N-methyl-D-aspartate receptor-dependent mechanism that is blocked by the Alzheimer drug memantine”. *J Biol Chem*. **282**:11590-11601.

Demuro A, Mina E, Kayed R, Milton SC, Parker I, Glabe CG (2005) “Calcium Dysregulation and Membrane Disruption as a Ubiquitous Neurotoxic Mechanism of Soluble Amyloid Oligomers”. *J Biol Chem*. **280**:17294-17300.

Deng H, Wang P, Jankovic J (2018) “The genetics of Parkinson disease”. *Ageing Res Rev*. **42**:72-85.

De-Paula VJ, Radanovic M, Diniz BS, Forlenza OV (2012) “Alzheimer's disease”. *Subcell Biochem*. **65**:329-352.

Deshpande P, Gogia N, Singh A (2019) “Exploring the efficacy of natural products in alleviating Alzheimer's disease”. *Neural Regen Res*. **14**:1321-1329.

De Strooper B, Saftig P, Craessaerts K, Vanderstichele H, Guhde G, Annaert W, Von Figura K, Van Leuven F. (1998) “Deficiency of presenilin-1 inhibits the normal cleavage of amyloid precursor protein”. *Nature*. **391**:387-390.

Deuschl G, Antonini A, Costa J, Śmiłowska K, Berg D, Corvol JC, Fabbrini G, Ferreira J, Foltynie T, Mir P, Schrag A, Seppi K, Taba P, Ruzicka E, Selikhova M, Henschke N, Villanueva G, Moro E (2022) “European Academy of Neurology/Movement Disorder Society - European Section guideline on the treatment of Parkinson's disease: I. Invasive therapies”. *Eur J Neurol*. **29**:2580-2595.

Dev S (1999) “Ancient-modern concordance in Ayurvedic plants: some examples”. *Environ Health Perspect*. **107**:783-789.

Diaz JC, Simakova O, Jacobson KA, Arispe N, Pollard HB (2009) “Small Molecule Blockers of the Alzheimer Abeta Calcium Channel Potently Protect Neurons from Abeta Cytotoxicity”. *Proc Natl Acad Sci USA*. **106**:3348-3353.

Di Veroli GY, Fornari C, Goldlust I, Mills G, Koh SB, Bramhall JL, Richards FM, Jodrell DI (2015) “An Automated Fitting Procedure and Software for Dose-Response Curves with Multiphasic Features”. *Sci Rep*. **5**:14701.

Du X, Wang X, Geng M (2018) “Alzheimer's disease hypothesis and related therapies”. *Transl Neurodegener*. **7**:2.

Dubois B, Feldman HH, Jacova C, Dekosky ST, Barberger-Gateau P, Cummings J, Delacourte A, Galasko D, Gauthier S, Jicha G, Meguro K, O'brien J, Pasquier F, Robert P, Rossor M, Salloway S, Stern Y, Visser PJ, Scheltens P (2007) “Research criteria for the diagnosis of Alzheimer's disease: revising the NINCDS-ADRDA criteria”. *Lancet Neurol*. **6**:734-746.

Dubois B, Hampel H, Feldman HH, Scheltens P, Aisen P, Andrieu S, Bakardjian H, Benali H, Bertram L, Blennow K, Broich K, Cavedo E, Crutch S, Dartigues JF, Duyckaerts C, Epelbaum S, Frisoni GB, Gauthier S, Genthon R, Gouw AA, Habert MO, Holtzman DM, Kivipelto M, Lista S, Molinuevo JL, O'Bryant SE, Rabinovici GD, Rowe C, Salloway S, Schneider LS, Sperling R, Teichmann M, Carrillo MC, Cummings J, Jack CR Jr (2016) “Proceedings of the Meeting of the International Working Group (IWG) and the American Alzheimer's Association on “The Preclinical State of AD” July 23, 2015; Washington DC, USA. Preclinical Alzheimer's disease: Definition, natural history, and diagnostic criteria”. *Alzheimers Dement*. **12**:292-323.

Eftekharzadeh B, Daigle JG, Kapinos LE, Coyne A, Schiantarelli J, Carlomagno Y, Cook C, Miller SJ, Dujardin S, Amaral AS, Grima JC, Bennett RE, Tepper K, DeTure M, Vanderburg CR, Corjuc BT, DeVos SL, Gonzalez JA, Chew J, Vidensky S, Gage FH, Mertens J, Troncoso J, Mandelkow E, Salvatella X, Lim RYH, Petrucelli L, Wegmann S, Rothstein JD, Hyman BT (2018) “Tau Protein Disrupts Nucleocytoplasmic Transport in Alzheimer's Disease”. *Neuron*. **99**:925-940.

Elghetany MT, Saleem A (1988) “Methods for staining amyloid in tissues: a review”. *Stain Technol*. **63**:201-212.

Emin D, Zhang YP, Lobanova E, Miller A, Li X, Xia Z, Dakin H, Sideris DI, Lam JYL, Ranasinghe RT, Kouli A, Zhao Y, De S, Knowles TPJ, Vendruscolo M, Ruggeri FS,

Aigbirhio FI, Williams-Gray CH, Klenerman D (2022) “Small soluble α-synuclein aggregates are the toxic species in Parkinson's disease”. *Nat Commun*. **13**:5512.

Errico S, Lucchesi G, Odino D, Osman EY, Cascella R, Neri L, Capitini C, Calamai M, Bemporad F, Cecchi C, Kinney WA, Barbut D, Relini A, Canale C, Caminati G, Limbocker R, Vendruscolo M, Zasloff M, Chiti F (2023) “Quantitative Attribution of the Protective Effects of Aminosterols against Protein Aggregates to Their Chemical Structures and Ability to Modulate Biological Membranes”. *J Med Chem*. **66**:9519-9536.

Errico S, Lucchesi G, Odino D, Muscat S, Capitini C, Bugelli C, Canale C, Ferrando R, Grasso G, Barbut D, Calamai M, Danani A, Zasloff M, Relini A, Caminati G, Vendruscolo M, Chiti F (2020) “Making biological membrane resistant to the toxicity of misfolded protein oligomers: a lesson from trodusquemine”. *Nanoscale*. **12**:22596-22614.

Errico S, Ramshini H, Capitini C, Canale C, Spaziano M, Barbut D, Calamai M, Zasloff M, Oropesa-Nuñez R, Vendruscolo M, Chiti F (2021) “Quantitative Measurement of the Affinity of Toxic and Nontoxic Misfolded Protein Oligomers for Lipid Bilayers and of its Modulation by Lipid Composition and Trodusquemine”. *ACS Chem Neurosci*. **12**:3189-3202.

Esparza TJ, Zhao H, Cirrito JR, Cairns NJ, Bateman RJ, Holtzman DM, Brody DL (2013) “Amyloid-β oligomerization in Alzheimer dementia versus high-pathology controls”. *Ann Neurol*. **73**:104-119.

Erten-Lyons D, Woltjer RL, Dodge H, Nixon R, Vorobik R, Calvert JF, Leahy M, Montine T, Kaye J (2009) “Factors associated with resistance to dementia despite high Alzheimer disease pathology”. *Neurology*. **72**:354-360.

Evangelisti E, Cascella R, Becatti M, Marrazza G, Dobson CM, Chiti F, Stefani M, Cecchi C (2016) “Binding affinity of amyloid oligomers to cellular membranes is a generic indicator of cellular dysfunction in protein misfolding diseases”. *Sci Rep*. **6**:32721.

Evangelisti E, Cecchi C, Cascella R, Sgromo C, Becatti M, Dobson CM, Chiti F, Stefani M (2012) “Membrane lipid composition and its physicochemical properties define cell vulnerability to aberrant protein oligomers”. *J Cell Sci*. **125**:2416-2427.

Evangelisti E, Zampagni M, Cascella R, Becatti M, Fiorillo C, Caselli A, Bagnoli S, Nacmias B, Cecchi C (2014) “Plasma membrane injury depends on bilayer lipid composition in Alzheimer's disease”. *J Alzheimers Dis*. **41**:289-300.

Evans E, Kwok R (1982) “Mechanical calorimetry of large dimyristoylphosphatidylcholine vesicles in the phase transition region”. *Biochemistry* **21**:4874-4879.

Evans PH (1993) “Free radicals in brain metabolism and pathology”. *Br Med Bull*. **49**:577-587.

Fagan AM, Roe CM, Xiong C, Mintun MA, Morris JC, Holtzman DM (2007) “Cerebrospinal fluid tau/beta-amyloid(42) ratio as a prediction of cognitive decline in nondemented older adults”. *Arch Neurol*. **64**:343-349.

Fani G, Chiti F (2022) “Mechanosensitivity of N-methyl-D-aspartate receptors (NMDAR) is the key through which amyloid beta oligomers activate them”. *Neural Regen Res*. **17**:1263-1264.

Fani G, La Torre CE, Cascella R, Cecchi C, Vendruscolo M, Chiti F (2022) “Misfolded Protein Oligomers Induce an Increase of Intracellular Ca2+ Causing an Escalation of Reactive Oxidative Species”. *Cell Mol Life Sci*. **79**:500.

Fani G, Mannini B, Vecchi G, Cascella R, Cecchi C, Dobson CM, Vendruscolo M, Chiti F (2021) “Aβ Oligomers Dysregulate Calcium Homeostasis by Mechanosensitive Activation of AMPA and NMDA Receptors”. *ACS Chem Neurosci.* **12**:766-781.

Feher M, Schmidt JM (2003) “Property distributions: differences between drugs, natural products, and molecules from combinatorial chemistry”. *J Chem Inf Comput Sci*. **43**:218-227.

Fornai M, Pellegrini C, Antonioli L, Segnani C, Ippolito C, Barocelli E, Ballabeni V, Vegezzi G, Al Harraq Z, Blandini F, Levandis G, Cerri S, Blandizzi C, Bernardini N, Colucci R (2016) “Enteric Dysfunctions in Experimental Parkinson's Disease: Alterations of Excitatory Cholinergic Neurotransmission Regulating Colonic Motility in Rats”. *J Pharmacol Exp Ther*. **356**:434-444.

Fox SH, Katzenschlager R, Lim SY, Barton B, de Bie RMA, Seppi K, Coelho M, Sampaio C (2018) “Movement Disorder Society Evidence-Based Medicine Committee. International Parkinson and movement disorder society evidence-based medicine review: Update on treatments for the motor symptoms of Parkinson's disease”. *Mov Disord*. **33**:1248-1266.

Francis PT, Palmer AM, Snape M, Wilcock GK (1999) “The cholinergic hypothesis of Alzheimer's disease: a review of progress”. *J Neurol Neurosurg Psychiatry*. **66**:137-147.

Frost B, Jacks RL, Diamond MI (2009) “Propagation of tau misfolding from the outside to the inside of a cell”. *J Biol Chem*. **284**:12845-12852.

Fujita A, Cheng J, Hirakawa M, Furukawa K, Kusunoki S, Fujimoto T (2007) “Gangliosides GM1 and GM3 in the living cell membrane form clusters susceptible to cholesterol depletion and chilling”. *Mol Biol Cell*. **18**:2112-2122.

Fusco G, Chen SW, Williamson PTF, Cascella R, Perni M, Jarvis JA, Cecchi C, Vendruscolo M, Chiti F, Cremades N, Ying L, Dobson CM, Simone AD (2017) “Structural Basis of Membrane Disruption and Cellular Toxicity by α-Synuclein Oligomers”. *Science.* **358**:1440−1443.

Gallardo R, Ranson NA, Radford SE (2020) “Amyloid structures: much more than just a cross-β fold”. *Curr Opin Struct Biol*. **60**:7-16.

Gallardo G, Holtzman DM (2019) “Amyloid-β and tau at the crossroads of Alzheimer’s disease”. *Adv. Exp. Med. Biol*. **1184**:187–203.

Gallardo J, Escalona-Noguero C, Sot B (2020) “Role of α-Synuclein Regions in Nucleation and Elongation of Amyloid Fiber Assembly”. *ACS Chem Neurosci*. **11**:872-879.

Galvagnion C (2017) “The Role of Lipids Interacting with α-Synuclein in the Pathogenesis of Parkinson's Disease”. *J Parkinsons Dis*. **7**:433-450.

Galvagnion C, Brown JW, Ouberai MM, Flagmeier P, Vendruscolo M, Buell AK, Sparr E, Dobson CM (2016) “Chemical properties of lipids strongly affect the kinetics of the membrane-induced aggregation of α-synuclein”. *Proc Natl Acad Sci U S A*. **113**:7065-7070.

Galvagnion C, Buell AK, Meisl G, Michaels TC, Vendruscolo M, Knowles TP, Dobson CM (2015) “Lipid vesicles trigger α-synuclein aggregation by stimulating primary nucleation”. *Nat Chem Biol*. **11**:229-234.

Galvagnion C, Marlet FR, Cerri S, Schapira AHV, Blandini F, Di Monte DA (2022) “Sphingolipid changes in Parkinson L444P GBA mutation fibroblasts promote α-synuclein aggregation”. *Brain*. **145**:1038-1051.

Gandy S, Simon AJ, Steele JW, Lublin AL, Lah JJ, Walker LC, Levey AI, Krafft GA, Levy E, Checler F, Glabe C, Bilker WB, Abel T, Schmeidler J, Ehrlich ME (2010) “Days to criterion as an indicator of toxicity associated with human Alzheimer amyloid-beta oligomers”. *Ann Neurol.* **68**:220-230.

George JM (2002) “The synucleins”. *Genome Biol*. 3:REVIEWS3002.

Glenner GG, Eanes ED, Page DL (1972) “The relation of the properties of Congo red-stained amyloid fibrils to the -conformation”. *J Histochem Cytochem*. **20**:821-826.

Goate A, Chartier-Harlin MC, Mullan M, Brown J, Crawford F, Fidani L, Giuffra L, Haynes A, Irving N, James L, et al (1991) “Segregation of a missense mutation in the amyloid precursor protein gene with familial Alzheimer's disease”. *Nature*. **349**:704-706.

Golbe LI, Di Iorio G, Bonavita V, Miller DC, Duvoisin RC (1990) “A large kindred with autosomal dominant Parkinson's disease”. *Ann Neurol*. **27**:276-282.

Gong Y, Chang L, Viola KL, Lacor PN, Lambert MP, Finch CE, Krafft GA, Klein WL (2003) “Alzheimer's disease-affected brain: presence of oligomeric A beta ligands (ADDLs) suggests a molecular basis for reversible memory loss”. *Proc Natl Acad Sci U S A*. **100**:10417-10422.

Gonzalez-Garcia M, Fusco G, De Simone A (2021). “Membrane Interactions and Toxicity by Misfolded Protein Oligomers”. *Front Cell Dev Biol* **9**:642623.

Gould SB (2018) “Membranes and evolution”. *Curr Biol*. **28**:R381-R385.

Götz J, Chen F, van Dorpe J, Nitsch RM (2001) “Formation of neurofibrillary tangles in P301l tau transgenic mice induced by Abeta 42 fibrils”. *Science*. **293**:1491-1495.

Gralle M, Ferreira ST (2007) “Structure and functions of the human amyloid precursor protein: the whole is more than the sum of its parts”. *Prog Neurobiol*. **82**:11-32.

Gras SL, Waddington LJ, Goldie KN (2011) “Transmission electron microscopy of amyloid fibrils”. *Methods Mol Biol*. **752**:197-214.

Groiss SJ, Wojtecki L, Südmeyer M, Schnitzler A (2009) “Deep brain stimulation in Parkinson's disease”. *Ther Adv Neurol Disord*. **2**:20-28.

Grover S, Pham T, Jones A, Sinobas-Pereira C, Villoch Diaz Maurino M, Garrad EC, Makoni NJ, Parks A, Domalewski RJ, Riggio G, An H, Chen K, Nichols MR (2023) “A new

class of monoclonal Aβ antibodies selectively targets and triggers deposition of Aβ protofibrils". *J Neurochem*. **165**:860-873.

Grundke-Iqbal I, Iqbal K, Quinlan M, Tung YC, Zaidi MS, Wisniewski HM (1986) "Microtubule-associated protein tau. A component of Alzheimer paired helical filaments". *J Biol Chem*. **261**:6084-6089.

Haass C, Selkoe DJ (2007) "Soluble protein oligomers in neurodegeneration: lessons from the Alzheimer's amyloid beta-peptide". *Nat Rev Mol Cell Biol*. **8**:101-112.

Habchi J, Chia S, Limbocker R, Mannini B, Ahn M, Perni M, Hansson O, Arosio P, Kumita JR, Challa PK, Cohen SIA, Linse S, Dobson CM, Knowles TPJ, Vendruscolo M (2017) "Systematic Development of Small Molecules to Inhibit Specific Microscopic Steps of Aβ42 Aggregation in Alzheimer's Disease". *Proc Natl Acad Sci USA*. **114**:E200−E208.

Hampel H, Mesulam MM, Cuello AC, Farlow MR, Giacobini E, Grossberg GT, Khachaturian AS, Vergallo A, Cavedo E, Snyder PJ, Khachaturian ZS (2018) "The cholinergic system in the pathophysiology and treatment of Alzheimer's disease". *Brain*. **141**:1917-1933.

Hardy JA, Higgins GA (1992) "Alzheimer's disease: the amyloid cascade hypothesis". *Science*. **256**:184-185.

Hardy JA, Selkoe DJ (2002) "The amyloid hypothesis of Alzheimer's disease: progress and problems on the road to therapeutics". *Science*. **297**:353-356.

Harvey AL, Edrada-Ebel R, Quinn RJ (2015) "The re-emergence of natural products for drug discovery in the genomics era". *Nat Rev Drug Discov*. **14**:111-129.

Hastie TJ, Tibshirani RJ (1990) "Generalized Additive Models". Chapman & Hall/CRC. ISBN 978-0-412-34390-2.

Hauser RA, Sutherland D, Madrid JA, Rol MA, Frucht S, Isaacson S, Pagan F, Maddux BN, Li G, Tse W, Walter BL, Kumar R, Kremens D, Lew MF, Ellenbogen A, Oguh O, Vasquez A, Kinney W, Lowery M, Resnick M, Huff N, Posner J, Ballman KV, Harvey BE, Camilleri M, Zasloff M, Barbut D (2019) "Targeting neurons in the gastrointestinal tract to treat Parkinson's disease". *Clin Park Relat Disord*. **1**:2-7.

Hayes MT (2019) "Parkinson's Disease and Parkinsonism". *Am J Med*. **132**:802-807.

Hippius H, Neundörfer G (2003) "The discovery of Alzheimer's disease". *Dialogues Clin Neurosci*. **5**:101-108.

Holtzman DM, Morris JC, Goate AM (2011) "Alzheimer's disease: the challenge of the second century". *Sci Transl Med*. **3**:77sr1.

Hong S, Ostaszewski BL, Yang T, O'Malley TT, Jin M, Yanagisawa K, Li S, Bartels T, Selkoe DJ (2014) "Soluble Aβ oligomers are rapidly sequestered from brain ISF in vivo and bind GM1 ganglioside on cellular membranes". *Neuron*. **82**:308-319.

Howard R, Liu KY (2020) "Questions EMERGE as Biogen claims aducanumab turnaround". *Nat Rev Neurol*. **16**:63-64.

Huang LK, Kuan YC, Lin HW, Hu CJ (2023) "Clinical trials of new drugs for Alzheimer disease: a 2020-2023 update". *J Biomed Sci*. **30**:83.

Hulette CM, Welsh-Bohmer KA, Murray MG, Saunders AM, Mash DC, McIntyre LM (1998) "Neuropathological and neuropsychological changes in "normal" aging: evidence for preclinical Alzheimer disease in cognitively normal individuals". *Journal of neuropathology and experimental neurology*. **57**:1168–1174.

Hunter R (1981) "Zeta Potential in Colloid Science". *Science Academic Press.*

Hussain I, Powell D, Howlett DR, Tew DG, Meek TD, Chapman C, Gloger IS, Murphy KE, Southan CD, Ryan DM, Smith TS, Simmons DL, Walsh FS, Dingwall C, Christie G (1999) "Identification of a novel aspartic protease (Asp 2) as beta-secretase. *Mol Cell Neurosci*. **14**:419-427.

Hutter JL, Bechhoefer J (1993) "Calibration of Atomic-Force Microscope Tips". *Rev Sci Instrum*, **64**:1868-1873.

Illinger D, Duportail G, Mely Y, Poirel-Morales N, Gerard D, Kuhry JG (1995) "A comparison of the fluorescence properties of TMA-DPH as a probe for plasma membrane and for endocytic membrane". *Biochim Biophys Acta*. **1239**:58.

Ingólfsson HI, Carpenter TS, Bhatia H, Bremer PT, Marrink SJ, Lightstone FC (2017) "Computational Lipidomics of the Neuronal Plasma Membrane". *Biophys J*. **113**:2271-2280.

Ingólfsson HI, Melo MN, van Eerden FJ, Arnarez C, Lopez CA, Wassenaar TA, Periole X, de Vries AH, Tieleman DP, Marrink SJ (2014). "Lipid organization of the plasma membrane" *J. Am. Chem. Soc*. **136**:14554-14559.

Iqbal K, Liu F, Gong CX, Alonso Adel C, Grundke-Iqbal I (2009) "Mechanisms of tau-induced neurodegeneration". *Acta Neuropathol*. **118**:53–69.

Israel MA, Yuan SH, Bardy C, Reyna SM, Mu Y, Herrera C, Hefferan MP, Van Gorp S, Nazor KL, Boscolo FS, Carson CT, Laurent LC, Marsala M, Gage FH, Remes AM, Koo EH, Goldstein LS (2012) "Probing sporadic and familial Alzheimer's disease using induced pluripotent stem cells". *Nature*. **482**:216-220.

Ittner LM, Ke YD, Delerue F, Bi M, Gladbach A, van Eersel J, Wölfing H, Chieng BC, Christie MJ, Napier IA, Eckert A, Staufenbiel M, Hardeman E, Götz J (2010) "Dendritic function of tau mediates amyloid-beta toxicity in Alzheimer's disease mouse models". *Cell*. **142**:387-397.

Jack CR Jr, Bennett DA, Blennow K, Carrillo MC, Dunn B, Haeberlein SB, Holtzman DM, Jagust W, Jessen F, Karlawish J, Liu E, Molinuevo JL, Montine T, Phelps C, Rankin KP, Rowe CC, Scheltens P, Siemers E, Snyder HM, Sperling R (2018) "Contributors. NIA-AA Research Framework: Toward a biological definition of Alzheimer's disease". *Alzheimers Dement*. **14**:535-562.

Jack CR Jr, Bennett DA, Blennow K, Carrillo MC, Feldman HH, Frisoni GB, Hampel H, Jagust WJ, Johnson KA, Knopman DS, Petersen RC, Scheltens P, Sperling RA, Dubois B (2016) "A/T/N: An unbiased descriptive classification scheme for Alzheimer disease biomarkers". *Neurology*. **87**:539-547.

Jack CR Jr, Therneau TM, Weigand SD, Wiste HJ, Knopman DS, Vemuri P, Lowe VJ, Mielke MM, Roberts RO, Machulda MM, Graff-Radford J, Jones DT, Schwarz CG, Gunter JL, Senjem ML, Rocca WA, Petersen RC (2019) "Prevalence of Biologically vs

Clinically Defined Alzheimer Spectrum Entities Using the National Institute on Aging-Alzheimer's Association Research Framework". *JAMA Neurol*. **76**:1174–1183.

Jackson RJ, Rudinskiy N, Herrmann AG, Croft S, Kim JM, Petrova V, Ramos-Rodriguez JJ, Pitstick R, Wegmann S, Garcia-Alloza M, Carlson GA, Hyman BT, Spires-Jones TL (2016) "Human tau increases amyloid β plaque size but not amyloid β-mediated synapse loss in a novel mouse model of Alzheimer's disease". *Eur J Neurosci*. **44**:3056-3066.

Jash A, Ubeyitogullari A, Rizvi SSH (2021) "Liposomes for oral delivery of protein and peptide-based therapeutics: challenges, formulation strategies, and advances". *J Mater Chem B* **9**:4773-4792.

Jiang W, Li S, Li X (2015) "Therapeutic potential of berberine against neurodegenerative diseases". *Sci China Life Sci*. **58**:564-569.

Jokar S, Khazaei S, Gameshgoli XE, Khafaji M, Yarani B, Sharifzadeh M, Beiki D, Bavi O (2020) "Amyloid β-Targeted Inhibitory Peptides for Alzheimer's Disease: Current State and Future Perspectives". *Alzheimer's Disease: Drug Discovery [Internet]. Brisbane (AU): Exon Publications*. Chapter 3.

Jones SR, Selinsky BS, Rao MN, Zhang X, Kinney WA, Tham FS (1998) "Efficient Route to 7α-(Benzoyloxy)-3-dioxolane Cholestan-24(R)-ol, a Key Intermediate in the Synthesis of Squalamine". *The Journal of Organic Chemistry*. **63**:3786-3789.

Kahle PJ (2008) "α-Synucleinopathy models and human neuropathology: Similarities and differences". *Acta Neuropathol* **115**:87–95.

Kaiser RD, London E (1998) "Location of diphenylhexatriene (DPH) and its derivatives within membranes: comparison of different fluorescence quenching analyses of membrane depth". *Biochemistry*. **37**:8180.

Kalia LV, Lang AE (2015) "Parkinson's disease". *Lancet*. **386**:896-912.

Kametani F, Hasegawa M (2018) "Reconsideration of Amyloid Hypothesis and Tau Hypothesis in Alzheimer's Disease". *Front Neurosci*. **12**:25.

Kang J, Lemaire HG, Unterbeck A, Salbaum JM, Masters CL, Grzeschik KH, Multhaup G, Beyreuther K, Müller-Hill B (1987) "The precursor of Alzheimer's disease amyloid A4 protein resembles a cell-surface receptor". *Nature*. **325**:733-736.

Kao YC, Ho PC, Tu YK, Jou IM, Tsai KJ (2020) "Lipids and Alzheimer's Disease". *Int J Mol Sci*. **21**:1505.

Karamanos TK, Kalverda AP, Thompson GS, Radford SE (2015) "Mechanisms of amyloid formation revealed by solution NMR". *Prog Nucl Magn Reson Spectrosc*. **88-89**:86-104.

Karran E, Mercken M, De Strooper B (2011) "The amyloid cascade hypothesis for Alzheimer's disease: an appraisal for the development of therapeutics". *Nat Rev Drug Discov*. **10**:698-712.

Karran E, De Strooper B (2022) "The amyloid hypothesis in Alzheimer disease: new insights from new therapeutics". *Nat Rev Drug Discov*. **21**:306-318.

Katzman R, Saitoh T (1991) “Advances in Alzheimer's disease”. *FASEB J*. **5**:278-286.

Katzman R, Terry R, DeTeresa R, Brown T, Davies P, Fuld P, Renbing X, Peck A (1988) “Clinical, pathological, and neurochemical changes in dementia: a subgroup with preserved mental status and numerous neocortical plaques”. *Annals of neurology*. **23**:138–144.

Kayed R, Head E, Thompson JL, McIntire TM, Milton SC, Cotman CW, Glabe CG (2003) “Common structure of soluble amyloid oligomers implies common mechanism of pathogenesis”. *Science*. **300**:486–489.

Kayed R, Head E, Sarsoza F, Saing T, Cotman CW, Necula M, Margol L, Wu J, Breydo L, Thompson JL, Rasool S, Gurlo T, Butler P, Glabe CG (2007) “Fibril specific, conformation dependent antibodies recognize a generic epitope common to amyloid fibrils and fibrillar oligomers that is absent in prefibrillar oligomers”. *Mol Neurodegener*. **2**:18.

Kayed R, Lasagna-Reeves CA (2013) “Molecular mechanisms of amyloid oligomers toxicity”. *J Alzheimers Dis*. **1**:S67-78.

Kayed R, Pensalfini A, Margol L, Sokolov Y, Sarsoza F, Head E, Hall J, Glabe C (2009) “Annular protofibrils are a structurally and functionally distinct type of amyloid oligomer”. *J Biol Chem*. **284**:4230-4237.

Karaman O, Çakın H, Alhudhaif A, Polat K (2021) “Robust automated Parkinson disease detection based on voice signals with transfer learning” *Expert Systems with Applications*, **178**:115013.

Kim J, Basak JM, Holtzman DM (2009) “The role of apolipoprotein E in Alzheimer's disease”. *Neuron*. **63**:287-303.

Kingwell K (2017) “Zeroing in on neurodegenerative α-synuclein”. *Nat Rev Drug Discov*. **16**:371-373.

Kinney JW, Bemiller SM, Murtishaw AS, Leisgang AM, Salazar AM, Lamb BT (2018) “Inflammation as a central mechanism in Alzheimer's disease”. *Alzheimers Dement (N Y).* **4**:575-590.

Klunk WE, Engler H, Nordberg A, Wang Y, Blomqvist G, Holt DP, Bergström M, Savitcheva I, Huang GF, Estrada S, Ausén B, Debnath ML, Barletta J, Price JC, Sandell J, Lopresti BJ, Wall A, Koivisto P, Antoni G, Mathis CA, Långström B (2004) “Imaging brain amyloid in Alzheimer's disease with Pittsburgh Compound-B”. *Ann Neurol*. **55**:306-319.

Knopman DS, Amieva H, Petersen RC, Chételat G, Holtzman DM, Hyman BT, Nixon RA, Jones DT (2021) “Alzheimer disease”. *Nat Rev Dis Primers*. **7**:33.

Kouli A, Torsney KM, Kuan WL (2018) “Parkinson’s Disease: Etiology, Neuropathology, and Pathogenesis. In: Stoker TB, Greenland JC, editors”. *Parkinson’s Disease: Pathogenesis and Clinical Aspects*. Chapter 1. PMID: 30702842.

Koushki K, Shahbaz SK, Mashayekhi K, Sadeghi M, Zayeri ZD, Taba MY, Banach M, Al-Rasadi K, Johnston TP, Sahebkar A (2021) “Anti-inflammatory Action of Statins in Cardiovascular Disease: The Role of Inflammasome and Toll-Like Receptor Pathways”. *Clin Rev Allergy Immunol*. **60**:175-199.

Kramer ML, Schulz-Schaeffer WJ (2007) “Presynaptic alpha-synuclein aggregates, not Lewy bodies, cause neurodegeneration in dementia with Lewy bodies”. *J Neurosci*. **27**:1405-1410.

Krishnan N, Koveal D, Miller DH, Xue B, Akshinthala SD, Kragelj J, Jensen MR, Gauss CM, Page R, Blackledge M, Muthuswamy SK, Peti W, Tonks NK (2014) “Targeting the disordered C terminus of PTP1B with an allosteric inhibitor”. *Nat Chem Biol*. **10**:558-566.

Krishnan R, Goodman JL, Mukhopadhyay S, Pacheco CD, Lemke EA, Deniz AA, Lindquist S (2012) “Conserved Features of Intermediates in Amyloid Assembly Determine Their Benign or Toxic States”. *Proc Nat. Acad Sci USA*. **109**:11172−11177.

Krüger R, Kuhn W, Müller T, Woitalla D, Graeber M, Kösel S, Przuntek H, Epplen JT, Schöls L, Riess O (1998) “Ala30Pro mutation in the gene encoding alpha-synuclein in Parkinson's disease”. *Nat Genet*. **18**:106-108.

Lakowicz JR (2006) “Principles of Fluorescence Spectroscopy”. *Springer, Berlin*. http://dx.doi.org/10.1007/978-0-387-46312-4

Ladiwala ARA, Litt J, Kane RS, Aucoin DS, Smith SO, Ranjan S, Davis J, Nostrand WEV, Tessier PM (2012) “Conformational Differences between Two Amyloid β Oligomers of Similar Size and Dissimilar Toxicity”. *J Biol Chem* **287**:24765−24773.

Lambert MP, Barlow AK, Chromy BA, Edwards C, Freed R, Liosatos M, Morgan TE, Rozovsky I, Trommer B, Viola KL, Wals P, Zhang C, Finch CE, Krafft GA, Klein WL (1998) “Diffusible, nonfibrillar ligands derived from Abeta1-42 are potent central nervous system neurotoxins”. *Proc Natl Acad Sci U S A*. **95**:6448-6453.

Lambert MP, Viola KL, Chromy BA, Chang L, Morgan TE, Yu J, Venton DL, Krafft GA, Finch CE, Klein WL (2001) “Vaccination with Soluble Abeta Oligomers Generates Toxicity-Neutralizing Antibodies”. *J Neurochem*. **79**:595-605.

Lantz KA, Hart SG, Planey SL, Roitman MF, Ruiz-White IA, Wolfe HR, McLane MP (2010) “Inhibition of PTP1B by trodusquemine (MSI-1436) causes fat-specific weight loss in diet-induced obese mice”. *Obesity (Silver Spring)*. **18**:1516-1523.

Lee HK, Velazquez Sanchez C, Chen M, Morin PJ, Wells JM, Hanlon EB, Xia W (2016) “Three-Dimensional Human Neuro-Spheroid Model of Alzheimer's Disease Based on Differentiated Induced Pluripotent Stem Cells”. *PLoS One*. **11**:e0163072.

Leri M, Bemporad F, Oropesa-Nuñez R, Canale C, Calamai M, Nosi D, Ramazzotti M, Giorgetti S, Pavone FS, Bellotti V, Stefani M, Bucciantini M (2016). “Molecular insights into cell toxicity of a novel familial amyloidogenic variant of β2-microglobulin” *J Cell Mol Med* **20**:1443-1456.

Leri M, Oropesa-Nuñez R, Canale C, Raimondi S, Giorgetti S, Bruzzone E, Bellotti V, Stefani M, Bucciantini M (2018). “Oleuropein aglycone: A polyphenol with different targets against amyloid toxicity” *Biochim Biophys Acta Gen Subj* **1862**:1432-1442.

Li S, Jin M, Koeglsperger T, Shepardson NE, Shankar GM, Selkoe DJ (2011) “Soluble Aβ oligomers inhibit long-term potentiation through a mechanism involving

excessive activation of extrasynaptic NR2B-containing NMDA receptors". *J Neurosci*. **31**:6627-6638.

Limbocker R, Chia S, Ruggeri FS, Perni M, Cascella R, Heller GT, Meisl G, Mannini B, Habchi J, Michaels TCT, Challa PK, Ahn M, Casford ST, Fernando N, Xu CK, Kloss ND, Cohen SIA, Kumita JR, Cecchi C, Zasloff M, Linse S, Knowles TPJ, Chiti F, Vendruscolo M, Dobson CM (2019) "Trodusquemine enhances Aβ42 aggregation but suppresses its toxicity by displacing oligomers from cell membranes". *Nat Commun*. **10**:225.

Limbocker R, Cremades N, Cascella R, Tessier PM, Vendruscolo M, Chiti F (2023) "Characterization of Pairs of Toxic and Nontoxic Misfolded Protein Oligomers Elucidates the Structural Determinants of Oligomer Toxicity in Protein Misfolding Diseases". *Acc Chem Res*. **56**:1395-1405.

Limbocker R, Errico S, Barbut D, Knowles TPJ, Vendruscolo M, Chiti F, Zasloff M (2022) "Squalamine and trodusquemine: two natural products for neurodegenerative diseases, from physical chemistry to the clinic". *Nat Prod Rep*. **39**:742-753.

Limbocker R, Mannini B, Ruggeri FS, Cascella R, Xu CK, Perni M, Chia S, Chen SW, Habchi J, Bigi A, Kreiser RP, Wright AK, Albright JA, Kartanas T, Kumita JR, Cremades N, Zasloff M, Cecchi C, Knowles TPJ, Chiti F, Vendruscolo M, Dobson CM (2020) "Trodusquemine displaces protein misfolded oligomers from cell membranes and abrogates their cytotoxicity through a generic mechanism". *Commun Biol*. **3**:435.

Lin CH, Lin JW, Liu YC, Chang CH, Wu RM (2014) "Risk of Parkinson's disease following severe constipation: a nationwide population-based cohort study". *Parkinsonism Relat Disord*. **20**:1371-1375.

Linse S, Scheidt T, Bernfur K, Vendruscolo M, Dobson CM, Cohen SIA, Sileikis E, Lundqvist M, Qian F, O'Malley T, Bussiere T, Weinreb PH, Xu CK, Meisl G, Devenish SRA, Knowles TPJ, Hansson O (2020) "Kinetic fingerprints differentiate the mechanisms of action of anti-Aβ antibodies". *Nat Struct Mol Biol*. **27**:1125-1133.

Litvinov DY, Savushkin EV, Dergunov AD (2018) "Intracellular and Plasma Membrane Events in Cholesterol Transport and Homeostasis". *J Lipids*. **2018**:3965054.

Liu L, Zhang K, Tan L, Chen YH, Cao YP (2015) "Alterations in cholesterol and ganglioside GM1 content of lipid rafts in platelets from patients with Alzheimer disease". *Alzheimer Dis Assoc Disord*. **29**:63-69.

Liu W, Liu P, Tao S, Deng Y, Li X, Lan T, Zhang X, Guo F, Huang W, Chen F, Huang H, Zhou SF (2008) "Berberine inhibits aldose reductase and oxidative stress in rat mesangial cells cultured under high glucose". *Arch Biochem Biophys*. **475**:128-134.

Liu Y, Thalamuthu A, Mather KA, Crawford J, Ulanova M, Wong MWK, Pickford R, Sachdev PS, Braidy N (2021) "Plasma lipidome is dysregulated in Alzheimer's disease and is associated with disease risk genes". *Transl Psychiatry*. **11**:344.

Liu Z, Zhou T, Ziegler AC, Dimitrion P, Zuo L (2017) "Oxidative Stress in Neurodegenerative Diseases: From Molecular Mechanisms to Clinical Applications". *Oxid Med Cell Longev*. **2017**:2525967.

Logovinsky V, Satlin A, Lai R, Swanson C, Kaplow J, Osswald G, Basun H, Lannfelt L (2016) "Safety and tolerability of BAN2401--a clinical study in Alzheimer's disease with a protofibril selective Aβ antibody". *Alzheimers Res Ther*. **8**:14.

Lökk J, Nilsson M (2010) "Frequency, type and factors associated with the use of complementary and alternative medicine in patients with Parkinson's disease at a neurological outpatient clinic". *Parkinsonism Relat Disord*. **16**:540-544.

Lord A, Gumucio A, Englund H, Sehlin D, Sundquist VS, Söderberg L, Möller C, Gellerfors P, Lannfelt L, Pettersson FE, Nilsson LN (2009) "An amyloid-beta protofibril-selective antibody prevents amyloid formation in a mouse model of Alzheimer's disease". *Neurobiol Dis*. **36**:425-434.

Loof A, Schoofs L (2019) "Alzheimer's Disease: Is a Dysfunctional Mevalonate Biosynthetic Pathway the Master-Inducer of Deleterious Changes in Cell Physiology?" *OBM Neurobiology*. **3**:1-1.

Lorenzen N, Nielsen SB, Buell AK, Kaspersen JD, Arosio P, Vad BS, Paslawski W, Christiansen G, Valnickova-Hansen Z, Andreasen M, Enghild JJ, Pedersen JS, Dobson CM, Knowles TP, Otzen DE (2014) "The role of stable α-synuclein oligomers in the molecular events underlying amyloid formation". *J Am Chem Soc*. **136**:3859-3868.

Lu JX, Qiang W, Yau WM, Schwieters CD, Meredith SC, Tycko R (2013) "Molecular structure of β-amyloid fibrils in Alzheimer's disease brain tissue". *Cell*. **154**:1257-1268.

Lúcio M, Ferreira H, Lima JL, Reis S (2006) "Interactions between oxicams and membrane bilayers: an explanation for their different COX selectivity". *Med Chem*. **2**:447-456.

Lundbaek JA, Collingwood SA, Ingólfsson HI, Kapoor R, Andersen OS (2010) "Lipid bilayer regulation of membrane protein function: gramicidin channels as molecular force probes". *J R Soc Interface*. **7**:373-395.

Mandelkow EM, Biernat J, Drewes G, Gustke N, Trinczek B, Mandelkow E (1995) "Tau domains, phosphorylation, and interactions with microtubules". *Neurobiol Aging*. **16**:355-362.

Mannini B, Cascella R, Zampagni M, van Waarde-Verhagen M, Meehan S, Roodveldt C, Campioni S, Boninsegna M, Penco A, Relini A, Kampinga HH, Dobson CM, Wilson MR, Cecchi C, Chiti F (2012) "Molecular mechanisms used by chaperones to reduce the toxicity of aberrant protein oligomers". *Proc Natl Acad Sci U S A*. **109**:12479-12484.

Mannini B, Mulvihill E, Sgromo C, Cascella R, Khodarahmi R, Ramazzotti M, Dobson CM, Cecchi C, Chiti F (2014) "Toxicity of protein oligomers is rationalized by a function combining size and surface hydrophobicity". *ACS Chem Biol*. **9**:2309-2317.

Maqoud F, Curci A, Scala R, Pannunzio A, Campanella F, Coluccia M, Passantino G, Zizzo N, Tricarico D (2018) "Cell Cycle Regulation by Ca 2+-Activated K^+ (BK) Channels Modulators in SH-SY5Y Neuroblastoma Cells". *Int J Mol Sci.* **19**:2442.

Markesbery WR (1997) “Oxidative stress hypothesis in Alzheimer's disease”. *Free Radic Biol Med*. **23**:134-147.

Martins IC, Kuperstein I, Wilkinson H, Maes E, Vanbrabant M, Jonckheere W, Van Gelder P, Hartmann D, D'Hooge R, De Strooper B, Schymkowitz J, Rousseau F (2008) “Lipids revert inert Abeta amyloid fibrils to neurotoxic protofibrils that affect learning in mice”. *EMBO J*. **27**:224-233.

Massoud F, Gauthier S (2010) “Update on the pharmacological treatment of Alzheimer's disease”. *Curr Neuropharmacol*. **8**:69-80.

Matsubara T, Iijima K, Yamamoto N, Yanagisawa K, Sato T (2013) “Density of GM1 in nanoclusters is a critical factor in the formation of a spherical assembly of amyloid β-protein on synaptic plasma membranes”. *Langmuir*. **29**:2258-2264.

Matsubara T, Yasumori H, Ito K, Shimoaka T, Hasegawa T, Sato T (2018) “Amyloid-β fibrils assembled on ganglioside-enriched membranes contain both parallel β-sheets and turns”. *J Biol Chem*. **293**:14146-14154.

Matsunaga S, Kishi T, Iwata N (2015) “Memantine monotherapy for Alzheimer's disease: a systematic review and meta-analysis”. *PLoS One*. **10**:e0123289.

Mattson MP, Magnus T (2006) “Ageing and neuronal vulnerability” *Nat Rev Neurosci*. **7**:278-294.

Mattsson N, Zetterberg H, Hansson O, Andreasen N, Parnetti L, Jonsson M, Herukka SK, van der Flier WM, Blankenstein MA, Ewers M, Rich K, Kaiser E, Verbeek M, Tsolaki M, Mulugeta E, Rosén E, Aarsland D, Visser PJ, Schröder J, Marcusson J, de Leon M, Hampel H, Scheltens P, Pirttilä T, Wallin A, Jönhagen ME, Minthon L, Winblad B, Blennow K (2009) “CSF biomarkers and incipient Alzheimer disease in patients with mild cognitive impairment”. *JAMA*. **302**:385-393.

McFarlane O, Kędziora-Kornatowska K (2020) “Cholesterol and Dementia: A Long and Complicated Relationship”. *Curr Aging Sci*. **13**:42-51.

McGleenon BM, Dynan KB, Passmore AP (1999) “Acetylcholinesterase inhibitors in Alzheimer's disease”. *Br J Clin Pharmacol*. **48**:471-480.

McKhann GM, Knopman DS, Chertkow H, Hyman BT, Jack CR Jr, Kawas CH, Klunk WE, Koroshetz WJ, Manly JJ, Mayeux R, Mohs RC, Morris JC, Rossor MN, Scheltens P, Carrillo MC, Thies B, Weintraub S, Phelps CH (2011) “The diagnosis of dementia due to Alzheimer's disease: recommendations from the National Institute on Aging-Alzheimer's Association workgroups on diagnostic guidelines for Alzheimer's disease”. *Alzheimers Dement*. **7**:263-269.

McLean CA, Cherny RA, Fraser FW, Fuller SJ, Smith MJ, Beyreuther K, Bush AI, Masters CL (1999) “Soluble pool of Abeta amyloid as a determinant of severity of neurodegeneration in Alzheimer's disease”. *Ann Neurol*. **46**:860-866.

Medeiros R, Baglietto-Vargas D, LaFerla FM (2011) “The role of tau in Alzheimer's disease and related disorders”. *CNS Neurosci Ther*. **17**:514-524.

Menon S, Mondal J (2023) “Conformational Plasticity in α-Synuclein and How Crowded Environment Modulates It”. *J Phys Chem B*. **127**:4032-4049.

Menšíková K, Matěj R, Colosimo C, Rosales R, Tučková L, Ehrmann J, Hraboš D, Kolaříková K, Vodička R, Vrtěl R, Procházka M, Nevrlý M, Kaiserová M, Kurčová S, Otruba P, Kaňovský P (2022) “Lewy body disease or diseases with Lewy bodies?” *NPJ Parkinsons Dis*. **8**:3.

Miguel-Álvarez M, Santos-Lozano A, Sanchis-Gomar F, Fiuza-Luces C, Pareja-Galeano H, Garatachea N, Lucia A (2015) “Non-steroidal anti-inflammatory drugs as a treatment for Alzheimer's disease: a systematic review and meta-analysis of treatment effect”. *Drugs Aging*. **32**:139-147.

Miller DW, Hague SM, Clarimon J, Baptista M, Gwinn-Hardy K, Cookson MR, Singleton AB (2004) “α-Synuclein in blood and brain from familial Parkinson disease with SNCA locus triplication”. *Neurology.* **62**:1835–1838

Mizuno T, Nakata M, Naiki H, Michikawa M, Wang R, Haass C, Yanagisawa K (1999) “Cholesterol-dependent generation of a seeding amyloid beta-protein in cell culture”. *J Biol Chem*. **274**:15110-15114.

Moghaddam HK, Baluchnejadmojarad T, Roghani M, Khaksari M, Norouzi P, Ahooie M, Mahboobi F (2014) “Berberine ameliorate oxidative stress and astrogliosis in the hippocampus of STZ-induced diabetic rats”. *Mol Neurobiol*. **49**:820-826.

Molander-Melin M, Blennow K, Bogdanovic N, Dellheden B, Månsson JE, Fredman P (2005) “Structural membrane alterations in Alzheimer brains found to be associated with regional disease development; increased density of gangliosides GM1 and GM2 and loss of cholesterol in detergent-resistant membrane domains”. *J Neurochem*. **92**:171-182.

Moore KS, Wehrli S, Roder H, Rogers M, Forrest JN Jr, McCrimmon D, Zasloff M (1993) “Squalamine: an aminosterol antibiotic from the shark”. *Proc Natl Acad Sci U S A*. **90**:1354-1358.

Morris KL, Serpell LC (2012) “X-ray fibre diffraction studies of amyloid fibrils”. *Methods Mol Biol*. **849**:121-135.

Moss DE (2020) “Improving Anti-Neurodegenerative Benefits of Acetylcholinesterase Inhibitors in Alzheimer's Disease: Are Irreversible Inhibitors the Future?” *Int J Mol Sci*. **21**:3438.

Moustafa AA, Chakravarthy S, Phillips JR, Gupta A, Keri S, Polner B, Frank MJ, Jahanshahi M (2016) “Motor symptoms in Parkinson's disease: A unified framework”. *Neurosci Biobehav Rev*. **68**:727-740.

Müller CP, Reichel M, Mühle C, Rhein C, Gulbins E, Kornhuber J (2015) “Brain membrane lipids in major depression and anxiety disorders”. *Biochim Biophys Acta*. **1851**:1052-1065.

Murphy DD, Rueter SM, Trojanowski JQ, Lee VM (2000) “Synucleins are developmentally expressed, and α-synuclein regulates the size of the presynaptic vesicular pool in primary hippocampal neurons”. *J Neurosci.* **20**:3214–3220.

Murphy MP, LeVine H 3rd (2010) “Alzheimer's disease and the amyloid-beta peptide”. *J Alzheimers Dis*. **19**:311-323.

Nelson R, Eisenberg D (2006) “Recent atomic models of amyloid fibril structure”. *Curr Opin Struct Biol*. **16**:260-265.

Niemelä PS, Hyvönen MT, Vattulainen I (2006) “Influence of chain length and unsaturation on sphingomyelin bilayers. *Biophys J*. **90**:851-863.

Nieto-Garai JA, Lorizate M, Contreras FX (2022) “Shedding light on membrane rafts structure and dynamics in living cells”. *Biochim Biophys Acta Biomembr*. **1864**:183813.

Nilsson MR (2004) “Techniques to study amyloid fibril formation in vitro”. *Methods*. **34**:151-160.

Olson MI, Shaw CM (1969) “Presenile dementia and Alzheimer's disease in mongolism”. *Brain*. **92**:147-156.

Orini S, Geroldi C, Zanetti O (2022) “The new therapy for Alzheimer's disease: from a hope for a few to a false hope?” *Aging Clin Exp Res*. **34**:3151-3153.

Oropesa-Nuñez R, Seghezza S, Dante S, Diaspro A, Cascella R, Cecchi C, Stefani M, Chiti F, Canale C (2016) “Interaction of toxic and non-toxic HypF-N oligomers with lipid bilayers investigated at high resolution with atomic force microscopy”. *Oncotarget*. **7**:44991-45004.

Padurariu M, Ciobica A, Lefter R, Serban IL, Stefanescu C, Chirita R (2013) “The oxidative stress hypothesis in Alzheimer's disease”. *Psychiatr Danub*. **25**:401-409.

Paleologou KE, Kragh CL, Mann DM, Salem SA, Al-Shami R, Allsop D, Hassan AH, Jensen PH, El-Agnaf OM (2009) “Detection of elevated levels of soluble alpha-synuclein oligomers in post-mortem brain extracts from patients with dementia with Lewy bodies”. *Brain*. **132**:1093-1101.

Panchal M, Loeper J, Cossec JC, Perruchini C, Lazar A, Pompon D, Duyckaerts C (2010) “Enrichment of cholesterol in microdissected Alzheimer's disease senile plaques as assessed by mass spectrometry”. *J Lipid Res*. **51**:598-605.

Pandey NR, Zhou X, Qin Z, Zaman T, Gomez-Smith M, Keyhanian K, Anisman H, Brunel JM, Stewart AF, Chen HH (2013) “The LIM domain only 4 protein is a metabolic responsive inhibitor of protein tyrosine phosphatase 1B that controls hypothalamic leptin signaling”. *J Neurosci*. **33**:12647-12655.

Pandey NR, Zhou X, Zaman T, Cruz SA, Qin Z, Lu M, Keyhanian K, Brunel JM, Stewart AF, Chen HH (2014) “LMO4 is required to maintain hypothalamic insulin signaling”. *Biochem Biophys Res Commun*. **450**:666-672.

Paravastu AK, Leapman RD, Yau WM, Tycko R (2008) “Molecular structural basis for polymorphism in Alzheimer’s β-amyloid fibrils”. *PNAS* **105**:18349–18354.

Parkinson J (1817) “An essay on the shaking palsy”. *Whittingham and Rowland for Sherwood, Needly and Jones, London.*

Paroni G, Bisceglia P, Seripa D (2019) “Understanding the Amyloid Hypothesis in Alzheimer's Disease”. *J Alzheimers Dis*. **68**:493-510.

Passeri E, Elkhoury K, Morsink M, Broersen K, Linder M, Tamayol A, Malaplate C, Yen FT, Arab-Tehrany E (2022) “Alzheimer's Disease: Treatment Strategies and Their Limitations”. *Int J Mol Sci*. **23**:13954.

Perni M, Flagmeier P, Limbocker R, Cascella R, Aprile FA, Galvagnion C, Heller GT, Meisl G, Chen SW, Kumita JR, Challa PK, Kirkegaard JB, Cohen SIA, Mannini B, Barbut D, Nollen EAA, Cecchi C, Cremades N, Knowles TPJ, Chiti F, Zasloff M, Vendruscolo M, Dobson CM (2018) “Multistep Inhibition of α-Synuclein Aggregation and Toxicity in Vitro and in Vivo by Trodusquemine”. *ACS Chem Biol*. **13**:2308-2319.

Perni M, Galvagnion C, Maltsev A, Meisl G, Müller MB, Challa PK, Kirkegaard JB, Flagmeier P, Cohen SI, Cascella R, Chen SW, Limbocker R, Sormanni P, Heller GT, Aprile FA, Cremades N, Cecchi C, Chiti F, Nollen EA, Knowles TP, Vendruscolo M, Bax A, Zasloff M, Dobson CM (2017) “A natural product inhibits the initiation of α-synuclein aggregation and suppresses its toxicity”. *Proc Natl Acad Sci U S A*. **114**:E1009-E1017.

Petersen RC, Aisen P, Boeve BF, Geda YE, Ivnik RJ, Knopman DS, Mielke M, Pankratz VS, Roberts R, Rocca WA, Weigand S, Weiner M, Wiste H, Jack CR Jr (2013) “Mild cognitive impairment due to Alzheimer disease in the community”. *Ann Neurol*. **74**:199-208.

Pickett EK, Herrmann AG, McQueen J, Abt K, Dando O, Tulloch J, Jain P, Dunnett S, Sohrabi S, Fjeldstad MP, Calkin W, Murison L, Jackson RJ, Tzioras M, Stevenson A, d'Orange M, Hooley M, Davies C, Colom-Cadena M, Anton-Fernandez A, King D, Oren I, Rose J, McKenzie CA, Allison E, Smith C, Hardt O, Henstridge CM, Hardingham GE, Spires-Jones TL (2019) “Amyloid Beta and Tau Cooperate to Cause Reversible Behavioral and Transcriptional Deficits in a Model of Alzheimer's Disease”. *Cell Rep*. **29**:3592-3604.

Pike L (2004) “Lipid rafts: heterogeneity on the high seas”. *Biochem. J*. **378**:281-292.

Pilitsis JG, Chu Y, Kordower J, Bergen DC, Cochran EJ, Bakay RA (2008) “Postmortem study of deep brain stimulation of the anterior thalamus: case report”. *Neurosurgery.* **62**:E530–E532.

Poirier MA, Xiao W, Macosko JC, Chan C, Shin YK, Bennett MK (1998) “The synaptic SNARE complex is a parallel four-stranded helical bundle”. *Nat Struct Biol*. **5**:765-769.

Polymeropoulos MH, Lavedan C, Leroy E, Ide SE, Dehejia A, Dutra A, Pike B, Root H, Rubenstein J, Boyer R, Stenroos ES, Chandrasekharappa S, Athanassiadou A, Papapetropoulos T, Johnson WG, Lazzarini AM, Duvoisin RC, Di Iorio G, Golbe LI, Nussbaum RL (1997) “Mutation in the alpha-synuclein gene identified in families with Parkinson's disease”. *Science*. **276**:2045-2047.

Pooler AM, Noble W, Hanger DP (2014) “A role for tau at the synapse in Alzheimer’s disease pathogenesis”. *Neuropharmacology* **76**:1–8

Postuma RB, Berg D, Stern M, Poewe W, Olanow CW, Oertel W, Obeso J, Marek K, Litvan I, Lang AE, Halliday G, Goetz CG, Gasser T, Dubois B, Chan P, Bloem BR, Adler CH, Deuschl G (2015) “MDS clinical diagnostic criteria for Parkinson's disease”. *Mov Disord*. **30**:1591-1601.

Price JL, Morris JC (1999) “Tangles and plaques in nondemented aging and “preclinical” Alzheimer’s disease”. *Annals of neurology*. **45**:358–368.

Qin Z, Zhang L, Cruz SA, Stewart AFR, Chen HH (2020) “Activation of tyrosine phosphatase PTP1B in pyramidal neurons impairs endocannabinoid signaling by tyrosine receptor kinase trkB and causes schizophrenia-like behaviors in mice”. *Neuropsychopharmacology*. **45**:1884-1895.

Quinn N (1995) “Drug treatment of Parkinson's disease”. *BMJ* **310**:575–579.

Ramakrishnan NA, Drescher MJ, Drescher DG (2012) “The SNARE complex in neuronal and sensory cells”. *Mol Cell Neurosci*. **50**:58-69.

Rao MN, Shinnar AE, Noecker LA, Chao TL, Feibush B, et al. (2000) “Aminosterols from the dogfish shark Squalus acanthias”. *J Nat Prod*. **63**:631-635.

Rees TM, Brimijoin S (2003) “The role of acetylcholinesterase in the pathogenesis of Alzheimer's disease”. *Drugs Today (Barc).* **39**:75-83.

Rego AC, Oliveira CR (2003) “Mitochondrial dysfunction and reactive oxygen species in excitotoxicity and apoptosis: implications for the pathogenesis of neurodegenerative diseases”. *Neurochem Res*. **28**:1563-1574.

Reich C, Horton MR, Krause B, Gast AP, Rädler JO, Nickel B (2008) “Asymmetric structural features in single supported lipid bilayers containing cholesterol and GM1 resolved with synchrotron X-Ray reflectivity”. *Biophys J*. **95**:657-668.

Reiman EM, Chen K, Liu X, Bandy D, Yu M, Lee W, Ayutyanont N, Keppler J, Reeder SA, Langbaum JB, Alexander GE, Klunk WE, Mathis CA, Price JC, Aizenstein HJ, DeKosky ST, Caselli RJ (2009) “Fibrillar amyloid-beta burden in cognitively normal people at 3 levels of genetic risk for Alzheimer's disease”. *Proc Natl Acad Sci U S A*. **106**:6820-6825.

Relini A, Torrassa S, Rolandi R, Gliozzi A, Rosano C, Canale C, Bolognesi M, Plakoutsi G, Bucciantini M, Chiti F, Stefani M (2004) “Monitoring the process of HypF fibrillization and liposome permeabilization by protofibrils”. *J Mol Biol*. **338**:943-957.

Ricciarelli R, Fedele E (2017) “The Amyloid Cascade Hypothesis in Alzheimer's Disease: It's Time to Change Our Mind”. *Curr Neuropharmacol*. **15**:926-935.

Rizo J (2018) “Mechanism of neurotransmitter release coming into focus”. *Protein Sci*. **27**:1364-1391.

Robakis NK, Ramakrishna N, Wolfe G, Wisniewski HM (1987) “Molecular cloning and characterization of a cDNA encoding the cerebrovascular and the neuritic plaque amyloid peptides”. *Proc Natl Acad Sci U S A*. **84**:4190-4194.

Roberts RF, Wade-Martins R, Alegre-Abarrategui J (2015) “Direct visualization of alpha-synuclein oligomers reveals previously undetected pathology in Parkinson's disease brain”. *Brain*. **138**:1642-1657.

Rogaev EI, Sherrington R, Rogaeva EA, Levesque G, Ikeda M, Liang Y, Chi H, Lin C, Holman K, Tsuda T, et al. (1995) “Familial Alzheimer's disease in kindreds with missense mutations in a gene on chromosome 1 related to the Alzheimer's disease type 3 gene”. *Nature*. **376**:775-778.

Rosano C, Zuccotti S, Bucciantini M, Stefani M, Ramponi G, Bolognesi M (2002) “Crystal Structure and Anion Binding in the Prokaryotic Hydrogenase Maturation Factor HypF Acylphosphataselike Domain”. *J Mol Biol*. **321**:785−796

Rudajev V, Novotny J (2022) “Cholesterol as a key player in amyloid β-mediated toxicity in Alzheimer's disease”. *Front Mol Neurosci*. **15**:937056.

Salmi C, Loncle C, Vidal N, Laget M, Letourneux Y, Brunel JM (2008) “Antimicrobial activities of 3-amino- and polyaminosterol analogues of squalamine and trodusquemine”. *J Enzyme Inhib Med Chem*. **23**:860-865.

Sarkar S (2018) “Neurofibrillary tangles mediated human neuronal tauopathies: insights from fly models”. *J Genet*. **97**:783-793.

Scheefhals N, MacGillavry HD (2018) “Functional organization of postsynaptic glutamate receptors”. *Mol Cell Neurosci*. **91**:82-94.

Scheltens P, De Strooper B, Kivipelto M, Holstege H, Chételat G, Teunissen CE, Cummings J, van der Flier WM (2021) “Alzheimer's disease”. *Lancet*. **397**:1577-1590.

Schneider L (2020) “A resurrection of aducanumab for Alzheimer's disease”. *Lancet Neurol*. **19**:111-112.

Seghezza S, Diaspro A, Canale C, Dante S (2014). “Cholesterol drives aβ(1-42) interaction with lipid rafts in model membranes” *Langmuir*. **30**:13934-13941

Selkoe DJ (2008) “Soluble oligomers of the amyloid beta-protein impair synaptic plasticity and behavior”. *Behav Brain Res*. **192**:106-113.

Selkoe DJ (1991) “The molecular pathology of Alzheimer's disease”. *Neuron*. **6**:487-498.

Selkoe DJ, Hardy J (2016) “The amyloid hypothesis of Alzheimer's disease at 25 years”. *EMBO Mol Med*. 8:595-608.

Selinsky BS, Smith R, Frangiosi A, Vonbaur B, Pedersen L (2000) “Squalamine is not a proton ionophore”. *Biochim Biophys Acta*. **1464**:135-141.

Selinsky BS, Zhou Z, Fojtik KG, Jones SR, Dollahon NR, et al. (1998) “The aminosterol antibiotic squalamine permeabilizes large unilamellar phospholipid vesicles”. *Biochim Biophys Acta.* **1370**:218-234.

Sengupta A, Kabat J, Novak M, Wu Q, Grundke-Iqbal I, Iqbal K (1998) “Phosphorylation of tau at both Thr 231 and Ser 262 is required for maximal inhibition of its binding to microtubules”. *Arch Biochem Biophys*. **357**:299–309.

Sengupta U, Nilson AN, Kayed R (2016) “The Role of Amyloid-β Oligomers in Toxicity, Propagation, and Immunotherapy”. *EBioMedicine*. **6**:42-49.

Serpell LC (2000) “Alzheimer's amyloid fibrils: structure and assembly”. *Biochim Biophys Acta*. **1502**:16-30.

Serrano-Pozo A, Das S, Hyman BT (2021) “APOE and Alzheimer's disease: advances in genetics, pathophysiology, and therapeutic approaches”. *Lancet Neurol*. **20**:68-80.

Seubert P, Vigo-Pelfrey C, Esch F, Lee M, Dovey H, Davis D, Sinha S, Schlossmacher M, Whaley J, Swindlehurst C, McCormack R, Wolfert R, Selkoe D, Lieberburg I, Schenk

D (1992) “Isolation and quantification of soluble Alzheimer's beta-peptide from biological fluids”. *Nature*. **359**:325-327.

Sevigny J, Chiao P, Bussière T, Weinreb PH, Williams L, Maier M, Dunstan R, Salloway S, Chen T, Ling Y, O'Gorman J, Qian F, Arastu M, Li M, Chollate S, Brennan MS, Quintero-Monzon O, Scannevin RH, Arnold HM, Engber T, Rhodes K, Ferrero J, Hang Y, Mikulskis A, Grimm J, Hock C, Nitsch RM, Sandrock A (2016) “The antibody aducanumab reduces Aβ plaques in Alzheimer's disease”. *Nature*. **537**:50-56.

Sezgin E, Levental I, Mayor S, Eggeling C (2017) “The mystery of membrane organization: composition, regulation and roles of lipid rafts”. *Nat Rev Mol Cell Biol*. **18**:361-374.

Shaheen SM, Shakil Ahmed FR, Hossen MN, Ahmed M, Amran MS, Ul Islam A (2006). “Liposomes as a carrier for advanced drug delivery”. *Pak J Biol Sci*. **9**:1181-1191.

Shankar GM, Li S, Mehta TH, Garcia-Munoz A, Shepardson NE, Smith I, Brett FM, Farrell MA, Rowan MJ, Lemere CA, Regan CM, Walsh DM, Sabatini BL, Selkoe DJ (2008) “Amyloid-beta protein dimers isolated directly from Alzheimer’s brains impair synaptic plasticity and memory”. *Nature medicine*. **14**:837–842.

Shaw KP, Brooks NJ, Clarke JA, Ces O, Seddon JM, Law RV (2012) “Pressure–Temperature Phase Behaviour of Natural Sphingomyelin Extracts”. *Soft Matter*. **8**:1070-1078.

Sherrington R, Rogaev EI, Liang Y, Rogaeva EA, Levesque G, Ikeda M, Chi H, Lin C, Li G, Holman K, Tsuda T, Mar L, Foncin JF, Bruni AC, Montesi MP, Sorbi S, Rainero I, Pinessi L, Nee L, Chumakov I, Pollen D, Brookes A, Sanseau P, Polinsky RJ, Wasco W, Da Silva HA, Haines JL, Perkicak-Vance MA, Tanzi RE, Roses AD, Fraser PE, Rommens JM, St George-Hyslop PH (1995) “Cloning of a gene bearing missense mutations in early-onset familial Alzheimer's disease”. *Nature*. **375**:754-760.

Shi M, Chu F, Zhu F, Zhu J (2022) “Impact of Anti-amyloid-β Monoclonal Antibodies on the Pathology and Clinical Profile of Alzheimer's Disease: A Focus on Aducanumab and Lecanemab”. *Front Aging Neurosci*. **14**:870517.

Shipton OA, Leitz JR, Dworzak J, Acton CE, Tunbridge EM, Denk F, Dawson HN, Vitek MP, Wade-Martins R, Paulsen O, Vargas-Caballero M (2011) “Tau protein is required for amyloid {beta}-induced impairment of hippocampal long-term potentiation”. *J Neurosci*. **31**:1688-1692.

Shoji M, Golde TE, Ghiso J, Cheung TT, Estus S, Shaffer LM, Cai XD, McKay DM, Tintner R, Frangione B, et al. (1992) “Production of the Alzheimer amyloid beta protein by normal proteolytic processing”. *Science*. **258**:126-129.

Shou JW, Shaw PC (2022) “Therapeutic Efficacies of Berberine against Neurological Disorders: An Update of Pharmacological Effects and Mechanisms”. *Cells*. **11**:796.

Sierra MB, Pedroni VI, Buffo FE, Disalvo EA, Morini MA (2016) “The Use of Zeta Potential as a Tool to Study Phase Transitions in Binary Phosphatidylcholines Mixtures”. *Colloids Surf B Biointerfaces*. **142**:199-206.

Sims JR, Zimmer JA, Evans CD, Lu M, Ardayfio P, Sparks J, Wessels AM, Shcherbinin S, Wang H, Monkul Nery ES, Collins EC, Solomon P, Salloway S, Apostolova LG,

Hansson O, Ritchie C, Brooks DA, Mintun M, Skovronsky DM; TRAILBLAZER-ALZ 2 Investigators (2023) “Donanemab in Early Symptomatic Alzheimer Disease: The TRAILBLAZER-ALZ 2 Randomized Clinical Trial”. *JAMA*. **330**:512-527.

Sinha S, Anderson JP, Barbour R, Basi GS, Caccavello R, Davis D, Doan M, Dovey HF, Frigon N, Hong J, Jacobson-Croak K, Jewett N, Keim P, Knops J, Lieberburg I, Power M, Tan H, Tatsuno G, Tung J, Schenk D, Seubert P, Suomensaari SM, Wang S, Walker D, Zhao J, McConlogue L, John V (1999) “Purification and cloning of amyloid precursor protein beta-secretase from human brain”. *Nature*. 402:537-40.

Sloane JA, Pietropaolo MF, Rosene DL, Moss MB, Peters A, Kemper T, Abraham CR (1997) “Lack of correlation between plaque burden and cognition in the aged monkey”. *Acta Neuropathol*. **94**:471-8.

Small SA, Duff K (2008) “Linking Abeta and tau in late-onset Alzheimer's disease: a dual pathway hypothesis”. *Neuron*. **60**:534-42.

Smith AM, Maguire-Nguyen KK, Rando TA, Zasloff MA, Strange KB, Yin VP (2017) “The protein tyrosine phosphatase 1B inhibitor MSI-1436 stimulates regeneration of heart and multiple other tissues”. *NPJ Regen Med*. **2**:4.

Snyder EM, Nong Y, Almeida CG, Paul S, Moran T, Choi EY, Nairn AC, Salter MW, Lombroso PJ, Gouras GK, Greengard P (2005) “Regulation of NMDA receptor trafficking by amyloid-beta”. *Nat Neurosci*. **8**:1051-8.

Söllner T, Bennett MK, Whiteheart SW, Scheller RH, Rothman JE (1993) “A protein assembly-disassembly pathway in vitro that may correspond to sequential steps of synaptic vesicle docking, activation, and fusion”. *Cell*. 75:409-18.

Song D, Hao J, Fan D (2020) “Biological properties and clinical applications of berberine”. *Front Med*. **14**:564-582.

Spillantini MG, Crowther RA, Jakes R, Hasegawa M, Goedert M (1998) “α-Synuclein in filamentous inclusions of Lewy bodies from Parkinson's disease and dementia with Lewy bodies”. *Proc Natl Acad Sci* **95**:6469–6473.

Spillantini MG, Schmidt ML, Lee VM, Trojanowski JQ, Jakes R, Goedert M (1997) “α-Synuclein in Lewy bodies”. *Nature*. **388**: 839–840.

Staneva G, Watanabe C, Puff N, Yordanova V, Seigneuret M, Angelova MI (2021) “Amyloid-β Interactions with Lipid Rafts in Biomimetic Systems: A Review of Laboratory Methods”. *Methods Mol Biol*. 2187:47-86.

Stefanis L (2012) “α-Synuclein in Parkinson's disease”. *Cold Spring Harb Perspect Med*. **2**:a009399.

Steiner H, Haass C (2000) “Intramembrane proteolysis by presenilins”. *Nat Rev Mol Cell Biol*. **1**:217-24.

Strittmatter WJ, Saunders AM, Schmechel D, Pericak-Vance M, Enghild J, Salvesen GS, Roses AD (1993) “Apolipoprotein E: high-avidity binding to beta-amyloid and increased frequency of type 4 allele in late-onset familial Alzheimer disease”. *Proc Natl Acad Sci U S A*. **90**:1977-81.

Sun J, Wang L, Bao H, Premi S, Das U, Chapman ER, Roy S (2019) “Functional cooperation of α-synuclein and VAMP2 in synaptic vesicle recycling”. *Proc Natl Acad Sci U S A*. **116**:11113-11115.

Sunde M, Blake C (1997) “The structure of amyloid fibrils by electron microscopy and X-ray diffraction”. *Adv Protein Chem*. **50**:123-59.

Swanson CJ, Zhang Y, Dhadda S, Wang J, Kaplow J, Lai RYK, Lannfelt L, Bradley H, Rabe M, Koyama A, Reyderman L, Berry DA, Berry S, Gordon R, Kramer LD, Cummings JL (2021) “A randomized, double-blind, phase 2b proof-of-concept clinical trial in early Alzheimer's disease with lecanemab, an anti-Aβ protofibril antibody”. *Alzheimers Res Ther*. **13**:80.

Takamori S, Holt M, Stenius K, Lemke EA, Grønborg M, Riedel D, Urlaub H, Schenck S, Brügger B, Ringler P, Müller SA, Rammner B, Gräter F, Hub JS, De Groot BL, Mieskes G, Moriyama Y, Klingauf J, Grubmüller H, Heuser J, Wieland F, Jahn R (2006). “Molecular anatomy of a trafficking organelle”. *Cell.* **127**:831-846.

Takashima A, Noguchi K, Sato K, Hoshino T, Imahori K (1993) “Tau protein kinase I is essential for amyloid beta-protein-induced neurotoxicity”. *Proc Natl Acad Sci U S A*. **90**:7789-93.

Tampi RR, Forester BP, Agronin M (2021) “Aducanumab: evidence from clinical trial data and controversies”. *Drugs Context*. **10**:2021-7-3.

Tan XS, Ma JY, Feng R, Ma C, Chen WJ, Sun YP, Fu J, Huang M, He CY, Shou JW, et al. (2013) “Tissue distribution of berberine and its metabolites after oral administration in rats”. *PLoS ONE*. 8:e77969

Tanzi RE, Gusella JF, Watkins PC, Bruns GA, St George-Hyslop P, Van Keuren ML, Patterson D, Pagan S, Kurnit DM, Neve RL (1987) “Amyloid beta protein gene: cDNA, mRNA distribution, and genetic linkage near the Alzheimer locus”. *Science*. **235**:880-4.

Tatini F, Pugliese AM, Traini C, Niccoli S, Maraula G, Ed Dami T, Mannini B, Scartabelli T, Pedata F, Casamenti F, Chiti F (2013) “Amyloid-β oligomer synaptotoxicity is mimicked by oligomers of the model protein HypF-N”. *Neurobiol Aging*. **34**:2100-9.

Tayeb HO, Yang HD, Price BH, Tarazi FI (2012) “Pharmacotherapies for Alzheimer's disease: beyond cholinesterase inhibitors”. *Pharmacol Ther*. **134**:8-25.

Terry AV Jr, Buccafusco JJ (2003) “The cholinergic hypothesis of age and Alzheimer's disease-related cognitive deficits: recent challenges and their implications for novel drug development”. *J Pharmacol Exp Ther*. **306**:821-7.

Thinakaran G, Koo EH (2008) “Amyloid precursor protein trafficking, processing, and function”. *J Biol Chem*. **283**:29615-9.

Thirunavukkuarasu S, Jares-Erijman EA, Jovin TM (2008) “Multiparametric fluorescence detection of early stages in the amyloid protein aggregation of pyrene-labeled alpha-synuclein”. *J Mol Biol*. **378**:1064-73.

Thompson D, Morrice N, Grant L, Le Sommer S, Lees EK, Mody N, Wilson HM, Delibegovic M (2017) “Pharmacological inhibition of protein tyrosine phosphatase 1B

protects against atherosclerotic plaque formation in the LDLR-/- mouse model of atherosclerosis". *Clin Sci (Lond).* **131**:2489-2501.

Tintore M, Vidal-Jordana A, Sastre-Garriga J (2019) "Treatment of multiple sclerosis - success from bench to bedside". *Nat Rev Neurol*. **15**:53-58.

Tiwari S, Atluri V, Kaushik A, Yndart A, Nair M (2019) "Alzheimer's disease: pathogenesis, diagnostics, and therapeutics". *Int J Nanomedicine*. **14**:5541-5554.

Ulmer TS, Bax A, Cole NB, Nussbaum RL (2005) "Structure and dynamics of micelle-bound human alpha-synuclein". *J Biol Chem*. **280**:9595-603.

van der Kant R, Goldstein LSB, Ossenkoppele R (2020) "Amyloid-β-independent regulators of tau pathology in Alzheimer disease". *Nat Rev Neurosci*. **21**:21-35.

van Dyck CH, Swanson CJ, Aisen P, Bateman RJ, Chen C, Gee M, Kanekiyo M, Li D, Reyderman L, Cohen S, Froelich L, Katayama S, Sabbagh M, Vellas B, Watson D, Dhadda S, Irizarry M, Kramer LD, Iwatsubo T (2022) "Lecanemab in Early Alzheimer's Disease". *N Engl J Med*. **388**:9-21.

van Meer G, Voelker DR, Feigenson GW (2008) "Membrane lipids: where they are and how they behave". *Nat Rev Mol Cell Biol*. **9**:112-24.

Vaz M, Silvestre S (2020) "Alzheimer's disease: Recent treatment strategies". *Eur J Pharmacol*. **887**:173554.

Visser PJ, Verhey F, Knol DL, Scheltens P, Wahlund LO, Freund-Levi Y, Tsolaki M, Minthon L, Wallin AK, Hampel H, Bürger K, Pirttila T, Soininen H, Rikkert MO, Verbeek MM, Spiru L, Blennow K (2009) "Prevalence and prognostic value of CSF markers of Alzheimer's disease pathology in patients with subjective cognitive impairment or mild cognitive impairment in the DESCRIPA study: a prospective cohort study". *Lancet Neurol*. **8**:619-27.

Waltenberger B, Mocan A, Šmejkal K, Heiss EH, Atanasov AG (2016) "Natural Products to Counteract the Epidemic of Cardiovascular and Metabolic Disorders". *Molecules*. **21**:807.

Wang X, Wang R, Xing D, Su H, Ma C, Ding Y, Du L (2005) "Kinetic difference of berberine between hippocampus and plasma in rat after intravenous administration of Coptidis rhizoma extract". *Life Sci*. **77**:3058–3067.

Wang ZX, Tan L, Liu J, Yu JT (2016) "The Essential Role of Soluble Aβ Oligomers in Alzheimer's Disease". *Mol Neurobiol*. **53**:1905-1924.

Wasmer C, Lange A, Van Melckebeke H, Siemer AB, Riek R, Meier BH (2008) "Amyloid fibrils of the HET-s(218–289) prion form a β solenoid with a triangular hydrophobic core". *Science*. **319**:1523–26.

Wehrli SL, Moore KS, Roder H, Durell S, Zasloff M (1993) "Structure of the novel steroidal antibiotic squalamine determined by two-dimensional NMR spectroscopy". *Steroids*. **58**:370-8.

Wells C, Brennan S, Keon M, Ooi L (2021) "The role of amyloid oligomers in neurodegenerative pathologies". *Int J Biol Macromol*. **181**:582-604.

Whitehouse PJ, Saini V (2022) “Making the Case for the Accelerated Withdrawal of Aducanumab”. *J Alzheimers Dis*. **87**:999-1001.

Williams TL, Serpell LC (2011) “Membrane and surface interactions of Alzheimer's Aβ peptide--insights into the mechanism of cytotoxicity”. *FEBS J*. **278**:3905-17.

Williams TL, Urbanc B, Marshall KE, Vadukul DM, Jenkins AT, Serpell LC (2015) “Europium as an inhibitor of Amyloid-β(1-42) induced membrane permeation”. *FEBS Lett*. **589**:3228-3236.

Xie A, Gao J, Xu L, Meng D (2014) “Shared mechanisms of neurodegeneration in Alzheimer's disease and Parkinson's disease”. *Biomed Res Int*. **2014**:648740.

Xie X, Chang X, Chen L, Huang K, Huang J, Wang S, Shen X, Liu P, Huang H (2013) “Berberine ameliorates experimental diabetes-induced renal inflammation and fibronectin by inhibiting the activation of RhoA/ROCK signaling”. *Mol Cell Endocrinol*. **381**:56-65.

Xu L , Bhattacharya S , Thompson D (2018) “The fold preference and thermodynamic stability of α-synuclein fibrils is encoded in the non-amyloid-β component region”. *Phys Chem Chem Phys*. **20**:4502-4512.

Xu X, Yi H, Wu J, Kuang T, Zhang J, Li Q, Du H, Xu T, Jiang G, Fan G (2021) “Therapeutic effect of berberine on metabolic diseases: Both pharmacological data and clinical evidence”. *Biomed Pharmacother*. **133**:110984.

Yakupova EI, Bobyleva LG, Vikhlyantsev IM, Bobylev AG (2019) “Congo Red and amyloids: history and relationship”. *Biosci Rep*. **39**:BSR20181415.

Yamamoto N, Matsubara T, Sato T, Yanagisawa K (2008) “Age-dependent high-density clustering of GM1 ganglioside at presynaptic neuritic terminals promotes amyloid beta-protein fibrillogenesis”. *Biochim Biophys Acta*. **1778**:2717-26.

Yanagisawa K (2005) “Cholesterol and amyloid beta fibrillogenesis”. *Subcell Biochem*. **38**:179-202.

Yiannopoulou KG, Papageorgiou SG (2020) “Current and Future Treatments in Alzheimer Disease: An Update”. *J Cent Nerv Syst Dis*. **12**:1179573520907397.

Yoo G, Shin YK, Lee NK (2023) “The Role of α-Synuclein in SNARE-mediated Synaptic Vesicle Fusion”. *J Mol Biol*. **435**:167775.

Zampagni M, Cascella R, Casamenti F, Grossi C, Evangelisti E, Wright D, Becatti M, Liguri G, Mannini B, Campioni S, Chiti F, Cecchi C (2011) “A comparison of the biochemical modifications caused by toxic and non-toxic protein oligomers in cells”. *J Cell Mol Med*. **15**:2106-16.

Zarranz JJ, Alegre J, Gómez-Esteban JC, Lezcano E, Ros R, Ampuero I, Vidal L, Hoenicka J, Rodriguez O, Atarés B, Llorens V, Gomez Tortosa E, del Ser T, Muñoz DG, de Yebenes JG (2004) “The new mutation, E46K, of alpha-synuclein causes Parkinson and Lewy body dementia”. *Ann Neurol*. **55**:164-73.

Zasloff M, Adams AP, Beckerman B, Campbell A, Han Z, et al. (2011) “Squalamine as a broad-spectrum systemic antiviral agent with therapeutic potential”. *Proc Natl Acad Sci U S A*. **108**:15978-15983.

Zasloff M, Williams JI, Chen Q, Anderson M, Maeder T, et al. (2001) “A spermine-coupled cholesterol metabolite from the shark with potent appetite suppressant and antidiabetic properties”. *Int J Obes Relat Metab Disord*. **25**:689-697.

Zhang X, Rao MN, Jones SR, Shao B, Feibush P, McGuigan M, Tzodikov N, Feibush B, Sharkansky I, Snyder B, Mallis LM, Sarkahian A, Wilder S, Turse JE, Kinney WA, Kjærsgaard HJ, Michalak RS (1998) “Synthesis of Squalamine Utilizing a Readily Accessible Spermidine Equivalent”. *J Org Chem*. **63**:8599-8603.

Zhu M, Li J, Fink AL (2003) “The association of alpha-synuclein with membranes affects bilayer structure, stability, and fibril formation”. *J Biol Chem*. **278**:40186-40197.